Sofia University "St. Kliment Ohridski

Faculty of Physics

Dobromir Stefanov Pressyanov

RADIOLOGICAL PROBLEMS RELATED TO RADON AND NEW METHODS FOR THEIR INVESTIGATION

Dissertation for acquiring the scientific degree of Doctor of the Physical Sciences

2012

Non scholae sed vitae discimus

Contents

I. INTRODUCTION

In 2009 the World Health Organization [1] recognized radon exposure as the second cause for lung cancer, after smoking. For never-smokers it was pointed out as reason number one. This grasps the essence of extensive radon measuring campaigns and epidemiological studies made in the previous decades [2-4]. As a result radon was recognized as one of the most dangerous environmental factors. However, the story of the radon's threat can be traced back to 15^{th} century, thus making it perhaps "the most ancient" one from the radiation stories. Extensive silver mining started in Schneeberg, Saxony, Germany at about 1470. Somewhat later, in 1516, similar mining activities commenced in Joachimsthal (now Jachymov, Czech republic). The first report about unusually high mortality of miners from a mysterious sickness was from Paracelsus in his book about the "Bergsucht" and other miner's diseases [5]. This book was written in 1537 but published after the death of Paracelsus, at 1567. Paracelsus labeled this disease as "Mala Metallorum". Agricola, who served as a physician in Jachymov in 1527-33 described the mining practice at that time in his famous book "De Re Metalica" [6]. The sickness was identified in 1879 as malignant tumors of the lung [7], further classified as bronchial cancer. At that time the cause of death of about 75% of the miners in Schneeberg was lung cancer.

The cause of this high lung cancer morbidity remained mysterious for a long time. Schuettmann [8] has concluded that H. E. Mueller, a mining director in Zwickau, Saxony first raised the hypothesis of possible causality between radium in ores and radon in mines' air, and lung cancer in miners. This hypothesis received an experimental support after more precise radon measurements were carried out in Schneeberg [9] and Jachymov [10]. However, the calculations of the bronchial dose by radon itself didn't reveal a dose that is sufficient to explain the high lung cancer morbidity [11].

The radiologically important radon isotopes are members of long radioactive families. The most important ones are ^{222}Rn, a member of ^{238}U family (Fig. I.1.) and ^{220}Rn (or thoron) of ^{232}Th family (Fig. I.2.). Once produced after the decay of radium (^{222}Rn is decay product of ^{226}Ra and ^{220}Rn of ^{224}Ra), the inert gas radon can easily migrate through cracks and pores of the soil/rock. Radon-222 gives birth to short lived progeny, which includes ^{218}Po, ^{214}Pb and ^{214}Bi + ^{214}Po (because of its very short half-life ^{214}Po is always in equilibrium with ^{214}Bi and is not considered separately). Respectively, ^{220}Rn decays to ^{216}Po, ^{212}Pb and ^{212}Bi + ^{212}Po/^{208}Tl (see Fig. I.2.). It was not until 1951 that William F. Bale [12] realized that the short lived decay products of radon are the factor that delivers high lung dose. It is interesting to note that as early as in this report Bale foresaw the problem of indoor radon, stating that his calculations suggest "that bronchial epithelium receives the highest radiation dosage of any human tissue under background conditions" [12]. It was quite an insightful remark up - nowadays, exposure to radon-222 is considered a serious health problem and large scale investigations and radon measuring campaigns have been organized worldwide. In the last years the interest to thoron (^{220}Rn) is also increasing [13, 14].

In Bulgaria there is a century-long tradition of radon measurements [15]. Since 1907 with hardly any interruption radon and later radon progeny have been measured in mineral spas, in underground mines, in the human environment and in laboratory research. While most of the published work in this field in Bulgaria up to date comes from the University of Sofia, by far the largest number of radon and radon progeny measurements have been made by the work-place radiation monitoring of uranium industry in Bulgaria [16]. After cessation of the uranium industry the radon measurements were focused on the environmental consequences of this industry and on studies in risk regions.

The author was involved in radon dosimetry in 1986, first as a health physicists in uranium industry. After 1990 the methodological research was

expanded towards problems raised by the increasing concern in radon exposure of the human population [17, 18]. The extensive epidemiological studies in the last two decades gave direct evidence for the radon risk of the human population and led to the decision of the International Commission on Radiological Protection to increase almost twice lung cancer risk coefficients for radon exposure [19].

In this thesis the author comprises his contributions to solve several problems related to radon. The output presented here is in the following directions:

- Methodological research on diffusion chambers with solid state nuclear track detectors (SSNTDs) for integrated measurements of ^{222}Rn. This includes study of properties of the used SSNTDs, investigations related to automatic counting of tracks, theoretical and experimental study of the distribution of ^{222}Rn progeny inside the chamber volume and traceability of the measurements;
- Methodological research on grab sampling and integrated measurements of ^{222}Rn progeny and ^{220}Rn progeny. Development and application of a method for integrated measurements of the individual concentrations of ^{218}Po, ^{214}Pb and ^{214}Bi+^{214}Po, as well as of ^{212}Pb and ^{212}Bi+^{212}Po;
- Comprehending Bulgarian miners' radon exposure data and using it in bio-medical research;
- Identification of radon risk areas in Bulgaria and organizing dedicated radon surveys. These areas include the town of Rakovski, the village of Eleshnitsa and the regions affected by the uranium industry near Sofia.
- Proposal of a new method for radon measurements based on radon absorption in bisphenol-A based polycarbonate materials. Theoretical and experimental study of this "polycarbonate" method

and its potential applications for measurements of ^{222}Rn in air, water and soil-gas.

- On the basis of the polycarbonate method proposal, research and application of new method for retrospective ^{222}Rn measurements, based on the use of home stored CDs/DVDs. These are made of bisphenol-A based polycarbonate material that can serve as radon detector. Theoretical and experimental study of this method.
- Proposal and experimental study of a method for retrospective measurements of thoron (^{220}Rn). It is again based on the use of CDs/DVDs stored indoors.
- Theoretical and experimental study of a method for radon measurement based on a radon absorber/radiator and coupled with it external SSNTD.

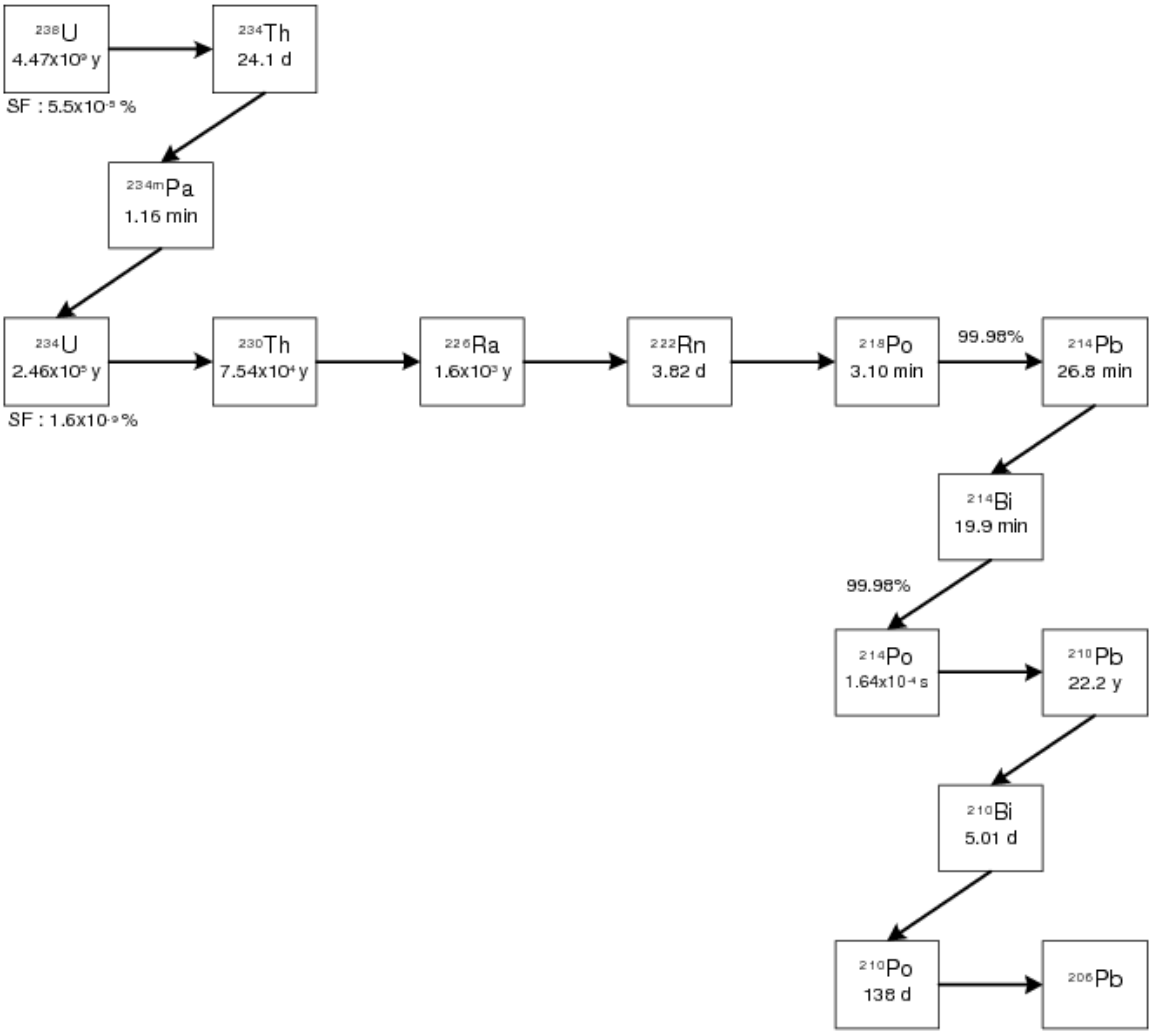

Figure I.1. The radioactive family of uranium (or uranium-radium). Transformations occurring with probability less than 0.15% are not included. Horizontal arrays correspond to α-decay and the tilted ones to β^- decay.

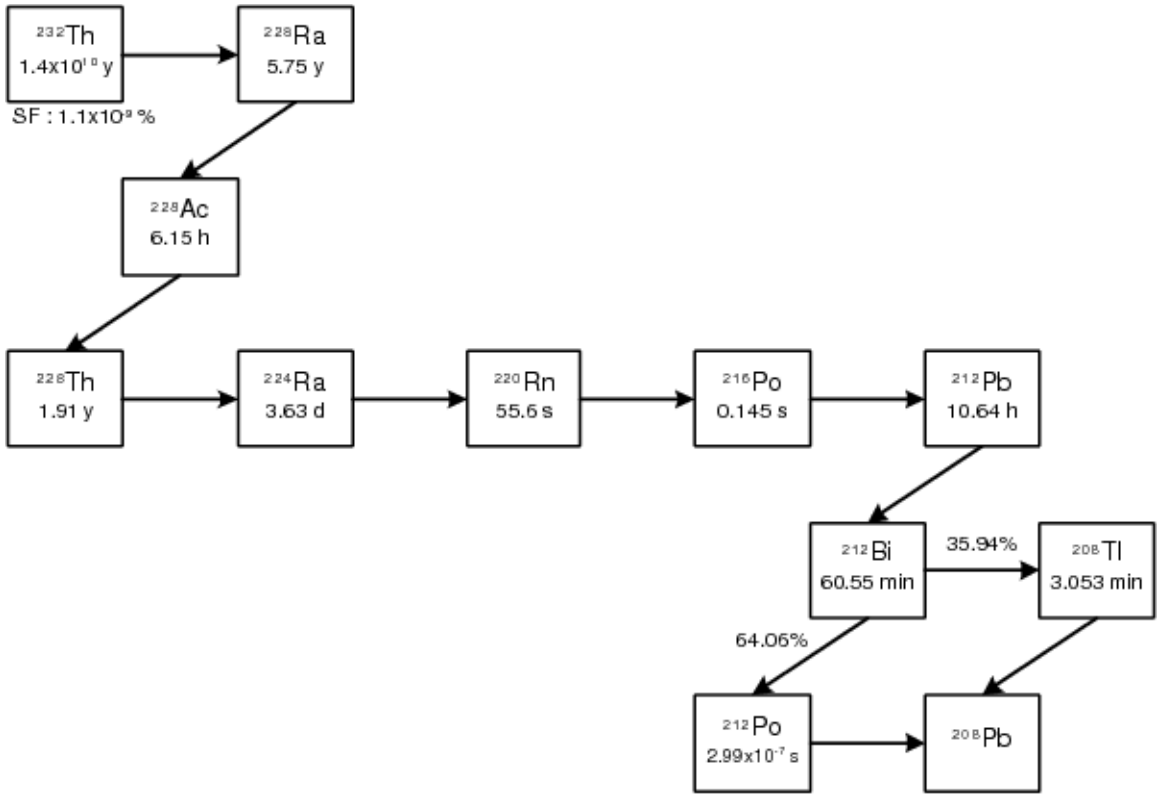

Figure I. 2. The radioactive family of thorium. Transformations occurring with probability less than 0.15% are not included. Horizontal arrays correspond to α-decay and the tilted ones to β^- decay.

II. METHODOLOGICAL ASPECTS OF INTEGRATED MEASUREMENTS OF ^{222}Rn BY DIFFUSION CHAMBERS

II.1. Solid state nuclear track detectors (SSNTDs) as a tool for radon measurements.

The technique of SSNTDs is perhaps the most widely used one in radon detection. It is based on the property of some dielectrics to "keep" for a long time defects in their structure that are created by heavy ions (in case of radon alpha particles are of primary interest). The first observation of such latent tracks was that of Young [20]. The applications boosted after extensive research and development carried out in the General Electric laboratories in 1960s [21]. In the past in Bulgaria this technique has been applied in nuclear research [22] and in geological exploration of uranium deposits [23]. The application of SSNTDs for environmental radon measurements in Bulgaria was initiated in the beginning of 1990s [24]. The first kind of SSNTD used for these measurements was that of Kodak-Pathe LR-115 type II. To utilize this technique in the Laboratory of Dosimetry and Radiation Protection at the University of Sofia substantial work was performed [25, 26]. The etching procedure, utilized for this kind of detector was as follows: Chemical etching with 10% solution of NaOH at 60^0 C for 120 min. After that the detectors are washed in water for 30 min and left (without agitation) for 2 min in 50% volume solution of ethanol. After the detectors dry out, the tracks are counted. In the first applications track counting was done visually - by a transmitted light microscope. Early studies were devoted to study the LR-115/II response to α-particles [25]. To create a track that will be etched the incident alpha particle should have energy and angle of incidence within the range that is specific for the particular kind of detector and etching conditions

[26]. The response function is described by the dependence of the registration efficiency on the energy and incident angle of alpha particles. The profile of the experimentally obtained in our laboratory response function is shown in Fig. II.1 [25].

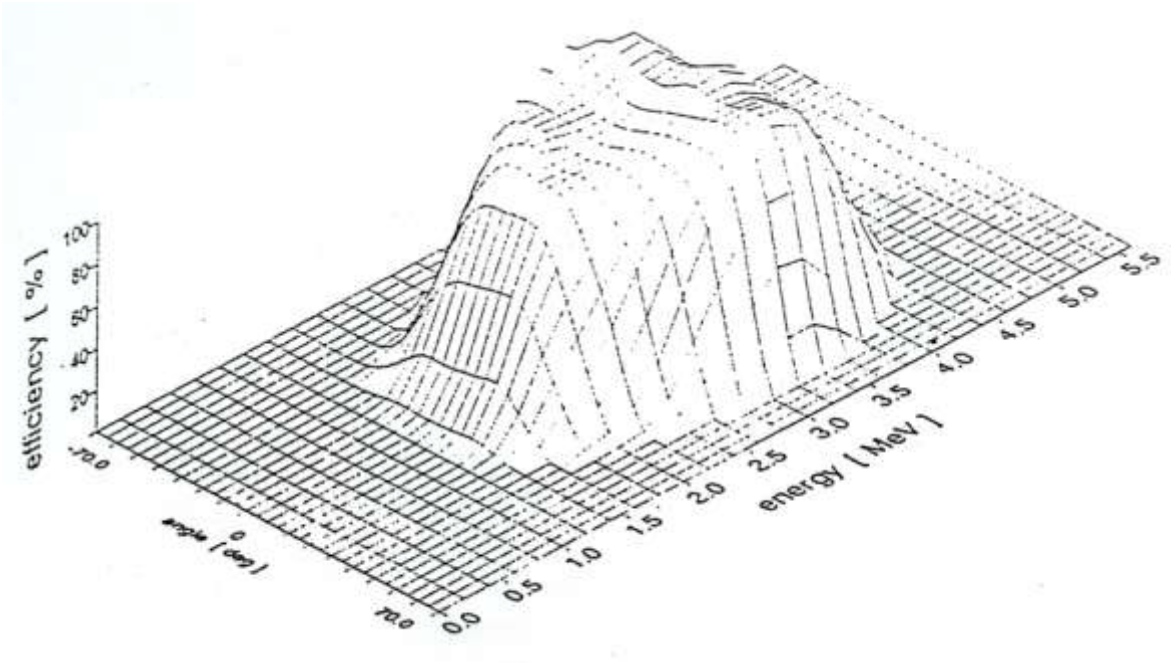

Figure II.1. The energy and angular response of Kodak Pathe LR-115 type II after etching with 10% NaOH at 60^0 C for 120 min. Visual counting by transmitted light microscope was applied. The efficiency is the ratio (per unit surface area) of etched tracks to the incident alpha particles.

The visual track counting is time and labor consuming. This is a technical limitation for large scale applications. Therefore, from the very beginning implementation of methods for automatic track counting was targeted. The attempts to adopt such methods developed by other authors [22, 27] revealed, that they don't cover the entire range we are interested in. The financial limitations hampered utilization of the commercially available image analyzers [28]. To overcome the limitations and to make a step ahead the obstructed total internal

reflection (TIR) of a laser beam was employed [29]. Figure II.2 illustrates the physical concept. A laser beam incident on the smooth surface at angle $\theta>\theta_0$ (θ_0=arcsin(n^{-1}), where n is the reflective index of the medium and θ_0 is the angle of TIR) undergoes a TIR. The etched tracks are "crater-like" defects on the surface, and the TIR condition is disturbed. First this approach has been used by Harvey and Weeks [30, 31] for 2 mm thick CR-39 detectors. We modified it to make the approach usable for thin Kodak-Pathe LR-15/II detectors. For that purpose a laboratory system was designed and constructed (in the Technical University, Varna), which is schematically shown in Fig. II.3. A 1 mW He-Ne laser of regulated (by the beam expander BE) beam width was used. The laser beam passes the beam splitter (BS). The part of the beam reflected by the BS is used by the laser beam intensity control (LBIC) system to compensate the instability of the laser beam. The SSNTD is placed (by immersion liquid) in optical contact with the prism P, so that the sensitivity surface of the detector looks to the microscope M. The photo-multiplier PM is installed on the microscope, and is operated as a photometer in photon counting mode. The experimentally obtained response, as a function of the track density, is given in Fig. II.4. The response is linear to about $5x10^4$ cm^{-2}, and increases sub-linearly to about $5x10^5$ cm^{-2}, where full saturation is reached. The saturation at high track density is due to the overlap of the images of the individual tracks. This version can be used for measuring track density in the range $10^3 - 10^5$ cm^{-2} (the relative uncertainty is about 50% at 500 cm^{-2} and decreases to about 10% and less at >2000 cm^{-2}).

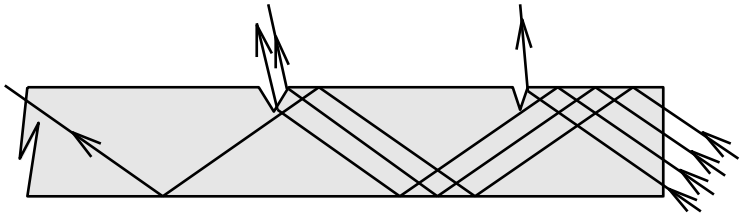

Figure II.2. The principle of track registration by obstructed TIR.

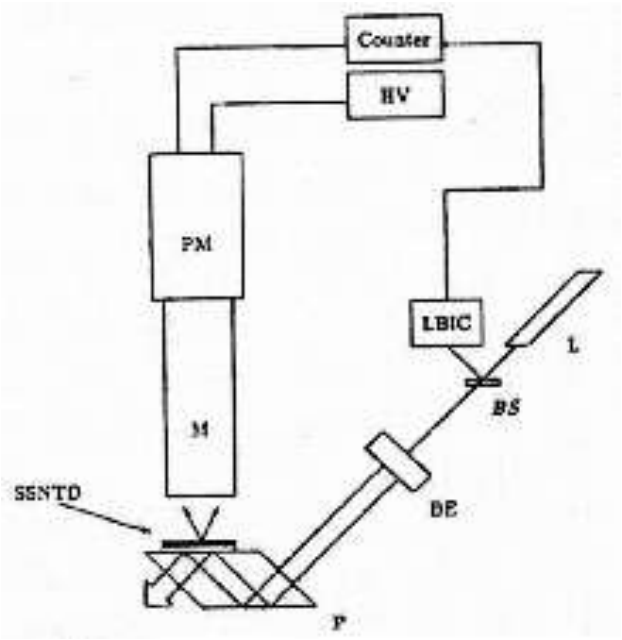

Figure II.3. A scheme of the equipment. Legend: L – laser tube, BS – beam splitter, BE – beam expander, LBIC – laser beam intensity control, P – prism, M – microscope, PM – photo multiplier, HV – high voltage. In the counter block the number of impulses from PM is divided by a factor proportional to the reference signal given by LBIC, and the result is displayed numerically.

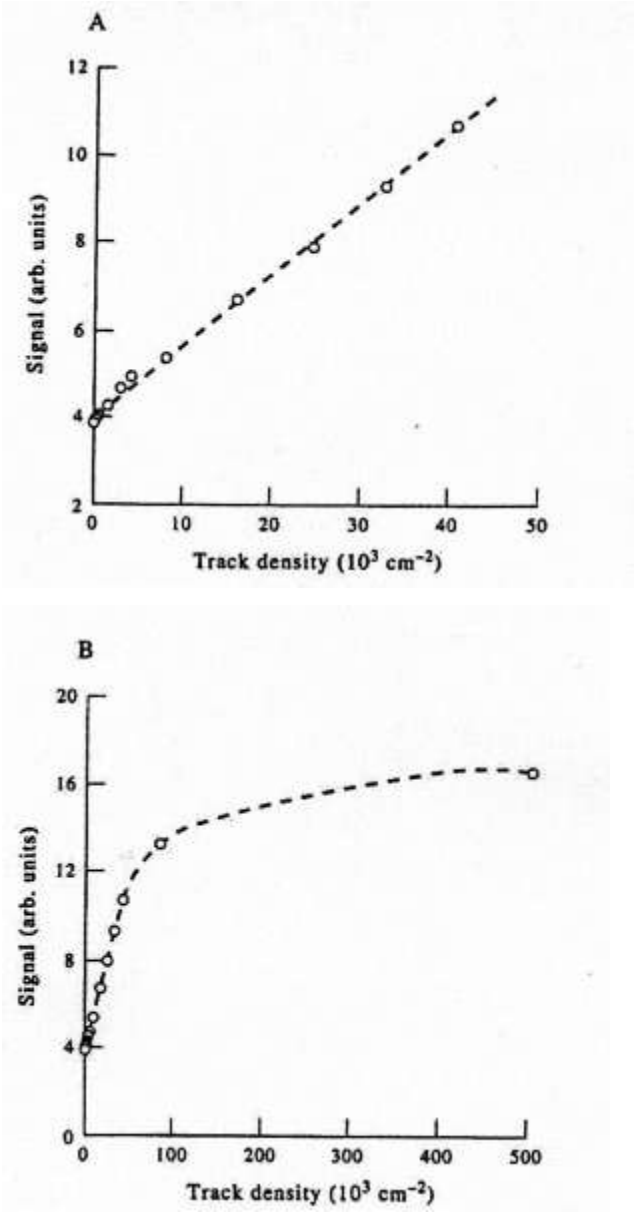

Figure II.4. Dependence of the mean signal on the track density, obtained in experiments with obstructed TIR of a laser light. Track density range: (A) 0 – $5x10^4$ cm^{-2}; (B) 0 – $5x10^5$ cm^{-2}.

A direction for substantial progress in automatic counting of chemically etched track detectors was opened with the utilization of high resolution computer scanners. First attempts in this direction started in the late 90-ies [32].

In 2004 a high resolution computer scanner EPSON Perfection 1650 Photo (1600x1600 dpi and 24-bit RGB color resolution) was successfully used to count chemically etched tracks both in transmitted light and in reflective mode [33]. The transmitted light mode was employed with Kodak-Pathe LR-115/II detectors. The tracks were counted with a dedicated computer code, following the procedure:

- From the scanned RGB bitmap image only the green component is analyzed. This is because of its highest contrast in the studied cases;
- An average density value (this is the pixels' intensity) and its standard deviation are calculated for the whole scanned field to estimate the background density;
- A threshold density value is then determined according to the background density and its standard deviation;
- All pixels are then successfully examined and all compact regions of pixels with density greater than the threshold density value are counted as tracks.

With this algorithm we have observed almost perfect correlation between automatic and visual track-counting modes (Fig II.5.).

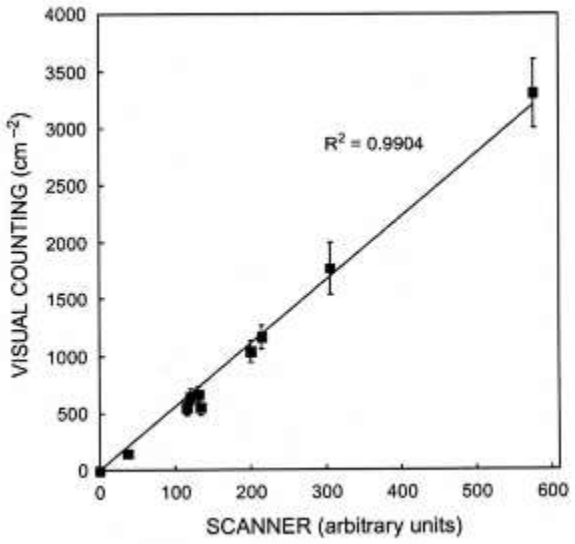

Figure II. 5. Comparison between results obtained by visual track counting and automatic counting by a computer scanner of tracks in SSNTD of Kodak Pathe LR-115 type II.

One principal practical goal of the research of the response and automatic track counting of Kodak Pathe LR-115/II was to use it in the design and practical applications of diffusion chambers for integrated measurements of ^{222}Rn.

II.2. Diffusion chambers for radon measurement.

II.2.1. Diffusion chambers for measurements in air

Diffusion chambers with solid state nuclear track detectors (SSNTDs) inside are one of the most commonly used instruments for integrated measurements of ^{222}Rn [34]. A photo of diffusion chambers used in the author's laboratory is shown in Fig. II. 6. In plastic chambers the ^{222}Rn gas enters the chamber through a polyethylene membrane that stops ^{222}Rn progeny (^{218}Po, ^{214}Pb and ^{214}Bi + ^{214}Po) and should also stop ^{220}Rn and ^{220}Rn progeny. In metal

chambers ^{222}Rn gas finds its "way through" small gaps that exist along the edge of the chamber cap. Inside the chamber ^{222}Rn gives birth to its progeny atoms that diffuse in air and are deposited on the inner walls. Alpha particles emitted from ^{222}Rn, ^{218}Po and ^{214}Po bombard the SSNTD surface and create tracks.

Figure II.6. Photo of two types of diffusion chambers used for practical investigations (left – metal chamber, right plastic chamber). The SSNTDs in both are Kodak Pathe LR-115 type II films.

Diffusion chambers with SSNTDs are extensively used for radon measurements in the environment [34, 35]. Their application for environmental studies in Bulgaria started in the 90s and raised many methodological questions that needed to be addressed, in order to warrant reliability. The size and construction of the diffusion chambers and the material of which they are made could vary. Therefore, it was necessary to perform a dedicated research of the physical processes in diffusion chambers that are of significance for creation of the track signal of the radon detectors.

The calibration factor (*CF*) of the chamber (*CF*=net track density/integrated ^{222}Rn concentration) depends on the source geometry – this is the distribution of the alpha emitters in the chamber volume and deposited progeny atoms on the inner surface of the wall. The computer simulations of other authors [36, 37] have shown that the distribution of radon progeny atoms on the

internal wall of the chamber is non-uniform and this affects the response of the chamber. Overall, our research was focused on the following:

- Calibration to ^{222}Rn. Study of the sensitivity to ^{220}Rn. Traceability to a primary ^{222}Rn standard;
- Numerical modeling and experiments on the physical processes that are of importance for the diffusion chambers' response;
- Analytical solution of the mathematical problem of ^{222}Rn progeny distribution in the volume of a cylindrical diffusion chamber.

To ensure the diffusion chambers' traceability to primary radon standard collaboration was built with Laboratoire National Henry Becquerel (LNHB) at CEA-Saclay, France. The employed approach was based on direct use of primary and secondary ^{222}Rn standards.

II. 2. 2. Traceability to a primary ^{222}Rn standard

The primary standard designed and constructed at LNHB-CEA, Saclay, France was used. It is based on ^{222}Rn condensed on a cold disk with well-defined size [38] and alpha counting in a defined solid angle. The alpha particles are counted by a surface barrier detector placed directly opposite the source. The source activity measured by the system is:

$$A = \dot{n}\frac{1}{G}, \qquad \text{(II.1)}$$

where A [Bq] is the activity, $\dot{n}$ is the counting rate [s^{-1}] in the 5.49 MeV alpha peak of ^{222}Rn. The quantity $\boldsymbol{G}$ is a "geometry factor", which is equal to the proportion of emitted alpha particles that are registered, provided that any alpha particle that falls on the detector surface is registered.

In the general case, the geometry factor and its uncertainty are calculated numerically by a dedicated computer code [39] that takes into account the "source-detector" geometry of the standard. It has been demonstrated [38] that the combined relative uncertainty (1 SD) of the determined activity is 0.5%.

After the absolute measurement is conducted and radon is re-vaporized, the gas is transferred to a container to provide secondary gas standards. The relative standard uncertainty of the ^{222}Rn activity in this secondary standard is of the order of 0.5%.

Having a precisely known ^{222}Rn activity makes it possible to calibrate radon measuring instruments in a radon chamber without the need of a reference instrument, provided that the chamber volume is precisely calibrated and its bias due to the instruments placed inside is either negligible or can be evaluated. For an activity A of the standard transferred into volume V, the integrated activity concentration I_A, for exposure time t_{exp} is [40]:

$$I_A = A\frac{1-\exp(-\lambda t_{\exp})}{\lambda V}. \qquad \text{(II.2)}$$

The radon chamber used was 1 m^3 BACCARA radon chamber developed in CEA-Saclay, France. A photo of this chamber is shown in Fig. II.7. In our calibration experiment the activity at the start of exposure was A = 13.90 ± 0.07 kBq. The exposure time was 101.50 ± 0.02 hours. The corresponding integrated activity concentration was I_A = 988 kBq h m^{-3}. The combined relative uncertainty of this value was 1.1% [40].

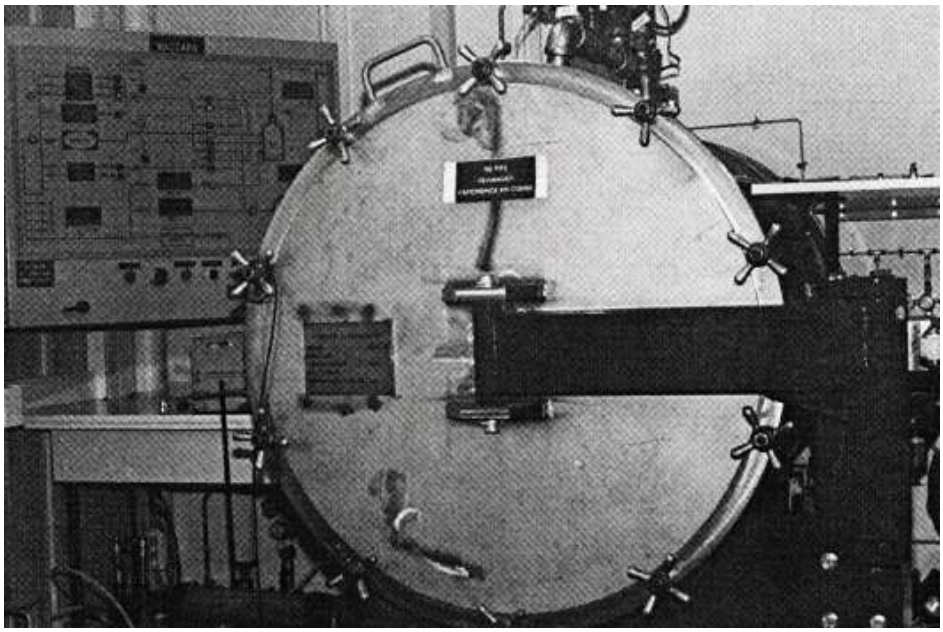

Figure II.7. A photo of BACCARA reference radon chamber.

The laboratory equipment used in this experiment fits the requirements for a reference system for test atmospheres with radon (STAR) that are specified in the recent IEC standard [41]. The diffusion chambers exposed were the plastic-ones, shown in Fig. II.6.

According to the *CF* definition: $CF=n_{tr}/I_A$, where n_{tr} is the area track density. The combined uncertainty of *CF* was determined according to Ref. [42] and is given by:

$$\frac{u_c(CF)}{CF}=\sqrt{\left(\frac{u(n_{tr})}{n_{tr}}\right)^2+\left(\frac{u(I_A)}{I_A}\right)^2}\ . \qquad \text{(II.3)}$$

Visual track counting by a transmitted light microscope was employed. The average *CF* of the plastic chambers used in this experiment (see Fig. **II.6,** right) was $CF = (1.97 \pm 0.08)$ cm^{-2} kBq^{-1} h^{-1} m^3. The *CF* here is expressed in

conventional units. However, one can note that its dimension is in fact the dimension of length. If the track density is expressed in cm^{-2} and the integrated ^{222}Rn activity concentration in Bq s cm^{-3} = cm^{-3}, then the *CF* is obtained in cm^{-2}/cm^{-3}=cm (*CF* in units of length is sometimes referred as "sensitivity" of the chamber). The relation between the numerical values in these units is as follows:

$$CF \text{ (cm)} = 0.2778\ C_F \text{ (cm}^{-2}\text{ kBq}^{-1}\text{ h}^{-1}\text{ m}^3\text{)}. \qquad \text{(II.4)}$$

In units *cm* the obtained C_F is 0.577 ± 0.022 *cm*.

II.2.3. Study of the physical processes in diffusion chambers.

The ^{222}Rn progeny atoms generated inside the chamber by the parent ^{222}Rn are distributed in the volume as well as deposited on the internal walls. This complicates the source geometry that is defined by the distribution of the alpha emitters ^{222}Rn, ^{218}Po and ^{214}Po. Monte Carlo simulations [43] have revealed that the uncertainty in sensitivity due to the unknown fraction of deposited radon progeny may approach 30% for cylindrical chambers of radius greater than 3 cm and of height greater than 4 cm.

In the theoretical studies we were focused on cylindrical geometry, as all diffusion chambers we have used are of cylindrical or close to cylindrical shape. Our first approach to the problem was by numerical modeling [44]. The model used considers diffusion of ^{222}Rn progeny atoms in a cylindrical cavity. The process was assumed to be stationary which is reasonable, because the time of exposure of diffusion chambers is much longer than the time needed for reaching equilibrium between ^{222}Rn and its progeny (3-4 h). The stationary problem is described by the equations:

$$D\Delta n_i - \lambda_i n_i + \lambda_{i-1} n_{i-1} = 0, \qquad \text{(II.5)}$$

where i=0,1,2,3 refer to ^{222}Rn, ^{218}Po, ^{214}Pb and ^{214}Bi, respectively (but the equations start with i=1), n_i are the atom concentrations, λ_i are decay constants and D is the diffusion coefficient, which is assumed to be the same for all of the ^{222}Rn progeny. The symbol Δ denotes the Laplacian operator ($\Delta = \frac{\partial^2}{\partial x^2} + \frac{\partial^2}{\partial y^2} + \frac{\partial^2}{\partial z^2}$). In cylindrical coordinates, in which angular dependence is missing due to the cylindrical symmetry of the problem, it takes the form $\Delta = \frac{1}{r}\frac{\partial}{\partial r}\left(r\frac{\partial}{\partial r}\right) + \frac{\partial^2}{\partial z^2}$.

A numerical modeling of the diffusion process in the cavity has been performed. The numerical modeling of the influence of the progeny atoms' reflection and recoil from the walls revealed that it is negligible [44]. After the distribution of ^{222}Rn progeny atoms concentration was obtained, the deposited fraction was calculated as 1- f_i, where f_i is the volume fraction of the i-th decay product:

$$f_i = \frac{\lambda_i \int_V n_i dV}{\lambda_0 n_0 V}, \qquad \text{(II.6)}$$

where V is the cavity volume. This fraction was calculated for cylindrical chambers of different diameter and height. The modeling was performed for different values of the diffusion coefficient of ^{222}Rn progeny atoms in air, which were reported in the literature. The modeling revealed that the deposited fractions of ^{214}Pb and ^{214}Bi are close to 100%, while that of ^{218}Po can vary in wider range. The results obtained for ^{218}Po are illustrated in Fig. II.8.

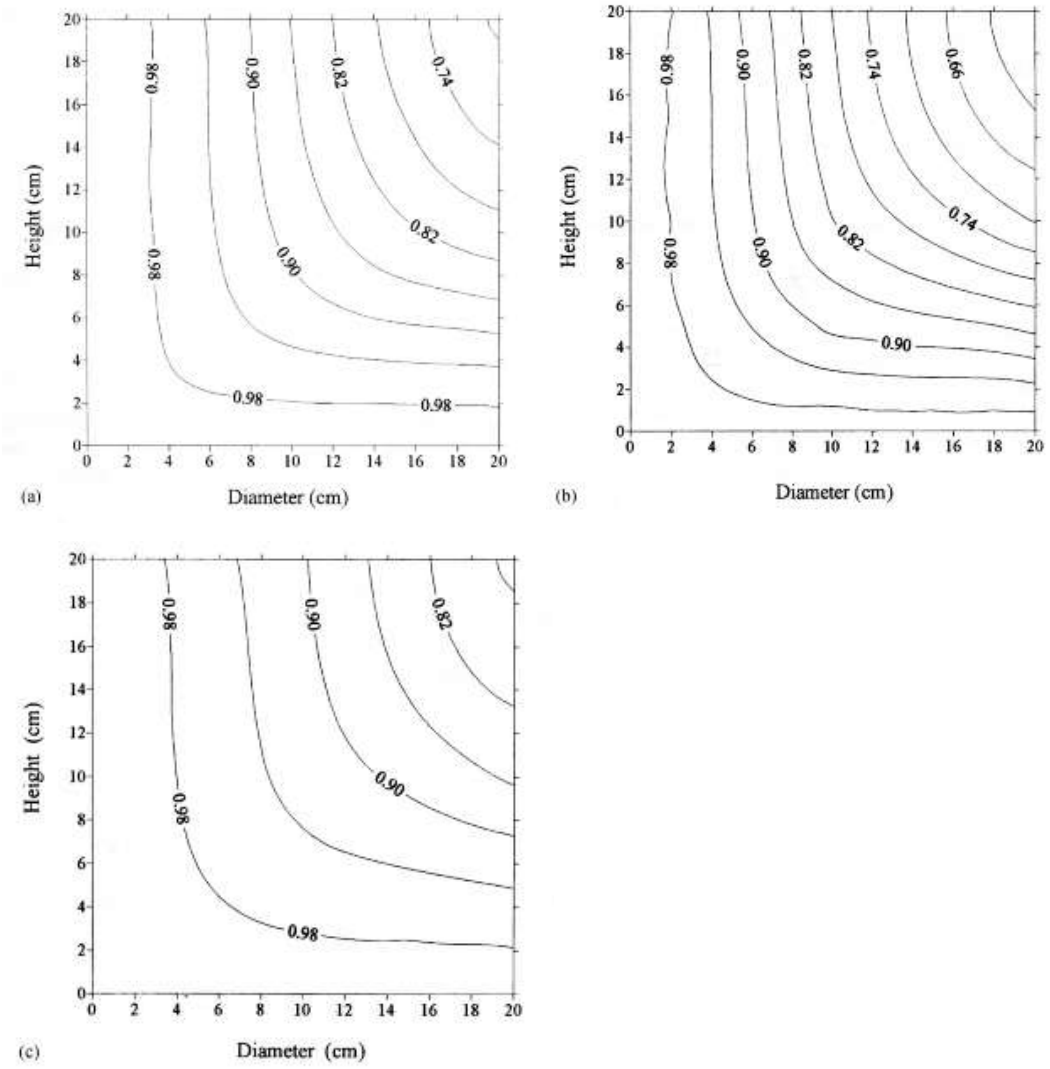

Figure II. 8. Deposited fraction of ^{218}Po atoms as a function of the diameter and height of the cylindrical chamber. Lines of equal deposition are drawn for diffusion coefficients of: (a) 0.054 $cm^2\ s^{-1}$; (b) 0.03 $cm^2\ s^{-1}$; (c) 0.085 $cm^2\ s^{-1}$.

Further, an experimental study with cylindrical diffusion chambers (diameter 8 cm and height 7.5 cm) was conducted. The diffusion chambers with SSNTD Kodak-Pathe LR-115 type II were exposed to an average ^{222}Rn concentration of 15.2 kBq m^{-3} for 16 days. The reference ^{222}Rn measurements were made with a calibrated radon monitor PRASSI, Model 5S (SILENA, Italy).

After exposure the SSNTDs were etched in 10% NaOH at 60^0 C for 120 min. The tracks were counted visually by a transmitted light microscope. The energy and angular response of the detectors was studied prior to these experiments [25]. Under the etching conditions used, the energy window for registration of alpha particles was 1.6-4.4 MeV and the critical angle (to the normal) was 59^0 – values very close to those obtained by other authors [45, 46]. The experimental C_F obtained for metal and plastic chambers was C_F =0.44 cm (±3.1%) and C_F =0.52 cm (±1.8%), respectively. Theoretical modeling shows that these values of C_F correspond to deposited fraction of ^{218}Po-atoms of 0.93 and 0.84, respectively. For D we considered a "typical" range of values: 0.03 – 0.085 cm^2 s^{-1} [47] with a "typical" mean 0.054 cm^2 s^{-1}. The experimental result for the metal chambers corresponds to the theoretical value (f_1=0.93) for "the mean" value of D = 0.054 cm^2 s^{-1}. The 15% higher C_F measured for plastic chambers corresponds to D<0.02 cm^2 s^{-1}. This could possibly be attributed to electrostatical forces (about 88% of the newly generated ^{218}Po are positive ions [47, 48]). This discrepancy should be addressed in further studies The deviation in C_F when D varies within the 0.03 – 0.085 cm^2 s^{-1} range, does not exceed 10% of the value corresponding to the mean D=0.054 cm^2 s^{-1}. Another source of uncertainty in the C_F might be related to different environmental conditions.

The experimental study suggests that, from methodological point of view, metal chambers are better choice than plastic ones. Therefore, a new experimental study was carried-out to utilize metal diffusion chambers for practical use. The metal diffusion chamber consists of tin can with a tin cap. In some of the cans few holes on the side wall of the chamber were made. The holes were covered with polyethylene foil from the inner side (Fig. II. 6.). In addition to the methodological advantages, the metal diffusion chambers also have advantages from practical point of view:

- They can be used multiple times and could easily be prepared for the next use;

- It is hard to destroy them accidentally during exposure;
- Some SSNTDS, like Kodak Pathe LR-115 type II can be damaged by the sunlight during exposure. Metal chamber keeps the detectors safe from the sunlight.

For the experiment, 11 metal diffusion chambers were constructed. They were of dimensions ∅75/80 mm. Nine of them were with perforated holes on the wall, covered with a diffusion membrane (polyethilenne, polyethilenne + texture). Two of the chambers were without any holes. The scheme of the experimental set-up used for exposure of the chambers is shown in Fig. II.9. The tracks were counted visually, by Nikon Eclipse E200 microscope and automatically, by two dedicated computer codes developed in the Faculty of Physics, University of Sofia [33]. For the visual counting at least 40 fields with equal area were randomly selected for each detector [49, 50]. In Fig II.10. the average track densities for the metal diffusion chambers are given. All chambers (incl. these without holes) give statistically consistent (after t-test) results. The calibration factor C_F obtained is as follows:

- Visual counting: 1.90 ± 0.12 cm^{-2} kBq^{-1} h^{-1} m^3
- Program 1: 1.11 ± 0.07 cm^{-2} kBq^{-1} h^{-1} m^3
- Program 2: 1.14 ± 0.07 cm^{-2} kBq^{-1} h^{-1} m^3

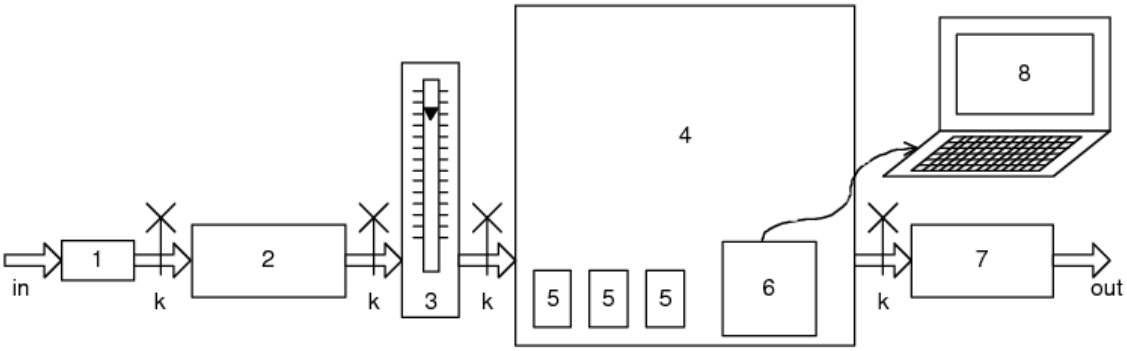

Figure II.9. Calibration set-up for diffusion chambers. Legend: 1 – dryer, 2 – radon source, 3 – rotameter, 5 – hermetic radon box, 5 – diffusion chambers, 6 – reference radonometer AlphaGUARD PQ 2000 PRO, 7 – pump, 8 – computer.

In this experiment plastic chambers were exposed as well. They gave the following average values for C_F:

- Visual counting: 2.41 ± 0.15 cm^{-2} kBq h^{-1} m^3
- Program 1: 1.50 ± 0.09 cm^{-2} kBq^{-1} h^{-1} m^3
- Program 2: 1.55 ± 0.10 cm^{-2} kBq^{-1} h^{-1} m^3

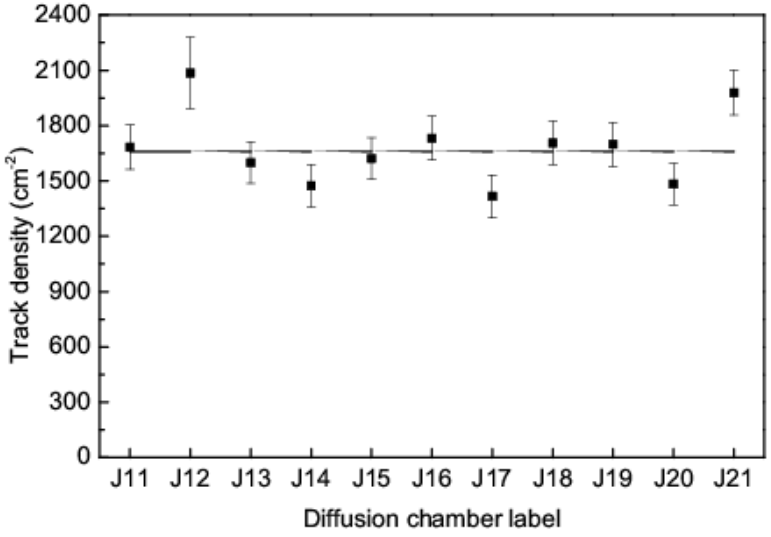

Figure II.10. Net track density obtained by different diffusion chambers (labeled J11 – J21) exposed at the same integrated ^{222}Rn concentration. The chambers J11 and J12 are without holes in the walls.

The "surprising" fact that chambers without holes have the same C_F as those with holes has important implications for the practice. It means that ^{222}Rn gas always finds its way through microscopic gaps along the edge of the cap and piercing holes is actually unnecessary. Therefore, diffusion chambers without holes were chosen for practical use in our work.

One problem discussed in the last few years in the scientific literature concerns the sensitivity of radon (^{222}Rn) detectors to thoron (^{220}Rn). This is an important problem as it appears that many commercial radon detectors are sensitive to thoron and if thoron is present the results for radon can be severely biased [51]. Therefore, in another experiment the sensitivity of the metal chambers (without holes) to thoron was studied. The obtained (after visual track counting) C_F (for thoron) was 0.096 ± 0.012 cm^{-2} kBq^{-1} h^{-1} m^3. Therefore, the thoron sensitivity of these diffusion chambers is only 5% of that to radon and they

rank among radon detectors with low sensitivity to thoron [51]. More details about thoron exposure experiments are given in Chapter VII.

II.3. Analytical model of ^{222}Rn progeny distribution inside a cylindrical diffusion chamber.

As Nikezic and Yu reported in 2004 in their review [35] the problem of uniformity or non-uniformity of deposition of radon progeny inside the chamber "has not been tackled yet". To address and solve this problem, the author proposed an analytical approach to calculate the distribution of ^{222}Rn progeny atoms in diffusion chambers.

II.3.1. General algorithm

The theoretical model is based on the set of equations that describe the molecular diffusion in air of atoms of non-branching decay chain with source activity concentration *a*:

$$\frac{\partial n_1}{\partial t} = D\left(\frac{\partial^2 n_1}{\partial x^2} + \frac{\partial^2 n_1}{\partial y^2} + \frac{\partial^2 n_1}{\partial z^2}\right) - \lambda_1 n_1 + a$$

$$\text{.....} \qquad \text{(II.7)}$$

$$\frac{\partial n_i}{\partial t} = D\left(\frac{\partial^2 n_i}{\partial x^2} + \frac{\partial^2 n_i}{\partial y^2} + \frac{\partial^2 n_i}{\partial z^2}\right) + \lambda_{i-1} n_{i-1} - \lambda_i n_i$$

where *a* is ^{222}Rn activity concentration ($a = \lambda_0 n_0$). Eq. (II.7) is considered with homogeneous initial and boundary conditions: $n_i\big|_{walls} = 0$. In the theoretical model the following assumptions are made:

- *D* is considered the same for all ^{222}Rn progeny isotopes.

- The effect of reflection and recoil of ^{222}Rn progeny atoms from the wall is neglected. Although after the alpha-decay of some 50% of ^{214}Pb atoms recoil back from walls in air, they are re-deposited almost entirely.
- Electric fields in the chamber are not considered.

Let's apply the following linear transformation:

$$\tilde{n}_i = \sum_{j=1}^{3} \Lambda_{ij} n_j , \qquad \text{(II.8)}$$

$$\tilde{a}_i = \Lambda_{i1} a ,$$

where:

$$\Lambda_{ij(i<j)} = 0, \Lambda_{ii} = 1 ,$$

$$\Lambda_{ij(i>j)} = \frac{\prod_{k=j}^{i-1} \lambda_k}{\prod_{l=j}^{i-1} (\lambda_l - \lambda_i)} . \qquad \text{(II.9)}$$

After this transformation is applied, the set of equations (II.7) splits into *k* independent equations:

$$\frac{\partial \tilde{n}_i}{\partial t} = D\left(\frac{\partial^2 \tilde{n}_i}{\partial x^2} + \frac{\partial^2 \tilde{n}_i}{\partial y^2} + \frac{\partial^2 \tilde{n}_i}{\partial z^2} \right) - \lambda_i \tilde{n}_i + \tilde{a}_i , \qquad \text{(II.10)}$$

with homogeneous initial and boundary conditions. The solution of this problem is:

$$\tilde{n}_i(x,y,z,t) = \iiint\limits_{V_{\xi\eta\zeta}} \int\limits_{\tau=0}^{t} \tilde{G}_i(x,y,z,t,\xi,\eta,\zeta,\tau)\tilde{a}_i(\xi,\eta,\zeta,\tau)d\xi d\eta d\zeta d\tau\,, \quad \text{(II.11)}$$

where $\tilde{G}_i$ is the Green function of the problem [52]. Taking into account eqs. (II.8) and (II.9), the solutions for n_i take the form:

$$\begin{aligned} n_i &= \sum_k \Lambda_{ik}^{-1}\Lambda_{k1} \iiint\limits_{V_{\xi\eta\zeta}} \int\limits_{\tau=0}^{t} \tilde{G}_k(x,y,z,t,\xi,\eta,\zeta,\tau)a(\xi,\eta,\zeta,\tau)d\xi d\eta d\zeta d\tau = \\ &= \iiint\limits_{V_{\xi\eta\zeta}} \int\limits_{\tau=0}^{t} G_{i1}(x,y,z,t,\xi,\eta,\zeta,\tau)a(\xi,\eta,\zeta,\tau)d\xi d\eta d\zeta d\tau, \end{aligned} \quad \text{(II.12)}$$

where G_{i1} can be considered as the corresponding element of a "matrix Green function":

$$G_{ij} = \sum_k \Lambda_{ik}^{-1}\tilde{G}_k\Lambda_{kj}\,. \quad \text{(II.13)}$$

The matrix Λ^{-1} is inverse of the matrix Λ. The inverse matrix elements are given by the expression [53]:

$$\Lambda_{ij(i<j)}^{-1} = 0,\ \Lambda_{ii}^{-1} = 1,\ \Lambda_{ij(i>j)}^{-1} = \frac{\prod\limits_{k=j}^{i-1}\lambda_k}{\prod\limits_{l=j+1}^{i}\left(\lambda_l - \lambda_j\right)}. \quad \text{(II.14)}$$

Using eqns (II.13) and (II.14) one can obtain [53]:

$$G_{11} = \tilde{G}_1, G_{i1(i>1)} = \left(\prod_{l=1}^{i-1} \lambda_l \right) \sum_{k=1}^{i} \frac{\tilde{G}_k}{\prod_{m=1, m\neq k}^{i} (\lambda_m - \lambda_k)} . \qquad \text{(II.15)}$$

II. 3. 2. Solutions for a cylindrical chamber

A substantial part of the diffusion chambers used in practice are cylindrical. Therefore, solutions for this case were studied in more detail. Consider finite circular cylinder of radius *R* and height *H*. The cylindrical coordinates *r,z* are used, where *r*=0 coincides with the axis of the cylinder. The coordinates of the circular bottom and top of the cylinder are *z=0* and *z=H*, respectively. The ^{222}Rn activity concentration is considered constant inside the chamber. In cylindrical coordinates, without angular dependence due to the cylindrical symmetry, the problem takes the form:

$$\frac{\partial \tilde{n}_k}{\partial t} = D\left(\left(\frac{\partial^2 \tilde{n}_k}{\partial r^2} + \frac{1}{r} \frac{\partial \tilde{n}_k}{\partial r} \right) + \frac{\partial^2 \tilde{n}_k}{\partial z^2} \right) - \lambda_k \tilde{n}_k + \tilde{a}_k . \qquad \text{(II.16)}$$

The Green function for this problem, constructed by the standard methods [54] is:

$$\tilde{G}_k = \frac{2}{\pi H R^2} \sum_{n=1}^{\infty} \sum_{m=1}^{\infty} \frac{J_0\left(\frac{\kappa_m}{R} r\right) J_0\left(\frac{\kappa_m}{R} \rho\right)}{J_1^2(\kappa_m)} \sin\left(\frac{n\pi}{H} z\right) \sin\left(\frac{n\pi}{H} \zeta\right) \exp\left(-\lambda_{nm}^k (t-\tau)\right) \qquad \text{(II.17)}$$

where J_0 and J_1 are the Bessel functions of zero and first order [55], κ_m are zeros of J_0 and the constants $\lambda_{nm}^{(k)}$ are given by the expression:

$$\lambda_{nm}^{(k)} = \lambda_k + D\left(\left(\frac{\kappa_m}{R}\right)^2 + \left(\frac{n\pi}{H}\right)^2\right). \qquad \text{(II.18)}$$

Using eqns (II.12, II.15 and II.17), the following solutions for the volume concentrations can be obtained:

$$n_1(r,z,t) = \frac{8a}{\pi}\sum_{n=0}^{\infty}\sum_{m=1}^{\infty}\frac{J_0\left(\frac{\kappa_m}{R}r\right)}{\kappa_m J_1(\kappa_m)}\sin\left(\frac{(2n+1)\pi}{H}z\right)\times\frac{1-\exp\left(-\lambda_{2n+1,m}^{(1)}t\right)}{(2n+1)\lambda_{2n+1,m}^{(1)}} \qquad \text{(II.19)}$$

$$n_{i(i>1)}(r,z,t) = \frac{8a}{\pi}\left(\prod_{q=1}^{i-1}\lambda_q\right)\sum_{k=1}^{i}\ \sum_{n=0}^{\infty}\sum_{m=1}^{\infty}\frac{J_0\left(\frac{\kappa_m}{R}r\right)}{\kappa_m J_1(\kappa_m)}\sin\left(\frac{(2n+1)\pi}{H}z\right)\times\frac{1-\exp\left(-\lambda_{2n+1,m}^{(k)}t\right)}{(2n+1)\lambda_{2n+1,m}^{(k)}\prod_{j=1,\,j\neq k}^{i}\left(\lambda_j-\lambda_k\right)}$$

For the particular case of the ^{222}Rn progeny chain the expressions for the activity concentrations C_{Ai} ($C_{Ai} = \lambda_i n_i$) of ^{218}Po, ^{214}Pb and ^{214}Bi in the inside air volume of the chamber are:

$$C_{A1}(r,z,t) = \frac{8a\lambda_1}{\pi}\sum_{n=0}^{\infty}\sum_{m=1}^{\infty}\frac{J_0\left(\frac{\kappa_m}{R}r\right)}{\kappa_m J_1(\kappa_m)}\sin\left(\frac{(2n+1)\pi}{H}z\right)\times\frac{1-\exp\left(-\lambda_{2n+1,m}^{(1)}t\right)}{(2n+1)\lambda_{2n+1,m}^{(1)}} \qquad \text{(II.20)}$$

$$C_{Ai(i>1)}(r,z,t)=\frac{8a}{\pi}\left(\prod_{q=1}^{i}\lambda_q\right)\sum_{k=1}^{i}\sum_{n=0}^{\infty}\sum_{m=1}^{\infty}\frac{J_0\left(\frac{\kappa_m}{R}r\right)}{\kappa_m J_1(\kappa_m)}\sin\left(\frac{(2n+1)\pi}{H}z\right)\times\frac{1-\exp\left(-\lambda_{2n+1,m}^{(k)}t\right)}{(2n+1)\lambda_{2n+1,m}^{(k)}\prod_{j=1,\,j\neq k}^{i}\left(\lambda_j-\lambda_k\right)}$$

II.3.3. Modeling volume fractions, equilibrium surface activities and sensitivity

Inside the chamber the ^{222}Rn progeny atoms are distributed partly in the air space of the cavity and partly on the internal surface of the walls. The activity concentrations in the air space of the cylindrical diffusion chamber are given by eqn (II.20). The activity concentrations under radioactive equilibrium are obtained when $t \to \infty$. The equilibrium fraction of the i-th nuclide that is in the air volume is:

$$f_i=\frac{\int_V \lambda_i n_i dV}{aV}=\frac{\int_V C_{Ai}dV}{aV}. \qquad \text{(II.21)}$$

Using (II.20) with $t \to \infty$, the following formula can be obtained [53]:

$$f_i=\frac{32}{\pi^2}\left(\prod_{q=1}^{i}\lambda_q\right)\sum_{k=1}^{i}\sum_{n=0}^{\infty}\sum_{m=1}^{\infty}\frac{1}{(2n+1)^2\kappa_m^2\lambda_{2n+1,m}^{(k)}\prod_{j=1,\,j\neq k}^{i}\left(\lambda_j-\lambda_k\right)}. \qquad \text{(II.22)}$$

The set of equations that describe the atoms deposition on the surface is:

$$\frac{dn_{S1}}{dt} = \Phi_{S1} - \lambda_1 n_{S1}$$
$$\text{.....} \qquad \text{(II.23)}$$
$$\frac{dn_{Si}}{dt} = \Phi_{Si} + \lambda_{i-1} n_{Si-1} - \lambda_i n_{Si}$$

where Φ_{Si} is the i-th atoms flux to the surface. According to the Fick's law, the flux is given by:

$$\Phi_{Si} = -D\frac{\partial n_i}{\partial \nu_S}, \qquad \text{(II.24)}$$

where $\partial n_i / \partial \nu_S$ is the directional derivative by the normal to the surface. For the case of cylinder:

$$\Phi_{Si}(\text{bottom}) = \Phi_{Si}(z=0) = D\left(\frac{\partial n_i}{\partial z}\right)_{z=0}$$
$$\Phi_{Si}(\text{top}) = \Phi_{Si}(z=H) = -D\left(\frac{\partial n_i}{\partial z}\right)_{z=H} \qquad \text{(II.25)}$$
$$\Phi_{Si}(\text{sidewall}) = \Phi_{\text{Si}}(r=R) = -D\left(\frac{\partial n_i}{\partial r}\right)_{r=R}$$

After the calculations are made, the following equilibrium surface activities are obtained:

- On the side-wall ($r=R$):

$$A_{Si} = \frac{8Da}{\pi R}\sum_{n=0}^{\infty}\sum_{m=1}^{\infty}\frac{1}{(2n+1)}\sin\left(\frac{(2n+1)\pi}{H}z\right)Q_{nm}^{(i)}. \qquad \text{(II.26)}$$

- On the bottom ($z=0$) and on the top ($z=H$):

$$A_{Si} = \frac{8Da}{H} \sum_{n=0}^{\infty} \sum_{m=1}^{\infty} \frac{1}{\kappa_m J_1(\kappa_m)} J_0\left(\frac{\kappa_m}{R} R\right) Q_{nm}^{(i)}. \qquad \text{(II.27)}$$

where:

$$Q_{nm}^{(1)} = \frac{1}{\lambda_{2n+1,m}^{(1)}}$$

$$Q_{nm}^{(2)} = Q_{nm}^{(1)} + \frac{\lambda_1}{\lambda_{2n+1,m}^{(1)}(\lambda_2 - \lambda_1)} + \frac{\lambda_1}{\lambda_{2n+1,m}^{(2)}(\lambda_1 - \lambda_2)}$$

$$Q_{nm}^{(3)} = Q_{nm}^{(2)} + \frac{\lambda_1\lambda_2}{\lambda_{2n+1,m}^{(1)}(\lambda_2 - \lambda_1)(\lambda_3 - \lambda_1)} + \frac{\lambda_1\lambda_2}{\lambda_{2n+1,m}^{(2)}(\lambda_1 - \lambda_2)(\lambda_3 - \lambda_2)} + \frac{\lambda_1\lambda_2}{\lambda_{2n+1,m}^{(3)}(\lambda_1 - \lambda_3)(\lambda_2 - \lambda_3)}$$

(II.28)

The diffusion coefficient of ^{222}Rn progeny in air can vary, depending on humidity, trace gases etc. [56]. First application of the proposed model was to study the dependence of the volume fractions f_i and sensitivity on the diffusion coefficient. In the theory of diffusion chambers the term "sensitivity" usually refers to C_F expressed in units of length (e.g. cm). The modeling was done for a cylindrical diffusion chamber of R=4 cm and H=7.5 cm. The sensitivity data used [26, 44] is for this chamber with SSNTD Kodak-Pathe LR-115/II. The considered interval for D is 0.005 – 0.1 cm^2 s^{-1}. This interval covers the range of D for unattached ^{222}Rn progeny in air [56].

The results for volume fractions f_i (deposited fraction = 1-f_i) are shown in Fig. II.11. The agreement between the present analytical approach and numerical

modeling (described in II.2.3.) was within 1%. The volume fraction of ^{218}Po (f_1) varies within 4-40% over the studied range of D, while f_2<5% and f_3<1% so ^{214}Bi (+^{214}Po) atoms are practically fully deposited. The sensitivity depends on f_i. Because these fractions depend on D, the dependence of sensitivity on D can be obtained. This dependence is shown in Fig. II.12. To obtain it, the results from the numerical modeling of the dependence of sensitivity on the deposited fraction of ^{222}Rn progeny [26, 44] were combined with the present results, illustrated in Fig. II.11. The influence of D for the studied chamber is more pronounced for D<0.04 $cm^2\ s^{-1}$.

Up to now, the experimental studies on the deposited fraction of ^{222}Rn progeny in diffusion chambers are scarce. Koo et al. [57, 58] reported f_1=0.4 for chambers made of different materials and of different size, including with size that is close to the modeled here. The experimental sensitivity obtained in Ref. [43] for metal diffusion chambers corresponds to volume fraction of ^{218}Po of 0.07. According to the present modeling, the result of Koo et al. [57, 58] corresponds to D of about 5.10^{-3} $cm^2\ s^{-1}$, while our result of Ref. [44] corresponds to an order of magnitude higher coefficient of diffusion. The data are not sufficient to speculate on this difference. For instance presence of aerosol particles in the chamber volume can change the behavior of ^{222}Rn progeny. Some of the atoms will attach to slowly diffusing aerosols, resulting in volume fraction that can be substantially higher than that in case of entirely unattached ^{222}Rn progeny.

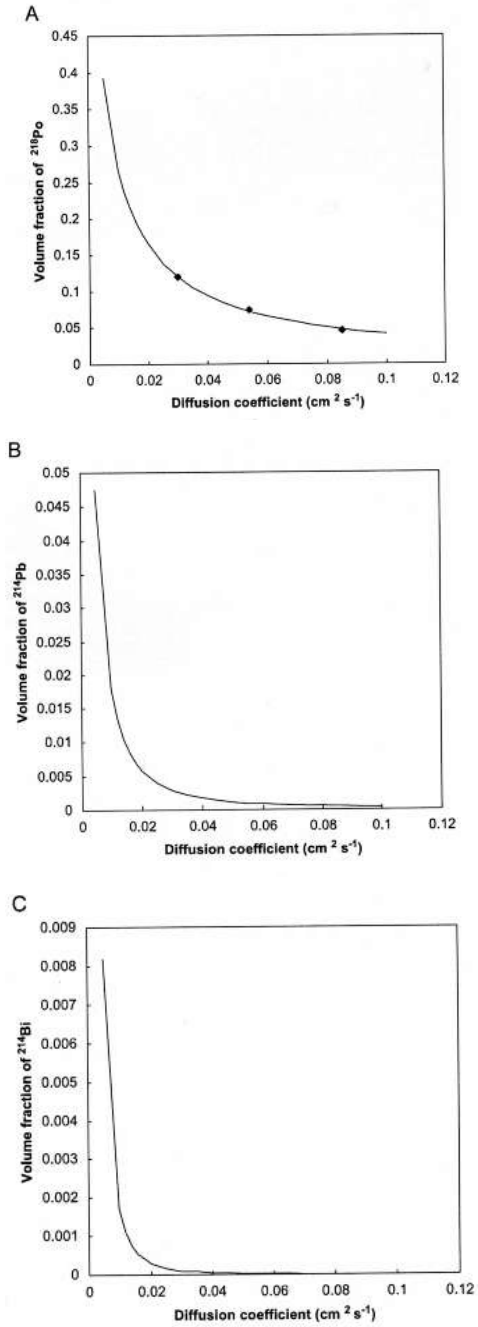

Figure II. 11. Dependence of the volume fractions of (A) ^{218}Po, (B) ^{214}Pb and (C) ^{214}Bi in the air inside a diffusion chamber on the diffusion coefficient of ^{222}Rn progeny in air. The lines are obtained by analytical solution and the points in A represent the results from a numerical simulation of the same chamber [44].

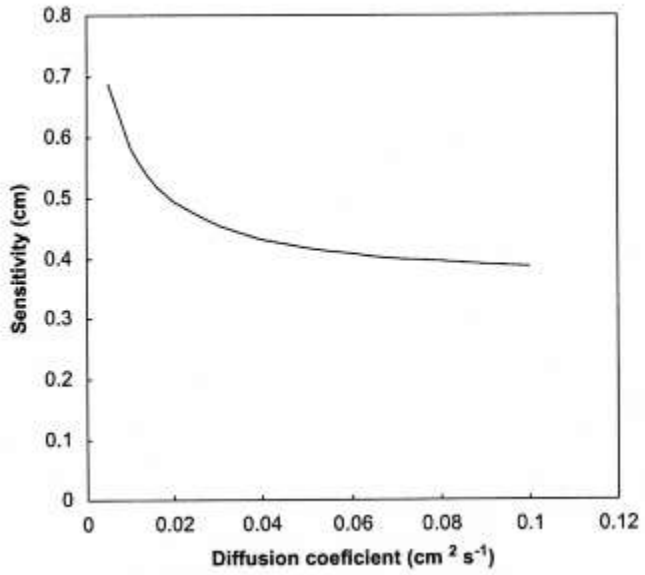

Figure II. 12. Dependence of the sensitivity of the cylindrical diffusion chamber of radius 4 cm and height 7.5 cm on the diffusion coefficient of ^{222}Rn progeny in air.

II.4. Diffusion chambers designed for radon in soil-gas.

Diffusion chambers with SSNTDs have also been used for soil-gas ^{222}Rn measurements. The principal limitation related to the usage of SSNTDs is the saturation effect observed at high concentrations. This can be avoided by reducing the exposure time. However, such a decision relies on preliminary information that the concentrations are high. On the other hand, short term measurements made at depths < 1 m are affected by the peculiar meteorological conditions during the exposure.

In the field work in areas affected by the uranium industry in Bulgaria we faced the problem to measure soil gas ^{222}Rn concentrations in wide range: from kBq m^{-3} to MBq m^{-3}. For concentrations > 0.5 MBq m^{-3} the SSNTD saturation is observed for less than two weeks of exposure. To overcome this problem, we

have proposed the approach to place both SSNTDs and thermoluminescent detectors (TLDs) inside the chamber.

Our arrangement employs a chamber with a SSNTD of Kodak-Pathe LR-115/II placed inside, together with two sets of dosimetrically thin TLDs (Fig. II.13.). One set of TLDs is open and the other one is covered with a 20 mg cm^{-2} plastic absorber. The used TLDs are ∅5 mm dishes filled with $CaSO_4$:Dy + B_4C. The B_4C admixture reduces the penetration of light through the TL material and makes the TLDs "surface sensitive" (or "dosimetrically thin", as they are usually called [59, 60]). As a result, the beta and gamma sensitivity is reduced significantly and TLDs become useful for registration of alpha particles. To subtract the small signal due to the gamma background, the differences between the signals from open and covered detectors are ascribed to ^{222}Rn. An advantage of the used TL material is its low fading – about 5% per six months [60]. The SSNTDs were etched at 10% NaOH at 60^0 C for 120 min. Calibration was made in a 2 m^3 radon box at the National Centre of Metrology, Bulgaria, at an average ^{222}Rn concentration of about $2.4x10^4$ Bq m^{-3}.

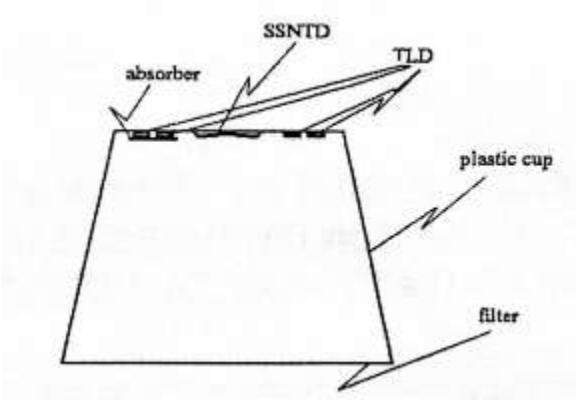

Figure II.13. A scheme of a diffusion chamber with TLDs and a SSNTD placed inside.

Measurements by this “soil-gas chambers” were made in areas contaminated by the uranium industry in Bulgaria [61]. The results obtained by SSNTDs are plotted against those obtained by TLDs in Fig. II.14. As seen, at high concentrations the linear correlation is frustrated due to the overlap of etched tracks (saturation effect). The advantage of using TLDs is to be able to assess concentrations above the range in which quantitative information could be derived by SSNTDs. As a result, the range of measurable concentrations is substantially expanded. For instance, for one month exposure time this range is from 100 Bq m^{-3} (SSNTD) up to 100 MBq m^{-3} (TLD). The upper limit is increased by more than two orders of magnitude compared to chambers with SSNTDs only . This type of soil-gas diffusion chambers were used in a radiological expertise about the environmental impact of the uranium mining and milling industry in Bulgaria [24].

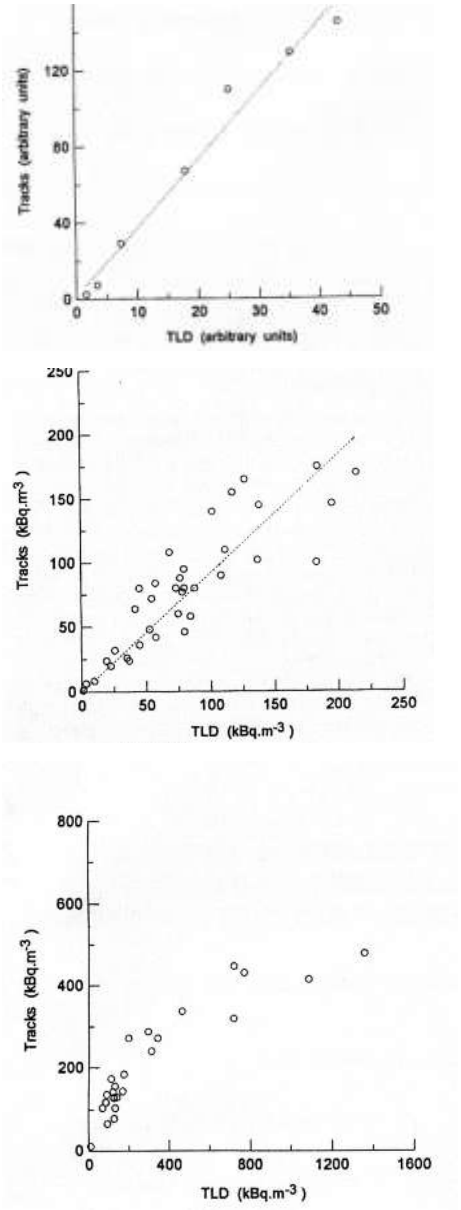

Figure II. 14. A laboratory comparison between TLD and SSNTD signal (top). Comparison between concentrations measured under real conditions by SSNTD and TLD at low/medium (middle) and high (bottom) concentrations.

III. MEASUREMENTS OF ^{222}Rn PROGENY AND ^{220}Rn PROGENY

The short-lived ^{222}Rn progeny (^{218}Po, ^{214}Pb and ^{214}Bi+^{214}Po) was identified in 1951 as the factor that contributes to the major part of the lung dose [12]. Since then lots of methods dealing with their measurements have been published [62-67]. Later, an attention was also given to measurement of ^{220}Rn progeny (the isotopes ^{212}Pb and ^{212}Bi+^{212}Po/^{208}Tl) [68]. Radon and thoron progeny atoms in the air originate from the parents: ^{222}Rn and ^{220}Rn and exist in two fractions [69, 70]:

- "Unattached" fraction of nanometric clusters. Their diameter is usually in the range 2-15 nm;
- Attached to aerosol fraction. Their diameter ranges between 40-400 nm.

The deposition pattern in the bronchial three and the relative importance for the dose of these two fractions is different. A number of methods for the differential measurements of the two fractions have been developed. Mostly, the methods employ the difference in their diffusion characteristics [71]. The review of these methods is out of the scope of this thesis.

In this chapter we focus on the following research problems :

- Development of a generalized algorithm for data processing of grab-sampling measurement of ^{222}Rn progeny and ^{220}Rn progeny;
- Design of short lived alpha-sources of energy 6.0 MeV and 7.69 MeV suitable for calibration of ^{222}Rn progeny detectors;
- Development of a method for integrated measurements of ^{222}Rn progeny and ^{220}Rn progeny, suitable for

measurements of the individual isotopes at environmental concentrations. Test of the method under laboratory and real conditions.

III.1. General mathematical algorithm for data processing of grab sampling measurements of ^{222}Rn and ^{220}Rn decay products.

The methods for measurement of ^{222}Rn and ^{220}Rn progeny concentrations in air include air sampling on aerosol filter and counting (in most cases α-counting) measurements of the filter in different time intervals [62-68]. If α-spectrometry is applied, the α-counting is made in different energy regions (or ROI – "regions of interest"). The "aerosol" radioactivity in the ambient air consists of the following components:

- ^{222}Rn short-lived progeny. Usually this component dominates in the total α-activity concentration [18];
- ^{220}Rn progeny. This component usually is much smaller than that related to ^{222}Rn and can dominate only in some peculiar cases;
- Long-lived radioactive aerosols. These can be both natural (e.g. ^{210}Pb, ^{210}Po etc.) and manmade. As a whole, the activity concentration of this component is orders of magnitude lower than that of the first two components [18]. Therefore, the third component will be ignored in the next considerations.

The equations, expressing the growth and decay of ^{222}Rn and ^{220}Rn progeny on the filter are:

$$\frac{dN_1}{dt} = \eta Q n_1 \Theta(T-t) - \lambda_1 N_1;$$
$$\frac{dN_2}{dt} = \eta Q n_2 \Theta(T-t) + \lambda_1 N_1 - \lambda_2 N_2;$$
$$\frac{dN_3}{dt} = \eta Q n_3 \Theta(T-t) + \lambda_2 N_2 - \lambda_3 N_3. \qquad \text{(III.1)}$$

$$\frac{dN_4}{dt} = \eta Q n_4 \Theta(T-t) - \lambda_4 N_4;$$
$$\frac{dN_5}{dt} = \eta Q n_5 \Theta(T-t) + \lambda_4 N_4 - \lambda_5 N_5.$$

where the first term at the right hand of (III.1) describes sampling (from $t = 0$ to $t = T$) and Θ is the Heaviside function ($\Theta(x \geq 0) = 1$, $\Theta(x < 0) = 0$), η is collection efficiency of the filter, Q is the air flow-rate, N_i is the number of the atoms on the filter and n_i are the atom concentrations in the air. The indices refer to : i=1 (^{218}Po), 2 (^{214}Pb), 3 (^{214}Bi), 4 (^{212}Pb) and 5 (^{212}Bi). In ^{220}Rn progeny measurements the first decay product after ^{220}Rn (^{216}Po) is usually ignored due to its short half-life (0.15 s).

Further, the general Bateman solution for the radioactive decay chains [72, 73] are adopted for the considered problem [74, 75]. If one substitutes:

$$\tilde{N}_1 = N_1;$$
$$\tilde{N}_2 = \frac{\lambda_1}{\lambda_1 - \lambda_2} N_1 + N_2;$$
$$\tilde{N}_3 = \frac{\lambda_1 \lambda_2}{(\lambda_1 - \lambda_3)(\lambda_2 - \lambda_3)} N_1 + \frac{\lambda_2}{\lambda_2 - \lambda_3} N_2 + N_3. \qquad \text{(III.2)}$$
$$\tilde{N}_4 = N_4;$$
$$\tilde{N}_5 = \frac{\lambda_4}{\lambda_4 - \lambda_5} N_4 + N_5.$$

Then, the variables $\tilde{N}_i$ satisfy the independent equations:

$$\frac{d\tilde{N}_i}{dt} = \eta Q \tilde{n}_i \Theta(T-t) - \lambda_i \tilde{N}_i \,, \qquad \text{(III.3)}$$

The relations between $\tilde{n}$ and n is the same as between $\tilde{N}$ and N. The solutions with zero initial conditions are:

$$\tilde{N}_i(t) = \frac{\eta Q \tilde{n}_i}{\lambda_i} f_i(t) \,, \qquad \text{(III.4)}$$

where:

$$f_i(t) = \left(1 - \exp\left(-\lambda_i t\right)\right)\Theta\left(T-t\right) + \left(\exp\left(\lambda_i T\right) - 1\right)\exp\left(-\lambda_i t\right)\Theta\left(t-T\right). \qquad \text{(III.5)}$$

If the background is ignored (which is reasonable for α-counting, in most cases) the counting rate $\dot{C}(t)$ at the moment t can be expressed as:

$$\dot{C}(t) = \sum_{i=1}^{5} \varepsilon_i \lambda_i N_i(t) = \sum_{i=1}^{5} x_i f_i(t) \,, \qquad \text{(III.6)}$$

where ε_i is the detection efficiency for the detected radiation that originates from the i-th nuclide. $f_i(t)$ are the functions given by eqn. (III.5) and the parameters x_i are linearly dependent on the activity concentrations C_{Ai} ($C_{Ai} = \lambda_i n_i$):

$$x_i = \sum_{j=1}^{5} R_{ij} C_{Aj} \,, \qquad \text{(III.7)}$$

where R_{ij} are the elements of the matrix:

$$R = \begin{pmatrix} {}_r R & 0 \\ 0 & {}_t R \end{pmatrix}, \text{where:}$$

$${}_r R = \eta Q \begin{pmatrix} \frac{1}{\lambda_1}\left(\varepsilon_1 - \frac{\lambda_2}{(\lambda_1-\lambda_2)}\varepsilon_2 + \frac{\lambda_2\lambda_3}{(\lambda_1-\lambda_2)(\lambda_1-\lambda_3)}\varepsilon_3\right) & 0 & 0 \\ \frac{1}{(\lambda_1-\lambda_2)}\varepsilon_2 - \frac{\lambda_3}{(\lambda_1-\lambda_2)(\lambda_2-\lambda_3)}\varepsilon_3 & \frac{1}{\lambda_2}\left(\varepsilon_2 - \frac{\lambda_3}{(\lambda_2-\lambda_3)}\varepsilon_3\right) & 0 \\ \frac{\lambda_2}{(\lambda_1-\lambda_3)(\lambda_2-\lambda_3)}\varepsilon_3 & \frac{1}{(\lambda_2-\lambda_3)}\varepsilon_3 & \frac{1}{\lambda_3}\varepsilon_3 \end{pmatrix}$$

$${}_t R = \eta Q \begin{pmatrix} \frac{1}{\lambda_4}\left(\varepsilon_4 - \frac{\lambda_5}{(\lambda_4-\lambda_5)}\varepsilon_5\right) & 0 \\ \frac{1}{(\lambda_4-\lambda_5)}\varepsilon_5 & \frac{1}{\lambda_5}\varepsilon_5 \end{pmatrix}$$

(III.8)

The matrix R may be considered as a direct sum of two matrixes: ${}_rR$ – 3x3 matrix (${}_rR_{ij}=R_{ij}$ when i≤3, j≤3) and ${}_tR$ – 2x2 matrix (${}_tR_{ij} = R_{ij}$ when i=4,5 and j=4,5) i. e. $R={}_rR\oplus {}_tR$. It should be noted that, in some cases, R can be singular. However, if both inverse matrices ${}_rR^{-1}$ and ${}_tR^{-1}$ exist, then:

$$R^{-1}={}_rR^{-1}\oplus {}_tR^{-1} \qquad \text{(III.9)}$$

The components of the inverse matrix, if it exists, are:

$$R^{-1}=\begin{pmatrix} {}_rR^{-1} & 0 \\ 0 & {}_tR^{-1} \end{pmatrix}, \text{ where}$$

$$ {}_rR^{-1}=\frac{1}{\eta Q}\begin{pmatrix} \dfrac{\lambda_1(\lambda_1-\lambda_2)(\lambda_1-\lambda_3)}{\varepsilon_1(\lambda_1-\lambda_2)(\lambda_1-\lambda_3)-\varepsilon_2\lambda_2(\lambda_1-\lambda_3)+\varepsilon_3\lambda_2\lambda_3} & 0 & 0 \\ \dfrac{-\lambda_1\lambda_2(\lambda_1-\lambda_3)}{\varepsilon_1(\lambda_1-\lambda_2)(\lambda_1-\lambda_3)-\varepsilon_2\lambda_2(\lambda_1-\lambda_3)+\varepsilon_3\lambda_2\lambda_3} & \dfrac{\lambda_2(\lambda_2-\lambda_3)}{\varepsilon_2(\lambda_2-\lambda_3)-\varepsilon_3\lambda_3} & 0 \\ \dfrac{\lambda_1\lambda_2\lambda_3}{\varepsilon_1(\lambda_1-\lambda_2)(\lambda_1-\lambda_3)-\varepsilon_2\lambda_2(\lambda_1-\lambda_3)+\varepsilon_3\lambda_2\lambda_3} & \dfrac{-\lambda_2\lambda_3}{\varepsilon_2(\lambda_2-\lambda_3)-\varepsilon_3\lambda_3} & \dfrac{\lambda_3}{\varepsilon_3} \end{pmatrix}$$

$$ {}_tR^{-1}=\frac{1}{\eta Q}\begin{pmatrix} \dfrac{\lambda_4(\lambda_4-\lambda_5)}{\varepsilon_4(\lambda_4-\lambda_5)-\varepsilon_5\lambda_5} & 0 \\ \dfrac{-\lambda_4\lambda_5}{\varepsilon_4(\lambda_4-\lambda_5)-\varepsilon_5\lambda_5} & \dfrac{\lambda_5}{\varepsilon_5} \end{pmatrix}$$

(III.10)

The counts obtained during the k-th measuring interval, that starts at $t_k^{(1)}$ and ends at $t_k^{(2)}$ can be expressed as:

$$C_k=\int_{t_k^{(1)}}^{t_k^{(2)}}\dot{C}(t)dt=\sum_{j=1}^{5}H_{kj}x_j\,, \qquad \text{(III.11)}$$

where:

$$H_{kj} = \int_{t_k^{(1)}}^{t_k^{(2)}} f_j(t)dt. \qquad \text{(III.11')}$$

The formulas (III.4 – III.11) can be incorporated in data processing of practically all counting methods for ^{222}Rn progeny and/or ^{220}Rn progeny measurements. This will be demonstrated for the case of α-counting methods for ^{222}Rn progeny measurement.

III.1.1. Applications for α-counting methods for ^{222}Rn progeny

In most situations in the reality the activity concentration of ^{222}Rn progeny is one – two (or more) orders of magnitude higher than that of ^{220}Rn progeny [14]. Therefore, in many cases in the environment and working places ^{220}Rn progeny can be ignored as being of secondary importance and methods estimate only C_{A1}, C_{A2} and C_{A3}. Some caution is needed, however, to verify whether this assumption is reasonable and the results for ^{222}Rn progeny are not biased because of significant presence of ^{220}Rn progeny.

III.1.1.1. Gross alpha-counting methods.

The most popular methods used in practice employ air sampling through a filter and gross α-counting of the filter in three different time intervals [e.g. 62, 63]. In the case of alpha counting $\varepsilon_2 = 0$. In addition, usually equal counting efficiency ($\varepsilon_1 = \varepsilon_3 = \varepsilon$) is assumed for 6.0 MeV and 7.69 MeV, but this assumption should be considered as conditional [76]. In case of counting in three time intervals the parameters x_i can be obtained by the expressions that follow from eqn. (III.11):

$$x_i = \sum_{j=1}^{3} H_{ij}^{-1} C_j \,, \qquad \text{(III.12)}$$

where H^{-1} is the inverse of H matrix. Respectively, C_{Ai} can be obtained as follows:

$$C_{Ai} = \sum_{j=1}^{3} {}_r R_{ij}^{-1} x_j = \sum_{j=1}^{3}\sum_{k=1}^{3} {}_r R_{ij}^{-1} H_{jk}^{-1} C_k \ . \qquad \text{(III. 13)}$$

The uncertainty in C_{Ai}, due to the counting statistics is given by the expression [74]:

$$u(C_{Ai}) = \left[\sum_{k=1}^{3}\sum_{l=1}^{3} {}_r R_{ik}^{-1} {}_r R_{il}^{-1} Cov(x_k, x_l) \right]^{1/2} . \qquad \text{(III.14)}$$

The covariance between x_k and x_l with Poisson statistics of the registered counts and counting in different, not overlapping intervals is:

$$Cov(x_k, x_l) = \sum_{m=1}^{3} H_{km}^{-1} H_{lm}^{-1} C_m \ . \qquad \text{(III. 15)}$$

That is, the resultant expression for the uncertainty due to the counting statistics is:

$$u(C_{Ai}) = \left(\sum_{k=1}^{3}\sum_{l=1}^{3}\sum_{m=1}^{3} {}_r R_{ik}^{-1} {}_r R_{il}^{-1} H_{km}^{-1} H_{lm}^{-1} C_m \right)^{1/2} . \qquad \text{(III.16)}$$

Other α-counting methods employ measurements in more than 3 intervals [65]. In these methods x_i parameters are estimated through the weighted least squares method. They are found as solutions of the equations [74, 75]:

$$\sum_{j=1}^{3}\left(\sum_{k=1}^{n}\frac{H_{ki}H_{kj}}{C_k}\right)x_j=\sum_{k=1}^{n}H_{ki}\,. \qquad \text{(III.17)}$$

Respectively: $Cov(x_i,x_j)=K_{ij}^{-1}$, where K^{-1} is the inverse matrix of the matrix with elements:

$$K_{ij}=\sum_{k}\frac{H_{ki}H_{kj}}{C_k}. \qquad \text{(III.18)}$$

After that C_{Ai} and $u(C_{Ai})$ can be calculated by eqns (III.13) and (III.14).

III.1.1.2. Alpha spectrometric methods for ^{222}Rn progeny

In these methods counting is performed in two spectral ROI: The ROI around 6.0 MeV is that of alpha particles of ^{218}Po and the ROI around 7.69 MeV of ^{214}Po alphas. In the first channel only $\varepsilon_1 \neq 0$, while in the second $\varepsilon_3 \neq 0$. If counting is in a vacuum chamber $\varepsilon_1 = \varepsilon_3$ = geometry efficiency. Only the matrix ${}_rR^{(2)}$, corresponding to the second channel, is regular. The alpha counts in the k-th channel registered in the i-th counting interval are:

$$C_i^{(k)}=\sum_{j=1}^{3}H_{ij}^{(k)}x_j^{(k)}\,. \qquad \text{(III.19)}$$

Where i=1,2…n (n ≥ 3), k=1,2. The index "i" starts with counting intervals in 6.0 MeV ROI and continues with these at 7.69 MeV ROI. It is different for the different time intervals as well as for identical intervals, but corresponding to different channels. It is helpful to substitute:

$$H_{ij}=\sum_{l=1}^{3}\sum_{v=1}^{3}H_{il}^{(k)}\,{}_rR_{lv}^{(k)}\,{}_rR_{vj}^{(2)-1}\,. \qquad \text{(III.20)}$$

If now the substitutions $C_i = C_i^{(k)}$ and $x_j = x_j^{(2)}$ are used, then eqn. (III.19) takes the form analogous to (III.11). The expressions for C_{Ai} and their counting uncertainty are analogous to eqns. (III.13) and (III.14) provided that ${}_rR^{(2)-1}$ is used instead ${}_rR^{-1}$.

III.1.1.3. Numerical solutions and practical implementation

The described algorithm encompasses practically all of the counting methods in which the problem is determined – i.e. in which the number of counting intervals is equal or greater than the number of the unknown concentrations that should be determined. In the case of ^{222}Rn progeny measurements this number is 3. When all ^{222}Rn and ^{220}Rn progenies are to be determined this number is 5. We will illustrate the approach numerically using as example the 3-interval gross alpha counting method of Kritidis et al. [67]. The method is only for ^{222}Rn progeny measurements and uses the following times of sampling/counting:

- Air sampling on a filter: 7 min (or T=7 min);
- First interval gross alpha counting: 30 s – 4 min after the end of sampling (that is $t_1^{(1)}$ = T+30 s = 7.5 min, resp $t_1^{(2)}$ = 11 min);
- Second interval: 5 – 24 min after the end of sampling;
- Third interval: 25 – 40 min after the end of sampling;

In this method (as in most of the other gross alpha counting methods) the efficiency is assumed to be equal for 6.0 MeV and 7.69 MeV alpha particles, i. e. $\varepsilon_1 = \varepsilon_2 = \varepsilon$. For the timing specified above and using standard numerical values for decay constants [77] one obtains:

$$H = \int_{t_k^{(1)}}^{t_k^{(2)}} f_j(t)dt = \begin{pmatrix} 102.9407 & 32.8178 & 42.0317 \\ 66.6017 & 131.0475 & 151.5723 \\ 0.6936 & 64.7099 & 63.4981 \end{pmatrix}. \qquad \text{(III.21)}$$

The unit of the matrix elements in H is (s). Respectively, the inverse matrix (units s^{-1}):

$$H^{-1} = \begin{pmatrix} 0.013386 & -0.005726 & 0.004806 \\ 0.037126 & -0.058583 & 0.11526 \\ -0.03798 & 0.05976 & -0.101768 \end{pmatrix}. \qquad \text{(III.22)}$$

The matrix R numerically is:

$$R = \eta Q \varepsilon \begin{pmatrix} 270.1995 & 0 & 0 \\ 1157.5902 & 9013.626 & 0 \\ -899.6672 & -6693.44 & 1722.9496 \end{pmatrix}. \qquad \text{(III.23)}$$

Respectively:

$$R^{-1} = \frac{1}{\eta Q \varepsilon} \begin{pmatrix} 3.70097 \times 10^{-3} & 0 & 0 \\ -4.7530 \times 10^{-4} & 1.10943 \times 10^{-4} & 0 \\ 8.60308 \times 10^{-5} & 4.31 \times 10^{-4} & 5.804 \times 10^{-4} \end{pmatrix}. \qquad \text{(III.24)}$$

The numbers inside the brackets of the matrix of *R* are in units (s*)* and that of R^{-1} are (s^{-1}). Respectively, the activity concentrations are obtained through eqn. (III.13) or in matrix form:

$$\begin{pmatrix} C_{A1} \\ C_{A2} \\ C_{A3} \end{pmatrix} = \frac{1}{\eta Q \varepsilon} \begin{pmatrix} 4.9542 \times 10^{-5} & -2.1190 \times 10^{-5} & 1.7788 \times 10^{-5} \\ -2.2437 \times 10^{-6} & -3.7780 \times 10^{-6} & 1.0503 \times 10^{-5} \\ -4.8910 \times 10^{-6} & 8.9449 \times 10^{-6} & -8.9737 \times 10^{-6} \end{pmatrix} \begin{pmatrix} C_1 \\ C_2 \\ C_3 \end{pmatrix}. \qquad \text{(III.25)}$$

In the above expression, if the flow rate Q is in units (m^3 s^{-1}) then the activity concentrations are obtained in Bq m^{-3}. In the original paper that describes the method [67] the flow rate is in L/min and the activity concentration in pCi/L. To obtain the numerical coefficients given in the original paper [67], the numbers in the 3x3 matrix in (III.25) should be multiplied by 1621.62 (= 60000/37).

We should also comment the methods in which gross counting is made in less than 3 intervals. Those that employ counting in one interval are usually methods for determination of the potential alpha energy concentration (PAEC – see the Glossary in Annex I) and will not be considered here. From two-interval counting methods the one most popular in Bulgaria was that of Markov et al. [63]. In the modified version of this method, described in [78] the three ^{222}Rn progeny activities are determined by counting in two intervals: 1-4 and 7-10 min after the end of sampling, which lasts 5 min. Re-calculated in SI units, the calculation in matrix form is:

$$\begin{pmatrix} C_{A1} \\ C_{A2} \\ C_{A3} \end{pmatrix} = \frac{1}{\eta Q \varepsilon} \begin{pmatrix} 7.2767\times10^{-5} & -7.2767\times10^{-5} \\ 0 & 1.85\times10^{-5} \\ -1.5047\times10^{-5} & 3.6815\times10^{-5} \end{pmatrix} \begin{pmatrix} C_1 \\ C_2 \end{pmatrix}, \qquad \text{(III.26)}$$

where Q is in (m^3 s^{-1}). However, this and other methods of this kind assume certain co-relation between C_{A1}, C_{A2} and C_{A3}. In the case of the method of Markov et al. [63], it can be shown that the relation is:

$$C_{A3} = -0.207 C_{A1} + 1.177 C_{A2}\,. \qquad \text{(III.27)}$$

Although the above relation gives realistic ratios between the individual activity concentrations, it cannot fully cover their range and all values that can be met in

reality. Therefore, the two-interval methods are somewhat "compromised" approach in the methodology.

Finally, we should comment that in regard to radon progeny, the levels (incl. in some legislative documents [79]) are expressed in terms of "equilibrium equivalent concentration (EEC)" or "potential alpha energy concentration (PAEC)". Their definitions are given in the Glossary section at the end. These are linear functions of individual activity concentration of radon progeny. The corresponding expressions are:

$$EEC = 0.105C_{A1} + 0.516C_{A2} + 0.379C_{A3}$$
$$PAEC\ (\text{MeV L}^{-1}) = 34.7EEC\ (\text{Bq m}^{-3}) \qquad \text{(III.28)}$$

III.2. Short-lived alpha sources of energies 6.0 MeV and 7.69 MeV for calibration purposes

This research was provoked by the fact, that there are no commercially available alpha sources of energies equal to that emitted by the measured ^{222}Rn progeny. This is because there are no long-lived isotopes that emit alpha energies in the region of interest. On the other side, the registration efficiency of some detectors depends on the energy of alpha particles. There are such indications for scintillation ZnS(Ag) detectors [76]. The problem is crucial for SSNTDs that are employed in devices for integrated measurements of ^{222}Rn progeny and ^{220}Rn progeny. This problem was addressed by the research community in different ways, among which:

- Combining experimental efficiency determined by certified source of other energy, that is available, with computer modeling of the dependence of detector efficiency on energy;

- Using alternative measurement of activity of ^{222}Rn progeny on the filter, e.g. by gamma spectrometry [80];
- Development of alpha sources of proper energy. This direction was addressed by preparation of low-emanating radium sources, that contain mix of alpha-energies including those of interest [81] and by the procedure developed by us [82], described in the present section.

In our research we have used the second and third of the above approaches and have contributed to the third. In particular, we focused on the possibility to prepare and use sufficiently pure (in the recommended time interval) monoenergetic alpha sources of energy 6.0 MeV and 7.69 MeV [82].

Sources of energy 6.0 MeV and 7.69 MeV could be prepared by sampling of ^{222}Rn progeny on a filter and proper timing. In calibration procedures what is actually needed is the exact number of α-particles emitted in a specified time interval and there is no need for the source to radiate much longer than the time necessary for the calibration procedure. The concept is to determine precisely the activity (or related parameters) of the individual radionuclides at the end of sampling by a reference measurement in vacuum with an α-spectrometer and to use them as input values to calculate with a sufficient precision the emission of α-particles with the required energy at any time interval of interest. The mathematical algorithm is based on Bateman equations.

III.2.1.Source of 7.69 MeV α-particles

First a filter sample is taken from ^{222}Rn progeny atmosphere. To have a pure 7.69 MeV source, after sampling the filter is left for 30 min, in order to wait for ^{218}Po to decay. The 7.69 MeV α-particles are emitted by ^{214}Po, which is always in equilibrium with ^{214}Bi. The emission rate of these α-particles is ruled by the ^{214}Bi activity ($A_3(t)$):

$$A_3(t) = \sum_{i=1}^{3} X_i \exp(-\lambda_i t), \qquad \text{(III.29)}$$

where X_i are known linear functions of the initial activity on the sample $A_i(0)$ (t=0 at the end of sampling). However, for the present algorithm they are considered as parameters, whose values should be best fitted using experimental data. For t>30 min the first term fades and:

$$A_3(t) = X_2 \exp(-\lambda_2 t) + X_3 \exp(-\lambda_3 t). \qquad \text{(III. 30)}$$

Respectively, the number of α-particles emitted in the interval (a,b) is given by:

$$N_3(t) = \int_a^b A_3(t)dt = \sum_{i=2}^{3} \frac{X_i}{\lambda_i}\left(\exp(-\lambda_i a) - \exp(-\lambda_i b)\right) = h_2(a,b)X_2 + h_3(a,b)X_3 . \qquad \text{(III. 31)}$$

The parameters X_2 and X_3 are determined by α-spectrometry in the region of interest (ROI) of the 7.69 MeV line for two time intervals. The number of counts in (t_{k1}, t_{k2}) is given by:

$$C_k = \varepsilon\left(h_2\left(t_{k1}, t_{k2}\right)X_2 + h_3\left(t_{k1}, t_{k2}\right)X_3\right) = \varepsilon\sum_{j=2}^{3} Q_{kj} X_j \ , \qquad \text{(III.32)}$$

where ε is the geometry efficiency for α-particle registration and Q_{kj} is 2x2 matrix with elements that are clear from eqn. (III.32). If C_1 and C_2 are the number of counts detected in two different time intervals, then:

$$X_i = \frac{1}{\varepsilon}\sum_{j=1}^{2}\left(Q^{-1}\right)_{ij} C_j \ , \qquad \text{(III.33)}$$

where Q^{-1} is the inverse of Q matrix. Respectively, the expression for N_3 is:

$$N_3 = \frac{1}{\varepsilon}\sum_{i=2}^{3}\sum_{j=1}^{2} h_i(a,b)\left(Q^{-1}\right)_{ij} C_j = \frac{1}{\varepsilon}\sum_{j=1}^{2} P_j C_j \ , \qquad \text{(III.34)}$$

where the definition of P_j is clear from the above equations.

The combined relative uncertainty in N_3 is given by the expression:

$$\left(\frac{u_c(N_3)}{N_3}\right)^2 = \left(\frac{u(\varepsilon)}{\varepsilon}\right)^2 + \frac{\sum_{j=1}^{2} P_j^2 C_j}{\left(\sum_{k=1}^{2} P_k C_k\right)^2} \ . \qquad \text{(III.35)}$$

Note that the time intervals (t_{11}, t_{12}) and (t_{21}, t_{22}) are different from the time interval (a,b) in which the source is used for calibration.

Thus, the basic steps in the technology for preparation of 7.69 MeV sources are:

- Taking a filter sample from ^{222}Rn progeny atmosphere;
- The filter is left for 30 min to leave ^{218}Po to decay;
- Making α-spectrometry reference measurements in two different time intervals. The number of counts in 7.69 MeV ROI are the input parameters to calculate the α-particles emission in the time interval (a,b) specified for calibration.

III.2.2. Source of 6.0 MeV α-particles

The source of these alphas is ^{218}Po. Its activity on the filter at the moment *t* after the end of sampling is given by:

$$A_1(t) = A_1(0)\exp(-\lambda_1 t), \qquad \text{(III.36)}$$

where $A_1(0)$ is the activity of ^{218}Po at t=0 (t=0 at the end of sampling). The number of α-particles emitted in the interval (*a, b*) is then:

$$N_1(a,b) = \int_a^b A_1(t)dt = \frac{A_1(0)}{\lambda_1}\left(\exp(-\lambda_1 a) - \exp(-\lambda_1 b)\right). \qquad \text{(III.37)}$$

Assume that 6.0 MeV α-particles are counted in vacuum by an α-spectrometer of geometry efficiency ε in some other time interval (t_1, t_2). The expected number of counts in the corresponding region of interest is:

$$C_1(t_1,t_2) = \varepsilon\int_{t1}^{t2} A_1(t)dt = \frac{\varepsilon A_1(0)}{\lambda_1}\left(\exp(-\lambda_1 t_1) - \exp(-\lambda_1 t_2)\right). \qquad \text{(III.387)}$$

Using the number of counts gathered from t_1 to t_2 the number of alpha particles emitted at any particular time interval can be specified.

The key approach to prepare a sufficiently pure 6.0 MeV source is to take a sample in the first few minutes after the radon box is filled with a pure ^{222}Rn gas. Under such circumstances there is an extremely high disequilibrium between the individual ^{222}Rn decay products and during the first minutes after sampling the activity of ^{218}Po on the source greatly dominates over those of ^{214}Pb and ^{214}Bi. The specific feature is that the 6.0 MeV α-sources are certified after their use for calibration. To demonstrate this approach we have made a mathematical simulation of the process. Some results are shown in Table III.1. As seen, in the first 6-7 min the contamination with 7.69 MeV α-particles could be less than 3%. During that time the source could be used for calibration as a practically pure 6.0 MeV α-source. Afterward it is still possible to certify the source with the demanded level of precision.

Table II.1. Emission of α-particles of energy 6.0 MeV and 7.69 MeV in the time interval (a, b) from a filter sample taken from ^{222}Rn progeny atmosphere of: C_{A1}=102000 Bq m^{-3}, C_{A2}=1350 Bq m^{-3}, C_{A3} = 16 Bq m^{-3}. Air flow rate of 10 L min^{-1} is assumed during the sampling.

Sampling (min)	(a-b) min	6.0 MeV	7.69 MeV	Contamination (ratio 7.69 to 6.0 MeV α-emission)
1.0	0.5 – 4	58800	440	0.75%
1.0	0.5 – 7	82700	1530	1.85%
1.0	1 – 7	71200	1500	2.1%
1.0	2 - 7	51700	1430	2.8%

III.3. Rotating filter method for integrated measurements of ^{222}Rn progeny and ^{220}Rn progeny.

This method was first proposed in 1991 [83]. The principal scheme of the device is shown in Fig. III.1. The filters rotate uniformly and each point passes consecutively by the inlet nozzle and by passive detectors placed above each filter. Because of the ^{222}Rn and ^{220}Rn progeny decay the signal of the detectors depends on their angular position and this is used to determine the individual integrated concentration of ^{222}Rn progeny and ^{220}Rn progeny. As the half lives of the short lived ^{222}Rn decay products and that of ^{220}Rn progeny differ substantially, two different angular velocity were used. The first corresponds to period of rotation of 1 hour and is used for measurement of ^{222}Rn progeny. The second one corresponds to 12 hours and is used for ^{220}Rn progeny. The first practical application of the rotating filter method used TLDs as detectors [84] and was aimed at measurements of ^{222}Rn progeny at relatively high concentrations, which are typical for mines and radon spas [84, 85]. The detectors used were dosimetrically thin TLDs made of $CaSO_4$: Dy. Further numerical analysis and practical experience [85, 86] revealed that this approach cannot warrant sufficient sensitivity and accuracy for measurement of environmental concentrations of ^{222}Rn progeny and ^{220}Rn progeny. Therefore, further research was focused on incorporating SSNTDs as detectors in these devices. The first successive development with SSNTD was of a device for integrated measurement of ^{220}Rn progeny [87] and after that a device for ^{222}Rn progeny measurement was also developed [88, 89]. Despite that the device for ^{222}Rn progeny measurement was developed later, from methodological point of view it is better to start with it.

III.3.1. Integrated measurements of ^{218}Po, ^{214}Pb and ^{214}Bi + ^{214}Po by rotating filter and SSNTDs

To develop a method oriented towards measurements of ^{222}Rn progeny, research was focused on the implementation of SSNTDs in a rotation filter device. This resulted in construction of a prototype, the principal scheme of which is shown in Fig. III.1. and its photo in Fig. III.2.

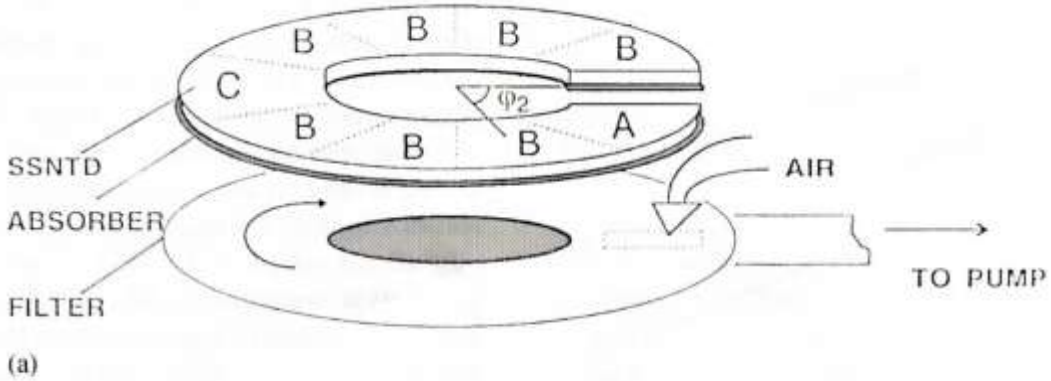

Figure III.1. A principal scheme of the rotating filter device designed for ^{222}Rn progeny. Each point of the rotating filter passes consecutively below SSNTD covered with different absorbers: **A** is scheduled to reduce the energy of 6.0 MeV (^{218}Po) α-particles to the energy window suitable for registration of α-tracks, **B** for 7.69 MeV alphas (^{214}Po) and **C** for 8.78 MeV alphas (^{212}Po). The angles φ_k of the centers of the sectors (φ_2 is illustrated) are measured from the start position of the inlet nozzle.

Figure III.2. A photo of the experimental device. Above: the device ready for use; below: The filter and the cap with SSNTD film covered with Mylar absorber foils.

This device operates as follows: During rotation each point of the filter passes consequently through the inlet nozzle and the detectors placed above the filter. Because of the ^{222}Rn progeny decay the signal of the detectors depends on their angular position and this is used to determine the individual integrated concentrations of ^{222}Rn progeny. In the version presented here the filter (0.8 μm Milipore filter) is moved with one rotation per hour by a synchronized motor connected to a gear-box. The detectors used were SSNTD of Kodak-Pathe LR-115 type II, shaped as shown in Fig. III.1. and covered by absorbers. The absorbers are used to reduce the energy of α-particles (6.0 MeV of ^{218}Po and 7.69 MeV of ^{214}Po) to the energy window of for registration of α-particles of the used detectors. The residual energies of the α-particles after passing through absorbers with different thickness are shown in Table III.2 a,b. They are calculated using ICRU Report 49 data [90].

Table III. 2a. Residual energies (MeV) of ^{222}Rn progeny and ^{220}Rn progeny α-particles that have traversed aluminum absorbers of different thickness. Incident angles are within the range 0-60^0.

Aluminum absorber thickness (μm)	6.0 MeV	7.69 MeV	8.78 MeV
10.4 μm (A-absorber)	2.2 – 4.4	4.7 – 6.3	6.1 – 7.5
25.2 μm (B-absorber)	0 - 0.85	0 - 3.9	0 - 5.4
41.9 μm (C-absorber)	-	-	0 - 2.3
43.3 μm (C-absorber)	-	-	0 - 1.9

Table III. 2b. Residual energies (MeV) of ^{222}Rn progeny and ^{220}Rn progeny α-particles that have traversed mylar absorbers of different thickness. Incident angles are within the range 0-60^0.

Absorber thickness (μm)	6.0 MeV	7.69 MeV	8.78 MeV
14 μm (A-absorber)	2.4 - 4.4	5.0 - 6.4	6.4 - 7.7
35 μm (B-absorber)	0 - 0.7	0 - 4.1	0 - 5.7
60 μm (C-absorber)	-	-	0 - 2.4

The whole device is mounted inside a metal housing, where the air enters through a hole situated above the inlet nozzle.

Further, the theoretical algorithm for data processing will be described. First consider a given point of the rotating filter which enters the inlet nozzle area at moment t=0 and passes it at moment $t = t_F$. The number of ^{222}Rn progeny atoms per unit area (n_{Si}) can be determined as solutions of the following equations:

$$\begin{aligned}
\frac{dn_{S1}}{dt} &= \eta V n_1 \Theta(t_F - t) - \lambda_1 n_{S1} \\
\frac{dn_{S2}}{dt} &= \eta V n_2 \Theta(t_F - t) + \lambda_1 n_{S1} - \lambda_2 n_{S2} \\
\frac{dn_{S3}}{dt} &= \eta V n_3 \Theta(t_F - t) + \lambda_2 n_{S2} - \lambda_3 n_{S3}
\end{aligned} \qquad \text{(III.39)}$$

where V is the linear air velocity through the filter (V=air flow rate/nozzle inlet area), n_i is the atom concentration in the air of the i-th nuclide while the considered filter point passes the inlet nozzle (the activity concentration is $C_{Ai} = \lambda_i n_i$). The sectors geometry is shown in Fig. III.3. Let a point of the detector be situated at an angle of φ, i. e. the filter point reaches it at the moment $t = \varphi/\omega$,

where ω is the angular velocity of the filter. The growth-rate of the track density at this angular position at the moment t is:

$$\dot{N}_{tr} = \varepsilon_1 \lambda_1 n_{S1}(t) + \varepsilon_3 \lambda_3 n_{S3}(t) . \qquad \text{(III.40)}$$

Using the known general solutions of eqn (III.39) the above equation takes the form:

$$\dot{N}_{tr} = \sum_{i=1}^{3} x_i(0)\, f_i(t) . \qquad \text{(III.41)}$$

The parameters $x_i(0)$ are linearly related to C_{Ai} through the ${}_rR$-matrix given in eqn. (III.8). For an arbitrary moment t during the first rotation, eqn. (III.40) can be generalized:

$$\dot{N}_{tr}(t,\varphi) = \sum_{i=1}^{3} x_i(t-\varphi/\omega)\, f_i\left(\frac{\varphi}{\omega}\right). \qquad \text{(III.42)}$$

The contribution of "previous rotations" to the signal should also be taken into account. Let air sampling (e.g. "exposure time") is from the time $t=0$ to $t=t_a$. Then the expression takes the form:

$$\dot{N}_{tr}(t,\varphi) = \sum_{i=1}^{3}\sum_{k=0}^{\infty} x_i(t-\varphi/\omega-kT)\, f_i(\varphi/\omega+kT)\Theta(t-\varphi/\omega-kT)\Theta(t_a-(t-\varphi/\omega-kT)), \qquad \text{(III.43)}$$

where $T=2\pi/\omega$ is the period of the filter rotation. The Heaviside functions account that $x_i(t)\neq 0$ only for $t_a>t>0$. Therefore, the track density accumulated at the moment t_m is:

$$N_{tr}(\varphi) = \int_0^{t_m} \dot{N}_{tr}(t,\varphi)dt\,. \qquad \text{(III.44)}$$

In the applications of this method, after the end of sampling the rotation of filter continues, until practically all deposited progeny atoms disintegrate (in the case of ^{222}Rn progeny 4-5 hours are sufficient). In this case t_m can be replaced with ∞:

$$N_{tr}(\varphi) = \int_0^{\infty} \dot{N}_{tr}(t,\varphi)dt = \sum_{i=1}^{3}\sum_{k=0}^{\infty} f_i\left(\varphi/\omega + kT\right)\int_0^{t_a} x_i(\tau)d\tau = \sum_{i=1}^{3} G_i(\varphi)X_i\,, \qquad \text{(III.45)}$$

where $X_i = \int_0^{t_a} x_i(\tau)d\tau$ and $G_i(\varphi) = \sum_{k=0}^{\infty} f_i\left(\varphi/\omega + kT\right)$.

The explicit formula for G_i is:

$$G_i(\varphi) = \frac{\left(\exp\left(\lambda_i t_F\right)-1\right)\exp\left(-\lambda_i\varphi/\omega\right)}{1-\exp\left(-2\pi\lambda_i/\omega\right)}\,. \qquad \text{(III.46)}$$

Then, the expression for the number of tracks at a sector with centre at an angle φ and half-with Δφ is:

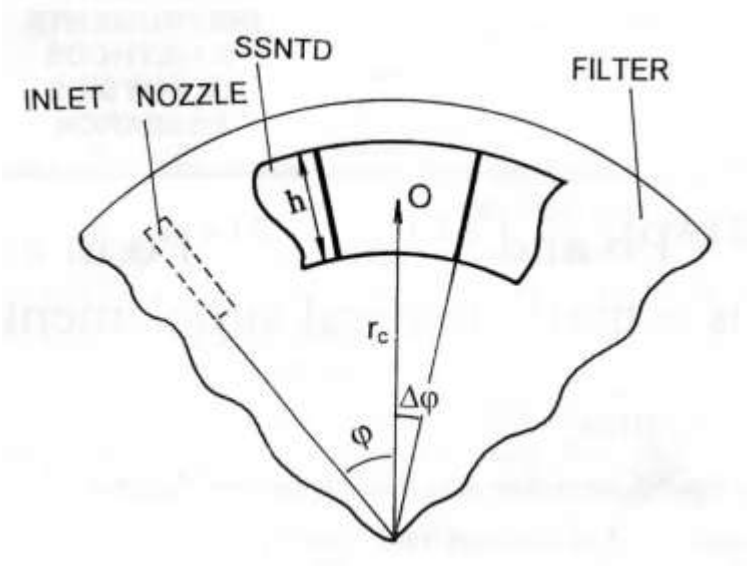

Figure III.3. Sector geometry: each point of the uniformly rotating (clockwise) filter passes consecutively by the inlet nozzle and different sectors of LR-115/II film.

$$C(\varphi) = \int_S N_{tr}(\varphi) dS = r_c h \int_{\varphi-\Delta\varphi}^{\varphi+\Delta\varphi} N_{tr}(\varphi) d\varphi = \sum_{i=1}^{3} X_i \left[G_i(\varphi) \frac{2hr_c\omega}{\lambda_i} sh(\lambda_i \Delta\varphi/\omega) \right] = \sum_{i=1}^{3} X_i \tilde{F}_i(\varphi)$$

.

(III.47)

The above algorithm was specified for "spectrometric" measurements, with different efficiency for A and B-sectors, using the approach explained in sub-section III.1.1.2. The net number of tracks in the k-th sector, whose center is placed at an angle φ_k is given by the expression:

$$C_k = C(\varphi_k) = \sum_{i=1}^{3} F_i(\varphi_k) X_i \ . \qquad \text{(III.48)}$$

The relationship between the integrated activity concentrations I_i and the parameters X_i is:

$$I_i = \sum_{j=1}^{3} {}_r R_{ij}^{-1} X_j \ , \qquad \text{(III.49)}$$

where:

$$ {}_r R^{-1} = \frac{1}{V\eta\varepsilon_3^{(B)}} \begin{pmatrix} \frac{\lambda_1(\lambda_1-\lambda_2)(\lambda_1-\lambda_3)}{\lambda_2\lambda_3} & 0 & 0 \\ -\frac{\lambda_1(\lambda_1-\lambda_3)}{\lambda_3} & -\frac{\lambda_2(\lambda_2-\lambda_3)}{\lambda_3} & 0 \\ \lambda_1 & \lambda_2 & \lambda_3 \end{pmatrix} . \qquad \text{(III.50)}$$

The relation between X_i and $I_i = \int_0^{t_a} C_{Ai}(t)dt$ is given by eqn. (III.49) and is the same as the relation between x_i and C_{Ai} in the theory of grab sampling measurements, described in section III.1.1.

Using the algorithm developed for spectrometric measurements the following explicit form for $F_i(\varphi_k)$ is obtained [89]:

$$F_i(\varphi_k) = \frac{2hr_c\omega}{\lambda_i} sh(\lambda_i \Delta\varphi_k/\omega) \frac{(\exp(\lambda_i t_F)-1)\exp(-\lambda_i(\varphi_k/\omega))}{1-\exp(-(2\pi/\omega)\lambda_i)} \times$$
$$\times \left[1+\delta_{k1}\left[(\varepsilon_3^{(A)}/\varepsilon_3^{(B)}) + \frac{(\lambda_1-\lambda_2)(\lambda_1-\lambda_3)\varepsilon_1^{(A)}}{\lambda_2\lambda_3\varepsilon_3^{(B)}}\delta_{i1} - 1\right]\right] . \qquad \text{(III.51)}$$

In the above expression δ_{ik} is the Kronecker symbol (δ_{ik} =1 if i=k and 0 if i≠k), h is the height of the sector and r_c is the radius of the circle passing through the

sector centers. As an illustration of the physics that underlies this theory a simulation of the angular dependence of the specific activity on the filter is made. The results are illustrated in Fig. III.4.

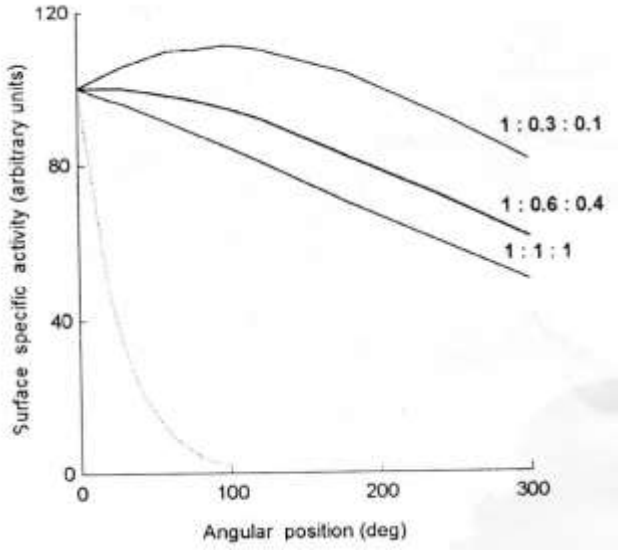

Figure III.4. Theoretical dependences of the surface specific activities of ^{218}Po (dotted line) and ^{214}Bi + ^{214}Po on the angular position. Assumed activity ratios (^{218}Po:^{214}Pb:^{214}Bi) are shown.

In real data processing, the calculation of integrated activity concentrations by eqn (III.49) should pass through determination of X_i parameters. The X_i parameters are determined by a least squares fit of the experimentally determined number of tracks in different sectors – through minimization of the form:

$$\sum_{k=1}^{n}\left[C_k - \sum_{i=1}^{3} F_i(\varphi_k) X_i\right]^2 . \qquad \text{(III.52)}$$

Uncertainties u_i in I_i were calculated as follows:

$$u_i = \left[\sum_{k=1}^{3} \sum_{l=1}^{3} R_{ik}^{-1} R_{il}^{-1} Cov(X_k X_l) \right]^{1/2}, \qquad \text{(III.53)}$$

where the co-variation $Cov(X_k,X_l)$ is given by the expression:

$$Cov(X_k, X_l) = \frac{\sum_{p=1}^{n} \left[C_p - \sum_{i=1}^{3} F_i(\varphi_p) X_i \right]^2}{n-3} \left(K^{-1} \right)_{kl}. \qquad \text{(III.54)}$$

In eqn. (III.54) K^{-1} is the inverse matrix of the matrix with elements:

$$K_{ij} = \sum_k F_i(\varphi_k) F_j(\varphi_k). \qquad \text{(III.55)}$$

III.3.1.1. Optimization of the design

The experimental uncertainties are significantly dependent on the choice and position of the different sectors, their number, etc. To optimize the design of the rotating filter devices numerical experiments were made. In these simulations the statistical uncertainty was ascribed to the track counting and a Poisson distribution of the number of tracks was assumed. First, the position of the A-sector was chosen. The starting angle for this sector was selected to be 2^0. The uncertainties in ^{218}Po, ^{214}Pb and ^{214}Bi were studied as dependent on the width of this sector. The B-sectors start immediately after the A-sector and every B-sector has 20^0 angular width. The results demonstrate that the uncertainty in ^{218}Po is decreasing for wider A-sector, while the uncertainty in ^{214}Bi is increasing. The uncertainty in ^{214}Pb is weakly dependent on this parameter. The criterion for an optimal width was to minimize the sum $\sigma_1^2+\sigma_2^2+\sigma_3^2$, where σ_i are the standard

deviations that corresponds to the Poisson counting statistics ($\sigma_i = u_i$ if the uncertainty is due only to the Poisson counting statistics). The results are illustrated in Fig. III.5. As seen, the optimal width of sector A is about 20^0 for a great variety of ratios ^{218}Po : ^{214}Pb : ^{214}Bi.

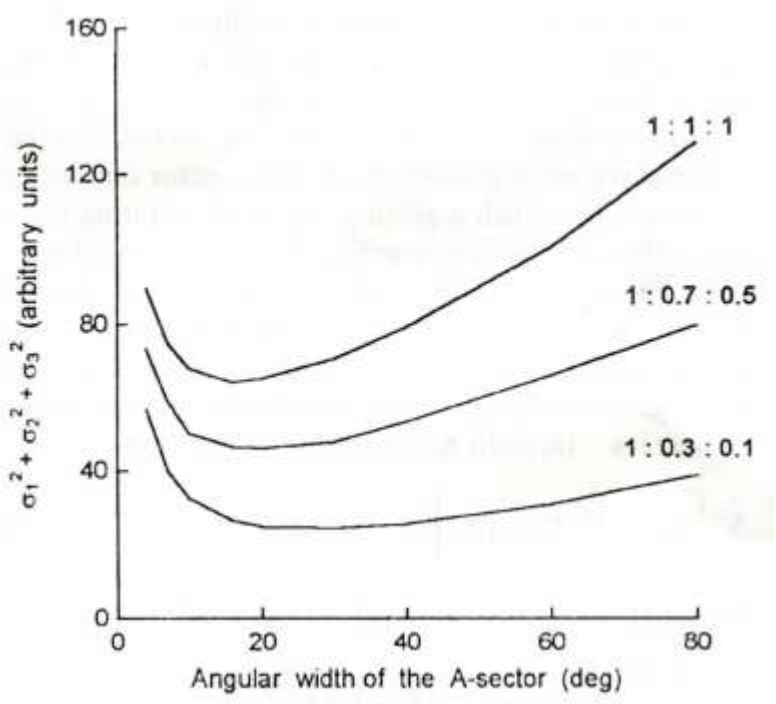

Figure III.5. Dependence of the quadratic sum of the Poisson counting statistic standard deviations on the angular width of the A-sector. Assumed activity ratios (^{218}Po:^{214}Pb:^{214}Bi) are shown.

The dependence of the uncertainties of ^{214}Pb and ^{214}Bi on the number of B-sectors is shown in Fig. III.6. As seen, if the number of sectors is small, the uncertainties grow rapidly. In our experiments the number of sectors used was usually ≥ 8.

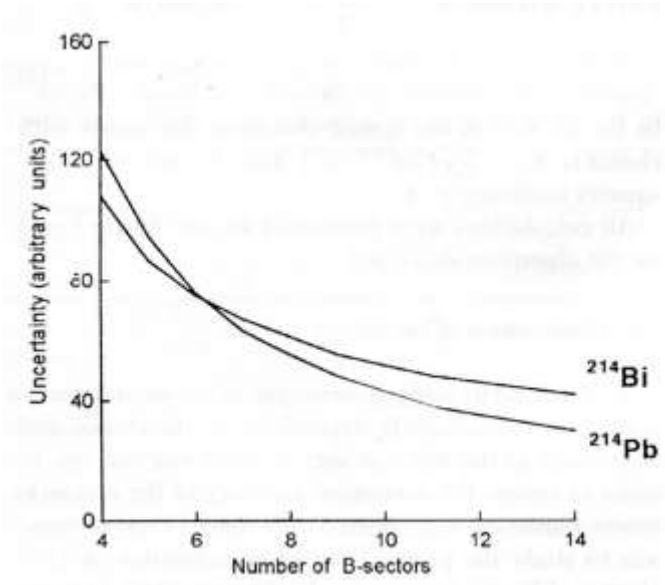

Figure III.6. Uncertainties of ^{214}Pb and ^{214}Bi as a function of the number of B-sectors.

III.3.1.2. Correction for ^{220}Rn-progeny presence

If short-lived ^{220}Rn progeny is present, it can affect the signal in both A- and B-sectors. However, the correction for ^{220}Rn progeny is much facilitated by the following reason: For the fixed period of rotation (1 h) the angular dependence of the surface specific activity of ^{212}Bi + ^{212}Po (both directly deposited and produced by the ^{212}Pb decay) is weak. For activity ratios ^{212}Bi : ^{212}Pb $\leq$ 1 (which is the real case, according to Reference [91]) the angular variation of the specific activity (max-min) is from 7% (^{212}Bi = ^{212}Pb) to less than 2% (^{212}Pb >> ^{212}Bi). If this activity is considered constant for all angular positions, it can be determined using the track density in the center of the C-sector, which is situated at some middle point (e.g. 180^0). Then, the deviation of this estimate from the real surface specific activity would not exceed $\pm$ 4%. This difference is sufficiently less than the normal experimental uncertainties expected in this type of measurements.

Experimentally, the correction for ^{220}Rn progeny was made as follows: If the net number of tracks in C-sector is C_T, the number of ^{212}Bi disintegrations in this sector will be $C_T/\varepsilon_5^{(C)}$. Taking this number as constant for all sectors, the expected number of tracks in the A-sector due to the ^{220}Rn progeny on the filter are: $0.36C_T\varepsilon_1^{(A)}/\varepsilon_5^{(C)}$ and in the B-sector (formed by the 8.78 MeV alpha particles of ^{212}Po): $C_T\varepsilon_5^{(B)}/\varepsilon_5^{(C)}$. Note that 0.36 is the probability of ^{212}Bi α-decay. These values are subtracted from the total number of tracks in the correspondent sectors.

The net-number of tracks in the C-sector can also be used for determination of the time integrated PAEC of ^{220}Rn progeny. The theoretical analysis showed that integrated PAEC(^{220}Rn) is proportional to C_T with less than 1% variation due to the differences in ^{212}Pb : ^{212}Bi ratio [86].

III.3.2. Determination of the registration efficiencies for 6.0 MeV, 7.69 MeV and 8.78 MeV α-particles

In our experimental work two approaches for experimental determination of the registration efficiencies were employed. The first was based on gamma-spectrometry and, as a concept, was used by other authors, too [80]. The second approach is based on the use of short-lived α-sources for calibration purposes [82]. The absorbers used in different experiments were aluminum foils or mylar foils of proper thickness.

Within the gamma-spectrometry approach, the efficiency $\varepsilon_1^{(A)}$ was determined in the following way: A grab sample of ^{220}Rn progeny was taken with a filter. After a delay time of 6 h the activities of ^{212}Pb, ^{212}Bi + ^{212}Po/^{208}Tl are in constant proportions (equilibrium state). Then, a SSNTD (covered with A-absorber) was fixed above the filter and was simultaneously placed on a HPGe detector with relative efficiency 24.9% and FWHM(1332 keV) = 1.77 keV. The

gamma spectrum was gathered for a controlled time (24 h). After that the SSNTD was etched and the number of tracks determined. The total number of ^{212}Bi disintegrations was determined by the net area of the 727 keV gamma line of ^{212}Bi and of the 860 keV gamma line of ^{208}Tl. There are two α-emitting ^{220}Rn daughters on the filter. The first one is ^{212}Bi that disintegrates with a probability about 36% by α-decay [77] emitting α-particles of energies 6.05 and 6.09 MeV. These alphas have energy very close to 6.0 MeV alphas of ^{218}Po and were used for determination of $\varepsilon_1^{(A)}$. The other α-source is ^{212}Po, but for the selected A-absorbers it could not contribute to tracks in the A-sector as the residual energy of the 8.78 MeV alphas after passing through the A-absorber is outside the energy window for registration.

The efficiencies $\varepsilon_3^{(B)}$ and $\varepsilon_3^{(A)}$ were determined as follows: A grab sample of ^{222}Rn progeny was taken with the filter. After a 30 min delay ^{218}Po atoms are essentially disintegrated and the only α-source on the filter is ^{214}Bi + ^{214}Po. Then, a SSNTD covered with A or B type of absorbers was fixed above the filter and the filter + SSNTD were simultaneously placed on the HPGe detector described above. The gamma spectrum was gathered for 4 h. After that the SSNTD was processed. The total number of ^{214}Bi disintegrations was determined by the net area of the 1120 keV gamma line.

The application of the second method was according to the methodology described in section III.1.1.3. The experiments were carried-out in the Laboratory of Sub-Atomic and Radiation Physics at the University of Ghent, Belgium. An experimental set-up with Si- alpha spectrometry detector (surface barrier) was constructed. All α-spectrometry measurements were made under vacuum. The experimentally obtained efficiencies for different absorbers, used in our experiments are summarized in Tables III.3. a-c.

Note that the value of $\varepsilon_3^{(A)}$ is only about 4% of the $\varepsilon_1^{(A)}$ value, therefore the present manner of registration could be considered as quasi-spectrometric regarding ^{218}Po and ^{214}Po alphas.

Table III.3a. Efficiency to 6.0 MeV α-particles.

Source	Absorber	Reference method	Efficiency
^{218}Po	Mylar 14 μm (A-absorber)	Alpha spectrometry	0.19 ± 0.01
^{212}Bi+^{212}Po	Aluminum 10.4 μm (A-absorber)	Gamma spectrometry using lines 727 keV (^{212}Bi) and 860 keV (^{208}Tl)	0.097 ± 0.007

Table III.3b. Efficiency to 7.69 MeV α-particles.

Source	Absorber	Reference method	Efficiency
^{214}Bi+^{214}Po	Mylar 35 μm (B-absorber)	Alpha spectrometry	0.14 ± 0.01
^{214}Bi+^{214}Po	Aluminum 25.2 μm (B-absorber)	Gamma spectrometry using line 1120 keV	0.087 ± 0.005
^{214}Bi+^{214}Po	Aluminum 10.4 μm (A-absorber)	Gamma spectrometry using line 1120 keV	0.0041 ± 0.0004

Table III.3c. Efficiency to 8.78 MeV α-particles.

Source	Absorber	Reference method	Efficiency
^{212}Bi+^{212}Po	Mylar 60 μm (C-absorber)	Alpha spectrometry	0.022 ± 0.001
^{212}Bi+^{212}Po	Aluminum 41.9 μm (C-absorber)	Gamma spectrometry using lines 727 keV (^{212}Bi) and 860 keV (^{208}Tl)	0.019 ± 0.002
^{212}Bi+^{212}Po	Aluminum 43.3 μm (C-absorber)	Gamma spectrometry using lines 727 keV (^{212}Bi) and 860 keV (^{208}Tl)	0.017 ± 0.001
^{212}Bi+^{212}Po	Aluminum 25.2 μm (B-absorber)	Gamma spectrometry using lines 727 keV (^{212}Bi) and 860 keV (^{208}Tl)	0.023 ± 0.005

The sector C is used to account for ^{220}Rn progeny availability, as described above.

III.3.3. Results of laboratory and field measurements

This section summarizes the results of different experiments on integrated measurements of ^{222}Rn progeny, carried-out in the interval 1996-2001 in the University of Sofia and in the University of Ghent, Belgium.

In the first experiments, made in Sofia, the absorbers were made of aluminum foil, with thickness specified in Table III.2a These measurements were made in an experimental basement where ^{222}Rn progeny concentrations varied within the range 15 – 200 Bq m^{-3} and ^{220}Rn progeny concentrations were from <0.5 to 3.5 Bq m^{-3}. The average ratio PAEC(^{220}Rn):PAEC(^{222}Rn) was about 0.4. The situation in this basement was similar to the situation in dwellings where both

^{222}Rn and ^{220}Rn are present. The reference measurements were made by the method of Kritidis et al. [67] – gross α-counting version. The bias due to the ^{220}Rn progeny presence was < 7%. Results from such comparative measurements are shown in Table III. 4:

Table III. 4. Integrated concentrations of ^{222}Rn progeny estimated by the rotating filter method compared with results from simultaneously made series of grab sampling measurements (Bq h m^{-3}).

Rotating filter method			**Grab samplings [67]**		
^{218}Po	**^{214}Pb**	**^{214}Bi**	**^{218}Po**	**^{214}Pb**	**^{214}Bi**
870 ± 150	930 ± 120	700 ± 140	830 ± 100	770 ± 25	590 ± 32
249 ± 21	101 ± 26	72 ± 20	234 ± 39	119 ± 9	60 ± 12
599 ± 72	369 ± 54	280 ± 60	554 ± 168	381 ± 55	329 ± 34
196 ± 16	62 ± 14	52 ± 15	159 ± 79	40 ± 20	20 ± 15
530 ± 40	446 ± 29	336 ± 40	659 ± 90	466 ± 60	390 ± 39
4500 ± 250	1410 ± 110	490 ± 70	5050 ± 460	1760 ± 190	570 ± 130

However, certain disadvantages of using Al-foils were noted. The most critical was that the thickness of these foils can vary thus introducing an additional source of experimental uncertainty. Therefore, for the next experiments the design was optimized. Instead of aluminum, mylar absorbers of 3 different thicknesses were used. The first, used for the « A-sector » of the detector was 14 μm thick, the next, used for the « B-sectors » was 35 μm thick and that used for the « C-sector » was 60 μm thick. These thicknesses were selected, in order to achieve « spectroscopic » mode of registration. The residual energies of α-particles for

different absorber thicknesses and incident angles are shown in Table III.2b. As seen in Table III. 2b, after the 14 μm absorber (A-sector) the residual energy of 7.69 MeV α-particles of ^{214}Po is outside the energy window of registration of the detectors. The same is true for 6.0 MeV alphas of ^{218}Po after 35 μm Mylar. Therefore, A-sector is used for registration of ^{218}Po α-particles and B-sectors are for ^{214}Po alphas. In all measurements presented furthermore ^{220}Rn progeny was either missing (laboratory experiments) or ^{222}Rn progeny greatly dominated. Therefore, correction for ^{220}Rn progeny was practically negligible.

The registration efficiency of the detectors in A and B and C sectors has been experimentally determined and is given in Tables III. 3.

First, laboratory experiments were made, with parallel grab-sampling measurements, by the method published in Ref. [67] - α-spectrometry version.

Table III.5. Integrated activity concentrations of individual ^{222}Rn short-lived decay products (in Bq h m^{-3}) measured using the rotating filter method during the laboratory tests. Results of parallel grab sampling measurements are given, for comparison.

Test	**Rotating filter**			**Grab samplings [67]**		
	^{218}Po	**^{214}Pb**	**^{214}Bi**	**^{218}Po**	**^{214}Pb**	**^{214}Bi**
1	117600±3900	70600±5300	60500±7600	107700±8600	75500±9000	54000±3800
2	113000±4000	69500±5000	79600±7200	106300±10700	75200±11000	76500±11500
3	88500±1500	11400±1300	<3900	104800±15900	13900±5200	2950±1170
4	118800±4000	38000±3800	6200±5500	139300±11000	29800±7950	14800±2200
5	91400±2800	39400±2900	23800±4100	101300±5800	46400±6400	25500±1500

Tables III. 4. and III. 5. provide laboratory test/verification of the rotating filter method over 3 orders of magnitude of integrated activity concentrations. After the method was tested in the laboratory a number of measurements under real conditions were made. The measurements were made indoors, in private houses, working places, storage rooms with radioactive minerals, public buildings and outdoors (in rainy weather under very low ^{222}Rn and ^{222}Rn progeny concentrations). In all measurements the flow rate used was 1 L/min. The results are presented in Table III.6. As seen, the method allows sufficiently precise

measurements over a vast range of ^{222}Rn progeny concentrations. Even concentrations of the order of 1.5 Bq m^{-3} are measurable with an uncertainty of about 10% or even less.

Table III. 6. Mean activity concentrations (= integrated activity concentration/exposure time) obtained by measurements by the rotating filter device under real conditions (in Bq m^{-3}).

Place	Exposure time	^{218}Po	^{214}Pb	^{214}Bi
House 1 (indoors)	177.25 h	122±5	50±4	32±5
House 2 (indoors)	100.83 h	476±30	410±30	390±34
Outdoors-rainy weather	232.33 h	1.49±0.13	1.32±0.12	1.28±0.15
House 3(indoors)	25.1 h	20.6±1.8	20.4±4.4	4.9±3.9
Public building-1 (basement)	6.83 h	61.0±3.7	29.7±3.4	19.5±4.0
Working place 1 (chemical laboratory) - 1^{st} measurement	43.17 h	59.25±6.2	37.1±5.8	26.2±6.6
Working place 1 - 2^{nd}	72.6 h	22.2±3.5	12.6±3.2	4.6±3.7
Working place 1 3^{rd}	3 h	17.3 ± 2.7	8.3 ± 2.0	3.3 ± 2.0
House 4 (indoors)	31.33 h	470±27	269±25	191±28

Working place 2 (factory) -1st measurement	6.8 h	58.2±3.4	16.8±2.5	16.8±3.5
Working place 2 – 2nd	8 h	69.0±4.8	28.5±4.4	26.3±5.0
Working place 2 – 3rd (overnight)	11.83 h	98.1±11.5	53.5±10.7	45.6±12.2
Working place 2 – 4th	8	54.0±4.0	18.9±3.7	15.5±4.3
Public building 2	8 h	19.1±3.1	10.8±2.9	8.8±3.2
Public building 2 – basement	64 h	146±12	121±11	81±12
Storage room 1 (uranium minerals)	2 h	9150±1100	8950±1050	4400±1200
Storage room 2 - ventilation off	15 h	339 ± 19	74 ± 43	65 ± 40
Storage room 2 - ventilation on – 1st	50.5 h	59.6 ± 4.0	12.1 ± 3.8	5.1 ± 4.4
Storage room 2- ventilation on – 2nd	92 h	72.0 ± 2.0	9.8 ± 2.2	13.0 ± 2.2

What is clearly seen from the table is that indoors, either in houses or in working places, the activity-ratios between different radionuclides (i.e. ^{218}Po, ^{214}Pb and ^{214}Bi + ^{214}Po) are quite different and site specific. This can question the common approach [92] to apply an uniform equilibrium factor, in order to

determine the exposures under real conditions. Recent publications also provide support for our scepticizm about the use of a constant equilibrium factor [93]. In the outdoor measurement the radionuclides seem to be close to equilibrium. We would also like to draw more attention to the results in the factory. There we coherently obtained ^{214}Pb and ^{214}Bi concentrations very close to each-other. Our experience, as well as former research over the mine atmosphere models [94], indicate that this is a sign of « air-rotation » - close circuit in the air ventilation stream. After we have diagnosed the ventilation mode, this appeared to be exactly the case as the heating and the ventilation system were linked and rotation of a substantial proportion of the air used for ventilation could be expected [95]. Therefore, the method offers good opportunities for diagnostic of the ventilation conditions at working places.

Notably, the ^{222}Rn progeny disequilibrium indoors and at working places differs significantly from place to place and, probably, the equilibrium factor is very site-specific [96]. Recent studies [93] also demonstrate that the F-factor can vary in a wide range, thus affecting substantially the lung dose estimates. The author feels that the direct characterization of radon and thoron progeny atmosphere in dwellings and working places is a problem that needs to be re-addressed by the radon expert community. The described rotating filter method smoothes the large time variations in the concentrations and, possibly, offers better opportunities for diagnostic of the ventilation conditions than the grab sampling methods.

III.3.4. Integrated measurements of ^{212}Pb and ^{212}Bi.

The concept of this method is to employ a filter that rotates with a period of 12 h and to cover the SSNTD with a sufficiently thick absorber so that only ^{212}Po α-particles (8.78 MeV) could be registered. The experiments were organized with SSNTD Kodak-Pathe LR-115/II covered with 11.7 mg cm^{-2} (43.3

μm) aluminum absorber (foil). The scheme of the arrangement is shown in Fig. III.7. For better experimental design first theoretical modeling of the angular dependence of the signal was made. The results are shown in Fig. III.8. As seen the theoretical curves obtained for different activity ratios of ^{212}Pb and ^{212}Bi differ for angles $<150^0$, which suggests that activity ratios within the whole expected range can be resolved.

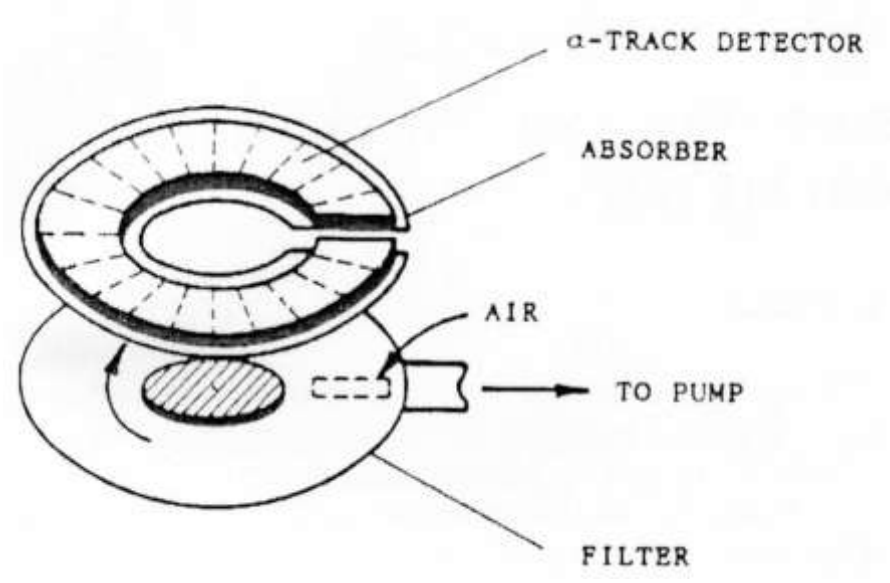

Figure III.7. A scheme of the experimental device for ^{220}Rn progeny measurement. The filter rotates with a period of 12 hours and the detector is covered by an absorber with appropriate thickness, so that only 8.78 MeV alphas can pass through it and be registered.

Considering the general algorithm restricted only to ^{220}Rn progeny one can obtain the following expression for the net-number of tracks on a sector with center at angle φ:

$$C(\varphi) = \sum_{i=4}^{5} F_i(\varphi) X_i \ , \qquad \text{(III.56)}$$

where F_i are:

$$F_i(\varphi) = \frac{2hr_c\omega}{\lambda_i} sh(\lambda_i \Delta\varphi/\omega) \frac{(\exp(\lambda_i t_F) - 1)\exp(-\lambda_i(\varphi/\omega))}{1 - \exp(-(2\pi/\omega)\lambda_i)}, \qquad \text{(III.57)}$$

The integrated activity concentrations $I_i = \int_0^{t_a} C_{Ai}(t)dt$ are linearly dependent on the X_i parameters in the following matrix expression:

$$\begin{pmatrix} I_4 \\ I_5 \end{pmatrix} = \frac{1}{V\eta} \begin{pmatrix} -\frac{\lambda_4(\lambda_4 - \lambda_5)}{\varepsilon\lambda_5} & 0 \\ \frac{\lambda_4}{\varepsilon} & \frac{\lambda_5}{\varepsilon} \end{pmatrix} \begin{pmatrix} X_4 \\ X_5 \end{pmatrix}, \qquad \text{(III.58)}$$

or:

$$I_i = \sum_{j=4}^{5} {}_t R_{ij}^{-1} X_j \,. \qquad \text{(III.59)}$$

In the rest the core of the algorithm remains the same as that for ^{222}Rn progeny. Using the experimentally obtained number of tracks $C_k = C(\varphi_k)$ for different sectors k, the parameters X_i and their covariation $Cov(X_i,X_j)$ have been determined through the least squares method.

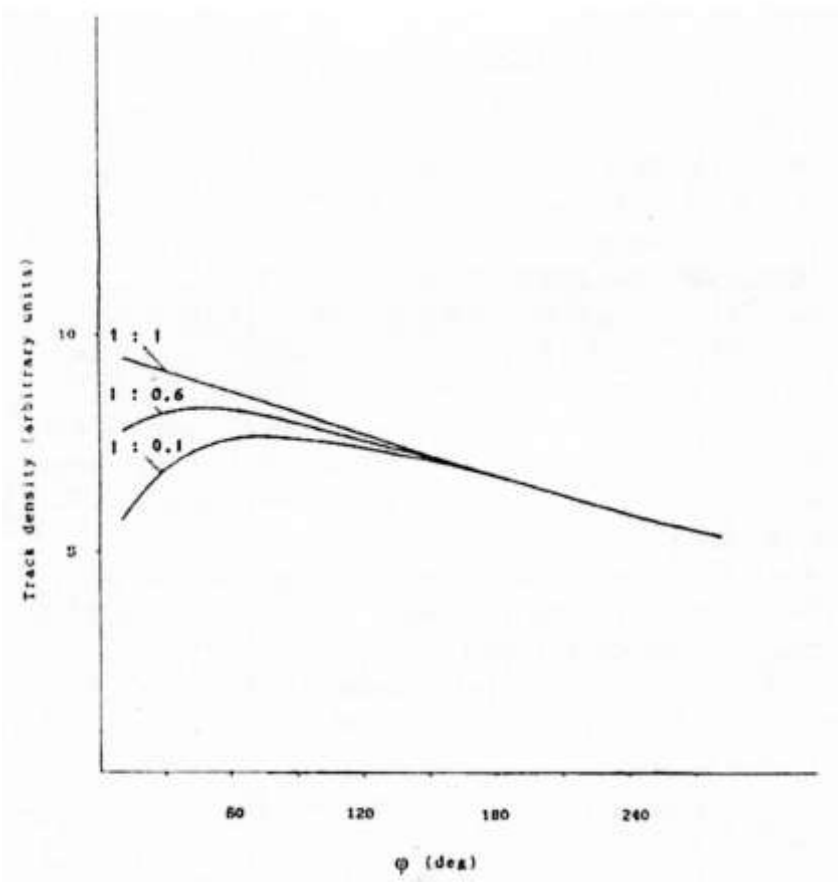

Figure III.8. A theoretical dependence of the track density on the angular position of the detector center, determined from the air inlet. The activity ratios (^{212}Pb:^{212}Bi) are shown.

To study the potential of this method for precise measurements and to optimize the device's design, a number of numerical simulations were made. The results for uncertainties at different integrated concentrations are shown in Fig. III.9. Both the effects of Poisson counting statistics and fluctuations in the absorber thickness were studied.

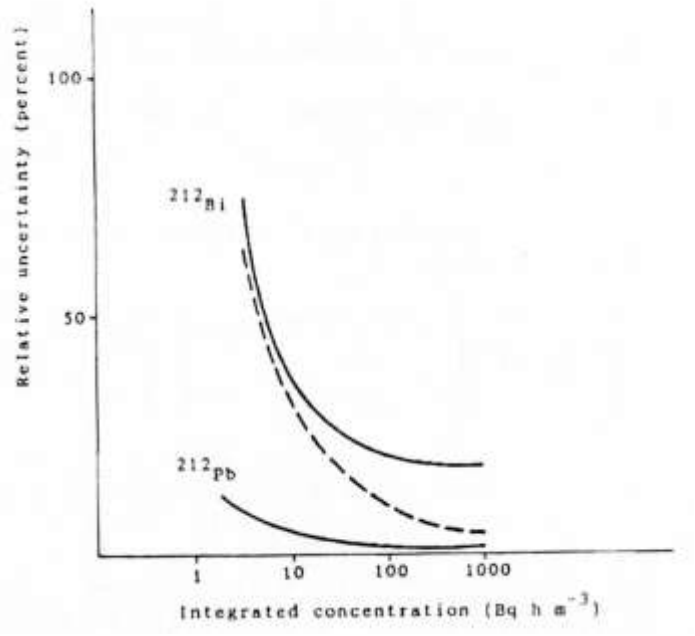

Figure III.9. Dependence of the relative uncertainty on the integrated activity concentration of the corresponding isotopes. The activity ratio ^{212}Pb:^{212}Bi = 1:0.5 is assumed. The dotted line represents ^{212}Bi relative uncertainty that is due only to counting statistics, if the absorber is with truly constant thickness of exactly 11.70 mg cm-^{2}. The solid lines correspond to the real Al-absorber, which has the above thickness, but is not ideally uniform (with a standard deviation of the thickness of 0.05 mg cm^{-2}).

The dependence of the relative uncertainty on the angular position of the first sector is shown in Fig. III.10. The curve for ^{212}Bi indicates that the first sector should be placed at as small as possible angle for better ^{212}Bi determination. The dependence of the relative uncertainty on the number of sectors is shown in Fig. III.11. It is clearly seen that at least 6-8 sectors should be used, but the improvement if they are > 10 is relatively slight.

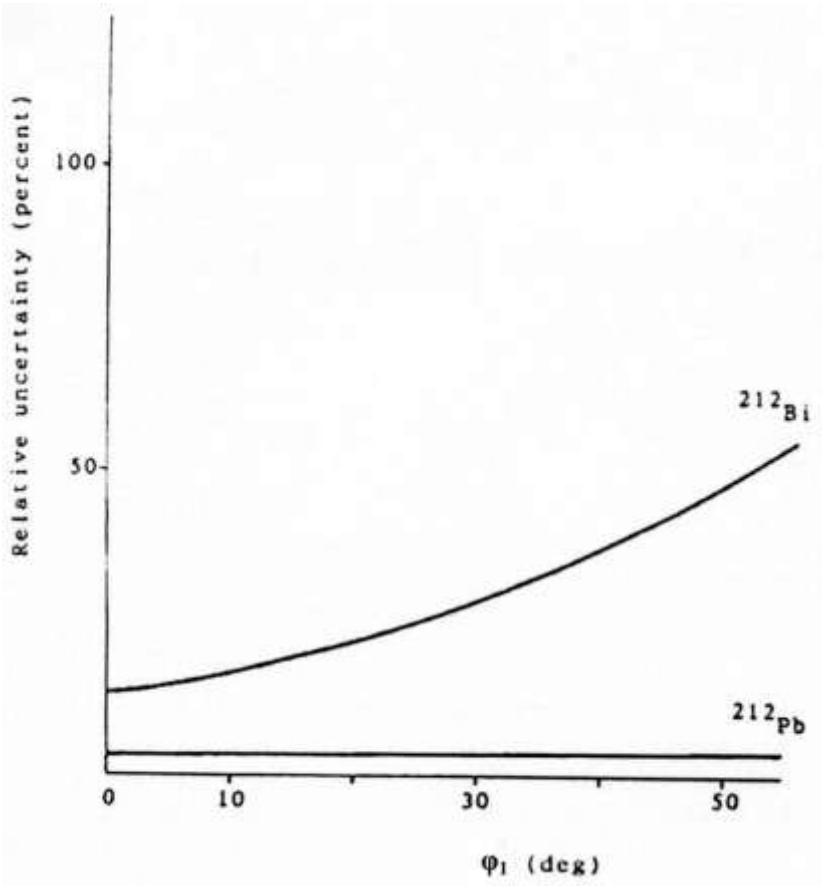

Figure III.10. A dependence of the uncertainties in the integrated concentrations of ^{220}Rn progeny on the angular position of the first sector in the rotating filter device. The assumed number of sectors is 10, each of 20^0 angular width.

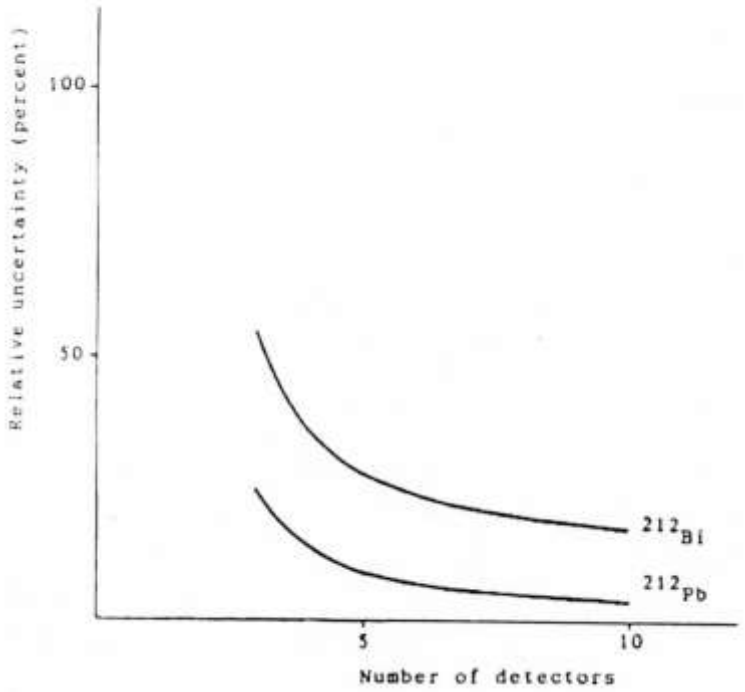

Figure III.11. A dependence of the uncertainties on the number of sectors. The first sector starts at 10^0 and the angular width of each sector is 20^0.

Experiments with this method were carried out in an artificial ^{220}Rn atmosphere in a 0.5 m^3 laboratory box. The quantitative correspondence between the results obtained by the present method and those obtained by grab sampling through the method [68] is illustrated in the Table III.7.

Table III. 7. Integrated measurements of ^{212}Pb and ^{212}Bi. Integrated activity concentration (Bq h m^{-3}) are given.

Isotope	Rotating filter	Grab sampling [68]
^{212}Pb	92.2 ± 6.1	88.5 ± 4.5
^{212}Bi	44.0 ± 10.5	36 ± 16

IV. RADON-RELATED RADIOLOGICAL PROBLEMS STUDIED IN BULGARIA.

There is a century long tradition in radon measurements in Bulgaria [15]. Since 1907 with hardly any interruption radon (and since the 1960s radon progeny) have been measured in mineral spas [96, 97], in the human environment and in the course of laboratory research. However, by far the largest number of measurements (>50000) have been done in the uranium industry and other underground mines [98-100]. The uranium industry (mining and milling) as an industrial branch operated in Bulgaria in the period 1945 – 1992. In the interval 1945 -1956 it was under Soviet administrative control and no radiation data is available from that time. In 1956 Bulgarian administration took the control positions in the branch and health physics group was established and operated till the cessation of the industry. Regular radon/radon progeny measurements have been made since 1958. They were reviewed, comprehended and the statistical extract published in the 1990s [16, 99,100]. The methodological research on grab-sampling measurements, incl. comparison of different methods, was performed by the author [101] and others [102, 103]. The comparison of different methods was partly provoked by the need to comprehend in an unified scheme the methods used in practice, in order to be able to calculate miners' exposure in an unambiguous way.

Although measurements of radon in the environment were performed before 1990, published information about them is scarce. However, since the 1990s public concern about the environmental issues increased, in particular about the radiological consequences of the uranium industry in Bulgaria [104, 105]. Notably, radon-related problems due to industrial activity can be found not only in uranium industry, but also in other mining and non-mining branches. A typical example in Bulgaria is the copper mining centre "Rosen" near Bourgas. Due to elevated uranium content in the cooper ore and to the practice to dispose

the wastes from the flotation factory in the Black sea, in the area of the bay of Vromos large areas were radioactively contaminated. Awareness of these problems put a priority on radon measurements in the human environment. In contrast to radiation monitoring in underground mines, where most of the measurements were grab-sampling for radon and/or radon progeny, in dwellings integrated long-term radon measurements are recommended [1].

In this chapter we emphasize on radon-related radiological research performed after 1992. This includes:

- Comprehending the large number of measurements carried-out in the mining industry and making analysis, in order to calculate the annual average radon progeny exposure in working places in the major Bulgarian uranium mines and in Bourgas copper mines.
- Providing dosimetry data to carry-out sound statistical analysis of the medical data on bronchial dysplasia (pre-neoplastic lesion) in underground miners and its relation to ^{222}Rn progeny exposure [106].
- Investigations on the radon problem in regions of increased radon risk. This included areas affected by the uranium industry (regions near Sofia – Bouchovo, Yana, Gorni Bogrov, Dolni Bogrov etc.; the region of Eleshnitsa – the second center of uranium industry in Bulgaria) as well as the town of Rakovsky - where chronically increased lung cancer incidence has been observed.

IV.1. Radon and radon progeny in underground mines in Bulgaria

Radon measurement in the Bulgarian uranium industry commenced in 1956 and since 1958 they had been conducted regularly till the cessation of this

industry in 1992. In mines outside the uranium industry, systematic radon/radon progeny measurements were made in the Bourgas copper mines of the group of "Rosen" (namely: "Propadnala voda", "Rosen" and "Meden rid"). There is also data on radon/radon progeny measurements in some other metal mines (e.g. "Obrochishte", "Bakadjik", some mines of GORUBSO Co.), but they were not systematic and could hardly be used for exposure evaluation.

Until 1972 the radiation monitoring of the underground mines was based only on radon measurements. In the interval 1972-79 parallel measurements of ^{222}Rn and the individual concentrations of its short-lived decay products were made. After 1980 the measured quantity was PAEC of ^{222}Rn decay products. Radon measurements have been made by ionization chambers SG-1M and that of ^{222}Rn progeny by aerosol radiometers type RV-4 (individual concentrations) and IZV-3 (only PAEC). The combined ^{222}Rn + ^{222}Rn progeny measurements in 1972-1979 were used to "glue" radon data before 1972 with radon progeny data after 1979. Different methods for ^{222}Rn progeny measurement were employed, but most of the measurements were made by those of Markov et al. [63] and that of Kapitanov et al. [107]. Both methods employ gross alpha counting in two intervals. After 1980 practically all measurements in underground mines were measurements of PAEC of radon progeny by aerosol radiometers IZV-3. The problems of comparison of different methods and the procedures of their calibration and performance testing have been discussed elsewhere [101, 102]. The general conclusion is that the relative uncertainty of a single measurement is in all cases less than 50% and in most cases less than 30% [99, 100].

After 1990 an extensive work started to comprehend the whole database of radiation measurements in underground mines. The goal targeted was: using measurements made in underground working places to calculate the annual average PAEC in any monitored mine for any monitored year. On this basis to calculate the "average radon progeny exposure" for any mine and for any year for which radiation data is available.

This exposure estimate actually refers to a "virtual" average miner. However, given the absence of detailed records of the distribution of miners in different working places, this was considered as the only possible task that can be addressed.

Traditionally, radon progeny exposure is expressed in units WLM (Working Level Month – see glossary before the Reference section). One WLM corresponds to exposure at PAEC of 1.3×10^5 MeV/L (or 1 WL) for 170 h [108]. The relation to SI units is 1 WLM = 12.75 J s m^{-3}. For any large mine (small mines were not included in the analysis for the absence of a systematic radiation data) the annual average PAEC at the underground working places was calculated. Using the annual working hours, which according to the Bulgarian legislation were 2000 h till 1961 and 1700 h after 1961, the "average annual exposure" was calculated. For the years till 1972, when only ^{222}Rn was measured, the approach was as follows. Using the data for the years 1972-79, the average equilibrium factor (F-factor) has been determined. As seen in Tables IV.1. and IV.2., the F-values differ among different mines, but for a single mine the variation is usually smaller. Therefore, in data analysis an individual F-factor for any single mine was applied. In this way the radon progeny exposure has been determined for every year since 1958. The algorithm to convert ^{222}Rn concentration to PAEC using F-factor is as follows:

$$EEC = 0.105C_{A1}+0.516C_{A2}+0.379C_{A3} = C_A(^{222}Rn).F \qquad (IV.1)$$

$$PAEC(WL) = PAEC\ (MeV\ L^{-1})/1.3\times10^5 = 2.67\times10^{-4}\ EEC(Bq\ m^{-3})$$

Table IV.1. F-factor in major uranium mines in Bulgaria.

Mine	Average F-factor	Range of values
9 Septemvri	0.47	0.42 – 0.53
Eleshnitsa 1	0.78	0.71 – 0.97
Eleshnitsa 2	0.86	0.79 – 0.97
Smolyan	0.74	0.63 – 1.0
Bjalata voda	0.72	0.66 – 0.87

For one mine (Seslavci) no F-factor data was available, therefore in the calculations the same F-factor as that in the close-by mine "9 Septemvri" was used. For other mines radiation monitoring started immediately in units of PAEC.

Table IV.2. F-factor in Bourgas cooper mines.

Mine	Average F-factor	Range of values
Propadnala voda	0.60	0.50 – 0.77
Rosen	0.53	0.37 – 0.62
Meden rid	0.48	0.40 – 0.67

The cumulated WLM exposure (CWLM) for a certain mine for the period since radiation monitoring there started was calculated as follows:

$$CWLM(n) = \sum_{i=i_0}^{n} WLM(i), \qquad \text{(IV.2)}$$

where i_0 is the year in which the radiation monitoring in this mine has started. In this way, the radon progeny exposure (WLM) of an "average miner" that has worked in this mine from the year n_1 to the year n_2 is calculated as $CWLM(n_2) - CWLM(n_1)$. The CWLM for uranium mines is illustrated in Fig. IV.1. and IV.2. and that for Bourgas cooper mines in Fig. IV. 3.

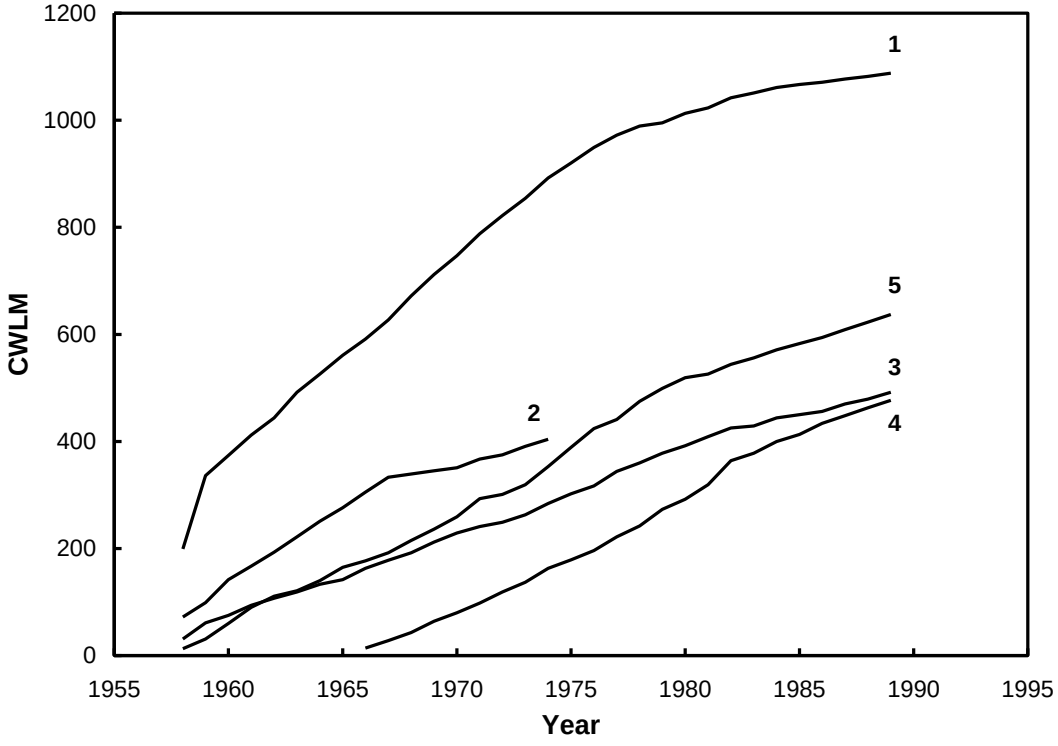

Figure IV. 1. Cumulated from the start of operation WLM exposure (CWLM) in uranium mines in which the work started before 1970 and part of the measurements are of ^{222}Rn gas alone. Legend: 1 – 9 Septemvri, 2 – Seslavci, 3 – Eleshnitsa 1, 4 – Eleshnitsa 2, 5 – Smolyan.

Figure IV. 2. Cumulated from the start of operation WLM exposure (CWLM) in uranium mines which work started after 1972. All radiation data is based on direct measurements of ^{222}Rn progeny. Legend: 1 – Bjala voda, 2 – Balkan, 3 – Smolyanovci, 4 – Eleshnitsa 3.

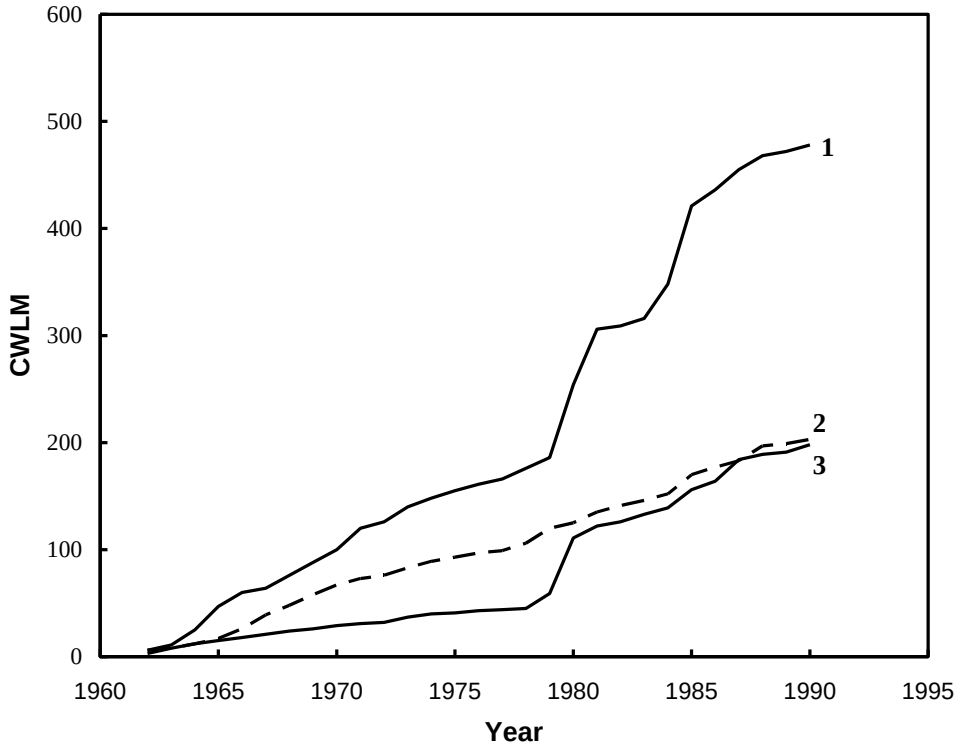

Figure IV. 3. Cumulated from the start of operation WLM exposure (CWLM) in Bourgas cooper mines of the group "Rosen". Legend: 1 – Propadnala voda, 2 – Rosen, 3 – Meden rid.

The error analysis in these WLM-estimates is problematic. From one side the radiation levels at different working places in one mine are different and from another almost every miner changes several working places within one year. Therefore, some "smoothing" of the individual exposures can be assumed, although the available database didn't allow us to make more detailed statistical analysis of the individual exposures. We used the results of the analysis of other authors based on similar data base [109, 110]. They evaluated that calculated by this approach individual exposures have uncertainty typically within 30%.

The evaluated exposures in different mines were used to study the correlation between ^{222}Rn progeny exposure of underground miners and respiratory pre-neoplastic lesions.

IV.2. Bronchial dysplasia in underground miners exposed to ^{222}Rn progeny

The development of bronchial malignancy involves progressive changes in the bronchial epithelium, from cell metaplasia to malignant transformation [111]. The occurrence and progress of metaplasia is dependent on smoking, toxic inhalants and inflammatory diseases. The stages that precede the development of carcinoma are reversible and lung cancer develops only in a small proportion of the cases of epithelial cell transformations. The examination of exfoliated metaplastic cells, found in the sputum, has shown that cell transformation occurs in the bronchial epithelium long before the development of clinical symptoms of lung cancer. These observations led to research on sputum cytology as a method for cancer prophylaxis in high risk groups [112-114] and it was also adopted in medical examinations of uranium miners [115]. To study possible dose-frequency response of proportions of miners with atypical metaplastic cells (to the level of notable dyspalsia, as defined in [106]) a cytological study has been carried-out in the 1990s in Bulgaria. The research team a included medical doctor, a physicist (the author – responsible for study design and miners' exposure estimates) and a statistician. The studied cohort was of 434 underground miners (334 exposed and a control group of 100 miners from a mine, where elevated levels of radon progeny were not found). The entire cohort was of active miners that had still worked underground at the time when the study had been made. They were selected at random from workers in five uranium and six metal mines in Bulgaria. The miners were classified into three categories of smokers: the smokers group included only people who smoked >10 cigarettes per day for at least five years.

The group of non-smokers included people who had never smoked. Ex-smokers and moderate smokers who were exposed to ^{222}Rn were constituted as a third group (there were no ex and moderate smokers among controls).

Sputum samples were taken and analyzed by the medical expert in the research group. The specimens were classified as having dysplasia following the definitions and classifications of Refs. [113-115].

The risk of dysplasia in relation to exposure to ^{222}Rn progeny, smoking, and underground work experience was studied by logistic regression analysis [116]. The determination of the 95% confidence intervals (95% CIs) was based on the likelihood ratio criterion. The data were analyzed by the statistical package SPSS/PC+, version 4.01.

In all the uranium mines and in three of the metal mines the data from long term radiation monitoring was available. The 233 miners from these mines were defined as group A. For each of them individual exposure was determined, as described in the previous section. In the remaining two metal mines, ^{222}Rn progeny has been measured since 1991. The results have shown elevated levels of ^{222}Rn progeny in the mines' atmospheres, but the real past exposures could not be determined directly. Their range was estimated by extrapolation, assuming the same annual exposure in the past as in the years for which data was available. The smokers and non-smokers from these mines were defined as group B. The ex and moderate smokers were defined as group C. A detailed description of the groups is shown in Table IV. 3.

Table IV.3. Description of the groups of miners.

	Group A (n=233)	Group B (n=79)	Group C (n=22)	Controls (n=100)
Smokers	140	55	-	42
Age (mean (SD, range) y)	40.3 (6.0, 20-59)	40.0 (8.2, 23-56)	37.3 (6.2, 25-44)	42.9 (5.3, 24-51)
Work duration (mean (SD, range) y)	9.5 (5.6, 1-24)	7.4 (5.3, 2-28)	8.1 (5.7, 2-21)	11.7 7.5, 1-25)

The data in Table IV.3 shows similar distributions of age and underground work practice for exposed and not exposed groups. Therefore, the exposures to silica, dust, and other toxic inhalants (not radon) were expected to be similar. The study showed 87 cases of dysplasia among the 334 miners in groups A, B, C (frequency 0.26, 95% CI = 0.21 – 0.31) versus three cases among the 100 controls (0.03, 95% CI: 0.007 – 0.077). Thus, the higher occurrence of dysplasia in exposed miners was significant ($P<0.0001$). This study also revealed dose-response correlation in the exposed group, which can be seen in Table IV.4.

Table IV. 4. Frequency of dysplasia by exposure

Group	Exposure (WLM)	Non-smokers		Smokers	
		Dysplasia/ total	Frequency (95% CI)	Dysplasia/ Total	Frequency (95% CI)
A	0 – 50	2/45	0.044 (0.007-0.132)	7/37	0.19 (0.085-0.335)
	50 – 150	7/27	0.26 (0.12-0.44)	26/77	0.34 (0.24-0.45)
	> 150	8/21	0.38 (0.19-0.59)	19/26	0.73 (0.54-0.88)
B	2 - 70	4/24	0.167 (0.054-0.348)	8/55	0.145 (0.069-0.255)
C	2.5 - 346			6/22	0.27 (0.11-0.48)
Controls		2/58	0.034 (0.006-0.10)	1/42	0.024 (0.001-0.10)

The stepwise logistic regression analysis made with data for group A revealed statistically significant correlation between the frequency of dysplasia and both ^{222}Rn progeny exposure ($P<0.0001$) and smoking ($P=0.0016$). The underground work experience did not fit the criteria for significance. These results suggest that the prevalence of the dysplasia frequency in the exposed group is probably related to ^{222}Rn progeny exposure. The relation of the risk of dysplasia and ^{222}Rn progeny exposure and smoking was quantified by logistic regression analysis. In the model employed the risk of dysplasia was estimated as:

$$\frac{\exp(-2.79+0.012WLM+1.089Sm)}{1+\exp(-2.79+0.012WLM+1.089Sm)}, \qquad \text{(IV.3)}$$

where smoking (*Sm*) is treated as dichotomous variable (0=non-smoker, 1=smoker). The numerical coefficients for smoking (1.089), exposure in WLM (0.012) and the constant (-2.79) are the maximum likelihood estimates derived by logistic regression. In general the results for groups B and C gave semiquantitative support to the exposure-response relation found for group A.

The conclusion from this study was that the miners' exposure to ^{222}Rn progeny results in a significantly increased frequency of squamous cell metaplasia. At the level of notable dysplasia this frequency follows an exposure-response relation.

IV.3. Radon in the environment in Bulgaria

Due to the limited resources available for radon studies in Bulgaria, large scale national survey and radon mapping of the country are not yet completed. Instead, in the last two decades the efforts were focused on relatively small scale studies in „radon risk areas". Up to now we have revealed and regularly studied three such areas:

- The village of Eleshnitsa. This was the second center of former uranium industry in Bulgaria. Radon concentrations in this village are increased in most of the dwellings as well as outdoors [24, 117];
- The town of Rakowski (population about 17 000).
- Areas near Sofia, affected by uranium industry. These include the town of Bouchovo (the main center of uranium mining and milling industry in Bulgaria) and several villages near by (Yana, Gorni Bogrov etc.).

IV.3.1. The case of Eleshnitsa

In Bulgaria, high concentrations of ^{222}Rn were observed in the village of Eleshnitsa (first outdoors [24, 117]). Large areas in this region are contaminated with wastes from the uranium industry. The region as a whole exhibits enhanced radioactivity associated with natural uranium. There was not any other industrial air pollution in this valley. To study the radon problem there, a systematic survey commenced in 1992. This included ^{222}Rn and ^{222}Rn progeny measurements outdoors and indoors, as well as measurements of the concentrations of ^{222}Rn in soil gas [24].

The basic methods used for ^{222}Rn progeny measurements were [63, 67]. About 400 grab samples were taken in 1992-1994 in different seasons and at random moments of the day and night. Similar measurements were also made indoors, in some dwellings.

The ambient concentrations of ^{222}Rn progeny showed diurnal pattern, illustrated in Fig. IV.4. This pattern is close to the "typical" for the outdoor air [118]. The PAEC varied in the interval from <200 MeV/L to about 14000 MeV/L. The averaged diurnal distribution for the period 1992-94 is shown in Fig. IV. 5. The average PAEC based on these measurements was found to be about 2300 MeV/L and the annual exposure due to outdoor radon was estimated to be about 0.9 WLM.

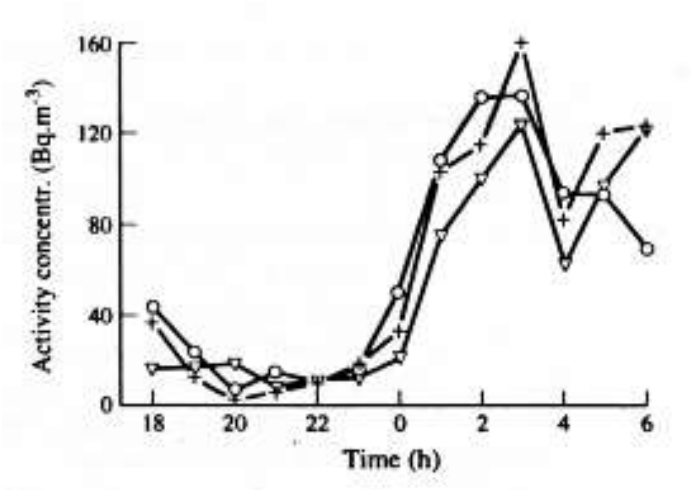

Figure IV. 4. Typical trend of the activity concentrations of ^{222}Rn progeny in late afternoons and nights. Legend: (○) ^{218}Po, (+) ^{214}Pb, (∇) ^{214}Bi.

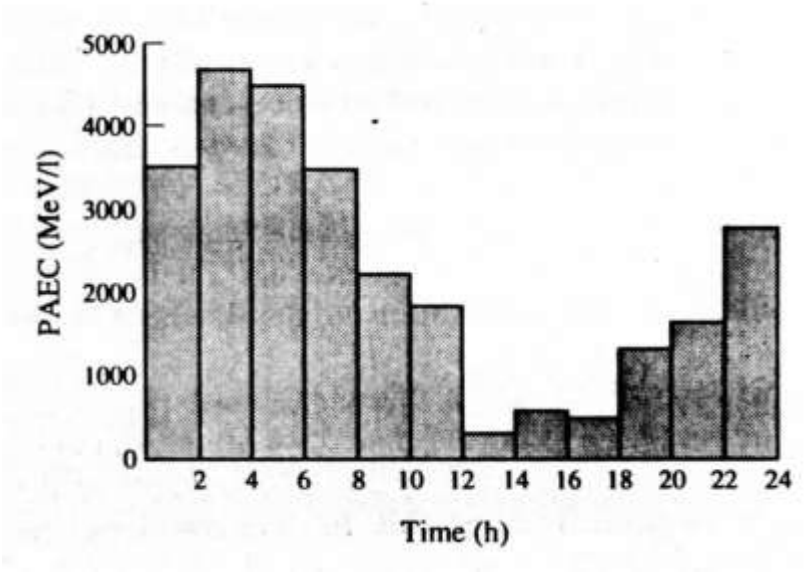

Figure IV.5. Daily variation of the PAEC outdoors in the village of Eleshnitsa.

IV.3.1.1. Sources of ^{222}Rn outdoors

The following potential sources of ^{222}Rn in the valley of Eleshnitsa have been considered:

- Radon exhalation from contaminated and non-contaminated areas;
- Exhaust air from mine ventilation;
- Natural exchange of air between open mine adits and pits.

^{222}Rn in soil gas was measured by integrated measurements through diffusion chambers with passive detectors placed inside (these were solid state nuclear track detectors Kodak-Pathe LR-115 type II and thermo-luminescent detectors of $CaSO_4$:Dy + 5% B_4C). The plastic boxes were buried at depth of 60 cm and left there for a controlled time.

The ^{222}Rn levels in soil-gas in non-contaminated soil in the village were relatively low. The average background value (at depth 60 cm) outside the valley was 4 kBq m^{-3} [24], while in the village it was 7 kBq m^{-3}. However, the area is surrounded by wastes and waste residuals from the former uranium mining and milling and the whole valley is of enhanced natural radioactivity and rich in surface radioactive anomalies. The soil gas concentrations there were substantially higher, the averages being in the range 50 – 400 kBq m^{-3} and up to 1400 kBq m^{-3} in some radioactive anomalies [24]. The measured soil-gas ^{222}Rn concentrations were higher in the summer.

There was not any data about the ambient ^{222}Rn concentrations in this valley before the beginning of uranium industry. This hampered evaluation of the impact of the uranium industry on radon contamination of the air. The main single source related to uranium industry was the central ventilation of the mines. It released, during mines' operation $(0.3 – 1)x10^7$ Bq/s in the atmosphere. About half of this amount was emitted near the village. In the first report on outdoor

radon in the valley [117], the mines ventilation was considered to be the most important cause for the elevated levels of outdoor radon. However, about 100 measurements in 1992 were in periods during which mine ventilation was stopped for a long time. Notably, no difference in the PAEC distribution was observed, the average value being the same: 2300 MeV/L. Based on these observations, we excluded the ventilation exhaust as dominating radon source for the village as a whole. The power of mine adits as radon sources was much smaller than that of the active ventilation. Among all sources of ^{222}Rn, probably the dominating is the exhalation from the large natural radioactive anomalies. The mining and milling wastes are serious sources, but based on the measured ^{222}Rn concentrations in the soil-gas and in the area of contaminated sites (0.2 km^2 mining and 0.42 km^2 milling wastes) they are unlikely to release more radon in the atmosphere than the anomalies and the sandstone hills surrounding the valley. The soil underlying the village has much lower concentrations of ^{222}Rn in soil gas and its contribution to the outdoor concentration is assumed to be of secondary importance.

IV.3.1.2. Indoor ^{222}Rn in the village of Eleshnitsa

Three campaigns of indoor ^{222}Rn measurements were carried-out in the interval 1995-2001. The measurements in 1998-99 covered one year period. They were made by diffusion chambers with Kodak Pathe LR-115/II detectors placed inside. The histograms of the distributions for living areas and basements are shown in Figs IV.6. and IV.7. In 2000-2001 a subset of measurements was made on the 1st and second floors. The statistical summary is shown in Table IV.5. During the measurement period the average outdoor ^{222}Rn concentration was about 80 Bq m^{-3} which corresponds to the early estimates and suggests that there is not a systematic trend in the outdoor radon concentrations in the village. In part

of the houses ^{222}Rn progeny measurements were made and the F-factor determined. The mean value of the equilibrium factor was F= 0.65.

Table IV. 5. Statistical summary of the whole-year (1998-1999) ^{222}Rn measurements in Eleshnitsa. Non-parametric analysis [119] is applied for the 95% CI of the median.

Floor	**Number of measurements**	**Arithmetic mean Bq m^{-3}**	**Median (95% CI) Bq m^{-3}**
Basement	36	490	245 (204 - 550)
1st floor	104	288	200 (180 – 251)
2nd floor	97	220	151 (138 – 175)
1st and 2nd floors	201	255	178 (164 – 190)

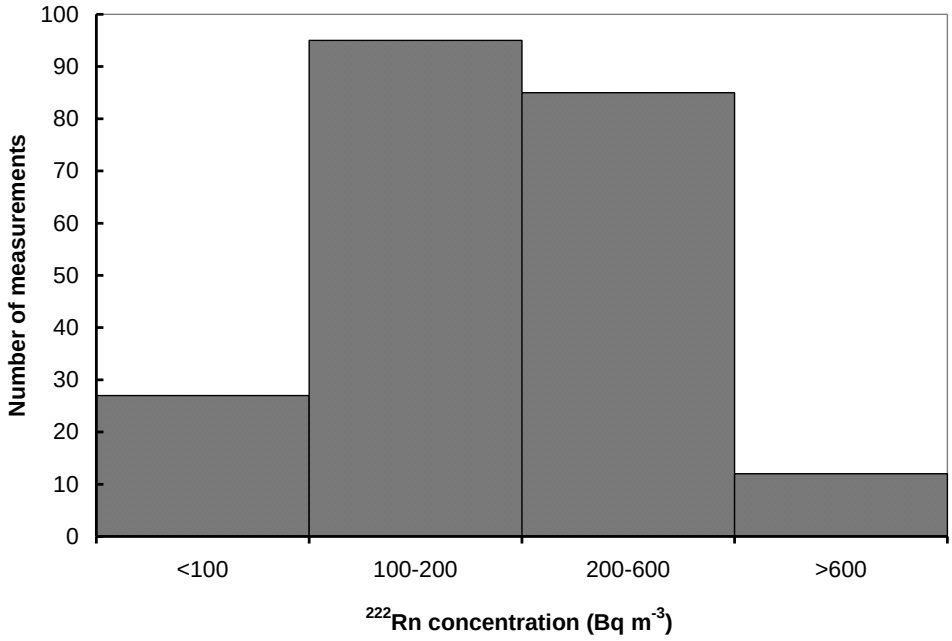

Figure IV.6. Histogram of ^{222}Rn concentrations measured in houses in the village of Eleshnitsa.

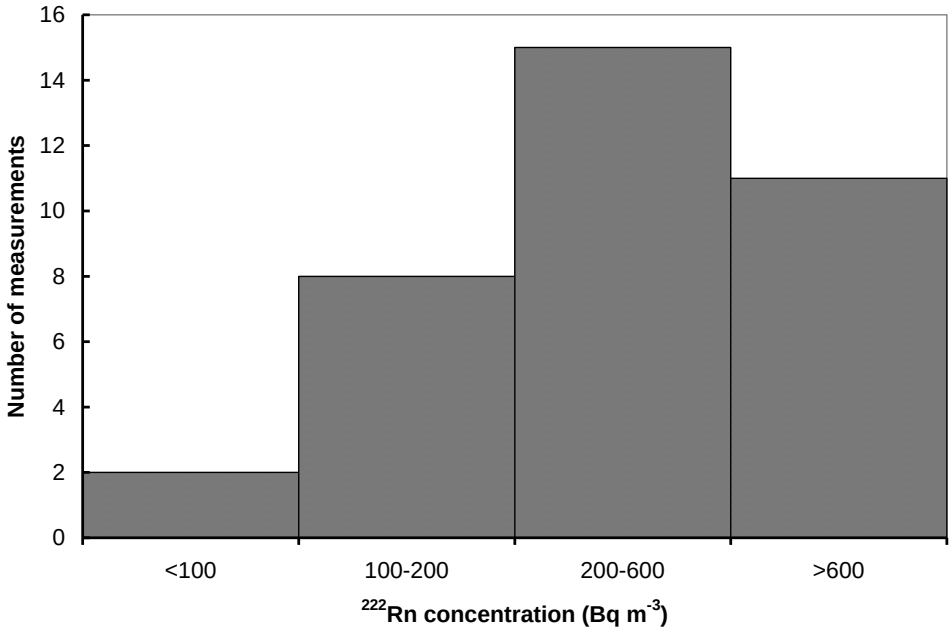

Figure IV.7. Histogram of ^{222}Rn concentrations in basements in the village of Eleshnitsa.

The concentrations on the first floor are on average significantly higher than that on the 2nd floor. The maximum concentration measured indoor was about 3300 Bq m^{-3}.

In conclusion the basic features of the radon problem in Eleshnitsa are:

- Relatively high outdoor ^{222}Rn and ^{222}Rn progeny concentrations were observed with the annual mean of ^{222}Rn being about 80 Bq m^{-3}. The diurnal variations were significant with night values normally exceeding by more than an order of magnitude those during the day. The reason for this feature is in the generally enhanced natural radioactivity in the valley where the village is situated and the specific meteorological conditions on the spot: poor air circulation and frequent air stagnation. The maximum in the concentrations is normally observed after midnight, under conditions of air stagnation and at that time normally full equilibrium between ^{222}Rn and ^{222}Rn progeny is observed. The seasonal maximum of outdoor radon is in the summer and the minimum in the winter, the difference being a factor of two. The soil gas ^{222}Rn concentrations are also higher in the summer.
- The results from the survey of ^{222}Rn indoors revealed an annual mean varying throughout the years within the range 205-255 Bq m^{-3}, a geometry mean within 162-178 Bq m^{-3} and, in about one third of the houses, concentrations exceeding 200 Bq m^{-3}.

An analysis of lung cancer incidence was not made in the village firstly because the population is too small and secondly, because a severe bias due to the high lung cancer incidence among the significant number of ex-uranium miners living in the village was anticipated.

IV.3.2. The case of the town of Rakovski

The unusually high lung-cancer incidence in the town of Rakovski (population about 17 000) has been observed since the National Cancer Registry of Bulgaria exists [120]. No local industrial activity or man-made pollutants could reasonably explain the risk. Based on the available information, it appears that the first radon measurements there were made in the winter of 1997-98 [121]. This winter (December-February) survey revealed average concentrations of about 360 Bq m^{-3} (range 25 – 1200 Bq m^{-3}). These results warned about the radon problem in the town and more detailed investigations were carried-out in 1999-2001 [122].

The basic method of measuring indoor ^{222}Rn concentrations was that of the diffusion chambers with alpha-track detectors Kodak-Pathe LR-115 type II. These chambers were calibrated with the primary ^{222}Rn standard in Laboratoire National Henry Becquerel, CEA-Saclay, France. Details of this procedure are provided in Chapter II.

In 1999-2000 parallel measurements were made in 61 houses with a case of lung cancer among the inhabitants, which was observed in the period 1981-1998 and in 136 houses without registered lung cancer cases. The average mean ^{222}Rn concentration was about 27% higher in the houses with lung-cancer case than the others, the difference being significant at 90% level. We still interpret this difference with caution, as only being indicative for possible contribution of the radon exposure to the increased risk.

The estimates of the annual mean concentrations are based on measurements in 157 randomly selected houses. The measurements were conducted from March 2000 to March 2001. The average annual mean concentration was 234 Bq m^{-3}, the geometry mean 186 Bq m^{-3} and in about 50% of the houses the annual mean concentrations were higher than 200 Bq m^{-3}. For

comparison, the world average proportion of homes exceeding this level is about 2% [2, 17, 18]. The distribution of the annual mean concentrations is shown in Fig. IV.8.

During the 2000-2001 survey a questionnaire was delivered to the inhabitants of the rooms where measurements were conducted. In this questionnaire, among other things, there was an inquiry about the smoking habits in the studied rooms. In 76 out of 157 houses an unambiguous answer was obtained. The distribution of concentrations in this sub-set was found to be alike in smoking and non-smoking rooms, the average annual mean being about 215 Bq m^{-3}, with only 2 Bq m^{-3} non-significant difference between smoking and non-smoking rooms. Therefore, we don't expect our findings to be strongly confounded by the smoking habits.

Preliminary study of smoking habits revealed, that the proportion of smokers among the men in Rakovski is about the same as among the men in the urban population of Bulgaria, while among women it is most probably lower than the average proportion of smokers among urban women.

The lung-cancer risk in Rakovski was analyzed using the data derived from the cancer registry. In Rakovski the mobility of the population is low. One reason is that this is the largest catholic center in Bulgaria, mostly orthodox country, and the level of migration is low. The lung cancer cases for a period of 19 years (1981-1999) were taken from the National Cancer Registry, Bulgaria. That Registry is population-based and has been collecting all new cancer cases, diagnosed since 1968. The reporting is fairly complete, as hospital departments, physicians and pathologists are obliged to report all new cancer cases all over the country. The expected number of cases was determined using cancer incidence data for the urban population of Bulgaria for the same time interval. The observed number was treated as a Poisson variable and the statistical analysis was made by conventional methods [119].

The essential features in the lung cancer incidence data, shown in Table IV.6. are as follows [123]:

a) Significantly increased risk – about twice for both sexes, compared to the urban population of the country, which has higher incidence than the rural one;
b) The relative risk for young males (≤ 49 yr.) is about 1.8 times higher than that for aged ≥ 50 yr., the difference being significant. The observed number of female lung cancer cases is too small to conclude about such an effect. No other cancers, except lung-cancer, showed significantly higher incidence rates than the control population.

These considerations should be classified as an "ecological study". These studies can be subject of uncontrolled bias of confounding factors [124] and cannot be considered as an evidence for real statistical correlation. However, the region of Rakovski is not an "unique radon hot-spot". Similar areas are also found elsewhere [125, 126]. Targeting population that lives at high radon exposures and has low residential mobility may help to improve the risk estimates [127]. In the present study there are several major indications that ^{222}Rn exposure may contribute to the lung cancer risk: a) equally increased relative risk for males (mostly smokers) and females (mostly non-smokers), b) indication for higher ^{222}Rn concentrations in houses with a case of lung cancer among the inhabitants, c) the significantly higher risk for young males.

Table IV.6. Cases of lung cancer in the town of Rakovski in 1981-1999 using the rates of the urban population of Bulgaria as a standard.

Group	Observed	Expected	SIR* (95% CI)	P-value
Males, ≤ 49y	34	10.28	3.31 (2.29-4.62)	$< 10^{-4}$
Males, >49y	140	74.36	1.88 (1.58-2.22)	$<10^{-6}$
Males, all ages	174	84.64	2.06 (1.76-2.39)	$<10^{-6}$
Females, all ages	27	14.19	1.90 (1.25-2.77)	$<10^{-2}$

- SIR = standard incidence ratio

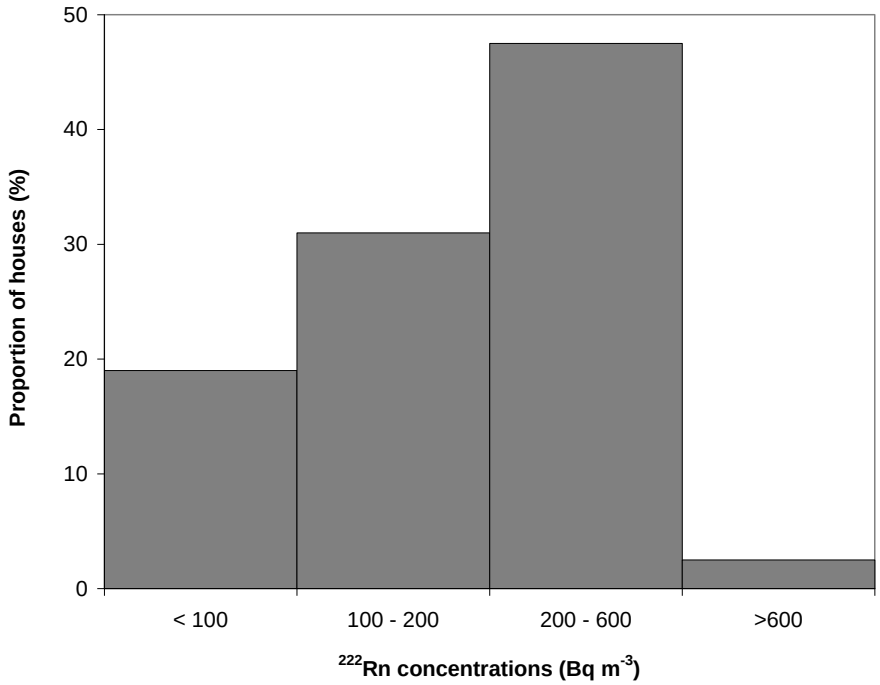

Fig. IV.8. Distribution of the annual mean ^{222}Rn concentrations in dwellings in the town of Rakovski obtained in the measuring campaign 2001/2002.

In conclusion we suggest that making an analytical epidemiological study in Rakovski and, eventually, pooling it with other risk groups in high radon areas may lead to more precise direct risk estimates in shorter time and with less

resources than pooling large epidemiological studies that are diluted by the great number of persons who live at low radon exposures.

IV.3.3. The case with areas affected by the uranium industry close to Sofia

Uranium industry in Bulgaria commenced in 1945 under Soviet control. The first mining centre was near the town of Bouchovo, about 23 km from the city of Sofia, the capital of the country. The uranium deposits in the region around Bouchovo have been object of interest, exploration and pilot technological attempts by German and Bulgarian experts and organizations, even before 1945, but not at industrial magnitude. As a result of mining and milling activities in the 40s and 50s and due to the absence of adequate radioactive waste management large areas have been radioactively contaminated. The contamination is mainly from the uranium milling wastes which were released freely in the environment till 1958. In the next decades several radiological investigations have been made in the affected region, but the number of radon and radon progeny measurements (mostly grab sampling measurements) was rather limited. Still, they indicated elevated radon concentrations in some dwellings [128, 129].

In 2003-2004 a radon survey was carried-out in areas near Sofia, affected by the uranium industry. The measurements were made by the commonly used diffusion chambers with Kodak-Pathe LR-115/II detectors exposed for 3 months. The histogram of the distribution is shown in Fig. IV.9.

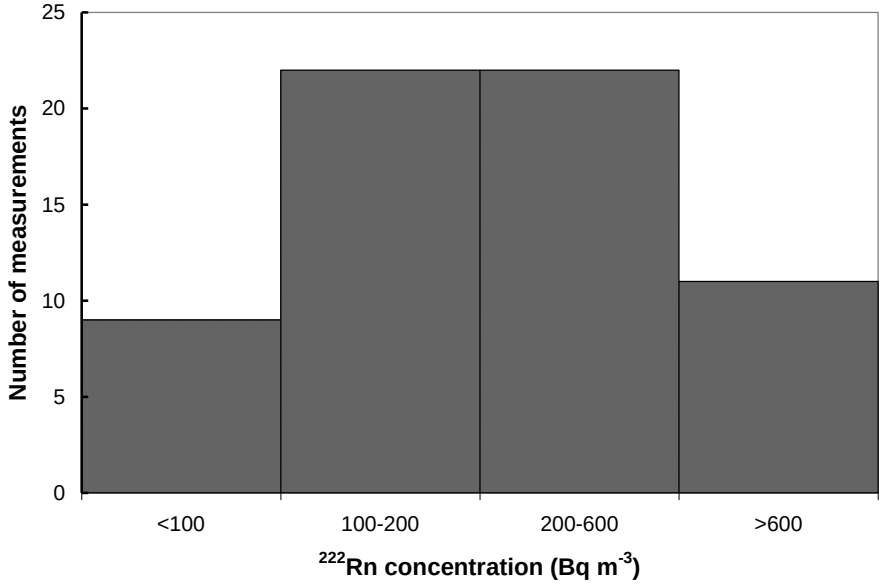

Figure IV. 9. The histogram of the distribution of ^{222}Rn concentrations in houses in Bouchovo, Yana, Gorni Bogtov and Seslavci.

Results clearly indicated that in about 50% of the dwellings in this area ^{222}Rn concentrations are > 200 Bq m^{-3}. This revealed radon prone area with significant radon risk. In a further study, still ongoing in this region, CDs/DVDs stored indoors are analyzed, using the CD-method for retrospective radon measurements [130, 131]. The pilot results also suggest elevated radon in this area [130].

In search of the source of radon indoors, ^{222}Rn measurements in soil gas were organized. These measurements were integrated, by diffusion chambers buried at depth 60 cm. The average background concentration was 6.0 ± 0.7 kBq m^{-3}. The levels in the contaminated areas were substantially higher: from 13 to 820 kBq m^{-3}, the last value being measured in the village of Yana. It should be also mentioned that the first radon mitigation systems in Bulgaria were installed in risk dwellings in this area. The author provided technical consultancy for their design and installation [132]. The technical design followed established technical standards and practices [133, 134]. Figure IV.10 illustrates the efficiency of the

combined (passive+active) mitigation system installed in the kindergarten of Gorni Bogrov.

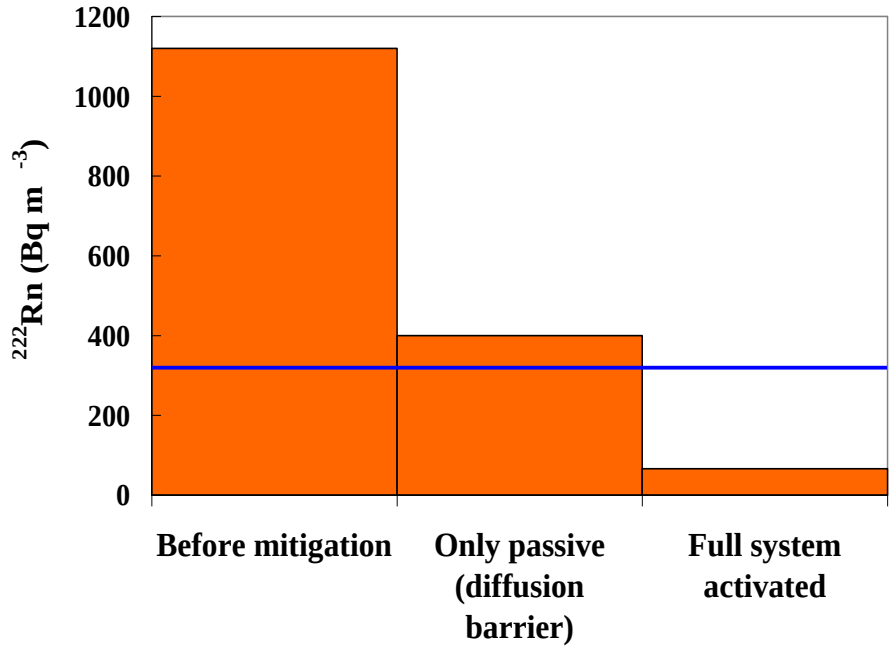

Figure IV.10. Reduction of ^{222}Rn concentrations by passive barrier alone (200 μm polyethilenne soil-gas retarder + 3 cm floor cement coat) and after the switching on the active sub-slab depressurization (full system). The horizontal line is the maximum permissible mean ^{222}Rn activity concentration (300 Bq m^{-3}) according to the current Bulgarian legislation [135].

The gathered experience allowed to test in 2012 an integrated approach to the radon problem in dwellings. Within this approach all steps of the basic process: "detection of the problem → diagnostic measurements → mitigation" are considered as an united whole. The results of its practical application in 2012, in which most of the methods described in this dissertation were used in practice is illustrated in Annex II.

V. POLYCARBONATE METHOD. KEY CONCEPT AND METHODOLOGICAL BACKGROUND.

To use polycarbonate materials of high radon absorption ability for measuring radon was first proposed by the author in 1999 and the first experiments were made in collaboration with researches from the University of Ghent, Belgium [136, 137]. This "polycarbonate method further" revealed a clear potential to contribute for efficient solution of some important problems in radon dosimetry [137-140] and for measurement of other radioactive noble gases [141, 142]. The chapters V, VI and VII are dedicated to radon-related research and applications of this method.

V.1. Key concepts

The properties of bisphenol-A polycarbonates (trade names: Makrofol, Lexan etc.) as SSNTDs were studied and used for decades [143]. More recently, their remarkable ability to absorb radon was mentioned in the literature [144], but considered as a potential source of error in radon measurements. The key concept of the first (and most studied and used) version of the polycarbonate method is to employ this absorption ability in combination with the track-etch properties of such polycarbonates as a new approach for quantitative measurements of ^{222}Rn [136, 137]. Probably, the most important achievement was the development of method for precise retrospective ^{222}Rn measurements using home stored CDs and DVDs [138, 139, 145, 146]. Bisphenol-A polycarbonates are widely used as a basic constructive material for compact discs (CDs) and digital verbatile discs (DVDs). Therefore, home-stored CDs or DVDs may serve as long-term retrospective radon detectors. Except measuring in air, measurements of ^{222}Rn in

water and soil-gas were recently initiated [146-148] by different versions of the polycarbonate method.

In brief, the method consists in the following: First, a polycarbonate specimen (e.g. Makrofol-foil, CD, DVD) is being exposed to radon. During exposure the ^{222}Rn atoms that are trapped on the polycarbonate surface further diffuse in depth. After decay they emit alpha-particles and give birth to decay products, two of which (^{218}Po and ^{214}Po) are also alpha emitters. As ^{222}Rn progeny atoms rest immobilized in the polycarbonate matrix at the point of their origin, their volume distribution is the same as that of ^{222}Rn. For a polycarbonate specimen placed in radon containing atmosphere one can distinguish "external" and "internal" alpha sources. "External" to the plastic volume are alpha-particles coming from the ambient radon (^{222}Rn and ^{220}Rn) and radon progeny, as well as those from the deposited on the surface radon progeny atoms (radon progeny plate-out). The "internal" source is the absorbed ^{222}Rn and its progeny. With the method, after exposure, we remove a sufficiently thick layer from the surface and etch electrochemically alpha tracks at that depth (Fig. V. 1). This way none of the alpha-particles from the external sources can reach the etched detection spot. The "external" sources are highly variable and dependent on particular behavior of radon and radon progeny in the ambient air and close to the surface. If the layer is thicker than 80 μm (76 μm if take into account that α-particles of energy below certain threshold cannot create tracks) any influence of the „external" alpha-particles is effectively cancelled out.

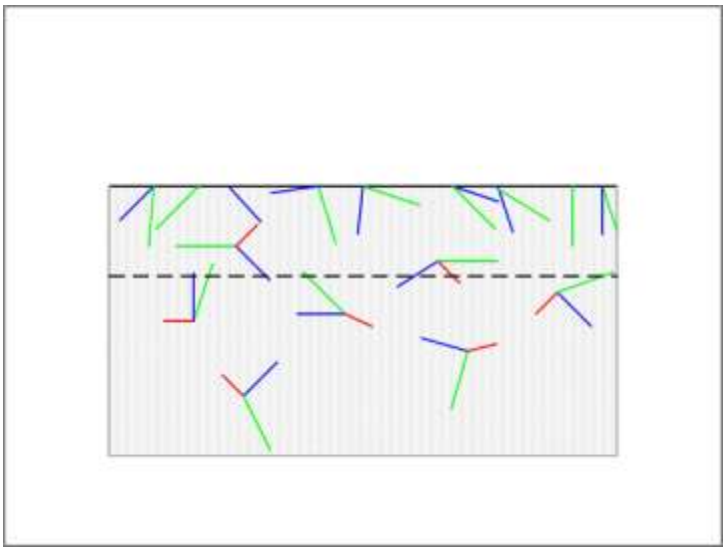

Fig. V. 1. Traces of alpha particles in the polycarbonate material. Beneath the dashed line (i.e. ≥ 76 μm beneath the surface), the traces are related only to the absorbed ^{222}Rn and its progeny (^{218}Po, ^{214}Pb, ^{214}Bi + ^{214}Po). Three alpha particles originate from one point – those of ^{222}Rn, ^{218}Po and ^{214}Po. The ^{222}Rn progeny atoms rest immobilized in the solid matrix and decay in the point of decay of the parent ^{222}Rn atom.

The first step of processing consists of removal, from the surface of the exposed polycarbonate specimen, of layer thicker than the maximum range of the alpha-particles from ^{222}Rn and ^{220}Rn progenies plate-out on the surface. This layer should be > 76 μm. Usually it is about 80 μm or more and is removed chemically. After that electrochemical etching (ECE) is applied and the tracks, which at that depth are related only to the absorbed ^{222}Rn, are counted.

V.1.1. Methodology

The methodology consists of the following steps:

- **Exposure of polycarbonate specimens** (or "detectors" as named further in the text) to radon. In retrospective mode the detectors (CDs/DVDs) are already exposed for long time (years). The exposure time with this method in air is relatively long, e.g. a year or more. However, laboratory exposures, as well as those in water and soil gas are usually shorter (days, weeks).
- **Outgasing.** After exposure the detectors are left in radon-free air to allow the absorbed radon to decay and degas for some time (about two weeks). The process of sorption and desorption of ^{222}Rn is described in section V.3. This process depends to some degree on the exposure time and the size of the specimens, but in any case the outgasing is effectively finished within about two weeks. Therefore, the time for outgasing of two weeks can be considered sufficient. The outgasing is of significance only for relatively short exposure times. In case of CDs/DVDs, already exposed retrospectively for years, skipping this step practically does not affect the results.
- **Removal of surface layer.** The necessary thickness (usually about 80 μm) is removed by chemical pre-etching (CPE). This is usually done by aqueous solution of 52% KOH (m/v) and 40% methanol (m/v) at 30^0 C. At this regime the bulk-etch velocity is about 1 μm min^{-1} and the targeted depth can be reached in a reasonable time.
- **Electrochemical etching.** The tracks at the studied depth are revealed by electrochemical etching (ECE) [149, 150]. The ECE process is performed at effective electric field in the range (for different experiments) 3.0 – 4.4 kV mm^{-1} at frequency 6 kHz (2kHz in the early experiments) and temperature 25^0 C. The etching solution is mixture of ethanol with 6M KOH solution with 1:4 volume ratio. The process starts with 30 min pre-etching with

the same solution. After pre-etching the electric field is applied for 3 hours. To apply the method for detectors of thickness 1.2 mm (CDs) or even more, a generator of variable effective voltage up to 4 kV was constructed by Ekotronik Ltd. (www.ekotronic.cz). A photo of the equipment that is installed and used at the Laboratory of Dosimetry and Radiation Protection at St. Kliment Ohridski University of Sofia is shown in Fig. V.2.

- **Track counting.** We employ mostly automatic counting by computer scanner. More details about the dedicated algorithm and software are given by Mitev et al. [151]. In some special cases visual counting, by a transmitted light microscope was done.

The "signal" of the detectors is the net track density at the studied depth. At any fixed depth (> 80 μm) it is almost perfectly correlated with the integrated ^{222}Rn activity concentration. This can be seen in Fig. V.3. This correlation is used to "calibrate" the detectors. One feature of this method, used with CDs/DVD is that two possible modes of calibration are possible: standard *(a priori)* and individual *a posteriori* calibration of detectors. These modes are discussed in the section VI.4.2.

Figure V.2. A photo of the experimental equipment used for CPE and ECE of polycarbonate detectors.

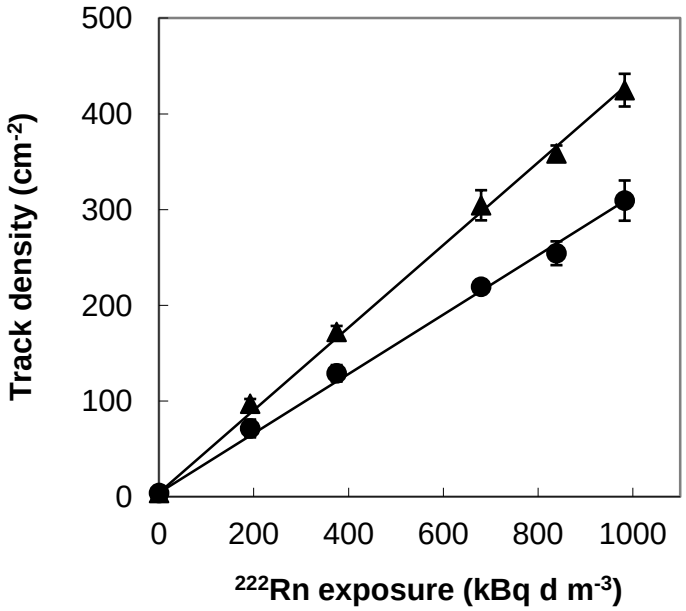

Fig. V. 3. Correlation between the net track density at depth 83 μm (▲) and 117 μm (●) beneath the front surface of Makrofol (300 μm thick plastic foil) and integrated ^{222}Rn activity concentration.

V. 2. Experimental studies

One of the first task addressed was to study of the possible influence of different factors to the experimental uncertainties. These factors include: the influence of the jewel cases of CDs, the effect of the humidity, the pressure, the temperature, dust and smoke-stained atmosphere, thoron (^{220}Rn) presence, the effect of ^{210}Po after long term exposures, laser light during rad/write of CDs/DVDs. To reveal the useful range of the method the background track density was studied and the range of concentrations quantitatively measurable by this method was evaluated.

V.2.1. Evidence that the signal at depths ≥80 μm is due only to the absorbed ^{222}Rn and its progeny.

Numerous tests have been conducted to study whether the plate-out of the ^{222}Rn progeny on the surface of the detectors contributes to the track density at the studied depths. The results are described in more detail elsewhere [137-140] and the essence is the following (all statements are valid for depth > 80 μm, but if ^{220}Rn is absent, they are true at > 64 μm):

- No tracks above the background have been observed after irradiation of the detector surface with 7.69 MeV alpha-particles with a flux up to 50,000 cm^{-2}.
- No difference in the track density has been observed when detectors were exposed bare and covered with a filter that allows radon to pass through but prevents radon progeny plate-out on the surface.
- In one experiment detectors were exposed to ^{220}Rn. In this experiment the experimentally determined alpha-particle flux from the plate-out of ^{220}Rn-progeny was about 730,000 cm^{-2}. This value was more than twice higher than the ^{222}Rn progeny plate-out alpha flux in the highest exposed group in ^{222}Rn laboratory experiments, but no significant effect was observed. The track density at 83 μm depth was 10.0 ± 1.2 cm^{-2}, while in the highest ^{222}Rn exposure group of detectors it was > 400 cm^{-2}. Even the small increase of the track density above the background (3.8 ± 1.1 cm^{-2}) could be due to the small amount of the absorbed ^{220}Rn, not to the plate-out contribution. Although, in principle, some plate-out contribution from the rare ^{212}Po long-range alpha-particles could be expected at 83 μm, the numerical estimates showed that this is negligible.

- After a set of 10 detectors were exposed to one and the same ^{222}Rn concentration, in half of them 83 μm were removed mechanically from the surface. This mechanical treatment removes virtually all latent tracks from "external sources". In the remaining half the same layer was removed by CPE. Afterward ECE was applied for both sets. The net-track density of the mechanically treated detectors was 297 ± 16 cm^{-2} and that of the detectors treated by CPE was 289 ± 22 cm^{-2}. We consider the statistically identical signal in both cases as a direct evidence for the absence of any plate-out contribution to the tracks at the studied depth.
- There is no difference in the signal between bare CDs and those exposed in their jewel cases. In these cases there is a small (≈1 mm) air gap between the front surface of the CD and the board of the case. Under such circumstances the plate-out on the surface is substantially lower than in the bare mode [152]. Therefore, a significant difference in plate-out contribution would result in a significant difference in the track density. However, there is no indication, even small, for such difference.

Given this evidence, we firmly interpret the tracks at a depth > 80 μm (76 μm) are related only to the absorbed ^{222}Rn and its progeny, thus any plate-out contribution being cancelled-out.

V.2. 2. Factors which influence has been studied

The prospects for implementation of this method seem to be considerable. Therefore, experiments were carried-out to study thoroughly the performance of the method and the influence of different indoor environmental factors that might contribute to the uncertainty. For all irradiation experiments, the detectors were

placed in hermetic laboratory vessels (0.23 m^3 glass bulbs or 0.011 m^3 metal pans). The radon was supplied by a certified source (Model Rn 1025 radium source; Pylon Electronics Inc., Canada). During the exposures the radon concentrations were followed by reference measurements with Lucas-cells, which were calibrated with a National Physical Laboratory (UK) primary radon standard. The uncertainty of a single measurement is less than 3%.

In many laboratory studies, spread over one decade time, the following environmental factors were found to have little or no effect:

- **Pressure**: Studied over 57 – 148 kPa range. The pressure experiment was performed with 3 sets of CDs exposed to the same integrated radon concentration (529 kBq d m^{-3}) at three different pressure levels (57.4 kPa, 100.6 kPa and 147.7 kPa at 23.5 °C). No significant effect seen [140] as seen in Fig. V.4.

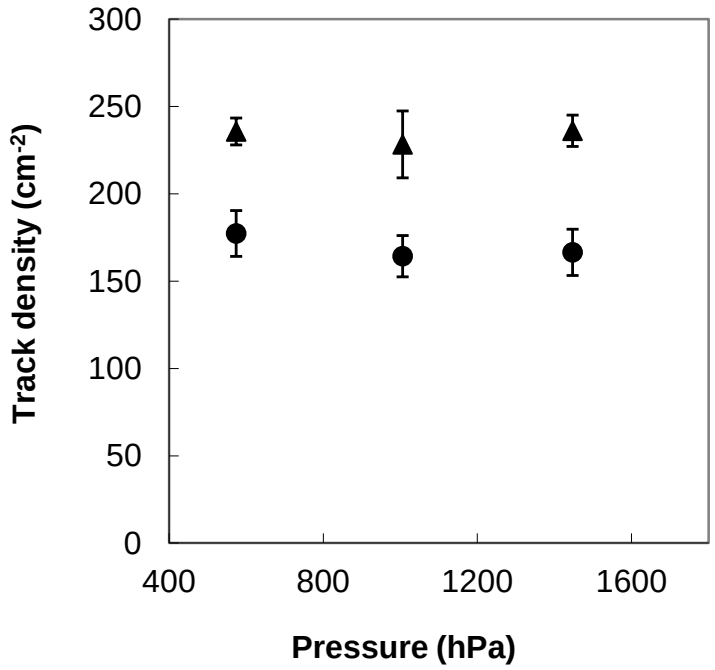

Figure V. 4. Signal at different pressure for 300 μm Makrofol (▲) and CD (●).

- **Cigarette smoke**: Studied in artificially created cigarette smoke much denser than what realistically can be found indoors. There was an indication for some 11% reduction of the track density in the smoke-stained detectors [140]. Since these detectors were much deeper colored than those exposed even in the most smoke-stained smoking rooms, it is unlikely that the effect of cigarette smoke under real living conditions will be stronger;
- **Dust deposition**: Studied with dust artificially deposited on the detector surface to a level that exceeded significantly what we observed on detectors, exposed even in the most dusty environment under real conditions. There was no difference between clean and dusty detectors [140];
- **Humidity**: Studied over 0 – 100% RH range. Not significant effect, however, some indication for reduced signal at RH=100% is noted [140]. To test whether the humidity has a noticeable effect on the CD's performance, 3 sets of CDs were exposed to ^{222}Rn under 3 levels of relative humidity (RH), RH=0%, 44% and 100% [139]. The track densities at RH=0% and 44% were practically the same, while there was an indication for some non-significant 6% reduction of the track density at 100% RH. Possibly, there is a real effect at the humidity levels that approach 100%, but its magnitude is certainly less than 10%;
- **Presence of ^{220}Rn**: Studied at ^{220}Rn integrated concentrations > 6 MBq d m^{-3}. The observed track density at 83 μm was slightly higher than the background (10.0 ± 1.2 cm^{-2} vs. 3.8 ± 1.1 cm^{-2}). Under similar integrated ^{222}Rn concentrations, the track density is at saturation level (>2000 cm^{-2}). The small excess above the background in this experiment could be due to a small amount of

^{220}Rn absorbed in the polycarbonate and diffused to depths from which α-particles can reach the depth of 83 μm beneath the surface.

Other studied factors include:

- **Mode of storage of CDs and DVDs used as retrospective ^{222}Rn detectors**. Normally, CDs are sold and stored in jewel cases. These are not hermetic and radon gas may enter freely. Still the possible difference in response due to the storage in jewel cases was examined. Two kinds of jewel cases were examined: the 10 mm high classical type and the more recent 5 mm high type. In all experiments bare CDs and CDs in jewel cases gave the same results within the experimental uncertainty. Therefore, it was concluded that there is no effect of jewel cases. This is also an indirect evidence for the absence of any plate-out contribution. The plate-out when the detector surface faces a narrow gap (as a CD in a jewel case) is substantially smaller in comparison to wider gaps [152] or to bare detectors. The absence of a significant difference in track density between bare and enclosed CDs is one more argument for the absence of any contribution from the plate-out to the tracks at the depths studied.
- **Response from either side of the Makrofol detector [153]**. Both sides of the employed as detectors Makrofol foils are different, one side being glossy and the other mat. Potentially, either one could be used as detector surface but it is not *a priori* clear if the response to radon will be the same. The knowledge whether both sides behave equally or not is also important for the modeling of the processes underlying the present method. In order to address this question, the following experiment was carried out. The glossy side of some detectors was hermetically covered with a 23μm thick Mylar foil by gluing the margins together. Other detectors were covered

on the mat side or on both sides. All 3 sets were exposed to the same integrated ^{222}Rn concentration (983 kBq d m^{-3}). The results are as follows:

- The track density at a depth of 83 μm of the detectors covered on both sides (7.8±1.1 cm^{-2}) is somewhat higher than the background of non-exposed detectors at the same depth (3.8±1.1 cm^{-2}). However, it is sufficiently low, so it might be assumed that mylar stops efficiently the radon penetration.
- The 83 μm track density of the detectors exposed to the mat side was 374 ± 36 cm^{-2}, while the density of those, exposed to the glossy side was 398 ± 35 cm^{-2}. Since the difference is not significant it appears that there is no sharp disparity in the absorption manner from both sides.

- **Effect of ^{210}Po in the detector volume after long exposure times**. For long exposure times the growing ^{210}Po activity in the detector volume may also contribute to the observed track density. This effect was studied by a theoretical modeling of the process. The growth of the ^{210}Po activity from the ^{222}Rn activity (taken constant over time) was determined by solving the known equations for the radioactive chain transformations [72, 73]. After the integration of the result over time, the correction factor was calculated which shows the relative increase of the track density compared to a short-term exposure to the same integrated ^{222}Rn concentration. The numerical values for the last factor are as follows:
  - 1-year exposure: 1.002,
  - 10 years: 1.042,
  - 20 years: 1.081.

Therefore, the bias due to the long-lived ^{222}Rn progeny is less than 10% for realistic exposure times and may be taken into account by a proper correction factor.

- **Fading of polycarbonates as nuclear track detectors.** There is several decades experience in use of polycarbonates as nuclear track detectors. In particular, Makrofol detectors have been regularly used in the Laboratory of Nuclear Physics at the University of Ghent, Belgium, since 1981. Since that time there is a many years' experience of storage of irradiated detectors in a protective box with aged, radon-free air, sometimes for years. All data strongly indicate the absence of fading in Makrofol [154].
- **Effect of the laser light on the tracks in Makrofol and CDs.** The effect of light on the track-etch properties of polycarbonates is a somewhat controversial issue. An effect of the light of strong 5-15 W lasers on the track-etch properties of alpha track detectors, CR-39 in particular, has been reported [155]. As the read-out of CDs is by a narrow laser beam (with a power of the order of 1mW), one may speculate whether this may have an effect on the latent tracks. Therefore, Jozef Buysse made some theoretical estimates to address this problem [154]. The laser light used for CDs has a wavelength of 780 nm that is converted to 500 nm in polycarbonates. The spot of light that hits the CD's upper surface has a diameter of 800 μm and is narrowed down to 1.7 μm at the registration layer level. The diameter of the spot at a depth of 80 μm will be approximately 750 μm, which corresponds to an area of 4.4×10^5 μm². The total area of the active part of the CD (between the diameters 46 and 117 mm of the total CD's diameter of 120 mm) is about 9.1×10^9 μm². For a typical playing time of 74 minutes, this means that the laser will see each spot during roughly 0.2 seconds. This is an average value since in reality the speed

of rotation is not constant. We could compare the laser beam power of 1 mW on a spot of $4.4x10^5$ μm^2 with the typical power of daylight at the earth's surface, which is between 250 and 400 W m^{-2} (or 0.11 to 0.18 mW on a $4.4x10^5$ μm^2 spot). Therefore, the laser flux is 5 to 9 times more intense than daylight at the earth's surface. Taking into account the difference in intensity, but assuming neither intensity nor wavelength effect, it might be concluded that playing a CD during 74 minutes is the same as exposing it during 1 to 2 seconds to daylight. Or playing a CD 1000 times would be equivalent to an exposition to daylight during 16 to 33 min. There is no indication, even small, for any effect of daylight on Makrofol for such times. The writing process in CD-Rs or CD-RWs takes place with a power in the range 4 to 14 mW, but the writing could be assumed as a much more rare action than reading and, in general, the above estimate is valid as well. In spite of no direct experimental evidence, the conclusion is that the possibility for a profound effect due to the laser light is probably small.

Notably, the only factor that demonstrated substantial influence over results was the temperature. The temperature effect is significant, as can be seen in Table V.1, where several experimental studies are summarized [139, 140, 153]. As seen, if take the temperature of 20^0 C as a reference value, the relative variation of the signal within $10 – 30^0$ C interval is -22 ÷ +12% at depth 80 μm, -32 ÷ + 33% at 120 μm and -44 ÷ +73% at depth 165 μm.

Table V. 1. Relative bias of CF at different temperatures. The temperature 20^0 C is taken as reference temperature

	Depth		
Temperature	**80 μm**	**120 μm**	**165 μm**
5^0 C	-37%	-48%	-55%
10^0 C	-22%	-32%	-44%
15^0 C	-10%	-16%	-26%
20^0 C	0%	0%	0%
25^0 C	7%	17%	33%
30^0 C	12%	33%	73%
35^0 C	14%	50%	121%
40^0 C	14%	68%	176%

To study the temperature effect dedicated experiments were carried-out in 2001-2003 [139, 140]. The essence of the results is presented in the next section.

V. 2. 3. Influence of the temperature

V.2.3.1. Basic experiments

In order to study the depth distribution under different temperatures, CDs of the type Kodak CD-R Ultima 80 700 MB were exposed under laboratory conditions (at the University of Ghent, Belgium) to controlled ^{222}Rn concentrations at 4 different temperatures (5^0C, 19.5^0C, 23.5^0C and 38^0C) [139]. The integrated ^{222}Rn concentrations were respectively 984, 1010, 1061 and 1011 kBq d m^{-3}, respectively. After the outgassing a layer was removed mechanically from the back so that the residual thickness of the etched spot, after CPE, was 230 μm. This way the thickness of all detectors, loaded for ECE, was alike and the regime of the ECE was fully equal for all detectors.

The track densities were determined in the range of depths between 70 μm and 300 μm beneath the surface, normally with a step of 10 μm. Each CD was treated for a different depth by CPE and after that the standard ECE and track counting were applied. The CPE for the depth distribution experiments was performed at 25^0C with aqueous solutions containing 52% KOH (m/v) and 40% methanol (m/v). By using this stronger solution the bulk etch velocity was increased to more than 70 μm per hour.

In order to compare the results obtained under different temperatures we used the CFs instead of the track densities, as the reference radon exposures were not exactly the same at the four different temperatures. The dependence of the CFs on the depth at the studied temperatures, in log-linear scale, is shown in Fig. V.5. The experimental results imply that the depth distributions of tracks (or *CF*s) at different temperatures are close to exponential.

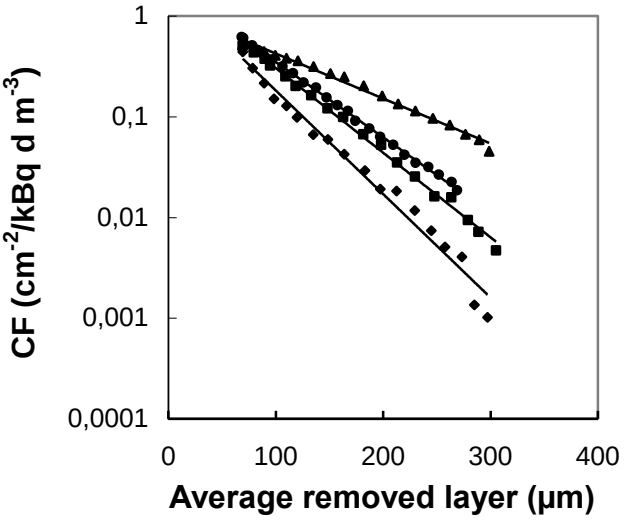

Figure V.5. The dependence of the *CF* on the depth beneath the front surface of the CD. The dependences are for 4 temperatures: (♦) 5^0 C, (■) 19.5^0 C, (●) 23.5^0 C and (▲) 38^0 C.

The straight lines in this scale correspond to the exponential dependence:

$$CF(t, d) = B(t) \exp(-\beta(t)d), \quad \text{(V.1)}$$

where $B(t)$ and $\beta(t)$ are functions of the temperature t (°C) and d is the depth (μm) beneath the front surface of the CD. The above should be used only if $d \geq 64$ μm (if only ^{222}Rn is present) or $d \geq 76$ μm (if ^{220}Rn is also present). At shallower depths the alphas from plate-outed progeny atoms contribute to the track density and the method cannot be used.

The regression analysis has been made by SPSS, version 9.0 statistical package. The slope of the lines (Fig. V. 5) increases with decreasing temperature. Although the experiments were performed at only four different temperatures, the general trend of the functions $B(t)$ and $\beta(t)$ can be seen in Fig. V. 6a,b.

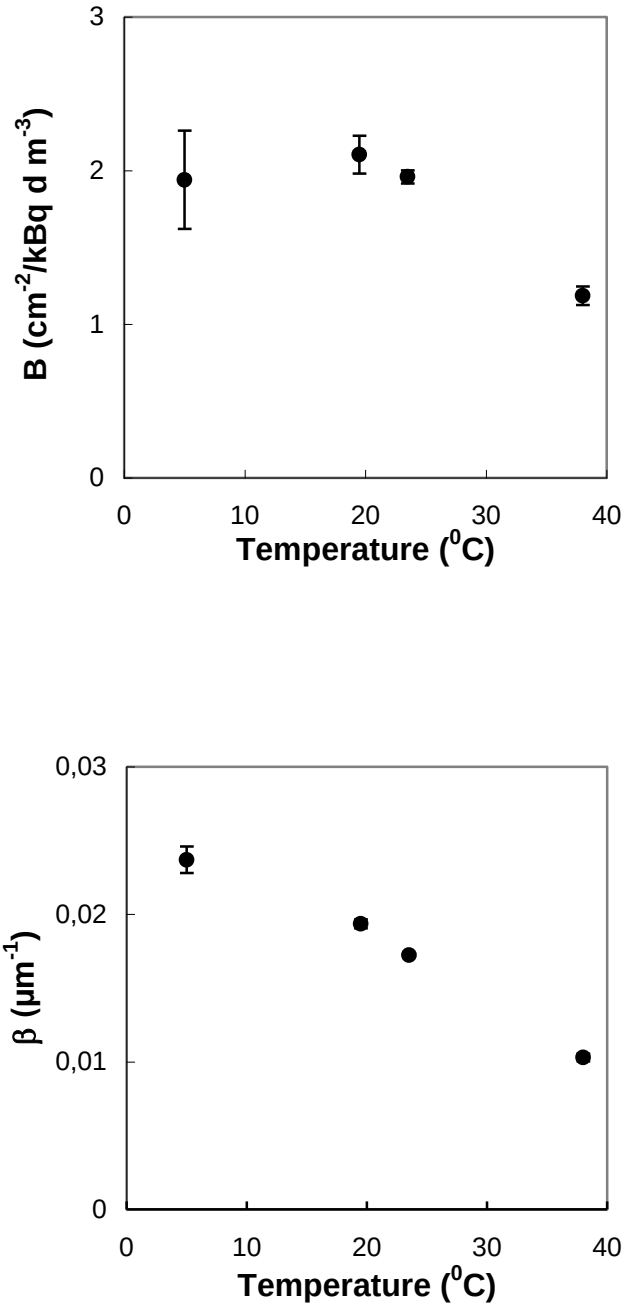

Figure V. 6a,b. The dependence of (a) parameter *B* and (b) parameter β on the temperature.

V.2.3.2. A posteriori temperature correction

The dependence of the "slope" (or factor β) on the temperature (Fig. V.6b.) could be successfully used to substantially reduce the temperature bias. To illustrate the potential of this approach, a simple case will be considered. The track counting is made in 2 different depths: 80 μm and 180 μm (the residual thickness being 230 μm in both cases). The uncertainty in the track density is assumed to be 10% and the uncertainty in the measured depth is assumed to be 3 μm. These values are realistic. For instance, the standard deviation of the track density ratio at 80 μm and 180 μm obtained at 23.5^0C was 8% and the basic uncertainty in the detector thickness measurements (by a micrometer or by a precise weighting before and after CPE) was normally less than 3 μm. Using Eq. (V. 1) one may obtain:

$$\begin{aligned} CF(d_1) &= \frac{n_1}{I} = B\exp(-\beta d_1) \\ CF(d_2) &= \frac{n_2}{I} = B\exp(-\beta d_2) \end{aligned} \qquad \text{(V. 2.)}$$

and by dividing the above two equations and taking a logarithm one may obtain:

$$\beta = \frac{Ln(\frac{n_1}{n_2})}{d_2 - d_1}, \qquad \text{(V. 3)}$$

where ***I*** is the integrated ^{222}Rn concentration, d_1 = 80 μm, d_2 = 180 μm and n_1 and n_2 are the corresponding net-track densities. Therefore, taking into account the propagation of the uncertainties one may obtain:

$$\frac{\sigma^2(\beta)}{\beta^2} = \frac{\sigma^2(Ln(\frac{n_1}{n_2}))}{(Ln(\frac{n_1}{n_2}))^2} + \frac{2\sigma^2(d)}{(d_2 - d_1)^2}, \qquad \text{(V. 4)}$$

where $\sigma(\beta)$ and $\sigma(d)=\sigma(d_1)=\sigma(d_2)$ are the uncertainties in the corresponding values. After it is noted that:

$$\sigma^2(Ln(\frac{n_1}{n_2})) = \sigma^2(Ln(n_1)) + \sigma^2(Ln(n_2)) = \frac{\sigma^2(n_1)}{n_1^2} + \frac{\sigma^2(n_2)}{n_2^2}, \qquad \text{(V. 4')}$$

and taking into account Eq. (V. 4), the following expression is obtained:

$$\frac{\sigma^2(\beta)}{\beta^2} = \frac{1}{(d_2 - d_1)^2}\left[\frac{\frac{\sigma^2(n_1)}{n_1^2} + \frac{\sigma^2(n_2)}{n_2^2}}{\beta^2} + 2\sigma^2(d)\right]. \qquad \text{(V. 4'')}$$

Under the assumptions made, the factor β will be determined with relative uncertainties as follows:

at 5^0C : 7.3%

at 20^0C: 8.4%

at 38^0C: 14.4%

Then, using the dependence illustrated on Fig. V. 6b one may estimate the average temperature during exposure. By converting the uncertainty in β into the uncertainty in *t*, the "*a posteriori*" temperature estimates imply the following uncertainties:

at 5^0C: $\pm 5.1^0$C

at 20^0C: $\pm 4.2^0$C

at 38^0C: $\pm 2.6^0$C

From the calculated average temperature with the above uncertainties a proper *CF* could be determined with an uncertainty that could be substantially less than 25%.

The potential of this approach can be demonstrated more directly if the *CF* is plotted against β as shown in Fig. V. 7. For a depth 80 μm one may see that a large uncertainty at small β (high temperatures) will be projected in a small uncertainty in the *CF* because of the small slope of the trend in that region of the graphic. With the above uncertainties in β, potentially, the CF at 80 μm could be "reconstructed" with an uncertainty of about 10% at 20^0C or even less in the region of high temperatures (as low as 4% at 38^0C). However, to achieve this the statistical power of the *CF*-β dependence should be sufficiently improved by adding points at other temperatures within the range that is realistic indoors. The analysis also showed that the accuracy of this a posteriori temperature correction is lower at low temperatures. For instance, the uncertainty in the reconstructed *CF* at 5^0C may approach 30%. However, we don't expect such low mean temperatures in inhabitable rooms.

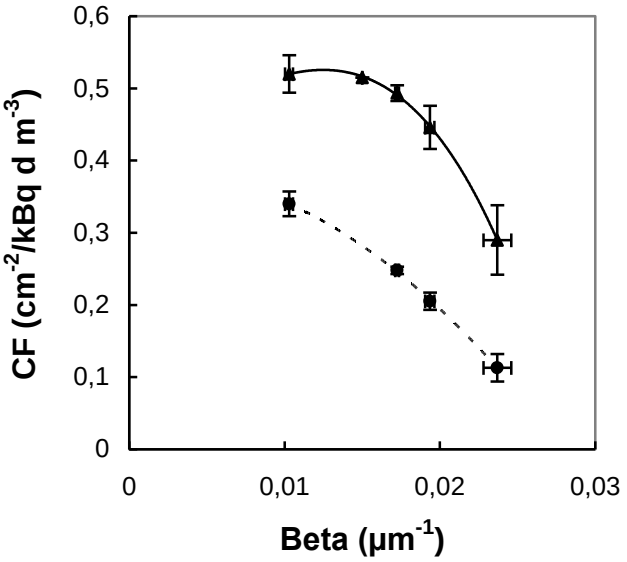

Figure V. 7. The dependence of the *CF* on β: (▲) at 80 μm, (●) at 120 μm. The lines are polynomial (2nd degree) interpolations.

The dependence of the *CF* on the temperature at the depths of 80 μm and 120 μm is shown in Fig. V. 8. As seen this dependence is markedly non-linear at 80 μm. A bias could be expected in the event of a highly non-stationary temperature regime with large amplitude. We evaluated its magnitude under the following extreme assumptions: exposure to radon for half of the time is at 5^0C and for the other half at 38^0C. At these rather unrealistic conditions the deviation in *CF* from its value at the mean temperature of 21.5^0C would be 16% at 80 μm and 4.5% at 120 μm. As seen, the results at a depth 120 μm are less biased under highly variable temperature conditions.

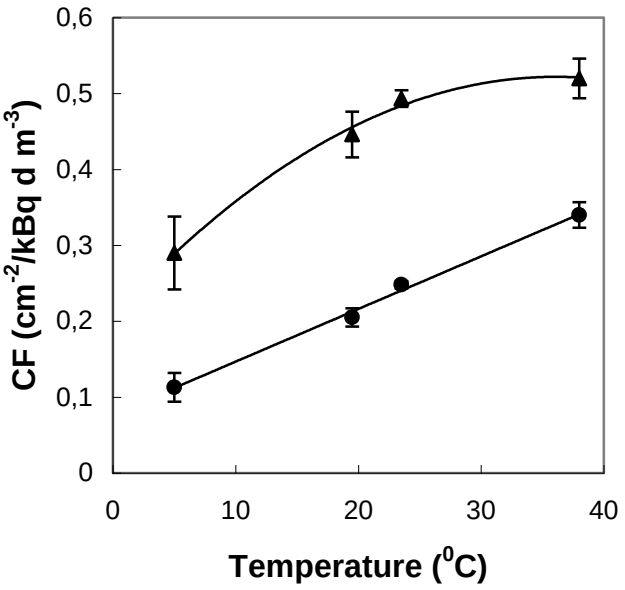

Figure V.8. The dependence of the *CF* on the temperature: (▲) at 80 μm, (●) at 120 μm. The lines are polynomial interpolation.

V.2.4. Field comparison

The comparative measurements were arranged in 23 houses in the town of Rakovski. The existing radon problem in this town is described in Chapter IV. In all of these houses, Makrofol foils (300 μm thick) and conventional diffusion chambers were placed close to each other and left for 301-day exposure [140]. After exposure, the Makrofol foils were treated by the standard etching/counting procedure. The results of this comparison are shown in Fig. V. 9. For calculating the concentrations by Makrofol detectors the *CF* at a temperature of 19.5^0 C was used. The general agreement between the concentrations measured by the polycarbonate method and by the conventional diffusion chambers is clearly visible. Because of the limited exposure time, the uncertainty in the Makrofol detectors was normally higher than 10%. The observed dispersion of the

experimental points could be partly explained by likely different temperature conditions during exposure. However, the slope of the trend line (1.03) suggests that the real average temperature is close to that assumed in the *CF*-value.

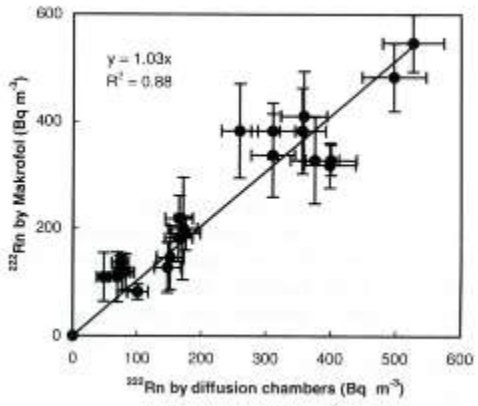

Figure V. 9. A comparison of the average ^{222}Rn concentrations obtained by the polycarbonate method (Makrofol) and by diffusion chambers with Kodak Pathe LR-115/II detectors.

V. 2. 5. Limits of precision and range of sensitivity

In order to study the limits of precision of the method, contributions to the uncertainty coming from the counting statistics, small variations in depth of the chemically removed layer and the effect of the long decay chain were analyzed.

V. 2. 5. 1. Standard deviation within a set of detectors

The standard deviation obtained within one set of equal detectors exposed under the same condition was normally less than 10% but, generally, higher than the expected value after Poisson counting statistics. With the track density range in the most laboratory experiments (100-700 cm^{-2}) and the counting area

examined (usually 2.5 cm^2 for Makrofol and 10 cm^2 for CDs), the Poisson standard deviation was 1.2 – 6%.

Without strong control, small variations in the depth of the CPE-removed layer are possible (usually within ± 5 μm but sometimes greater). Variation in the removed layer affects the results by two "mechanisms": Let's for instance the removed layer is a bit greater than the targeted one. This way, the studied depth will be greater and the signal will be lower, because it decreases in depth. From the other hand, with greater removed layer the residual thickness (*h*) of the detector, loaded for ECE will be smaller, therefore the effective electric field (*U/h*) higher. At higher fields the ECE efficiency is higher, resulting in an increase of the signal. As seen, both "mechanisms" work in a partly compensating ways. The resultant uncertainty, incurred on the results has been studied by analysis of the full set of the available experimental data and by theoretical modeling using the described in section V. 3. theoretical model. Both approaches gave similar results. For illustration we will use the two most frequently used polycarbonate detectors: Makrofol of 300 μm thickness, etched at 800 V effective, and CDs of 1.2 mm thickness, etched at 3.3 kV effective. In both cases we will assume target surface removal of 80 μm. The analysis shows that 3 μm variation in the thickness of the removed layer incurs uncertainty of 3.5% for 300 μm Makrofol and 5.5% for CDs. The correspondent results for 5 μm variation are 6% and 9%, respectively. Such uncertainties may compete the contribution of the Poisson statistics to the total uncertainty and in some cases can dominate.

V. 2. 5. 2. Effect of the long decay chain.

When the "counting time" of the long decay chain is long enough, compared to the half-life of the nuclides, there is a probability to observe tracks not only from the alpha of the parent atom, but also from some of its progeny atoms. As a result part of the tracks are correlated and the standard deviation could be different than what is

expected according to counting statistics. Analysis of this "effect of long decay chains" has been of concern for a long time and was addressed with regard to ^{222}Rn measurements by [156].

To analyze the effect for the present case, the geometry of the source should be considered. According to previous studies, we assume that the energy window for the employed ECE mode is 0.5 – 2.0 MeV and the average critical angle is about 43° [157]. The "source" comprises the radionuclides ^{222}Rn, ^{218}Po and ^{214}Po, each emitting alpha particles of different energy and therefore coming from different distances to the detection point. This is illustrated on Fig. V. 10. To simplify the analysis we will assume a homogenous activity distribution and absence of migration of the progeny atom in the lattice. As seen in Fig. V. 10 there is a small overlap only between the ^{222}Rn and ^{218}Po detection volumes. When an alpha particle from a ^{222}Rn atom is detected, it is not possible to detect the alpha particle from the ^{214}Po atom that is matched to the same ^{222}Rn atom. The same is valid between ^{218}Po and ^{214}Po, too. With regard to the couple ^{222}Rn-^{218}Po, even if one assumes registration on the detection spot of all alphas emitted in the detection volume (which is a tremendous exaggeration) only 17% of the tracks from ^{222}Rn will be coupled with a progeny ^{218}Po-atom track. Using the approach of Ref. [156] for this case, it was found that the multiplying factor for the standard deviation is about 1.03. Because of the last assumption this is a conservative estimate and the real factor is even closer to unity. The fact that the real activity distribution is not uniform cannot change the picture dramatically. Therefore, the effect of long decay chain is negligible for the present method.

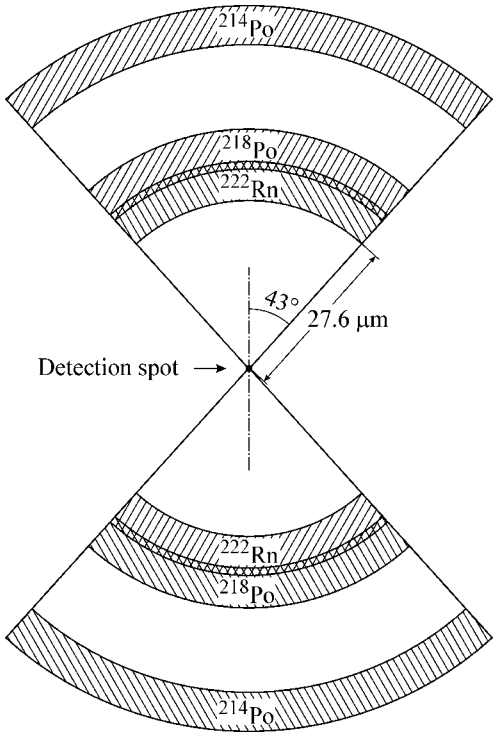

Figure V.10. The volumes in the polycarbonate material, from which alpha particles emitted from the correspondent radionuclides can be registered at the detection spot.

The major factor that contributes to the larger uncertainty than expected with Poisson statistics is probably the thickness variation of the removed layer. This implies the possibility, by using a strong control for the removed layer, to achieve precise measurements, within a few percent uncertainties. This reflected to our measurement strategy: While in the first experiments we have controlled the thickness of the removed layer with 3 – 5 μm accuracy, now we have tightened this control to 1-2 μm. With such accuracy in measured depth, a good counting statistics, tightened calibration and *a posteriori* correction procedures, the method potentially can arrive at potential precision that is better than 10%.

V.2.5. 3. Range of sensitivity of the method

The sensitivity of the method is evaluated by minimum detectable ^{222}Rn activity concentrations (MDAC). The approach followed is that of [158]. In the alpha-tracks mode it depends on the background track density. The estimates for MDAC at different modes of measurement are shown in Table V.2.

Table V. 2. The minimum detectable activity concentration (MDAC) is given as a measure for the sensitivity of the method. The assumed effective electric field for ECE is 3.3 kV/mm. Results with CDs and different "exposure scenario" are given.

Measurement conditions	**MDAC**
CD exposed in air for 10 y - α-tracks at depth 80 μm beneath the surface	3 Bq m^{-3}
CD exposed in air for 10 y - α-tracks at depth 200 μm beneath the surface	21 Bq m^{-3}
CD exposed in soil-gas for 1 week - α-tracks at 80 μm	1500 Bq m^{-3}
CD exposed in soil-gas for 1 week - α-tracks at 200 μm	10500 Bq m^{-3}

The upper limit of detection corresponds to the signal at which "saturation" occurs – a situation at which, because of the very high track density the individual tracks overlap and can not be counted. In our case it happens at track density about 2000 cm^{-2} with automatic track counting. With visual counting this level is somewhat higher, but maximum to about 4000 cm^{-2}. The upper limit of detection can be enhanced by decreasing *CF* in two ways: By removing thicker layer from the surface or by reducing the ECE efficiency, through applying lower HV. Flexibly combining both ways, we can measure practically all ^{222}Rn concentrations that can be met in practice. For instance removing 500 μm from a

CD surface and applying 1600 V effective, the saturation level corresponds to 10 y exposure at ^{222}Rn concentration of 10 MBq m^{-3}. At 80 μm removal and 3300 V effective, the saturation for the same exposure time is at 2 kBq m^{-3}. Of course, regimes scheduled for high concentration will not provide the best sensitivity at low and *vice versa*. More details are given in section V.3.2.

V.3. Theoretical modeling

V.3.1. Sorption and Desorption of Radioactive Noble Gases in Polycarbonates

V.3.1.1. Theoretical model

Although experimental results about the desorption rate were presented in the first report on the polycarbonate method [136], the numerous possibilities for practical application of the method revealed the need for a detailed quantitative description of the sorption/desorption processes. The objective of this section is to present a theoretical study of the processes of sorption and desorption of radon in polycarbonates. Although used in this thesis for radon only, the method is usable also for other radioactive noble gases [142]. The theoretical model considers the diffusion of RNGs in the polycarbonate material, taking into account the radioactive decay [159]. Once a radon atom is caught in the polycarbonate matrix, its further transport in it is considered to be ruled by diffusion and radioactive decay. The equation describing the transport of one radioactive isotope is:

$$\frac{\partial n}{\partial t} = D\left(\frac{\partial^2 n}{\partial x^2} + \frac{\partial^2 n}{\partial y^2} + \frac{\partial^2 n}{\partial z^2}\right) - \lambda n\,, \qquad \text{(V.5)}$$

where n is the radon atoms concentration, D is the diffusion coefficient of the atoms in the polycarbonate material and λ is the corresponding decay constant. This equation is considered with initial conditions $n(x,y,z,t=0) = n_0(x,y,z)$ and boundary conditions: $n(x,y,z)\big|_S = c(t)$ (boundary concentration). This problem is considered in the literature and the general solution is given by the expression [52]:

$$n(x,y,z,t) = \iiint_{V_{\xi\eta\zeta}} G(x,y,z,t,\xi,\eta,\zeta,\tau=0) n_0(\xi,\eta,\zeta) d\xi d\eta d\zeta - \\ - D \oint_{S_{\xi\eta\zeta}} \int_0^t \frac{\partial G(x,y,z,t,\xi,\eta,\zeta,\tau)}{\partial \nu_{\xi\eta\zeta}} c(\tau) dS_{\xi\eta\zeta} d\tau \qquad , \qquad \text{(V.6)}$$

where $V_{\xi\eta\zeta}$ is the volume of the specimen and $S_{\xi\eta\zeta}$ is its surface in the ξ,η,ζ coordinates, $G(x,y,z,t,\ \xi,\eta,\zeta,\tau)$ is the Green function for the problem (V.5) and $\partial G/\partial \nu$ is its directional derivative to the normal of $S_{\xi\eta\zeta}$. The following processes can be distinguished:

- Sorption of RNG with zero initial concentration in the specimen (n_0=0). In this case the first term in (V.2) is zero and the solution is:

$$n_S(x,y,z,t) = -D \oint_{S_{\xi\eta\zeta}} \int_0^t \frac{\partial G(x,y,z,t,\xi,\eta,\zeta,\tau)}{\partial \nu_{\xi\eta\zeta}} c(\tau) dS_{\xi\eta\zeta} d\tau\,. \qquad \text{(V.7)}$$

It should be noted that the boundary concentration $c(t)$ is the RNG concentration in the polycarbonate at the boundary of the sample. It is proportional to the ambient concentration $c_A(t)$ ($c(t)=Kc_A(t)$) in the air or in the water in which the polycarbonate sample is exposed. The dimensionless partition coefficient K is

proportional to the "solubility" of the RNG in the polycarbonate under the considered conditions.

- Desorption in atmosphere free from RNG ($c_a=0$) after previous sorption for time T. In this case only the first term of (V.2) plays for the solution:

$$n_d(x,y,z,t) = \iiint_{V_{\xi\eta\zeta}} G(x,y,z,t,\xi,\eta,\zeta,\tau=0) n_0(\xi,\eta,\zeta) d\xi d\eta d\zeta \,, \qquad \text{(V.8)}$$

where $n_0(\xi,\eta,\zeta) = n_S(\xi,\eta,\zeta,T)$.

V.3.1.2. Solution for a thin plate

Consider an axis *Ox* that is perpendicular to the plate surface, so that $x=0$ and L are the coordinates of the surfaces, where L is the plate thickness. "Thin plate" means that L is much lower than the other dimensions. Neglecting the edge effects, Eq. (V.1) takes one-dimensional form:

$$\frac{\partial n}{\partial t} = D\frac{\partial^2 n}{\partial x^2} - \lambda n \,. \qquad \text{(V.9)}$$

For this case the general solution takes the form:

$$n(x,t) = \int_0^L G(x,\xi,t,\tau=0) n_0(\xi) d\xi + D\int_0^t \left[\left(\frac{\partial G(x,\xi=0,t,\tau)}{\partial \xi} - \frac{\partial G(x,\xi=L,t,\tau)}{\partial \xi} \right) c(\tau) \right] d\tau$$

. (V.10)

The Green function for this problem is [160]:

$$G(x,\xi,t,\tau)=\frac{2}{L}\sum_{n=1}^{\infty}\sin\left(\frac{n\pi}{L}x\right)\sin\left(\frac{n\pi}{L}\xi\right)\exp(-\lambda_n(t-\tau)), \qquad \text{(V.11)}$$

where: $\lambda_n=\lambda+\left(\frac{n\pi}{L}\right)^2 D=\lambda\left[1+\left(\frac{n\pi L_D}{L}\right)^2\right]$, (V.12)

and $L_D=\sqrt{\frac{D}{\lambda}}$ is the diffusion length. Using the equations (V.6 – V.8) the solutions that describe sorption and desorption processes can be obtained. In sorption experiments, organized to verify the theory, two modes of exposure were used:

- Mode A: exposure to constant concentrations. This corresponds to constant boundary conditions $c(t) = c$ = const.
- Mode B: exposure to concentrations that decrease due to the radioactive decay. In this case $c(t) = c.exp(-\lambda t)$.

Desorption process is considered to happen in radon-free ambient. The correspondent solutions for sorption n_S and for desorption n_d are:

For mode **A**:

$$n_S(x,t)=\frac{4Dc}{L}\sum_{k=0}^{\infty}\frac{\frac{(2k+1)\pi}{L}}{\lambda_{2k+1}}\left(1-\exp(-\lambda_{2k+1}t)\right)\sin\left(\frac{(2k+1)\pi}{L}x\right), \qquad \text{(V.13)}$$

and:

$$n_d(x,t)=\frac{4Dc}{L}\sum_{k=0}^{\infty}\frac{\frac{(2k+1)\pi}{L}}{\lambda_{2k+1}}\left(1-\exp(-\lambda_{2k+1}T)\right)\sin\left(\frac{(2k+1)\pi}{L}x\right)\exp(-\lambda_{2k+1}t).$$

(V.14)

For mode **B**:

$$n_S(x,t) = \frac{4Dc}{L}\sum_{k=0}^{\infty}\frac{\frac{(2k+1)\pi}{L}}{\lambda_{2k+1}-\lambda}\left(\exp(-\lambda t)-\exp(-\lambda_{2k+1}t)\right)\sin\left(\frac{(2k+1)\pi}{L}x\right). \qquad \text{(V.15)}$$

and:

$$n_d(x,t) = \frac{4Dc}{L}\sum_{k=0}^{\infty}\frac{\frac{(2k+1)\pi}{L}}{\lambda_{2k+1}-\lambda}\left(\exp(-\lambda T)-\exp(-\lambda_{2k+1}T)\right)\sin\left(\frac{(2k+1)\pi}{L}x\right)\exp(-\lambda_{2k+1}t)$$

(V.16)

The activity $A(t) = \lambda\int_V n(V,t)dt$, where the integration is over the volume of the sample, for mode A and B is:

A: $$A(t) = \frac{8\lambda^2 ScL_D^2}{L}\sum_{k=0}^{\infty}\frac{1-\exp(-\lambda_{2k+1}T)}{\lambda_{2k+1}}\exp(-\lambda_{2k+1}t). \qquad \text{(V.17)}$$

B: $$A(t) = \frac{8\lambda^2 ScL_D^2}{L}\sum_{k=0}^{\infty}\frac{\exp(-\lambda T)-\exp(-\lambda_{2k+1}T)}{\lambda_{2k+1}-\lambda}\exp(-\lambda_{2k+1}t). \qquad \text{(V.18)}$$

V.3.1.3. Solution for a cylinder

The another specific case of specimens shape that was considered was that of cylinders. Consider a finite circular cylinder of radius *R* and height *H*. The

cylindrical coordinates *r,z* are used, where *r = 0* coincides with the axis of the cylinder *z*. The coordinates of the circular bottom and top of the cylinder are *z=0* and *H*, respectively. In cylindrical coordinates Eq. (V.1) takes the form:

$$\frac{\partial n}{\partial t} = D\left(\frac{1}{r}\frac{\partial}{\partial r}\left(r\frac{\partial n}{\partial r}\right)+\frac{\partial^2 n}{\partial z^2}\right)-\lambda n\,. \tag{V.19}$$

The Green function for the problem (V.19) is:

$$G(r,\rho,z,\zeta,t,\tau) = \frac{2}{\pi R^2 H}\sum_{n=1}^{\infty}\sum_{m=1}^{\infty}\frac{J_0\left(\frac{\kappa_m}{R}r\right)J_0\left(\frac{\kappa_m}{R}\rho\right)}{J_1^2(\kappa_m)}\sin\left(\frac{n\pi}{H}z\right)\sin\left(\frac{n\pi}{H}\zeta\right)\exp(-\lambda_{n,m}(t-\tau)) \tag{V.20}$$

where J_0 and J_1 are the Bessel functions of zero and first order [55], κ_m is the m-th zero of J_0 and $\lambda_{nm}=\lambda(1+(\kappa_m L_D/R)^2+(n\pi L_D/H)^2)$.

Subsequently, the solutions for mode A are:

$$n_S(r,z,t) = 8Dc\sum_{k=0}^{\infty}\sum_{m=1}^{\infty}\left(\frac{1}{H^2}\frac{(2k+1)\pi}{\kappa_m}+\frac{1}{R^2}\frac{\kappa_m}{(2k+1)\pi}\right)\frac{J_0\left(\frac{\kappa_m}{R}r\right)}{J_1(\kappa_m)}\sin\left(\frac{(2k+1)\pi}{H}z\right)\frac{1-\exp(-\lambda_{2k+1,m}t)}{\lambda_{2k+1,m}} \tag{V.21}$$

$$n_d(r,z,t) = 8Dc\sum_{k=0}^{\infty}\sum_{m=1}^{\infty}\left(\frac{1}{H^2}\frac{(2k+1)\pi}{\kappa_m}+\frac{1}{R^2}\frac{\kappa_m}{(2k+1)\pi}\right)\frac{J_0\left(\frac{\kappa_m}{R}r\right)}{J_1(\kappa_m)}\sin\left(\frac{(2k+1)\pi}{H}z\right)\frac{1-\exp(-\lambda_{2k+1,m}T)}{\lambda_{2k+1,m}}\exp(-\lambda_{2k+1,m}t) \tag{V.22}$$

For mode B:

$$n_S(r,z,t) = 8Dc\sum_{k=0}^{\infty}\sum_{m=1}^{\infty}\left(\frac{1}{H^2}\frac{(2k+1)\pi}{\kappa_m}+\frac{1}{R^2}\frac{\kappa_m}{(2k+1)\pi}\right)\frac{J_0\left(\frac{\kappa_m}{R}r\right)}{J_1(\kappa_m)}\sin\left(\frac{(2k+1)\pi}{H}z\right)\frac{\exp(-\lambda t)-\exp(-\lambda_{2k+1,m}t)}{\lambda_{2k+1,m}-\lambda}$$

(V.23)

$$n_S(r,z,t) = 8Dc\sum_{k=0}^{\infty}\sum_{m=1}^{\infty}\left(\frac{1}{H^2}\frac{(2k+1)\pi}{\kappa_m}+\frac{1}{R^2}\frac{\kappa_m}{(2k+1)\pi}\right)\frac{J_0\left(\frac{\kappa_m}{R}r\right)}{J_1(\kappa_m)}\sin\left(\frac{(2k+1)\pi}{H}z\right)\frac{\exp(-\lambda T)-\exp(-\lambda_{2k+1,m}T)}{\lambda_{2k+1,m}-\lambda}\exp(-\lambda_{2k+1,m}t)$$

(V.24)

Respectively, for the activity one obtains:

Mode **A**:

$$A(t) = 32\lambda^2 cV\sum_{k=0}^{\infty}\sum_{m=1}^{\infty}\left(\frac{L_D^2}{H^2\kappa_m^2}+\frac{L_D^2}{\pi R^2(2k+1)^2}\right)\frac{1-\exp(-\lambda_{2k+1,m}T)}{\lambda_{2k+1,m}}\exp(-\lambda_{2k+1,m}t)$$

(V.25)

Mode **B**:

$$A(t) = 32\lambda^2 cV\sum_{k=0}^{\infty}\sum_{m=1}^{\infty}\left(\frac{L_D^2}{H^2\kappa_m^2}+\frac{L_D^2}{\pi R^2(2k+1)^2}\right)\frac{\exp(-\lambda T)-\exp(-\lambda_{2k+1,m}T)}{\lambda_{2k+1,m}-\lambda}\exp(-\lambda_{2k+1,m}t)$$

(V.26)

V. 3. 1. 4. Experiments to verify the model

Series of experiments were carried out to verify the developed analytical model of the sorption/desorption processes [159, 161-163]. The experiments were with 3 different RNG isotopes: ^{222}Rn, ^{133}Xe and ^{85}Kr. Five kinds of polycarbonate samples were used: plates with thickness 0.25, 0.3, 0.5 and 0.7 mm, and cylindrical grains. The plates were made of Makrofol, while the grains were made of Makrolon. The grains had the shape of an elliptical cylinder with height H=2.65 mm and semi-axes a=1.78 and b=1.17 mm. For the theoretical model this was approximated with a circular cylinder of radius R=1.49 mm and height H=2.65 mm. The perimeter of a cyrcle with radius 1.49 mm is the same as that of the described ellipse.

In the experiments polycarbonate samples were exposed to air or water with high activity concentration of one of the RNG isotopes. The experiments were performed at ambient temperature of about 25^0 C. The samples were exposed to high RNG concentrations for the following reasons:

- To obtain sufficiently good counting statistics for straightforward quantitative follow-up of sorption/desorption process.
- To be able to neglect the background RNG concentration and to consider that desorption is in a RNG-free atmosphere.

After the exposure, all specimens were taken out from exposure vessels for desorption and laboratory measurements. While exposure were either in air or in water, the desorption was always in air. The experimental points were very well fitted by the theoretical model [159]. The correspondence between theory and experiment can be best illustrated by experiments that were dedicated and used to obtain, experimentally, the diffusion length and the partition coefficient.

The above theoretical model can be used to calculate the RNG activity in the exposed polycarbonate specimen:

$$A(t) = \lambda \iiint_V n(x, y, z, t)dxdydz, \qquad \text{(V.27)}$$

where the integration is over the volume of the polycarbonate. The basic concept of data processing is in the relation between the activity *A(t)* at a moment *t* (after the end of exposure) and the activity concentration C_A in the ambient media:

$$A(t) = KC_A VF(t,T), \qquad \text{(V.28)}$$

where *V* is the volume of the specimen, *T* is the exposure time and the "timing function" *F(t,T)* can be obtained from the mathematical algorithm described above. By definition, the partition coefficient *K* is the equilibrium ratio between radon concentration in the thin surface layer of the plastic and in the ambient medium. The explicit form of *F(t,T)* for some particular cases, covered by dedicated experiments are:

- For plate geometry and constant concentrations:

$$F(t,T) = \frac{8\lambda L_D^2}{L^2} \sum_{k=0}^{\infty} \frac{1-\exp(-\lambda_{2k+1}T)}{\lambda_{2k+1}} \exp(-\lambda_{2k+1}t) \qquad \text{(V. 29)}$$

- For cylindrical geometry and constant concentrations:

$$F(t,T) = 32\lambda \sum_{k=0}^{\infty} \sum_{m=1}^{\infty} \left(\frac{L_D^2}{H^2 \kappa_m^2} + \frac{L_D^2}{\pi R^2 (2k+1)^2} \right) \frac{1-\exp(-\lambda_{2k+1,m}T)}{\lambda_{2k+1,m}} \exp(-\lambda_{2k+1,m}t)$$

(V.30)

On the basis of this theoretical model we proposed a simple method for simultaneous quantitative determination of both *K* and *D*-values of radon in materials [163]. The method is based on exposing the specimens to controlled

^{222}Rn concentration and after that measuring radon activity in the specimens in a series of time intervals. The necessary experimental set-up includes:

- A chamber/container where the specimen can be left in contact with radon-containing media for a controlled time;
- Reference radon monitor;
- Counting equipment for measurement of the activity absorbed in the exposed specimens.

The scheme of the experimental set-up, based on activity measurement by gamma spectrometry, is illustrated in Fig. V. 11.

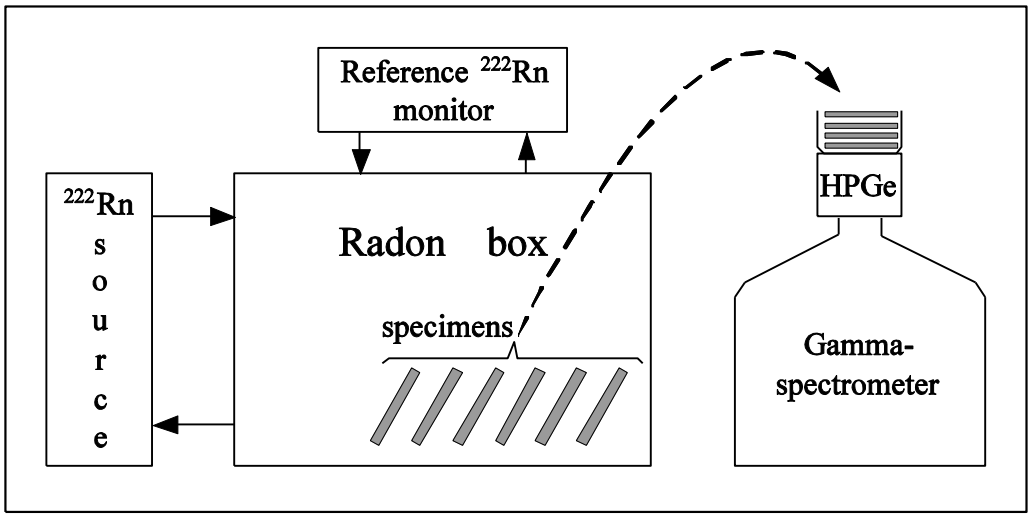

Figure V. 11. A schematic diagram of the laboratory equipment used in the experiments.

The basic idea of the method is to use a sequence of counting measurements of the specimen to determine the diffusion length and the solubility. The first approach, applied in Ref. [159] was to determine the diffusion length was to measure the specimen sufficiently long time after the exposure, when only the exponential term containing λ_1 remains significant (as λ_1

$< \lambda_3 < ... < \lambda_{2k+1}$). Then the experimental results are presented in semi-logarithmic scale and linearly fitted. The slope of the linear fit gives the constant λ_1, which is enough to determine L_D and respectively D. In this way, L_D and D could be determined without quantitative information for the reference ^{222}Rn concentration. Once the value of L_D is known, the function $F(T,t)$ can be parameterized. After that, using the reference ambient ^{222}Rn concentration and counting data from the activity measurements of the specimen, and using Eq.(V. 28) the value of K can be determined [142]:

$$K = \frac{N}{\varepsilon C_A V \int_{t_1}^{t_2} F(T,t)dt}, \qquad \text{(V.31)}$$

where N is the net-number of counts registered in the time interval (t_1, t_2) and ε is the counting efficiency of the detector.

Our experience with processing data from many experiments showed that, in the above method for determination of L_D, the time required to wait before the measurements could in some cases be so long that the residual activity in the plastic is not enough for good counting statistics (such is the case when $L_D << L$). Therefore, the methodology was further improved using non-linear fitting with two or more exponential terms [163]. The fitting function is obtained from Eq.(V.28) and Eq.(V.29), as the constants λ_{2k+1} are expressed by Eq.(V.12) and the summing is limited to a reasonable number of terms m. The obtained fitting functions $A(t)$ depends only on the two parameters K and L_D (for given exposure conditions). This approach is allows the values of K and L_D to be determined simultaneously (if all exposure conditions are known) by multi-exponential fitting of the experimental data with the proper $A(t)$ function. It must be noted that this approach also allows the value of L_D to be determined without knowing the ambient concentration C_A. The non-linear curve fitting is performed with TableCurve 2D v5.0 software using its user-defined function option. Furthermore,

this software also calculates the uncertainty of K and L_D values. The uncertainties in D were calculated using the standard algorithms for propagation of uncertainties [42]. A major advantage of this approach is that it could be applied to experimental data obtained shortly after the end of exposure. We studied the performance of the algorithm for determination of the diffusion length of a material for which L_D was already known. The non-linear fitting was performed on data from measurements after the 5^{th} hour of desorption and the sum was restricted to the 5^{th} term. The obtained value coincided with the known value within less than 1%.

All experiments were carried-out using the experimental set-up schematically shown in Fig. V. 11. Here, we present results obtained for 4 plastic materials. The first three, called A, B and C were the specimens supplied in the course of an international intercomparison on diffusion coefficient determination, organized in 2009 [164]. The fourth material was bisphenol-A polycarbonate (Makrofol foil of thickness 250 μm). The controlled ^{222}Rn concentration was supplied by a certified ^{226}Ra source with activity 104.5×10^3 Bq ± 1.5% (referred to 01.05.2006), emanation power 0.998 and ^{222}Rn output 0.2188 Bq/s. The reference monitor used was AlphaGUARD radonometer (AlphaGUARD PQ 2000 PRO, Genitron GmbH, Germany). After exposure, the activity in the specimens was measured by HPGe gamma spectrometer (relative efficiency of 24.9% and resolution (FWHM) of 1.9 keV for the 1332 keV gamma-line of ^{60}Co). Examples of experimental desorption curves are shown in Figs. V. 12 and V. 13. Such dependences have been experimentally obtained and analyzed for all studied specimens. Using this experimental data, the values of K and D were determined as described above. We have also calculated the permeability of each plastic membrane.

The results are shown in Table V.3. Compared to results from studies of other plastics [165, 166], the diffusion coefficient of radon in the materials A, B, C has similar values. The results for bisphenol-A are substantially different,

which again demonstrates the unique properties of this polymer as radon absorber. Notably, the permeability constant determined for polycarbonate in another study [167] is also lower than that of the other studied plastics (except mylar), but the authors have not specified the type of polycarbonate. Our method is the first method based on measuring desorption to evaluate the "effective diffusion coefficient" (that is the product KD) in plastics. Most of the widely used methods are based on radon penetration through membranes [168, 169]. In this respect it is worth to mention, that the organizers of the international intercomparison in their report [170] quote that "the great success of the comparison measurements was the agreement of Czech results and results measured by Bulgarian laboratory".

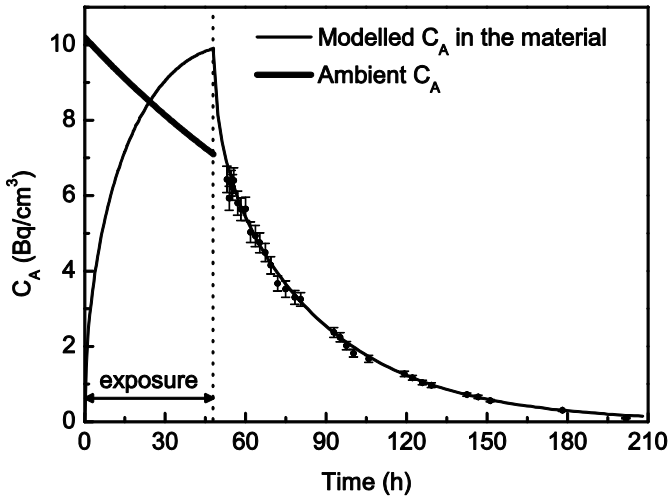

Figure V. 12. Desorption from the specimen A. The thin line is the theoretical dependence (inclusive of sorption). The thick line is the ambient ^{222}Rn activity concentration during exposure. The decrease is due to the radioactive decay.

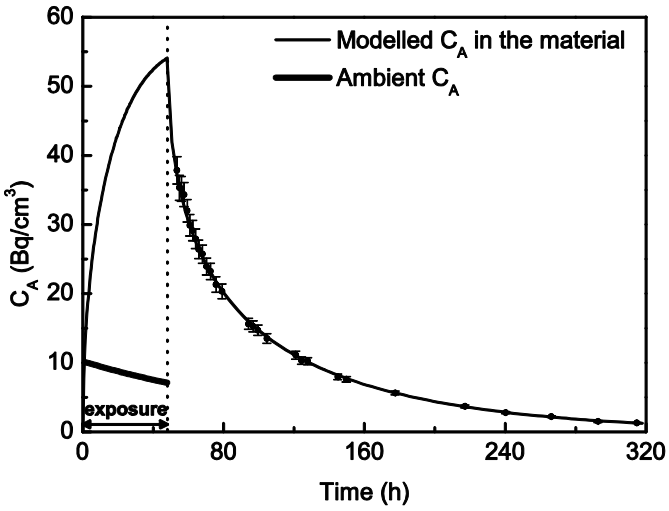

Figure V. 13. Desorption from the polycarbonate (Makrofol) 250 μm thick specimen. The thin line is the theoretical dependence (inlusive of sorption). The thick line is the ambient ^{222}Rn activity concentration during exposure. The decrease is due to the radioactive decay. The partition coefficient of radon in this material is substantially greater than in material A, which is illustrated in Fig. V. 12.

Table V. 3. Results obtained for the diffusion length, the diffusion coefficient, the partition coefficient and the "effective coefficient of diffusion" (*p=KD*) of radon in the studied plastics [163].

Material	L_D [μm]	D [m^2s^{-1}]	K	$p=KD$
A	721 ± 9.0	(1.09 ± 0.02) x10^{-12}	2.21 ± 0.13	(2.40 ± 0.15) x10^{-12}
B	1463 ± 33	(4.48 ± 0.10) x10^{-12}	2.17 ± 0.14	(9.72 ± 0.66) x10^{-12}
C	1437 ± 94	(4.32 ± 0.28) x10^{-12}	2.40 ± 0.22	(1.04 ± 0.12) x10^{-11}
Bisphenol-A	50.8 ± 1.0	(5.40 ± 0.12) x10^{-15}	27.6 ± 1.6	(1.49 ± 0.09) x10^{-13}

V.3.2. Modeling detection based on absorption in polycarbonates and track-etch counting

In this section we describe a theoretical model suitable for electrochemically etched (ECE) Makrofol or equivalent detectors [171]. It is based on volume distribution of absorbed in the polycarbonate material ^{222}Rn and its progeny, and the response function of Makrofol alpha-track detector. The "response function" is the detection efficiency as a function of energy and angle of incidence of the alpha-particle. The numerical modeling consists of two steps:

- Modeling the volume distribution of absorbed ^{222}Rn and its progeny;
- Using results from the previous step, the track density in relation to the integrated ^{222}Rn concentration is modeled, taking into account the characteristics of the particular ECE process. As a result the

"calibration factor" (*CF*) is theoretically obtained (*CF* = net track density/integrated ^{222}Rn activity concentration).

The model has been applied for ECE regimes used in previous experiments. Comparison with experimental results shows very good agreement thus demonstrating the usefulness of the model.

V.3.2.1. Absorption process

After ^{222}Rn atoms enter from air in the polycarbonate matrix, they further diffuse into the material. In practical applications to now we are interested in plate specimens (foils of Makrofol, pieces of CDs and DVDs) which thickness is much less than their diameter (if round) or other characteristic surface dimension. In such case the process can be described mathematically as one-dimensional diffusion problem:

$$\frac{\partial c_1}{\partial t} = D\frac{\partial^2 c_1}{\partial x^2} - \lambda_1 c_1 , \qquad \text{(V.32)}$$

where c_1 is the ^{222}Rn atom concentration in the polycarbonate, x is the axial coordinate, λ_1 is the ^{222}Rn decay constant and D is the diffusion coefficient of ^{222}Rn atoms in the polycarbonate material. The equilibrium volume distribution is obtained by solving the stationary diffusion problem:

$$D\frac{d^2 c_1}{dx^2} - \lambda_1 c_1 = 0 , \qquad \text{(V.33)}$$

The equation (V.33) is considered with boundary conditions valid if ^{222}Rn enters from the both sides of the plastic: $c_1(0) = c_1(L) = Kc$, where L is the thickness of the plastic, c is the ^{222}Rn concentration in air and K is the partition coefficient of

^{222}Rn from air into the polycarbonate material. The solution of this problem is obtained by standard algorithms:

$$c_1(x) = Kc\left[A\exp\left(-\frac{x}{L_D}\right) + B\exp\left(\frac{x}{L_D}\right)\right], \tag{V.34}$$

where $L_D = \sqrt{D/\lambda_1}$ is the diffusion length of ^{222}Rn in the polycarbonate material, and:

$$A = \frac{\exp(L/L_D) - 1}{\exp\left(\frac{L}{L_D}\right) - \exp\left(-\frac{L}{L_D}\right)}, \tag{V.34'}$$

$$B = \frac{1 - \exp\left(-\frac{L}{L_D}\right)}{\exp\left(\frac{L}{L_D}\right) - \exp\left(-\frac{L}{L_D}\right)}$$

The graphic of such equilibrium distribution of ^{222}Rn is shown in Fig. V.14.

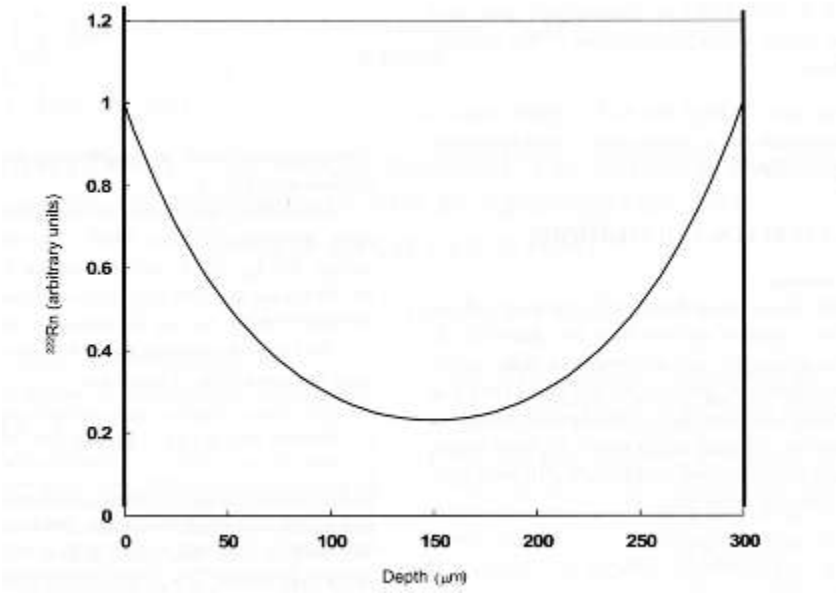

Figure V.14. The equilibrium concentration profile of ^{222}Rn absorbed in 300 μm-thick Makrofol foil.

For CDs the eqn. (3) can be simplified. The CD thickness is about 1.1 mm while experimentally obtained values for L_D for a realistic indoor temperature range (5 – 38^0 C) is 40 – 100 μm (0.04 – 0.1 mm) [139, 159]. As can be shown in this case, for depths x < 300 μm, the deviations of *A* from one and of *B* from zero are negligible. Therefore:

$$c_1(x) = Kc \exp\left(-\frac{x}{L_D}\right), \qquad \text{(V.35)}$$

in accordance with experimental findings for exponential depth distribution in CDs [139]. We should note that (V.35) can be applied only for thick specimens, e.g. CDs and DVDs. In some experiments thinner (300 μm) Makrofol foils have been used. Despite that in this case again A >> B, the exact eqn. (V.34) was used in modeling.

V.3.2.2. Modeling of detection properties

Detection properties are described by the "response function" of the detector under the particular ECE conditions. This function for Makrofol was studied by Vancraeynest et al. [149], using 300μm thick detectors. The ECE is made with solution that consists of a mixture of ethanol and 6N KOH solution with a volume ratio 1:4. The process is done at 25.0^0 C. After 30 min pre-etching an alternating HV (800 V effective, 2 kHz) is applied for 3 h. In our experiments the etching solution and ECE timing were the same but there was some difference in the applied electric field. Therefore, present model uses the response function obtained by Vancraeynest et al. [149] but modified, as further described, for variations in the electric field applied for ECE.

Alpha tracks related to ^{222}Rn are formed by 3 alpha-emitting isotopes: ^{222}Rn, ^{218}Po and ^{214}Po (always in equilibrium with ^{214}Bi). Consider the track density at depth "x" beneath the front surface of the detector. The geometry of alpha-particles irradiation is shown in Fig. V. 15. The tracks in spot with area ΔS can be etched if alpha-particles coming from the front or the back-side of the spot hit the surface under angle to the normal $\theta < \theta_c$. Because ^{222}Rn progeny atoms rest immobilized in the polycarbonate matrix, their volume distribution is the same as that of ^{222}Rn. Consider small volume dV situated so that emitted there alpha-particles can reach the detection spot (Fig. V. 15). The number of alpha-particles from the i-th isotope (i=1,2,3 refer to ^{222}Rn, ^{218}Po, ^{214}Po) that hit the spot with area ΔS per unit time is:

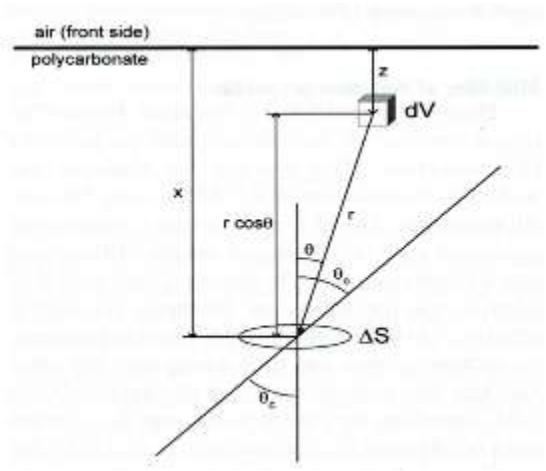

Figure V. 15. Geometry of the irradiation by α-particles of a detection spot ΔS at depth x beneath the front surface. The critical angle θ_c is the maximum incident angle at which etched tracks can be revealed.

$$d\dot{N}_i = \frac{\Delta S \cos\theta}{4\pi r^2} \lambda_i c_i dV \,. \tag{V.36}$$

However, after etching alpha-tracks appear only if the incident energy of the alpha-particle and the angle θ are within the range where tracks can be revealed. The response function $\Theta(E,\theta)$ is:

$$\Theta(E,\theta) = \begin{cases} 1 - \text{if alpha-tracks appear for these } E,\theta \\ 0 - \text{otherwise} \end{cases} \tag{V.37}$$

We will assume $x > \max\{R_1,R_2,R_3\}$, where R_i is the range of the alpha-particles from the corresponding radionuclide in the polycarbonate material. This means that alpha-particles coming only from the inside of the polycarbonate material can reach the detection spot. Therefore, the partial track density-rate due to alpha-particles from i-indexed isotope atoms in dV (dV is at depth z) is:

$$d\dot{n}_i = \frac{\cos\theta}{4\pi r^2} a_i \Theta(E,\theta) dV = K c_A \frac{\cos\theta}{4\pi r^2}\left[A\exp\left(-\frac{z}{L_D}\right) + B\exp\left(\frac{z}{L_D}\right)\right]\Theta(E,\theta)dV\,, \quad \text{(V.38)}$$

where $a_i=\lambda_i c_i$ is the activity concentration of the i-th isotope (under the considered equilibrium $a_1 = a_2 = a_3$). Integrating over the volume and by exposure time one obtains:

$$n_i = \int_0^{T_{\exp}} \int_V \frac{\cos\theta}{4\pi r^2} a_i \Theta(E,\theta) dV dt = K I_0 \int_{\{r,\theta\}} \frac{\cos\theta}{4\pi r^2}\left[A\exp\left(-\frac{z}{L_D}\right) + B\exp\left(\frac{z}{L_D}\right)\right] dV\,, \quad \text{(V.39)}$$

where: $I_0 = \int_0^{T_{\exp}} c_A dt$ is the integrated ambient ^{222}Rn activity concentration and $\{r,\theta\}$ is the volume from which alpha-particles hit the spot so that tracks are revealed. To take the volume integral note that (Fig. V. 15): $z = x - r\cos\theta$. Therefore:

$$n_i = K I_0 \iint_{\{r,\theta\}} \left[A\exp\left(-\frac{x - r\cos\theta}{L_D}\right) + B\exp\left(\frac{x - r\cos\theta}{L_D}\right)\right] \frac{\cos\theta}{4\pi r^2} 2\pi r^2 \sin\theta dr d\theta =$$
$$= \frac{1}{2} K I_0 \iint_{\{r,\theta\}} \left[A\exp\left(-\frac{x - r\cos\theta}{L_D}\right) + B\exp\left(\frac{x - r\cos\theta}{L_D}\right)\right] \cos\theta\sin\theta dr d\theta \quad \text{(V.40)}$$

After transforming and accounting for alphas coming from the back-side of the spot:

$$n_i = \frac{1}{2} K I_0 \left[\left(A\exp(-\frac{x}{L_D}) + B\exp(\frac{x}{L_D})\right) \int_0^{\theta_c} \int_{\rho_1(\theta)}^{\rho_2(\theta)} \left(e^{\frac{r\cos\theta}{L_D}} + e^{-\frac{r\cos\theta}{L_D}}\right) \cos\theta\sin\theta dr d\theta \right]. \quad \text{(V.41)}$$

Where $\rho_1(\theta)$ and $\rho_2(\theta)$ correspond to the distance, from which the alphas arrive with highest and lowest detection energy for the respective angle θ. These distances are:

$$\begin{aligned}\rho_1(\theta) &= R_i - R(E_U(\theta)),\\ \rho_2(\theta) &= R_i - R(E_L(\theta))\end{aligned}, \tag{V.42}$$

where $R(E)$ is the range of alpha-particle with energy E in the polycarbonate material [90]. $E_L(\theta)$ and $E_U(\theta)$ are respectively the lowest and highest detection energy for alphas incident at angle θ. Taking the integral over r one can obtain:

$$\begin{aligned}&\int_{R_i-R(E_U)}^{R_i-R(E_L)} e^{-\frac{r\cos\theta}{L_D}}\,dr = \frac{L_D}{\cos\theta}e^{-\frac{R_i\cos\theta}{L_D}}\left(e^{\frac{R(E_U)}{L_D}\cos\theta} - e^{\frac{R(E_L)}{L_D}\cos\theta}\right)\\ &\int_{R_i-R(E_U)}^{R_i-R(E_L)} e^{\frac{r\cos\theta}{L_D}}\,dr = \frac{L_D}{\cos\theta}e^{\frac{R_i\cos\theta}{L_D}}\left(e^{-\frac{R(E_L)}{L_D}\cos\theta} - e^{-\frac{R(E_U)}{L_D}\cos\theta}\right)\end{aligned}. \tag{V.43}$$

Therefore, after substitution in (V.41):

$$n_i = \frac{1}{2}KI_0L_D\left[A\exp\left(-\frac{x}{L_D}\right) + B\exp\left(\frac{x}{L_D}\right)\right]J_i, \tag{V.44}$$

where:

$$J_i = \int_0^{\theta_c}\left[e^{\frac{R_i}{L_D}\cos\theta}\left(e^{-\frac{R(E_L)}{L_D}\cos\theta} - e^{-\frac{R(E_U)}{L_D}\cos\theta}\right) + e^{-\frac{R_i}{L_D}\cos\theta}\left(e^{\frac{R(E_U)}{L_D}\cos\theta} - e^{\frac{R(E_L)}{L_D}\cos\theta}\right)\right]\sin\theta d\theta \tag{V.45}$$

Summing by all 3 alpha-sources within the detector volume one obtains:

$$n = \frac{1}{2} K I_0 L_D \left[A \exp\left(-\frac{x}{L_D} \right) + B \exp\left(\frac{x}{L_D} \right) \right] J , \qquad \text{(V.46)}$$

where $J = J_1 + J_2 + J_3$. As $n = CF \times I_0$, the expression for CF is:

$$CF = \frac{1}{2} K L_D \left[A \exp\left(-\frac{x}{L_D} \right) + B \exp\left(\frac{x}{L_D} \right) \right] J . \qquad \text{(V.47)}$$

The parameter J (e.g. J_1, J_2, J_3) was numerically calculated using (V.45) and the response function, obtained by Vancraeynest et al. [149]. The CF given by (V.47), refer to effective ECE voltage 800V, applied to Makrofol detectors of thickness 300 μm. This corresponds to effective electric field of 2.67 kV mm^{-1} which is further considered as a reference.

As experiments with this method were made with various electric fields – with strength up to 3.64 kV mm^{-1}, the model has to take into account the different ECE efficiency at different electric fields. This dependence was studied by De Vos [172] and will be present in the following form:

$$\varepsilon(U, h) = 5.7638 \left(\frac{h}{U} \right)^2 - 9.9644 \left(\frac{h}{U} \right) + 3.921 , \qquad \text{(V.48)}$$

where h (μm) is the thickness of the detector loaded for ECE and $U(V)$ is the effective applied voltage. The efficiency (V.48) is normalized so that for the reference field $\varepsilon(800\ V,\ 300\ \mu m)=1$. In the proposed model the applied HV frequency is not taken into account, assuming that its influence is weak in the range of frequencies (2 – 6 kHz) used in our experiments [171]. Therefore, the

expression for *CF* modified for different *U* and *h*, that is for different electric fields, is:

$$CF = \frac{1}{2} KL_D \left(A e^{-\frac{x}{L_D}} + B e^{\frac{x}{L_D}} \right) J\varepsilon(U,h) . \qquad \text{(V.49)}$$

For the case of thick samples (CDs and DVDs) the eqn. (V.49) simplifies:

$$CF = \frac{1}{2} KL_D \exp(-\frac{x}{L_D}) J\varepsilon(U,h) , \qquad \text{(V.50)}$$

respectively, the uncertainty is:

$$\frac{u(CF)}{CF} = \sqrt{\frac{u^2(K)}{K^2} + \frac{u^2(L_D)}{L_D^2}\left(1 + \frac{x^2}{L_D^2}\right) + \frac{u^2(x)}{L_D^2}} , \qquad \text{(V.51)}$$

where *s* is the uncertainty in the corresponding quantities. The contribution of uncertainties in $\varepsilon(U,h)$ and in the response function is not considered.

Note that the units of *CF* in (V.49-V.50) are units of length (e.g. μm if L_D is expressed in μm). To obtain it in more commonly used units, e.g. cm^{-2}/kBq h m^{-3}, the following numerical relation (equivalent to (II.4)) can be used:

$$CF\ [\text{cm}^{-2}/\text{kBq h m}^{-3}] = \frac{CF[\mu\text{m}]}{2778} . \qquad \text{(V.52)}$$

V.3.2.3. Parameterization of the model

To calculate the *CF* according to eqn. (V.49) the input data for the partition coefficient and the diffusion length of ^{222}Rn in the polycarbonate material is needed. As both the partition coefficient and the diffusion length depend on the temperature data for different controlled temperatures was used. The results from our previous laboratory experiments [139,140] were used as data source. In that work *CF*s and depth distribution of track density were experimentally studied in experiments conducted at 4 well controlled temperatures (5^0 C, 19.5^0C, 23.5^0C and 38^0 C). The observed depth distribution was exponential. Presented in log-linear scale the exponent is straight line and by its slope the diffusion length can be directly determined. Using L_D and (V.45) the parameter J for the corresponding temperature was numerically calculated. At the next step the partition coefficient was determined using the experimentally obtained *CF* and (V.50):

$$K = \frac{2CF(x)}{L_D J \varepsilon(U,h)} \exp\left(\frac{x}{L_D}\right), \tag{V.53}$$

respectively its uncertainty is:

$$\frac{u(K)}{K} = \sqrt{\frac{u^2(CF)}{CF^2} + \frac{u^2(L_D)}{L_D^2}\left(1+\frac{x^2}{L_D^2}\right) + \frac{u^2(x)}{L_D^2}}\,. \tag{V.54}$$

The results, obtained for L_D, J and K are presented in Table V.4. The *CF*s at two depths (80 μm and 120 μm) were used to calculate K and the correspondent values are practically identical. The results are plotted in Fig. V.16a-c and the fitting curves (polynomials) were provisionally used for simulating the temperature dependence in the temperature range 5 – 38^0 C. This way, using eqn.

(18) a *CF* can be modeled for any temperature within the specified range, and for different *U* and *h*. To compare with experimental values the results from independent, not used for parameterization, experiments were used.

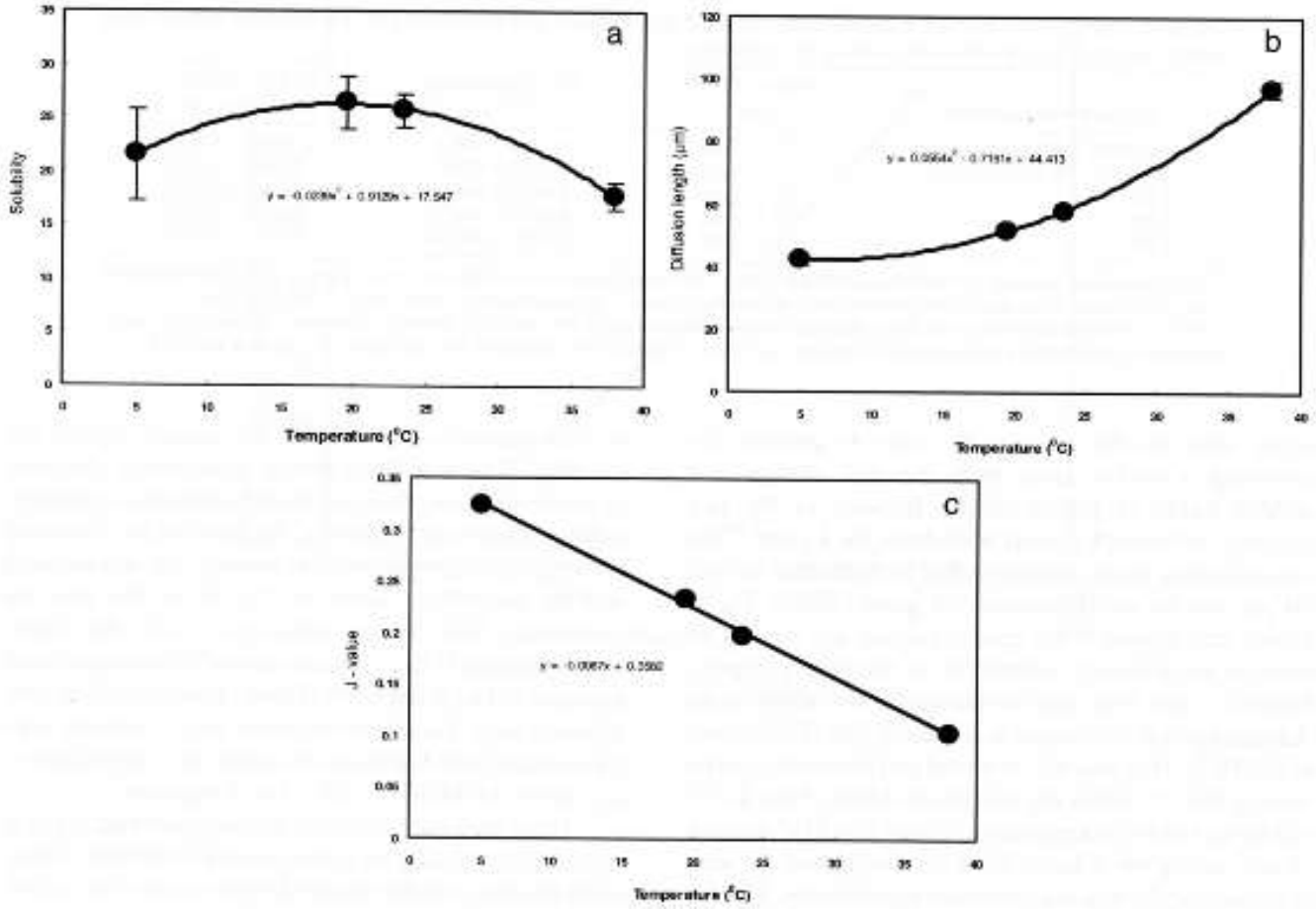

Figure V. 16. Experimentally obtained values for the partition coefficient (solubility) (a), $\boldsymbol{L_D}$ (b) and $\boldsymbol{J}$ (c). The fitting curves represent the provisional temperature dependences used in the model.

Table V.4. Numerical values used for model parametrization. One standard deviation is given as an uncertainty.

Temperature ^{0}C	L_D (μm)	J	K, according to CF at 80 μm	K, according to CF at 120 μm
5	42.2±1.6	0.3229	21.5±4.3	22.1±4.8
19.5	51.7±0.8	0.2338	26.4±2.5	26.5±2.4
23.5	58.0±0.5	0.1979	25.7±1.5	26.0±1.5
38	97.2±2.5	0.1034	17.8±1.2	17.8±1.3

V.3.2.4. Comparison with experimental CFs

Up to now in experimental studies with the polycarbonate method 300 μm Makrofol foils and CDs were used. In the initial experiments made in 1999-2004 a HV generator with fixed parameters was used for ECE (800 V effective, 2 kHz). These parameters are identical to these used by Vancraeynest et al. [149]. However, the field is not identical as in our methodology 80 μm or more are first removed from the surface. Therefore the thickness of foils loaded for ECE was max. 220 μm. The same was valid for CDs as their thickness was first reduced mechanically to 300 μm and after they were treated for surface layer removal and ECE under the standard way. After 2005, a generator of regulated up to 4 kV effective HV and frequency of 6 kHz was used, to avoid the time and labor consuming mechanical reduction of CDs thickness [139]. The CDs of thickness about 1 mm (this is the residual thickness after removal of 80 μm from the surface) were etched at 3.3 kV effective. The different from the reference field conditions were taken into account through $\varepsilon(U,h)$ function. The influence of the changed frequency on the etching process can be ignored [173].

The results are presented in Table V.5. As seen, there is very good correspondence between theoretical and experimental values. These experimental

values are from independent experiments, not used for the parametrization of the theoretical model. This fact is convincing for the usefulness of the proposed model.

Table V.5. Comparison between experimentally obtained and theoretically calculated CFs for different experimental series. One standard deviation is given as an uncertainty.

Polycarbonate specimens	**Depth for ECE (μm)**	**CF-experimental (cm^{-2}/kBq h m^{-3})**	**CF-model (cm^{-2}/kBq h m^{-3})**
Makrofol, 300 μm thick foil	83 ± 3	0.018 ± 0.001	0.019 ± 0.002
Makrofol, 300 μm thick foil	117 ± 3	0.013 ± 0.001	0.0142 ± 0.0016
CD	83 ± 3	0.0172 ± 0.0012	0.0182 ± 0.0021
CD	117 ± 3	0.0112 ± 0.0016	0.0111 ± 0.0013

The set of input values for our model is relatively limited. Further studies are going to focus more closely to solubility and diffusion length of ^{222}Rn in polycarbonates and parameterization of the model can be, eventually, refined.

V.3.2.5. Using the model for optimization of the measurement design

Such optimization can be illustrated on the example of measuring design for high ^{222}Rn concentrations. In the last years pilot measurements of ^{222}Rn in soil gas and water by the polycarbonate method were organized [146]. Some were made in radon spas or in areas radioactively contaminated by former uranium industry. In number of cases the radon concentrations were high and a problem with saturation of track-density have arisen. With automatic counting by computer scanner [151] the saturation occurs at track density about 2000 cm^{-2}, albeit visual counting is still possible up to about 4000 cm^{-2}. Expanding the upper limit of the measurable range is possible by removing thicker layer from the disk surface and etching tracks at greater depth. Because of the fast decrease of the track density with depth, levels corresponding to saturation at say 80 μm can be easily measured at greater depth. This is illustrated on Fig. V. 17. However, the bias due to the unknown temperature during exposure is stronger at greater depths [139]. This bias was modeled and the results can be seen in Fig. V. 18, where the maximum relative bias in *CF* due to the unknown temperature within 10 – 30^0 C range is shown, taking the value at 20^0 C as a reference. As seen at greater depths this bias increases significantly. Still the temperature bias can be corrected a posteriori as discussed in previous sections but this needs etching and counting tracks at different depths. Alternatively, the range of measurable concentrations might be expanded upward by etching at one and the same depth (e.g. 80 μm) but by decreasing HV (e.g. by decreasing ε). This strategy was also modeled and the results are shown in Fig. V.19. In this case the temperature bias remains unchanged, while the "upper measurable level" raises.

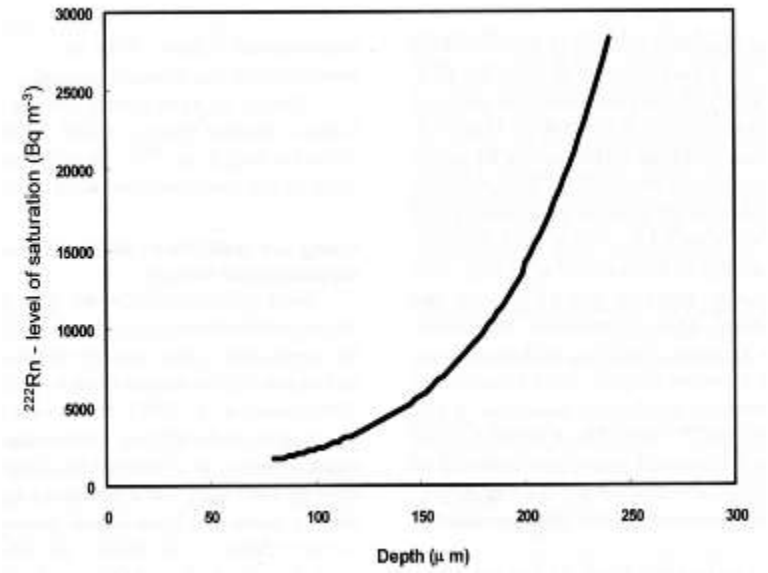

Figure V. 17. ^{222}Rn concentrations that lead to track-density saturation for 10-y exposure time as dependent on the depth at which ECE is made.

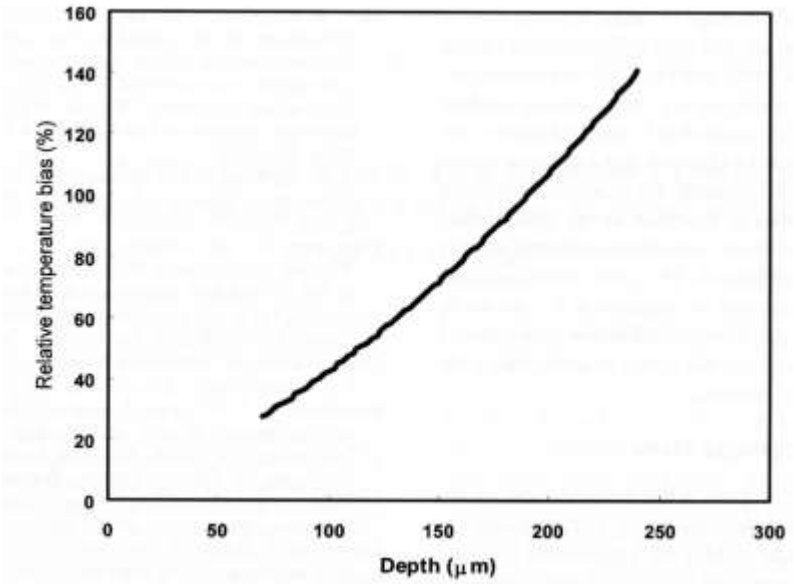

Figure V. 18. Relative temperature bias (for $\pm 10^0$ C variation around 20^0 C temperature at different depths for ECE.

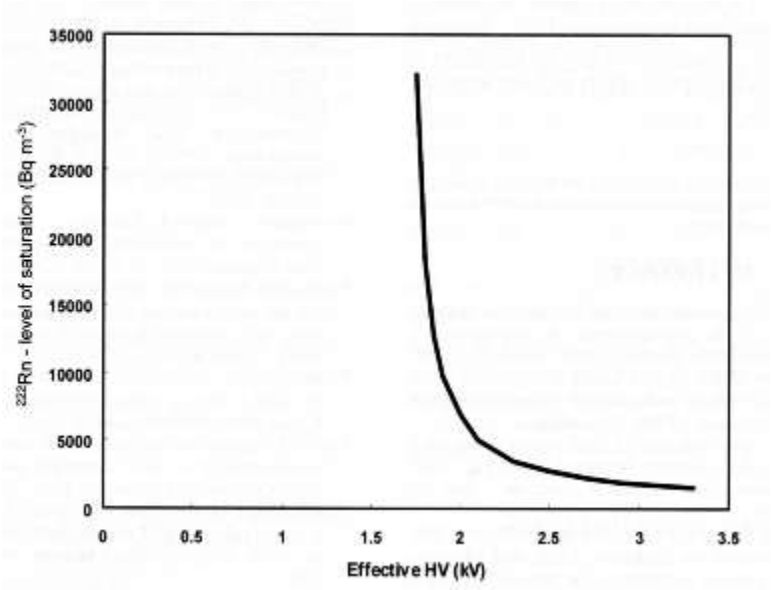

Figure V. 19. ^{222}Rn concentrations that lead to track-density saturation at depth 80 μm for a 10-y exposure time as a function of the effective ECE voltage.

Up to now our studies on polycarbonate method were focused mostly on home stored CDs/DVDs as they seem the most suitable choice for retrospective detectors (see next Chapter). However, a wide variety of polycarbonates are used nowadays. Printer parts, casings of irons, lighting covers, helmet, protective glasses, road reflectors – all are made of such materials [172] and this list is not exhaustive. We can foresee that strategies – e.g. for mapping outdoor ^{222}Rn concentrations, monitoring in working places etc. can be based on application of different polycarbonate specimens. Present model can be usable for Makrofol equivalent materials. Its application is foreseen on the design step, when the necessary sensitivity should be evaluated and the measurement design optimized. The good correspondence to experiments encouraged us to expand the model to other construction of absorption-based radon dosemeters – e. g. in which the absorption foil serves as radiator for an external alpha-track detector.

In summary, we conclude that this model can be usable in practical applications of the polycarbonate method for ^{222}Rn measurements.

VI. RETROSPECTIVE RADON MEASUREMENTS BY CDs/DVDs

VI.1. The need of retrospective radon measurements

Current risk estimates are based on epidemiological studies of two groups:

- Underground miners;
- The general public.

In most studies on miners "radon history" is usually documented by long term radiation monitoring [175, 109, 110]. The group of miners consists almost entirely of males whose exposure has started at age ≥ 18 y. Until recently epidemiological studies on miners were the only source for quantitative (extrapolated) risk estimates of the general population. In the 90s many case-control studies among the public were initiated in an attempt to obtain more direct risk estimates [176, 177]. In these studies males and females, whose exposure had started at different ages, were included. However, radon measurements in the studied houses gave results only about current concentrations and the history of radon exposure of the inhabitants was generally unknown.

As already it was mentioned, nowadays radon exposure is recognized as the second cause of lung cancer, after smoking, and the first cause for people who have never smoked [1]. There are studies which suggest a possible correlation between leukemia and radon exposure [178,179]. Most of the exposure related to radon is incurred indoors. Radon and radon progeny concentrations vary largely (up to orders of magnitude) with time. This makes instantaneous, grab sampling measurements crude and unrepresentative [1]. The preferred method for radon measurements is that of integrated measurements by passive detectors. The

typical duration of such measurements is from several months to one year. In this way most of the time variations are smoothed. However, year-to-year variations and changes after major building reconstructions still contribute to the bias in exposure estimates [180-183]. The two most important goals for ^{222}Rn measurements indoors are:

- Identifying dwellings with elevated radon concentrations and delineating of risk areas;
- Risk estimation due to ^{222}Rn exposure. This includes more precise lung cancer risk estimates as well as addressing the possibility that ^{222}Rn contributes to other malignancies.

The malignant diseases, lung cancer in particular, are multi-stage processes that take years and even decades to develop. Current scientific knowledge provides evidence that exposure within the interval 5 – 35 years prior to the clinical manifestation of lung cancer can contribute to the risk [184]. Making a realistic estimate of the "past exposure" is a serious problem for the exposure estimates in epidemiological studies [185-187]. Still, the epidemiological studies are based on prospective radon measurements. Only in a few small studies direct retrospective measurements by the glass implanted method (see e.g. [188-190]) were attempted. In other 3 epidemiological studies conducted in the last decade, a separate analysis was made, restricted only to persons that had not changed their house for the last 30 years. In all three studies this stratification resulted in higher risk estimates than after common analysis [1].

The problem of the risk estimation can be directly addressed only by retrospective measurements, e.g. measurements that estimate past exposure. This problem has attracted the attention of many researchers during the last three decades. The gathered knowledge on risk formation leads to the following criteria that have to be met by a method for retrospective measurements suitable for practical use:

- The method should cover sufficiently long time interval in the past (years);
- The obtained mean ^{222}Rn concentration should be with reasonably low uncertainty and the probability for large errors should be minimal;
- The method should be suitable for large-scale measuring campaigns, e.g. it should combine low price and easy handling of detectors;
- The range of sensitivity should cover the range of indoor ^{222}Rn concentrations that can be met in practice – i.e. concentrations at the level of 40 Bq m^{-3} should be measured with a good accuracy;
- The method should be applicable in case of changes of residence.
- Ideally, thoron should also be measured in retrospect [191].

VI. 2. Overview of the techniques for retrospective ^{222}Rn measurements

This section focuses on four methods for retrospective ^{222}Rn measurements, known before the CD/DVD method was proposed. They are: the method of glass-implanted ^{210}Pb (also referred as surface-trap method), the volume-trap method, the method of eyeglass lenses, the method of ^{210}Pb accumulated in the skeleton and the CD/DVD method. Table V.1. summarizes the physical processes on which the methods are based, the stages of the measurement and the factors, affecting the results of four of these methods (the fifth method, which is based on ^{210}Pb in the skeleton, is excluded from table VI.1, because it has very limited applicability, as explained further on).

Table VI.1. Physical characteristics of the four most promising methods for retrospective measurement of ^{222}Rn

METHOD	Glass- implanted $^{210}Pb/^{210}Po$	Volume traps	Eye-glass lenses	Absorption in CD/DVD
PHYSICAL PROCESS DURING EXPOSURE	- Plate out of RnP on a glass (e.g. picture frame glass) - Recoil implantation of ^{210}Pb atoms in the glass surface	- Diffusion of ^{222}Rn in spongy materials (e.g. mattresses) - Deposition of ^{210}Pb in the cavities of the material	- Diffusion of ^{222}Rn between the person's face and the eye-glass lenses - alpha-tracks formed in CR39 lenses by ^{222}Rn and RnP	- Absorption of ^{222}Rn in the CD/DVD's material - alpha-tracks formed in disk's material by the absorbed ^{222}Rn and its progeny
MEASUREMENT STAGES	Measurements of $^{210}Pb/^{210}Po$ surface activity by: - alpha-tracks in SSNTD attached and exposed on the glass surface or	Measurements of $^{210}Pb/^{210}Po$ deposited in the material volume: - taking a sample of the material and - radiochemical extraction and alpha-	Measurements of ^{222}Rn and RnP by etching the CR39 lenses for alpha-tracks	Measurements of ^{222}Rn by: - removing at least 80 microns of the disk's surface to cancel the plate-out effect and

	- alpha-spectrometry of a glass sample	spectrometry of ^{210}Po		- etching the tracks in the disk at a certain depth
FACTORS AFFECTING RESULTS	- aerosol concentration - ventilation - surface-to-volume ratio of the room - deposition rate of the attached and the unattached fraction - cleaning	- adsorption of ^{222}Rn on the material - dust in the material - recycled materials - determination of the sample volume	- individual face geometry - habits for cleaning the glasses - habits for wearing the glasses - differences in the track-properties of the lenses	- temperature (could be accounted for a posteriori) - small differences in the track-properties (could be accounted for a posteriori)

VI. 2.1. Method of Glass-Implanted ^{210}Pb

In the beginning of the 20th century it was observed that glasses that had been in contact with ^{222}Rn remained radioactive even after their surface was cleaned. Hahn and Meitner [192] explained the phenomena as recoil implantation of radioactive nuclei produced from alpha-decaying nuclides. Almost 80 years later, after the problem with ^{222}Rn exposure in homes was realized, it was proposed that the implantation of long-lived radon progeny in glass surfaces could be used for retrospective assessment of radon exposure [193, 194]. Retrospective measurements of ^{222}Rn by the proposed method are based on measurement of the activity of ^{210}Po in the glass surfaces of objects found in the studied buildings. The obtained signal is not directly related to the activity concentration of radon in the air, but rather to the activity of short-lived radon progeny plated-out on the surface. The physical processes and features behind the method of glass-implanted ^{210}Pb are illustrated in Figure VI.1. The alpha-decay of ^{218}Po and ^{214}Po plated-out on a glass surface could lead (with theoretical probability of about 50%) to implantation of the nuclei of their products (^{214}Pb and ^{210}Pb) in the glass (Figure VI.1). As a result, ^{210}Pb is accumulated in the surface layer of the glass (up to 100 nm depth). The lifetime of ^{210}Pb (which has half-life of 22.3 y) is comparable to the characteristic latent period of the lung cancer. The measurements of long-lived radon progeny, implanted in the thin surface layer, are influenced by the background volume activity of the glass. Background signal is lowest when alpha-particles are measured. After two disintegrations the nucleus of ^{210}Pb becomes ^{210}Po, which emits alpha-particles (Figure VI. 1). Therefore, by measuring ^{210}Po better signal to background ratio could be achieved.

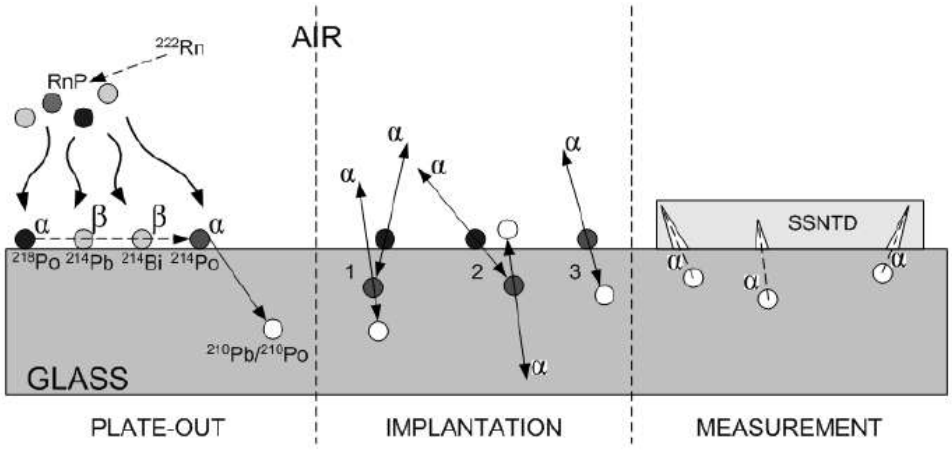

Figure VI. 1. Principles of the glass-implanted method: During the exposure, the short-lived radon progeny present in the air is plated-out on the glass surface (left). When the plated-out ^{218}Po and ^{214}Po decay, they emit alpha-particles. The recoil energy is just enough to implant ^{218}Po and ^{214}Po decay products in the glass surface (middle). This leads to accumulation of ^{210}Pb (half-life of 22.3y). The activity of the implanted ^{210}Pb could be estimated by measuring the glass' surface alpha-activity due to ^{210}Po. That could be done by placing a SSNTD on the glass surface (right).

The assessment of the past ^{222}Rn exposure by the glass-implanted ^{210}Pb includes the following steps:

- Measurement of the specific activity of ^{210}Po in the studied glass surface.
- Modeling the process of recoil implantation.
- Modeling the process of deposition of radon short-lived progeny on the particular glass surface.
- Estimating the time integrated activity concentration of ^{222}Rn in the air.

The most challenging step is the third, since it requires modeling of the complex behavior of radon progeny in the air, which is influenced by many factors. As one

of the authors of the method admits, this modeling could generate unstable results [195]. The methodological studies on the glass-implanted method are briefly described below.

VI. 2.1.1. Measurement of the Specific Activity of ^{210}Po in the Studied Glass Surface

Several nondestructive methods were developed for measurement of the specific activity of ^{210}Po. One of them is alpha-spectrometry by pulse ionization chamber (PIC) [196], in which the studied surface is used as cathode. The spectra obtained in such measurements consist of a relatively constant background and a distinct peak formed by the alpha-particles of ^{210}Po with energy of 5.3 MeV [196]. The narrow peak confirms that ^{210}Po is distributed in a thin surface layer of the glass. The background is formed by alpha-particles emitted by the natural radionuclides present in the glass (like ^{238}U, ^{232}Th and their progenies). The studies show that the background emission rate of alpha-particles in different glasses could vary substantially [197]. Therefore, background should be estimated for each measurement.

Detectors like PICs or wide-area silicon detectors are not suitable for measurements in numerous buildings. At present, these detectors are only used for laboratory studies and calibration purposes [198]. The measurements in homes are performed by solid state nuclear track detectors (SSNTD).

Several different techniques for measurement of ^{210}Po in glass using SSNTDs have been applied so far. In all of them the track detectors are placed directly on the glass surface in the studied home and are exposed for a certain time (usually several months). One widely applied technique uses two different track detectors – one is of the type CR-39 and the other is LR-115 [197]. For that exposure geometry the LR-115 detector is sensitive only to the background and is used to evaluate and subtract the background from the signal formed in the CR-39

detector (which is sensitive to both ^{210}Po and background alpha-particles). Experiments with unexposed glasses show that the standard deviation of the "zero" signal, obtained with this technique, corresponds to ^{210}Po specific activity of about 1 Bq m^{-2}, which roughly corresponds to cumulative radon exposure of 1 kBq y m^{-3} [197]. Calibration exposures of CR-39 detectors using glass sources with referent ^{210}Po activity show that the calibration factor could be determined with uncertainty of about 10% [198].

VI. 2.1.2. Modeling the Process of Recoil Implantation

In this step the ratio between the surface activity of ^{210}Po and the activity of short-lived radon progeny plated-out on the glass is evaluated. Experimental studies were conducted aiming to test whether this ratio varies for different surfaces and whether it is influenced by factors, unrelated to radon. The conclusions of these studies could be summarized as:

- It could be assumed that the only cause for ^{210}Pb accumulation in glass surfaces is ^{222}Rn in the air. The quantity of ^{210}Pb related to cigarette smoke could be neglected [199]. In addition, it was shown that ^{210}Pb distribution in the glass stays constant (diffusion of radon progeny in the glass is not observed at room temperature) [200].
- Some of the implanted activity could be removed by cleaning with common detergents [201]. This is due to corrosion of the surface of the glass, which is more pronounced at higher humidity [201,202].
- For dusty or greasy surfaces the probability for implantation is reduced, due to the small range of recoiled nuclei [195].

Usually, it is assumed that when surfaces are carefully chosen the last effect could be neglected. The effect of cleaning is taken into account by introducing a parameter in the models. Numerical studies showed that typically this parameter

could change the final result for radon activity concentration by less than 12% [203]. The same studies showed that the effect of modeling the implantation probabilities is 11% [203].

VI. 2.1.3. Modeling the Process of Deposition of Radon. Short-Lived Progeny on the Particular Glass Surface.

This step estimates the percent of short-lived radon progenies plated-out on the glass surface per one ^{222}Rn atom in the air. Based on the Jacobi room model [204], several different models for the deposition of radon progeny are developed [203, 205, 206]. All models are stationary and assume that the distribution of radon and its progeny in the room air is homogenous. Because of the last assumption, the models should not be used for surfaces that are partially covered by shelves or other objects or are near heaters, air conditioners and electronic equipment. The main parameters of the developed models are the aerosol concentration, the ventilation rate, the surface to volume ratio of the room and the deposition velocities of the attached and unattached fractions of short-lived radon progeny. There are some noticeable differences in the published models. For instance, the model in Ref. [206] neglects the deposition velocity of the attached fraction, while in Ref. [203] it is stated that both deposition velocities (of the attached and the unattached fraction) influence the results. In Ref. [203] the sensitivity of the result for the activity concentration of radon on the parameters of the used model is analyzed. All parameters have significant effect on the estimate of ^{222}Rn activity concentration, even when no extreme values of the parameters are considered. Moreover, some researchers have estimated the uncertainty of the results related to modeling the deposition of radon progeny on the glass. For this goal, the statistical distribution of the input parameters is described based on experimental results. Then, the frequency of obtaining different radon activity concentrations for a fixed value of the ^{210}Po surface

activity is studied. For standard room conditions and average values of the input parameters, the uncertainty related to modeling the deposition of radon progenies is estimated at 40-60% [203, 205, 206]. However, extreme conditions in the room or poor choice of surfaces could lead to a much higher error in the result.

A possibility to improve the results of the modeling is to restrict the interval in which the deposition velocities of short-lived radon progeny have varied. To achieve this, the contemporary deposition velocity is determined by additional SSNTDs, exposed together with those used for measurement of the ^{210}Po surface activity [207]. Such measurements reduce the uncertainty related to modeling, but could lead to errors in case when the conditions in the studied room differ from those in the past.

VI. 2.1.4. Estimating the Integrated Activity Concentration of ^{222}Rn in the Air

As a result of the previous steps the ratio between the number of ^{210}Pb nuclei implanted in the glass per unit time and the activity concentration of ^{222}Rn in the air is found. However, the present activity of ^{210}Pb (and respectively of ^{210}Po) depends on the time that has passed since the implantation occurred. Therefore, the present activity is influenced by the time dependence of the activity concentration of ^{222}Rn during the glass exposure. Since this time dependence is unknown, it is assumed ^{222}Rn activity concentration is constant during the exposure. On one hand, this is a potential source of error. On the other hand, in Ref. [195] it is pointed out that the dependence of the signal on the time since implantation could be used to weight the result for the current risk. In Fig. VI. 2 it is shown that the time dependence of the ^{210}Po surface activity might be similar to the dependence of the risk for lung cancer on the time since the exposure occurred. This hypothesis has not been proven by epidemiological studies yet.

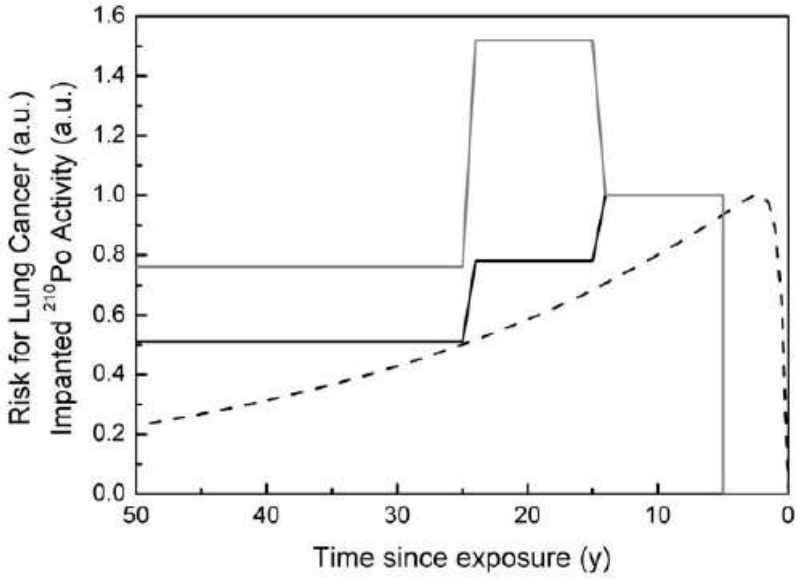

Figure VI. 2. The dashed line represents the surface activity of ^{210}Po in the glass as a function of the time passed since the implantation of ^{210}Pb. The solid lines represent the relative risk for development of lung cancer as a function of the time passed since the exposure (solid black line according to [208], solid grey line according to [209]).

VI. 2.1.5. Performance of the Method under Real Conditions

According to the methodological studies, the typical uncertainty of the method of glass-implanted ^{210}Pb is about 50-70% for standard room conditions and adequately chosen glass surfaces. However, real tests of the method are conducted in real homes with different ventilation and aerosol concentrations. The main questions that are addressed are:

- Could suitable glass surfaces be found in all homes?
- Are the results obtained with different objects from a room or with different objects of a person reproducible?

- And most importantly, do the results correlate well with the time integrated radon activity concentration, to which the studied glass was exposed?

When measurements are performed in homes the glass surfaces should be chosen, so that their age is known and the deposition velocity of radon progeny on them is close to average for the room. In addition, the quality of measurements of ^{210}Po on the surface should be guaranteed (e.g. the surfaces should be smooth and not exposed to direct sunlight, to which the SSNTDs are sensitive). Detailed criteria for choosing glass surfaces are given in Ref. [210, 211]. It is concluded that in most rooms suitable surfaces could be found, but the SSNTDs should be placed by well-trained operators. Despite the followed protocols for choice of glass surfaces, differences between the signal from different surfaces in the same room are found. For example, a study including 14 carefully chosen surfaces in a room showed that the signal (per unit exposure) has standard deviation of 20% [210]. In Ref. [212] a comparison between results obtained by two objects of the same person, is presented. The study includes 225 couples of objects, exposed for at least 20 years. A good correlation is found (with correlation coefficient R=0.77), but in some cases the results obtained by the two objects differ several times. Consequently, it is recommended that simultaneous measurements on several surfaces are performed in each home [195, 202].

The performance of the method was tested in an intercomparison between four laboratories, conducted in 17 homes with high radon activity concentration [203]. All laboratories used CR-39 detectors, calibrated with the same sources. The obtained mean relative variation in the determined ^{210}Po surface activities was 30% (half difference between the maximum and minimum value divided by the mean value determined by the laboratories). The mean relative variation in the determined radon activity concentration was 60%.

In several studies the results obtained by the glass-implanted ^{210}Pb method are compared with independently obtained estimates of the radon activity concentration. One of the studies includes 1089 measurements in homes in Iowa, USA, where elevated radon activity concentrations are found [207]. The study was part of an epidemiological study, involving women that have lived in their present homes for at least 20 years. The integrated activity concentrations of ^{222}Rn to which the glass surfaces were exposed was estimated based on contemporary cumulative measurements of radon. This estimate correlates with the measured surface activity of ^{210}Po (R=0.7) [207]. However, the results show that the same ^{210}Po activity in the glass might correspond to ^{222}Rn concentrations different by a factor of 10. According to [207], the correlation is significantly improved (R=0.84) when the present deposition velocities of radon progeny are taken into account.

In Ref. [214] results from several smaller studies are summarized. In most of them the correlation coefficient between the retrospectively estimated activity concentrations of ^{222}Rn and the independent estimates by other methods vary between 0.6 and 0.8 [212, 214]. Better correlation is obtained in two other studies. In the first, new glass objects are bought and are left in homes and schools for several years. Measurements of the activity concentration of ^{222}Rn are carried out throughout the whole exposure period the objects are exposed. The observed correlation coefficient in this study is R=0.9, but in some cases the activity concentrations of radon estimated by the two approaches differ 2-3 times [215]. The other study is carried out in buildings in which prospective measurements had been carried out systematically for the last 10 years. The correlation coefficient between the results obtained by retrospective and prospective measurements is R=0.92. In some of the studies worse correlation is found for smoking rooms than for nonsmoking [190, 211, 214]. This is explained by the fact that it is harder to model the behavior of short-lived radon progeny in smoking rooms, because the

frequency of smoking and ventilation should be accounted for. Similar problem is found for rooms with lots of electronic equipment [214].

It should be noted that, according to the modeling, the surface activity of ^{210}Po is expected to depend largely on the unattached fraction activity [203, 206]. This is due to the fact that the deposition velocity of the unattached fraction is much higher than this of the attached fraction. It is speculated that by combining the glass-implanted ^{210}Pb method with a retrospective method that directly estimates ^{222}Rn activity concentration (like the volume-trap) better estimates of the dose in the lungs could be achieved [216].

VI. 2.2. Volume-Trap Method

A detailed concept for the volume trap method was published in 1996 [217]. Like the glass-implanted ^{210}Pb method it uses the long-lived radon progeny, but in a substantially different way. The method is based on the ability of radon to diffuse freely into spongy materials. The decay of ^{222}Rn inside these materials leads to accumulation of long-lived radon progeny inside the material's pores. In this case, the spongy materials serve as volume traps for the long-lived radon progeny. An advantage of this method over the glass-implanted ^{210}Pb method is that the trapped activity does not depend on the behavior of short-lived radon progeny in the air, which could not penetrate inside the pores. Therefore, the signal is directly related to ^{222}Rn activity concentration. The method is applied by measurement of the activity of ^{210}Po in spongy material (like filling of mattresses or furniture). For this purpose samples of the interior of the object are taken. The surface of the object should be avoided, because the signal could be influenced by short-lived radon progeny from the air.

Usually ^{210}Po is extracted chemically and the extraction efficiency is determined by a tracer isotope (^{208}Po) [218]. Then, the activity of ^{210}Po (as well as that of the tracer) is determined by alpha-spectrometry. Details of the

radiochemical procedure are given in Ref. [218]. The most convenient material for the volume-trap method proved to be the filling of mattresses or furniture, which is polyester sponge, wool, cotton, etc. The following problems could lead to errors in the estimated ^{222}Rn activity concentration:

- Estimate of the volume of the sample during exposure.
- Differences in the ability of the materials to adsorb radon, which leads to differences in the ratio between signal and activity concentration of ^{222}Rn in the air.
- Objects that are very dusty and do not have clean interior.
- It is practically impossible to find out whether the material was recycled and reused.
- The method is destructive. The price of the objects may be high and their owners might not agree to provide them.

The lower detection limit of the method is not explicitly stated, but in Ref. [218] integrated activity concentrations of 1.2 kBq y m^{-3} are considered low and it is stated that in this case alpha-spectrometry measurements continue for several days. The declared uncertainty of the method is 30% [219]. Good agreement between results of the volume-trap method and independently estimated activity concentrations of ^{222}Rn is observed [219, 220]. The method has not been used for large measuring campaigns yet.

VI. 2.3. Eyeglass Lenses Method

The concept of the eyeglass lenses method was outlined by Fleischer [221]. One of the most widely used contemporary materials for lenses is CR-39 [221-223]. The alpha-particles emitted by ^{222}Rn and its progeny form tracks in the eyeglass lenses made from this material. It is assumed that the track density is

proportional to the integrated radon activity concentration. However, the signal depends on the complex behavior of the short-lived radon progeny in the air. The authors of the method note that it is better to develop the tracks on the inward-facing surface of the lenses (the one towards the face of the person). The tracks on this side are formed by radon progeny that has diffused in the air gap between the face and the glasses, which leads to more reproducible results. Moreover, the inner side is the one that is polished when the glasses are produced, which "resets" the signal. The experimental studies have shown that the track density on the lenses is higher at greater distances from the nose. This makes the exposure reconstruction complex. In addition, the habits of the owner of the glasses should be known – how long he/she wears the glasses, how often the glasses are cleaned, etc. Another methodological difficulty arises from the fact that the track properties of the lenses might differ significantly (up to 5 times differences are observed [223]). Therefore, individual calibration of each lens should be made by additional exposure.

The major obstacles for applying this method in epidemiological studies are that many people do not wear glasses and that the lenses of glasses are usually changed every several years. An advantage of the method is that the glasses act like personal dosemeters [224]. When the exposure is evaluated it is not necessary to carry out measurements in different rooms or to make assumptions about the exposure outside the person's home. Results show that the method allows measurements of ^{222}Rn activity concentrations in a wide range – from tens to several thousand Bq m^{-3}. Taking into account the drawbacks of the eyeglass lenses method, its author comments that the method should be applied as a supplement to other retrospective methods [223].

VI. 2.4. Method of ^{210}Pb Accumulated in the Skeleton

Another approach for retrospective measurements of ^{222}Rn that has been offered includes in-vivo measurement of the activity of ^{210}Pb accumulated in the skeleton of the exposed persons. The roots of this method lie in the miners' studies in the 60-ies of the last century [225-227]. Studies are undergoing in which the activity of ^{210}Pb in different bones is measured by low background gamma-spectrometry (see, for example Ref. [228]). The measurements should be carried in a shielded room, using detectors sensitive to the gamma-rays of ^{210}Pb (which have relatively low energy: 46.5 keV). A major problem in this approach is the fact that on average only 2% of the ^{210}Pb in the human skeleton could be attributed to inhalation of radon progeny [229]. About 86% is swallowed and about 12% is directly inhaled from the atmosphere [229]. Moreover, about 75% could be added by smoking or consuming alcohol. In Ref. [229] it is said that a measurable increase in the activity of ^{210}Pb in the skeleton could be found in people exposed for a long time to high radon activity concentrations (such as 20 years exposure to 2000 Bq m^{-3}). These estimates are made on the basis of studies of exposed miners. At this stage, the method is not applicable except for people exposed to very high concentrations of ^{222}Rn. For this reason this method will not be further discussed and commented on.

VI. 3. Compact Disk (CD/DVD) Method

The method is based on the same concept, described and discussed in Chapter V. The key idea is to combine the high radon absorption ability of some polycarbonates (bisphenol-A based, like Makrofol®, Makrolon®, Lexan®, Iupilon®) with their track-etch properties [136]. These polycarbonates are the basic constructive materials of the commercially available CDs/DVDs. On this basis a new method for integrated radon measurements (prospective or

retrospective) was developed. As the CD/DVD absorbs ^{222}Rn, the alpha-tracks inside the CD/DVD are related to the absorbed ^{222}Rn. However, the signal (the net track density) near the disk's surface is influenced by the plate-out. In order to cancel that influence, the tracks are developed (etched) at depth greater than the range of the alpha particles of ^{222}Rn and ^{220}Rn progeny with highest energy. For this purpose a surface layer with the necessary thickness is removed prior to the track etching. It was shown experimentally and theoretically that the thickness of the removed layer should be ≥ 76 μm. After the layer is chemically removed, the alpha tracks at that depth are etched electrochemically and counted (either visually or automatically). The track density is almost perfectly correlated with the integrated ^{222}Rn exposure. This became the fundament of the proposed CD/DVD method that employs home stored CDs or DVDs as retrospective radon detectors [138, 139]. In the last decade substantial experimental and theoretical work, dedicated on this method, was performed. The results of it are summarized in the following sections.

VI. 3.1. Principles of the Methodology

Albeit the CD/DVD method was proposed in 2001 [138], a version that can be considered "ready for use" was developed in 2005 [145]. After the exposed disks are collected, the following basic steps are carried out in the laboratory:

- Chemical pre-etching (CPE) to reach depth ≥ 76 μm;
- Electrochemical etching (ECE);
- Counting (automatic) of alpha tracks.

VI. 3.2. Preparation of Specimens

The preparation of the disks for etching starts with cutting a "specimen for etching". In principle, etching of the entire disk surface is possible, but for better productivity usually about a quarter of the disk is used. If DVDs have to be etched, after being cut they are split into two pieces (as the DVD consists of two thinner disks stuck together) and only that with the front surface (the surface that faces the laser of the CD/DVD reader) is etched. The thickness of the CD-pieces before etching is usually 1100 – 1200 μm and that of the DVDs after splitting is about 550 – 600 μm. Figure VI. 3 provides photos of the different stages of disk preparation and etching.

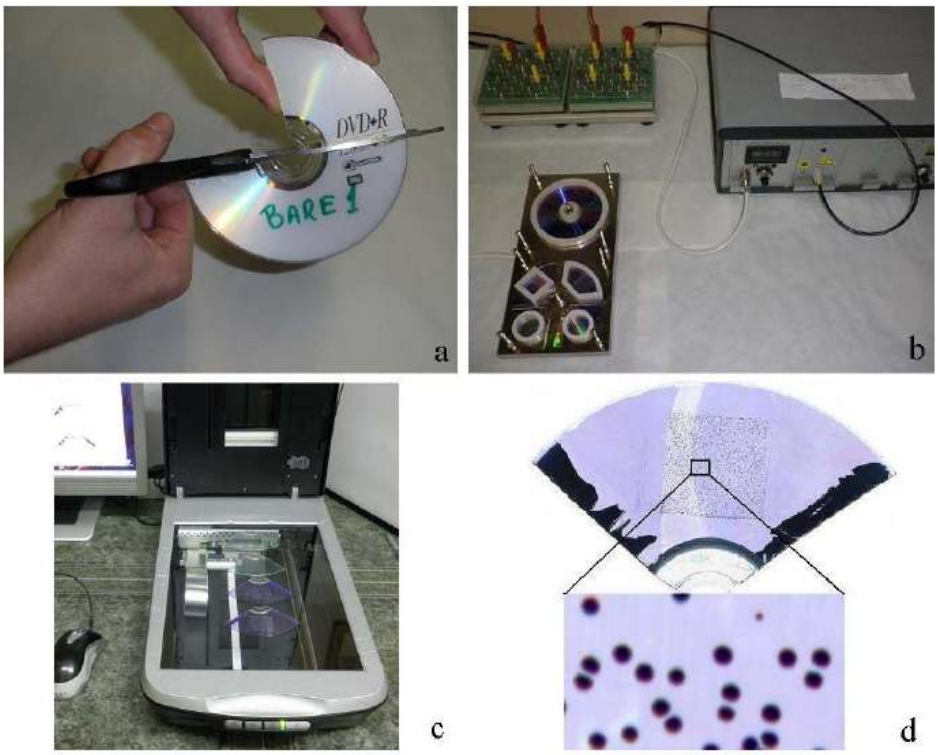

Figure VI. 3. Processing of the compact disks. After the exposed disks are gathered, one quarter of each disk is cut for further analysis (a). The disk pieces are chemically pre-etched and then electrochemically etched using the set-up shown in (b). Then, the etched part is scanned by a computer scanner (c) and the images are stored (d). The images are processed by dedicated software, which determines the track density [151].

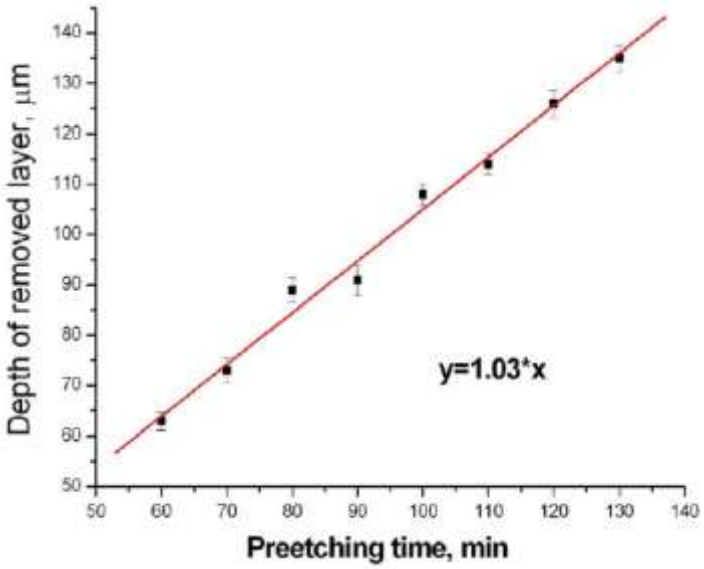

Figure VI. 4. Dependence of the thickness of the layer removed by chemical pre-etching on the pre-etching duration, obtained for the conditions described in the text. The etching rate (here 1.03 µm/min) could vary to some extent for different disks [230].

VI. 3.3. Chemical Pre-Etching

CPE is the process used to remove a layer with the desired thickness from the surface. We perform CPE at 300 C with a solution of KOH, water and methanol in mass ratios: 1:0.937:0.702. First KOH and water are mixed, and then methanol is added just before every pre-etching. The thickness of the removed layer is controlled by the pre-etching duration . In Figure VI. 4. the dependence between the removed layer and the duration of CPE is shown. According to these results, the dependence is linear and the CPE rate in this regime is about 60 µm/h. However, the actual removed thickness can vary and is always determined precisely by measurements with a micrometer before and after the CPE. The accuracy of this measurement is within ± 1 µm. In our practice, the standard

deviation in the thickness of the removed layer, determined by measurements at different points on a disk, is typically 1.5 - 3 μm.

VI. 3.4. Electrochemical Etching and Track-Counting

The alpha tracks in the CDs/DVDs are developed by electrochemical etching (ECE) with a solution described in [149,150] at 3 kV/mm effective high voltage (6 kHz frequency) at 250 C for 3 h. After the ECE, the developed tracks are counted manually (by an operator with an optical microscope) or automatically by means of a computer scanner and a specially developed algorithm for counting of ECE tracks in CDs. The manual counting is tiresome and time consuming and is not suitable for large radon measurement campaigns. It is further impeded by the fact that the number of tracks formed in the CD per year under typical indoor radon concentrations is relatively small. In contrast, the automatic counting with the help of a computer scanner is fast, easy to operate and very suitable for large measurement campaigns.

However, the automatic counting algorithm must cope with several difficulties which are specific to the CD/DVD method. First, the ECE tracks are large (around 0.1 mm in diameter) and have a specific dendrite structure which is visualized as dark and light zones on the track image This makes it difficult to automatically separate adjacent tracks without segmenting the single track. Second, at the time of etching the compact disks have already been used for over several years and their surface is often scratched. These scratches are developed during the CPE and ECE processes and introduces artifacts in the final images, which must be discarded by the counting algorithm. Thus, the application of other automatic algorithms, developed for etching other detector types (e.g. the one described in [33]), for counting ECE tracks in CDs/DVDs is not always reliable. To overcome these difficulties a dedicated algorithm for counting ECE tracks in CDs was developed. The algorithm uses specific global and local filters, object

filters and other criteria to discard artifacts and to estimate reliably the track density. A detailed description of the algorithm and its validation is published in [151]. The algorithm successfully identifies the large dendrite- shaped ECE tracks and separates clusters of tracks. It discards artifacts formed during the etching process and scratches which are common to home stored CDs. These features allow reliable counting in extreme cases of low (background) or high track densities (up to 2000 cm^{-2}, at depth 80 μm this corresponds e.g to 5 y exposure at > 2000 Bq m^{-3})). The performance of the algorithm is validated by comparison to manual counting for a wide span of track densities. The range of radon concentrations measurable with the CD/DVD method combined with automatic counting covers practically the whole range of radon concentrations encountered in dwellings (from a few to 100 000 Bq m^{-3} for 5 years exposure of the disks [151]). The automatic counting is between two and ten times faster than manual counting (depending on track density) and allows saving of the scanned and counted images for archive or for quality control. The automatic counting is currently in routine use for measurements by the CD/DVD method.

VI. 3.5. Calibration

One of the most important questions in retrospective radon measurements is whether there are individual differences between different objects used as "radon witnesses". One of the essential benefits of the CD-method is that every disk can be individually calibrated a posteriori – e.g. after the exposure under real conditions [130]. In concept, this mode of calibration employs the same equipment needed for the standard a priori calibration of new disks. The calibration exposure should be at constant temperature, ideally the same as the average room temperature during the real exposure (i.e. 20 – 22^0 C). The scheme of the used calibration equipment is shown in Fig. VI. 5. The ^{222}Rn source used in our experiments is a certified emanating ^{226}Ra source with activity 104.5 ± 1.5%

kBq. The hermetic "radon box" is usually with volume of 50 L, but in some situations smaller boxes (e.g. 10 L) are also used. The ^{222}Rn concentrations during exposure are followed by a reference monitor AlphaGUARD (Genitron GmbH, Germany) or, since 2012, RAD 7 (Durrige Inc., USA). Two modes of exposure can be employed: open and closed system. In open-system mode, ^{222}Rn concentrations can be kept constant by providing a constant air flow-rate. In closed-system mode, once the ^{222}Rn activity is transferred to the radon box, the box is kept closed during the exposure. In this mode, the concentrations during exposure decrease due to the radioactive decay of ^{222}Rn (provided that the box is hermetic). Normally, the open mode is preferred, but the closed one allows to reach much higher reference concentrations and thus the exposure time is reduced substantially.

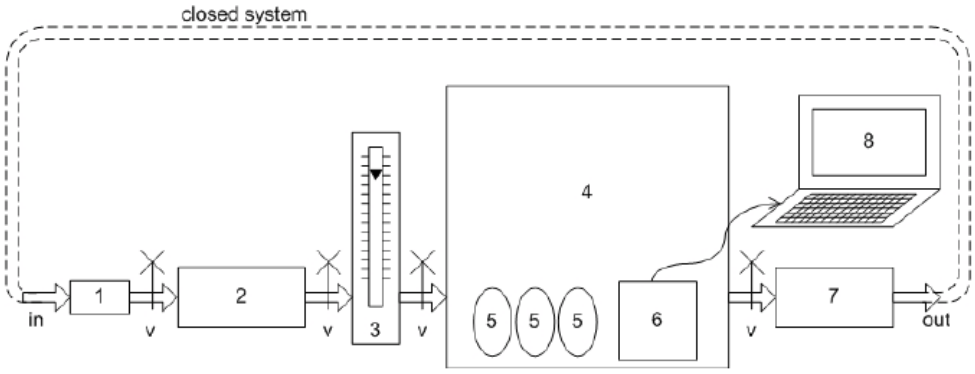

Figure VI. 5. Scheme of the calibration set-up: 1. Air-drying filter; 2. ^{222}Rn source; 3. Flow-meter; 4. Hermetic radon box; 5. CD/DVD; 6. Radon monitor AlphaGUARD PQ 2000 PRO; 7. Pump; 8. Computer; V – Valves. In the case of an open system, the pump ensures constant air-flow through the system, which is additionally controlled by the flow-meter. The activity concentration in the radon box is continuously monitored by the radon monitor and the measurements are stored in the computer. In close system the outlet of system is connected to its inlet. During the exposure the radon box is isolated to prevent activity leakage.

After exposure, the disks are left for at least two weeks in radon free atmosphere to degas. During this time the absorbed activity decreases due to radioactive decay and out-gasing. A theoretical model that describes this process is presented in Chapter V, along with experimental results verifying the model. Figure VI. 6 illustrates the decrease of ^{222}Rn activity inside an exposed disk. After calibration exposure, the disks are etched and the calibration factor is determined. In a priori calibration the net track density is the track density after the background is subtracted. However, in a posteriori calibration a piece of the analyzed disk is additionally exposed to referent radon activity concentration. In this case the "net track density" is that due to the calibration exposure: the difference between the track density of the piece exposed for calibration and the track density of piece that is not additionally exposed.

The *CF* also depends on the temperature. The concept of a posteriori temperature correction is described in Section V. 2. 3. 2. In our practice we usually apply an "average" *CF* to obtain a preliminary estimate. We always perform individual calibration, if the estimated concentrations are greater than 100 Bq m^{-3}.

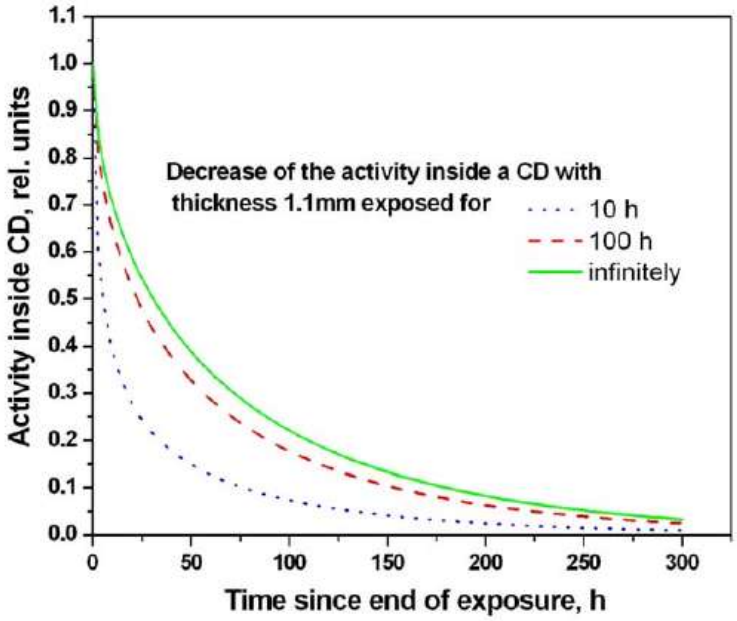

Figure VI. 6. Decrease of ^{222}Rn activity (desorption + radioactive decay) inside a compact disk (with 1.1 mm thickness) after the end of exposure. The lines are obtained by modeling [159] for different exposure durations. After about 2 weeks the activity left in the disk is negligible. The activity in thinner disks (DVDs) decreases faster.

VI. 3.6. Background Track Density

To study the "background" we have used 19 CDs/DVDs, randomly purchased from different shops. The background signal was determined at depth of 80 μm. The average track density obtained was 6.3 ± 2.4 cm^{-2}. Only one disk had abnormally high track density of 48 cm^{-2}. The estimates show that the above value for the background track density could lead to a maximum underestimation of the activity concentration of ^{222}Rn by 13 Bq m^{-3} for disks exposed 5 years [231, 232]. It follows that there is no danger of omitting buildings with high radon levels.

VI. 3.7. Uncertainty Budget

The uncertainty budget is shown in Table VI. 2. As seen, the typical uncertainty can be 16% when individual CF is applied. Rarely, the uncertainty can reach 60%. In these cases the maximum contribution to the total uncertainty comes from the uncertainty of the exposure time ("dating uncertainty") and the uncertainty due to the unknown temperature during exposure. As noted, the unknown temperature could be estimated and the signal corrected a posteriori. The dating uncertainty is a significant component in the uncertainty of the results of all types of retrospective methods.

Table VI. 2. Uncertainty budget of the CD/DVD method. The components of the relative uncertainty are estimated (at the level of 1 σ). The typical combined uncertainty is given for three different cases – when average calibration coefficient is used, when individual calibration coefficient is used and when both individual calibration and temperature correction are performed

Calibration type	Uncertainty type	Typical, %	Maximal, %	Comment
Standard	Statistical (track density) + calibration	19	19	
Individual	Statistical (track density) + calibration	9	17	
Standard/Individual	Exposure time	10	50	Maximal for disks exposed 1-2 years
Standard/Individual	Temperature related	15 (at 80 μm)	26 (at 120 μm)	No temperature correction, average temperature $22^0 \pm 4^0$C
Individual	Temperature related, after a posteriori temperature correction	8.4 (80 μm, 20^0 C)		
Standard	Combined	26	60	
Individual	Combined	20	60	
Individual, with a posteriori temperature correction	Combined	16		

VI. 4. Practical Applications of the CD/DVD for ^{222}Rn Measurements

VI. 4. 1. Real retrospective measurements by CDs/DVDs in dwellings

In real retrospective measurement the following questions were first addressed:

a) Whether different CDs taken from the same place give comparable results?

b) Will CD results match with independent estimates of retrospective ^{222}Rn concentrations based on past ^{222}Rn measurements by conventional methods?

To answer the first question we tried, whenever possible, to obtain more than one CD for analysis. Up to now we have obtained more than one disk from 8 different dwellings. From two of them 4 different CDs were obtained, from the remaining we received 2 or 3 disks. In all 8 cases the results with different disks gave statistically identical results. Results, obtained for a building in which we have obtained 4 different CDs are shown in Fig. VI. 7. As can be seen, different CDs give the same retrospective ^{222}Rn concentration within the experimental uncertainty. This conclusion is supported by results from other houses, from which we have obtained several CDs for analysis.

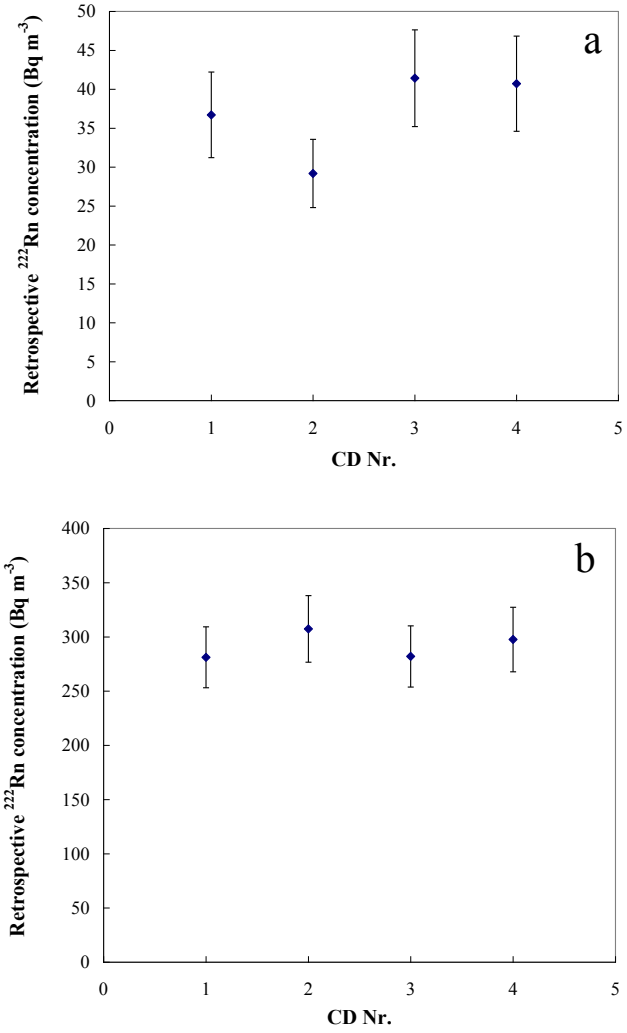

Figure VI. 7. Average retrospective ^{222}Rn concentrations measured by different CDs from the same place, a) dwelling with average ^{222}Rn concentration, b) dwelling with elevated ^{222}Rn concentration.

For twelve disks it was possible to make a comparison with alternatively determined retrospective ^{222}Rn concentrations by past measurements with diffusion chambers. All disks have been exposed since before the measurements by diffusion chambers were performed. Ten of the disks are from dwellings and

two from outdoor sites. In the studied dwellings during the interval in which the CDs were exposed no significant repairs or substantial changes (e. g. in the heating installation) were made. These disks have been exposed in places where long-term measurements by diffusion chambers were made in the past. They were done by conventionally used diffusion chambers with alpha-track detectors of Kodak-Pathe LR-115 type II. The diffusion chambers used are traceable to a primary ^{222}Rn standard, as described in Chapter II . There is a very good correspondence between the results obtained from CDs and those estimated from past measurements by diffusion chambers (Fig. VI. 8). More comparisons will be made in the future, but the pilot results seem promising.

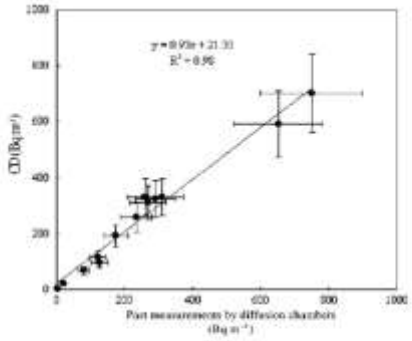

Figure VI.8. Correlation between measurements in places with known radon history. Retrospective ^{222}Rn concentrations by CDs are compared with average ^{222}Rn concentrations in the past, measured by diffusion chambers.

In practical applications the first step is to obtain one or more CD/DVD from the studied house. The general rule is to look for old disks and to try and date them in the best possible way. It can be useful that the year of production is marked on many commercial CDs and DVDs. However, in our opinion, the basic approach for dating is by personal communication with the disks' owners. Our experience indicates that, even though dating of each CD in the household can be problematic, in all houses there are some disks which the inhabitants can date with an accuracy of one year or even better. The disks are further processed in the laboratory. The DVDs, which are made of two thinner disks stuck together, are first split and only the lower half of the DVD is analyzed. The CDs are etched at their original thickness.

VI. 4. 2. A priori and a posteriori calibration

As it was already mentioned, the polycarbonate method allows two types of calibration - standard (or a priori) and a posteriori calibration. The standard calibration is done by exposure of new CDs/DVDs to reference ^{222}Rn concentrations, while in a posteriori mode pieces of old, already exposed in real conditions disks are additionally exposed to reference concentrations. The calibration exposure time is usually less than a few days. After the exposure the disks are left to degas for at least 2 weeks to allow all radon absorbed in the polycarbonate to degas or decay. After degassing the disks are treated by CPE and ECE as described above. As a result of the standard calibration, the calibration factor CF_{st} is determined:

$$CF_{st} = \frac{n}{I_{ref}}, \qquad \text{(VI.1)}$$

where $\boldsymbol{I_{ref}}$ is the reference integrated activity concentration during exposure and $\boldsymbol{n}$ is the net track density at a certain depth beneath the CD surface.

A benefit of the method is the possibility to apply a posteriori calibration to account for eventual differences in the properties of different CDs/DVDs used as radon detectors. In a posteriori mode an exposed disk taken from a studied dwelling is divided in several pieces, one of which is exposed additionally to reference radon concentration. After that, this piece is etched together with another, not additionally exposed, piece of the same disk. The difference between the average track densities of the two pieces gives the individual calibration factor $(CF_{a\ posteriori})$ of the studied CD:

$$CF_{aposteriori} = \frac{\Delta n}{I_{ref}}, \qquad \text{(VI. 2)}$$

where, Δn is the increment in track density due to the a posteriori exposure. In this way an individual calibration factor of each disk can be determined after the exposure.

The results from the standard calibration of 14 different CDs and DVDs are shown in Fig. VI.9. For most of the disks the CF_{st} is within 1 standard deviation (SD) of the average CF_{st}. Only one can be considered an "outlier" with *CF* 30% lower than the average. We can conclude that the studied set of new CDs/DVDs available on the market does not vary significantly in sensitivity to radon. From 5 brands we have calibrated both CDs and DVDs. Generally, CDs and DVDs of the same brand give similar results (circled on Fig. VI.9), with some indication for somewhat higher *CF* of DVDs. This will be better examined in the future, with larger number of CD+DVD couples. The SD of the entire group (CDs + DVDs) of calibrated disks is 13%. In general, this can be considered as the best achievable accuracy after a priori calibration. Better control on the uncertainty can be achieved by individual a posteriori calibration.

A posteriori calibration was made for a set of 16 CDs of different brands. Notably, the average *CF* obtained for this set of disks is the same as the a priori determined *CF* (0.0193 ± 0.0039 cm^{-2}/kBq h m^{-3} vs 0.193 ± 0.0026 cm^{-2}/kBq hm^{-3} for a priori calibrated set). The maximum difference between individual *CF* and

the average was about 40%. Such differences are a serious argument in favor of individual a posteriori calibration.

If the standard (a priori determined) calibration factor is used, in most cases the results will presumably be within ±13% of the true radon exposure. However, the potential of the method for precise measurements is much better. To study it, we have modeled the uncertainties at different Rn-levels both for a priori and a posteriori calibration. The counted number of tracks on a virtual 4 cm^2 field were considered as Poisson variables and standard algorithms for error propagation were applied [42]. The reference integrated ^{222}Rn concentration used for calibration was assumed to be $2x10^4$ kBq h m^{-3} known with 5% uncertainty. The results are shown in Fig. VI.10. With a posteriori calibration the individual uncertainty decreases to about 7% and then increases due to the decrease in the relative difference between the original track density and the track density after the calibration exposure. By selecting appropriate conditions for the a posteriori calibration, accuracy better than 10% can be targeted for a wide range of concentrations. Notably, the best accuracy with the studied model is observed at about 200 Bq m^{-3}, a level at which the action limit in some countries is set.

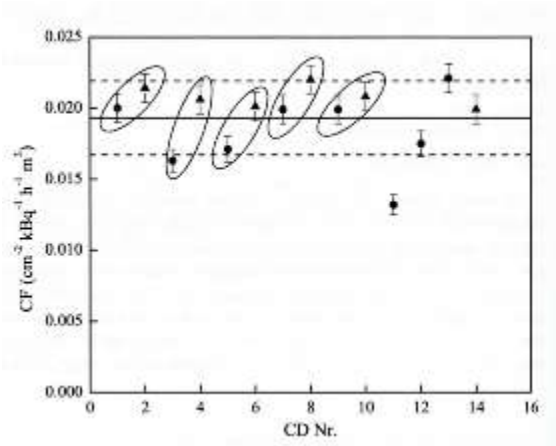

Figure VI. 9. Standard (a priori) CFs of 8 new CDs (●) and 6 new DVDs (▲) of different brands. The circled are one brand couples: CD (left) and DVD (right). The brands from left to right are: Mr. Data, Sony, HP, Verbatim, Princo.

The average CF (solid line) and the borders of the ± 1 SD interval (dashed lines) are shown.

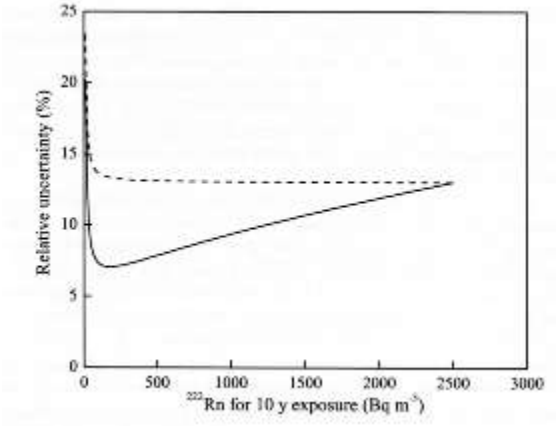

Figure VI. 10. Modeled relative uncertainty after standard (dashed line) and a posteriori (solid line) calibration under assumptions described in the text.

VI. 4. 3. Pilot surveys

Most of the pilot radon measurements by CDs/DVDs were carried out in dwellings in the city of Sofia or in areas in Bulgaria where radon concentrations are elevated. Results from pilot retrospective radon measurements with CDs/DVDs can be seen on Fig. VI.11. The bars numbered from 1 to 25 represent radon activity concentrations in random dwellings in the city of Sofia. With one exception they do not exceed 100 $Bq.m^{-3}$ and the average value is close to the weighted average indoor radon concentration of about 40 $Bq.m^{-3}$. The bars numbered from 43 to 49 represent measurements in buildings in the region of Bouchovo. This region is affected by former uranium mining and for each of the studied buildings previous measurements have shown elevated radon concentrations. The results from retrospective measurements also indicate that radon activity concentrations in these buildings are considerably above the average. The bars numbered from 26 to 42 represent measurements in dwellings in the village of Eleshnitsa. The village is situated in a valley of enhanced natural

radioactivity and was a center of uranium mining and milling. Previous measurements in this village have shown elevated indoor and outdoor radon concentrations [24]. In most cases the activity concentration of radon exceeds 100 $Bq.m^{-3}$.

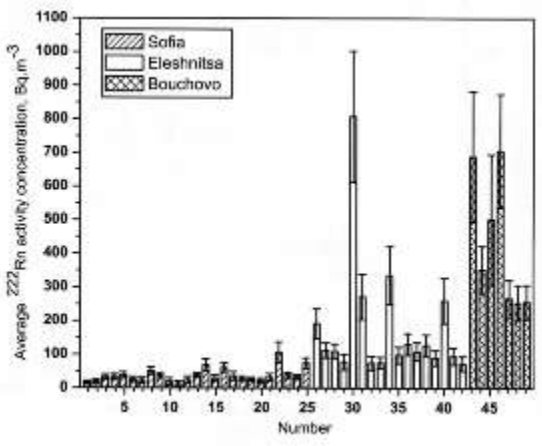

Figure VI. 11. Average retrospective radon concentrations measured by CDs exposed in dwellings. Sofia is a "normal", while Eleshnitsa and Bouchovo are radon prone areas. Vertical bars represent 1 SD uncertainty.

Even though the pilot results presented here are not sufficient for detailed mapping of the regions of interest, the number of measurements can be increased quite rapidly. At the moment up to 24 disks per day can be processed simultaneously in our laboratory. Since CDs/DVDs are available in the majority of households, the method has a potential for large-scale use.

In the last 3 years we have tried to organize measuring campaigns using the CD-method. A major advantage of this approach is that it allows the entire campaign to be organized remotely, e.g. the disks could be collected by post. Results obtained in our studies on this approach for normal and radon-prone areas are shown in Figure VI. 12 [230]. The radon-prone regions are well known from previous data and this was confirmed by the pilot CD/DVD-based survey.

Therefore, we conclude that the method can be used for identification of radon-prone areas and for radon mapping.

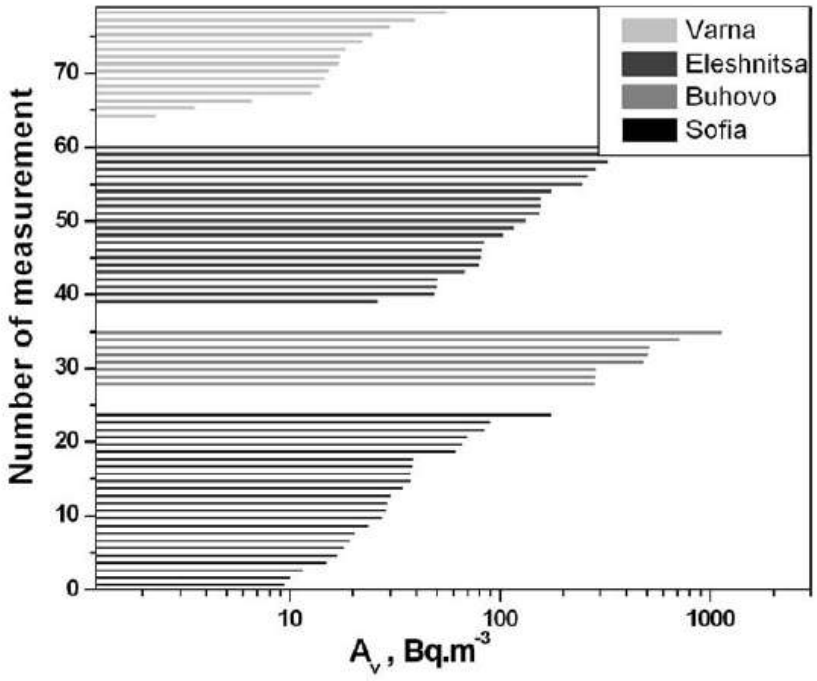

Figure VI. 12. Results of retrospective radon measurements by CDs/DVDs performed in normal (Varna and Sofia cities) and radon-prone (Buhovo town and Eleshnitsa village) areas in Bulgaria.

In the course of the first measurements under real condition carried out with the CD/DVD method some logistical points related to the organization of large-scale surveys arose. These questions are related to the logistic of such surveys. So far our experience in this field is in intermediate stage. To address the above issues we organized pilot radon surveys in several regions in Bulgaria [130, 231-233]:

- Two radon-prone regions;
- The city of Sofia ;

- The region of Varna and Dobritch cities .

Normally, the "disk age" is provided by its owner. This mode of dating is somewhat subjective and therefore, we should be aware about the possible bias/uncertainty in the results because of this. As a more objective manner for dating we explored the possibility to use the record/production date of the CDs/DVDs (excluding rewritable disks). Such information is not always available and we succeeded to obtain it for less than a third of the analyzed disks. The dates, according to the two dating approaches, correlate well and in most cases the differences between them are within 10% [231]. However, in 12% of the disks greater differences were observed [231]. As noted above, one of the aims of the pilot surveys organized in Sofia and Varna was to study the reaction of the participants. In Sofia there were 4 active contact persons, while in Varna the contact person was one. The contact persons were responsible to:

- Provide a short information about radon, based on the "core messages" of the World Health Organization [1];
- Inform the participants that their participation is voluntary and anonymous;
- Provide a short info about the CD-method and ask for one or more CD/DVD for which dating information is available.

The percentage of contacted persons that agreed to participate and to give disks for analysis was 32% in Varna (if the numbers are considered as Poisson variables, the 95% confidence interval (CI) of this percentage is 18 – 52%) and 50% in Sofia (95%CI: 37 – 65%) [231-233]. On this basis we expect that in Bulgaria, between a third and a half of the people will react positively and will provide at least one dated disk after a single personal contact. Also small part of the contacted people (<20% in our surveys) steadfastly refuse to participate. Even

from this preliminary experience some practical conclusions can be drawn. For instance, if radon survey in 1000 homes is planned, the number of contacted persons should be at least 2000, while probably 3000 will suffice. Further work will focus on remote measurements and will supplement the experience in the organization of efficient large-scale radon surveys.

VI. 4. 4. Detection of Changes in Concentrations in the Past

One additional possibility for practical application was recently explored [231, 233]. It is important to know whether large changes in radon concentrations occurred in the past. This is particularly important for dwellings with radon mitigation installation, the efficiency of which should be followed. The concept is to analyze two or more disks of different age. This makes it possible to evaluate differentially the concentrations in different time intervals, as shown in Figure VI.13. In the hypothetical example shown in Fig. VI.13, two disks are analyzed: a 5-year old and a 10-year old. It is assumed that the average concentrations determined by the two disks for the covered intervals are each estimated with uncertainty of 15 % and the ages of the disks are know with uncertainty 10%. Then, the average concentration for the first 5-year interval can be reconstructed with an uncertainty of about 35%. This approach was already applied in practice for a building with passive mitigation and the obtained estimate for the efficiency of the mitigation system agreed well with that obtained by prospective measurements.

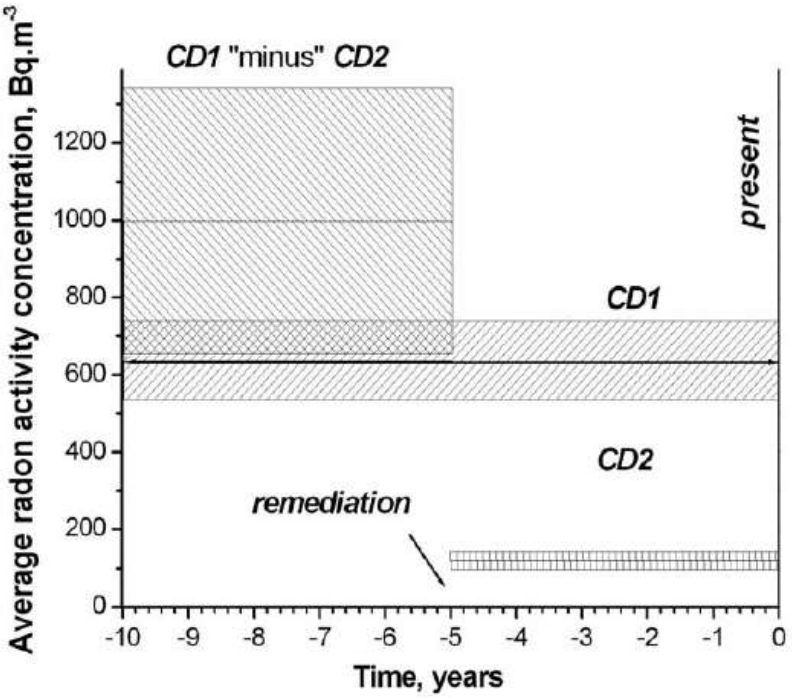

Figure VI. 13. Example of detection of changes in radon concentrations in the past by two disks exposed for different time – 5 and 10 years. It is assumed that remediation is carried out before CD2 is bought. The difference in the signal accumulated in the disks allows estimation of the average activity concentration of radon before the remediation and the resulting decrease.

VI. 5. Summary of the main methods for retrospective measurements and advantages of the CD/DVD method

The four methods for retrospective radon measurements, considered in this chapter, are summarized in Tables VI. 3 – VI. 5. Due to the relatively short time interval covered by the eyeglass lenses method, its author comments that it could be used subsidiary to another method. On the other hand, the volume trap method could cover sufficiently long periods in the past and has relatively low uncertainty. However, the major disadvantage of this method, which impedes its

application in large scale surveys, is the relatively complicated methodology and the fact that it is destructive. Up-to-now, two methods were used for radon surveys: the glass-implanted method and the CD/DVD method. If we consider the criteria formulated in the introduction of this chapter, the only method that meets all of them is the CD/DVD method. It is reliable, with simple methodology and covers the whole range of indoor ^{222}Rn concentrations observed in practice. It also offers the possibility for parallel retrospective measurements of both ^{222}Rn and ^{220}Rn by a single CD or DVD, that will be considered in the next chapter. Moreover, based on the methods' performance under real conditions, we conclude that the CD/DVD method demonstrates clear advantages in terms of both large scale applicability and accuracy. In 2010 this method was tested and certified by the accredited radon calibration laboratory of Bundesamt für Strahlenschutz, Germany (Certificate DKD-K-23001, Nr. 523/2010).

Table VI. 3. Methods for retrospective measurement of ^{222}Rn: Object used for the measurements. The comparison points are selected, because they are either important for identifying dwellings/public buildings with radon problem or for improving risk estimation

METHOD	Glass- implanted $^{210}Pb/^{210}Po$	Volume traps	Eye-glass lenses	Absorption in CD/DVD
OBJECT: a) type b) maximum age c) available record of age d) availability - in homes - in public buildings e) moved when the owners are moving f) destroyed in the analysis	a) glass surfaces b) very long c) possible for picture frames d) - yes, in most rooms - yes e) some objects – picture frames f) no	a) fillings of matresses/ furniture b) up to 20-30 years c) no d) - yes, in some rooms - sometimes e) sometimes f) yes, relatively high price of objects	a) eyeglass lenses b) up to 5 years c) yes, exact record d) objects are personal e) N/A f) yes, but old lenses could be used	a) CDs/DVDs b) widely used for over 20 years c) sometimes – by production date or dates of files d) – yes, in one room -yes, in offices, schools, kindergardens e) yes f) yes, but disks are cheap

Table VI. 4. Methods for retrospective measurement of ^{222}Rn: Characteristics of the methodology. The comparison points are selected

METHOD	Glass- implanted $^{210}Pb/^{210}Po$	Volume traps	Eye-glass lenses	Absorption in CD/DVD
METHODOLOGY a) signal related to b) additional info needed c) individual calibration of objects d) typical uncertainty e) maximum error f) range of CA for 10y g) additional info for: - changes in CA with time - radon progeny h) measurements of ^{220}Rn (thoron)	a) plated-out radon progeny b) for the object age, habits of occupants for ventillation smoking, heating, etc. c) not possible d) 50-70% e) by a factor of 10 f) >100 Bq m^{-3} g) in theory: signal is weighted for risk signal is corellated with fp h) not studied	a) ^{222}Rn in the air b) just for object's age c) possible but would take >1 y d) about 30% e) could be high if objects are recycled f) >100 Bq m^{-3} g) - not studied no h) not studied	a) radon progeny in the air between the face and the glasses b) for the object age, assumption for F, habits of the glass wearer c) yes, a posteriori calibration d) not estimated e) not estimated f) N/A g) not studied h) not studied	a) ^{222}Rn in the air b) just for object's age c) recommended, takes 2 weeks d) 20% or 16% with temperature correction e) 60% for 1-2 year-old disks f) > 7 Bq m^{-3} g) - significant changes in C_A could be detected using 2 or more disks with different age no h) yes, research is ongoing

Table VI. 5. Methods for retrospective measurement of ^{222}Rn: Applicability for large scale campaigns. The comparison points are selected

METHOD	Glass- implanted $^{210}Pb/^{210}Po$	Volume traps	Eye-glass lenses	Absorption in CD/DVD
APPLICABILITY FOR LARGE SCALE CAMPAINGS a) visits needed b) price of analysis c) necessary equipment d) duration of analysis	a) 2 visits needed b) low c) for etching and counting tracks d) several months, simultaneously in many homes	a) 1 visit needed b) relatively high c) radiochemical laboratory, alpha-spectrometry d) a few days per measurement	a) remote measurement b) low c) for etching and counting tracks and calibration exposures d) a few days, simultaneously	a) remote measurement b) low c) for etching and counting tracks and calibration exposures d) 2 weeks, simultaneously

VII. OTHER APPLICATIONS OF THE POLYCARBONATE METHOD

VII. 1. Measurements of ^{222}Rn in water by absorption in polycarbonates

The approach based on the ability of some polycarbonates to absorb radon can be expanded for quantitative measurements of ^{222}Rn in water and in soil gas. In this case the measurements are prospective: the polycarbonate specimen is left for exposure that is usually short-term (days or weeks) and afterwards measured. Despite that in many cases the absorbed activity is sufficient to be measured by detecting beta or gamma radiation, [147] the best sensitivity is achieved by etching and counting alpha-tracks, using the same methodology employed for measurements in air. Benefits of this method in the case of radon in water measurements is that the specimens can be exposed directly in the water source (e.g. directly in the water supply of a village). Thus, the activity of radon in domestic drinking water can be determined "at the source" as recommended by the Commission of the European Communities [234].

Concentrations of ^{222}Rn in water are of interest for radiation protection [235], radon spa balneology [96, 97] and seismology [236, 237]. To date most of the methods used for measurement of ^{222}Rn in water are based on laboratory analysis of water samples by means of liquid scintillation counting, emanometry by ionization or scintillation chambers, or gamma spectrometry [238]. First demonstration of the feasibility to employ absorption in polycarbonates for quantitative measurement of ^{222}Rn in water was published by Pressyanov et al. [147]. In these experiments square samples of Makrofol (thickness 0.3 mm, area 8.75 cm^2) were placed in hermetic vessels filled with water with different activity concentrations of ^{222}Rn. The activity concentration of ^{222}Rn in each vessel was prepared by mixing water with high ^{222}Rn concentration (taken from the mineral spa "Momin prohod") and radon-free distilled water in known proportions. The activity concentration of ^{222}Rn in the mineral water was 1595 Bq L^{-1} ± 6% (1σ confidence level). It was determined by gamma spectrometry with HPGe detector (ORTEC, relative efficiency of 24.9% and 1.9 keV resolution for the 1332 keV line of

^{60}Co) in geometry "Marinelli" beaker 1000 cm^3, using 295 and 352 keV gamma-lines of ^{214}Pb. The activity concentration of ^{222}Rn in each vessel was calculated using the known ratio of the volumes of the mineral and distilled water.

The detectors were exposed for a controlled time (48 h). The measurements of the detectors started 3 h after their removal from the vessels (in order to eliminate the contribution of the surface plate-out of the short-lived ^{222}Rn progeny). The radiation from the short-lived progeny, generated by ^{222}Rn absorbed in the detector volume, was measured by gross beta counting and gamma spectrometry.

The correlations between the signal of the detectors and the activity concentration of ^{222}Rn are shown in Figs. VII.1 and VII.2. As can be seen, the correlations are very good in both beta counting and gamma spectrometry. The minimum detectable activity concentration (MDAC) was estimated using the approach described in [158]. Assuming 1 h counting time, the estimated MDAC was about 20 Bq L^{-1} both for beta counting and gamma spectrometry. Therefore, this method is applicable for measurement of radon concentration in drinking water since its estimated MDAC is sufficiently lower than the recommended by the Commission of the European Communities reference concentration of 100 Bq L^{-1} [234].

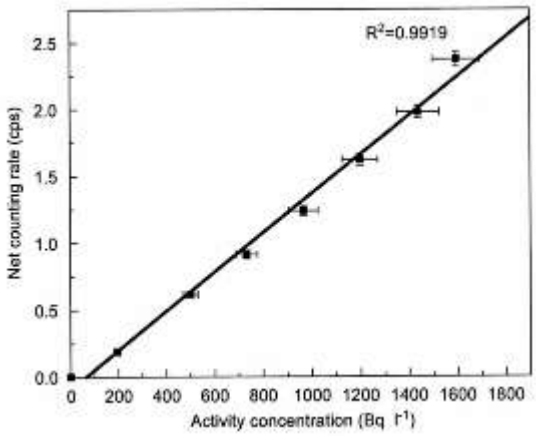

Figure VII. 1. Correlation between the measured net beta counting rate and the activity concentration of ^{222}Rn in the water samples in which the polycarbonates were exposed.

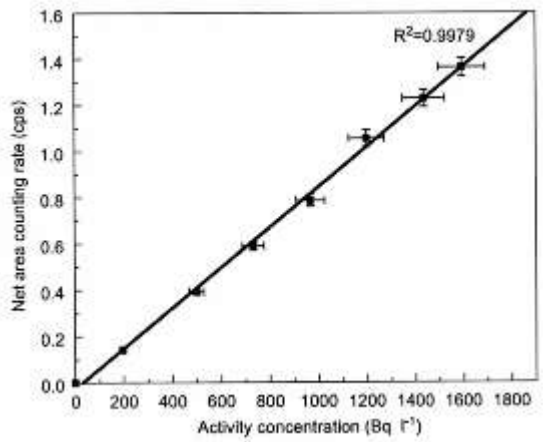

Figure VII. 2. Correlation between the measured net area counting rate of the 352 keV full-energy peak of ^{214}Pb and the activity concentration of ^{222}Rn in the water.

The MDAC can be significantly lowered if the detectors are etched for alpha tracks. Therefore, dedicated research was carried-out in this direction [148]. Interesting observation valid for the "track version" of the method for water is that water can be ignored as a direct source of α-particles, provided that there are no other α-emitters present in the water in concentrations comparable to that of radon. This is because of the very high partition coefficient (K=100) for the bisphenol-A polycarbonate in water [142]. A dedicated theoretical model was developed to evaluate the track density as a function of depth between the surface. Results are illustrated in Fig. VII. 3. As seen, the signal has maximum at a depth 40 – 60 μm beneath the surface. Also from the model it follows that the surface track density due to radon and its progenies in the water is only about 2% of this due to radon and its progenies inside the polycarbonate. It appears that in this case even the tracks on the surface are almost entirely due to the absorbed in the polycarbonate radon and the step "removal of a surface layer" can be, eventually, skipped.

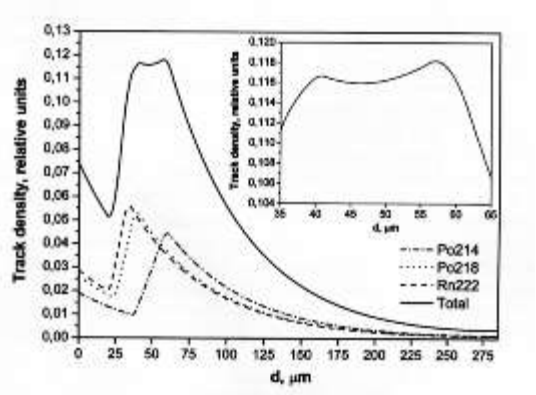

Figure VII. 3. In-depth track density distribution inside polycarbonate detectors with thickness L=570 μm exposed in water at temperature 21^0 C, obtained by theoretical model presented in Ref. [148]. The distribution is symmetrical with respect to the middle of the detector and half of it is shown. The solid line represents the total track density, obtained by summing the three components due to ^{222}Rn and its progeny (dashed lines). The region where the track density is highest is shown magnified.

In the first experiments polycarbonate detectors were placed in water with known activity concentrations of ^{222}Rn. Well water was used with ^{222}Rn activity concentration of 195.2 Bq L^{-1} ± 4.6%. This value was estimated by gamma-spectrometry with HPGe detector of relative efficiency of 24.9% and FWHM of 1.9 keV for the 1332 keV gamma-line of ^{60}Co. The gamma-lines of ^{214}Pb with energies 295 keV and 352 keV were used for the analysis. The detectors were exposed in 2 L plastic bottles that were tested to be hermetic to radon. For each bottle the integrated activity concentration in the water was determined as:

$$I = \frac{C_{A0}}{\lambda}\left(1 - e^{-\lambda T}\right), \qquad \text{(VII.1)}$$

where C_{A0} is the initial activity concentration of radon in the bottle, λ is the decay constant of ^{222}Rn and T is the exposure time. Different initial concentrations were prepared in the same way, as in the pilot series described above. However, in this experiment the exposure time for the specimens in different bottles varied (in the interval

3 – 572 h, but in most cases less than 168 h). During the exposure the bottles were stored in a room with temperature of 21 ± 2^0 C and after the exposure the detectors were left to degas for a month at the same temperature.

The correlation between the net track density and the integrated ^{222}Rn activity concentrations are shown for three different depths beneath the detector surface at Fig. VII.4 a-c. The results clearly show that alpha-track etching of Makrofol detectors exposed in water can be used for quantitative measurement of ^{222}Rn in water. Moreover, we have used this method in the 2009 intercomparison of radon-in-water measurements conducted by the Nuclear Chemistry Laboratory at the New York State Department of Health [239]. Our results agreed with the reference concentration within 10% [239]. Our successful participation in this intercomparison is an argument in favor of the feasibility of this method.

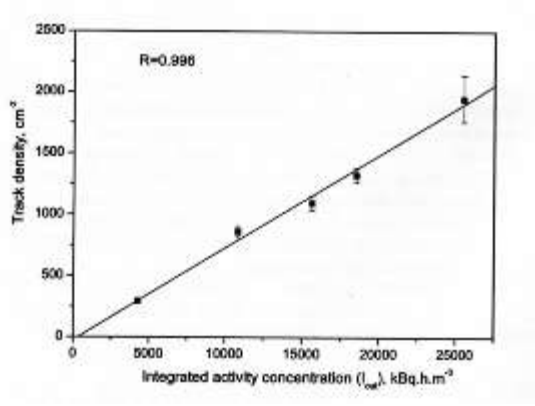

(a)

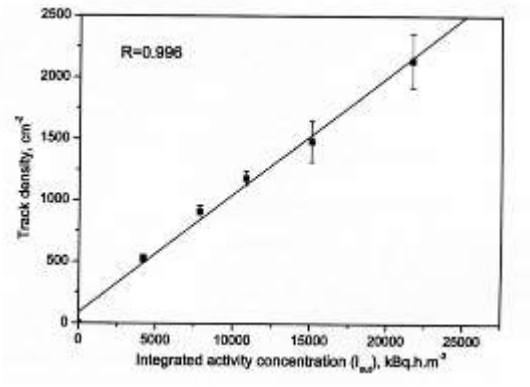

(b)

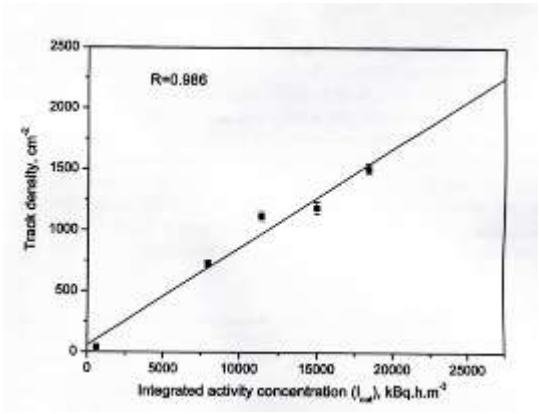

(c)

Figure VII.4. Dependence of the net track density on the integrated activity concentration of ^{222}Rn in the water. The track density is at: (a) depth 80 μm, (b) depth 60 μm, (c) at the surface.

The lower limit of the method was evaluated by the MDAC following the approach of Currie [158]. More details about this procedure are provided elsewhere [148]. The obtained results for 30 days exposure time are given in Table VII.1.

Table VII.1. Detection limit for ^{222}Rn in water determined by etching polycarbonate detectors, exposed in water, at different depth.

Depth (μm)	0	60	80
MDAC (Bq L^{-1})	0.069	0.058	0.073

An advantage of the proposed method for measurement of ^{222}Rn is that measurements could be made directly in the water source. Despite the relatively long time required for exposure, simultaneous measurements can be made in a large number of points. This is useful for monitoring or environmental surveys of water supplies.

VII. 2. External absorber as radiator

A new concept for radon monitors was recently proposed by [240-243]. The concept is to couple a SSNTD with external foil that absorbs radon and serves as a radiator. The first experiments, presented in Ref. [240] revealed a great potential for practical applications. These new dosemeters are remarkable with their compactness and can easily be fitted in many different objects like personal film or TLD dosemeters, document cases, staff-officer badges etc. To study the potential of this approach, a theoretical and experimental research was carried-out.

VII.2.1. Modeling response of radon track detectors with solid absorbers as radiators.

VII.2.1.1. Source geometry

Once radon atom is caught by a surface trap it further diffuses through the absorber volume. The model considers gas penetration from the both sides of the plate plastic radiator. This case can be considered as common, as the detector is not in hermetic contact with the absorber and radon penetrates freely through the small gap between the detector and absorber. We have considered two types of absorbers made from polycarbonate foils of high radon absorption ability [244]. The first type (Fig. VII.5) was monolithic absorber. The concentration profile in such absorber is by the theoretical model described in Chapter V.3.2 and illustrated on Fig. VII. 5. (right). The second type (Fig. VII.6) was composite absorber (C-absorber): a stack of several thin absorber foils stuck together but so that radon can diffuse freely between them. The resultant concentration profile in C-absorber is stuck by individual profiles of the foils, each foil considered as M-absorber (Fig. VII. 6). For 80 μm C-absorber of 4x20 μm thick absorber foils the maximum deviation of the real concentration profile from the homogenous one was within 3%. In modeling we have approximated this profile with "homogenous radon distribution".

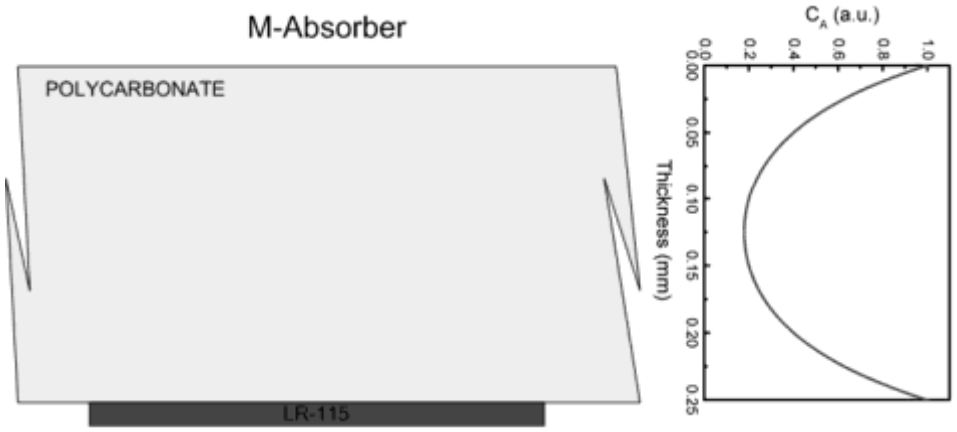

Figure VII.5. Illustration of exposure geometry of LR-115/II detector with monolithic absorber (M-absorber) of 250 μm thick Makrofol DE foil. Radon enters freely from both sides and decreases in depth due to radioactive decay. On the right the activity concentration profile is shown.

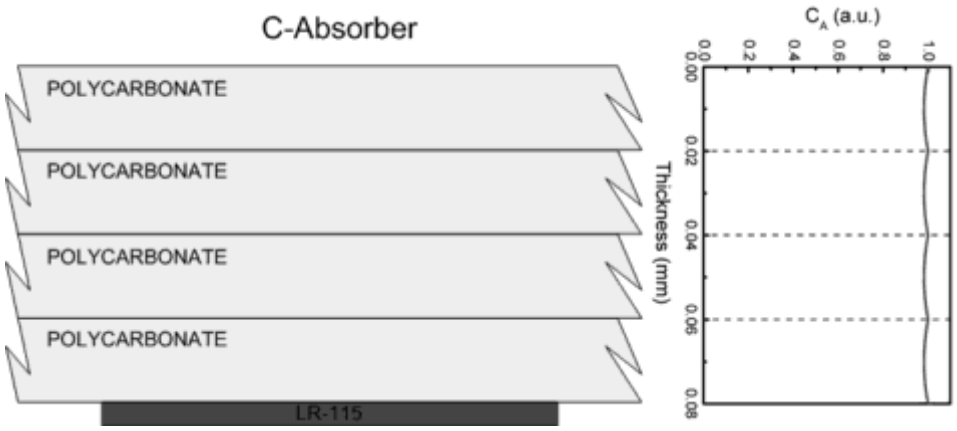

Figure VII.6. Exposure geometry with composite absorber (C-absorber) made of 4 Makrofol N foils with thickness 20 μm. Radon enters freely from both sides of each foil and its concentration profile is almost constant.

VII.2.1.2. Detector response

Detection properties of a SSNTD are described by the "response function" of the detector. The response function $\Theta(E,\theta)$ is 1 – if α-tracks appear for alphas of energy E and incidence angle θ, and 0 otherwise. Alpha tracks related to ^{222}Rn are formed by 3 alpha emitting isotopes: ^{222}Rn, ^{218}Po and ^{214}Po (always in equilibrium with ^{214}Bi). The concentration profile of ^{218}Po and ^{214}Po is the same as that of ^{222}Rn as decay atoms stay immobilized in the solid matrix. The detection geometry – absorber + detector in contact with its surface is shown in Fig. VII. 7. In the present model we assume that tracks are formed only by alpha particles that originate from the interior of the absorber. This corresponds to the physical reality when:

- The absorber is sufficiently thick, so the alphas from the front space and from the radon progeny plate-out on the front surface cannot create tracks. For example with LR-115/II detectors this is ensured by > 50 μm thick polycarbonate absorber;
- The gap between the detector and the back surface of the absorber (Fig. VII.7) is very small (e.g. of the order of micrometers) so the plate-out on the surfaces there can be neglected.

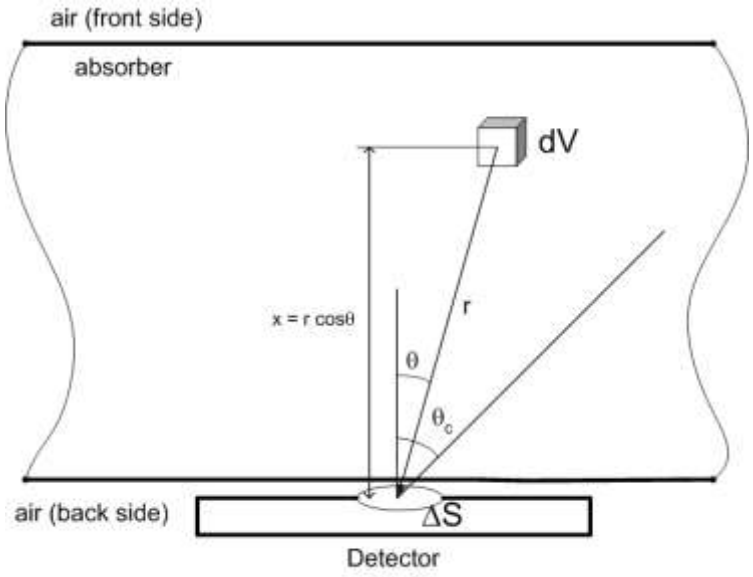

Figure VII.7. Geometry of the irradiation by alpha particles of a detection spot ΔS. The critical angle θ_c is the maximum incident angle at which etched tracks can be revealed.

Under these assumptions, the partial track density from the alphas of the i-th nuclide (i=1,2,3 refer to ^{222}Rn, ^{218}Po and ^{214}Po, respectively) is given by the expression:

$$d\dot{n}_i = \frac{\cos\theta}{4\pi r^2} a_i \Theta(E,\theta) dV \qquad \text{(VII.2)}$$

where $a_i = \lambda_i c_i$ is the activity concentration of the i-th isotope. Under equilibrium $a_1 = a_2 = a_3$. Taking into account eqn (V.34) one obtains:

$$n_i = \int_0^T \iint_V \frac{\cos\theta}{4\pi r^2} a_i \Theta(E,\theta) dV dt = K I_0 \int_{\{r,\theta\}} \frac{\cos\theta}{4\pi r^2} \left[A\exp(-x/L_D) + B\exp(x/L_D) \right] dV \qquad \text{(VII.3)}$$

where $\{r,\theta\}$ is the partial volume from which the alpha particles can hit the detection spot so the etched track will be revealed and I_0 is the integrated ambient ^{222}Rn activity concentration. Taking into account that $x = r\cos\theta$:

$$n_i = \frac{1}{2} K I_0 \int_0^{\theta_c} \int_{r_1(\theta)}^{r_2(\theta)} \left(A \exp\left(-\frac{r\cos\theta}{L_D} \right) + B \exp\left(\frac{r\cos\theta}{L_D} \right) \right) \sin\theta \cos\theta \, d\theta \, dr \, . \qquad \text{(VII.4)}$$

Physically, the meaning of the distances r_1 and r_2 is that the α-particle of energy E_i, emitted from a distance in the interval (r_1, r_2) arrives at the detection point with energy within the detection window, e.g. within the interval (E_L, E_U). Let $R_U(\theta)$ and $R_L(\theta)$ are the α-particles ranges corresponding to the energy of the upper $(E_U(\theta))$ and lower $(E_L(\theta))$ energy threshold for detection at this angle θ. For detectors Kodak Pathe LR-115/II always $R_U(\theta) \leq R_i$, where R_i is the range of α-particles from the i-th isotope. In such case $r_2(\theta)=R_i-R_L(\theta)$ and $r_1(\theta)=R_i-R_U(\theta)$. However, for CR-39 detectors there are angles ($\theta < \theta_1$) for which $R_U(\theta)>R_i$. In this case $r_1=0$. The range-energy dependence of [90] has been used, along with the response function to obtain the functions $R_U(\theta)$ and $R_L(\theta)$. These functions for Kodak Pathe LR-115/II and absorber of Makrofol are shown in Fig. VII. 8.

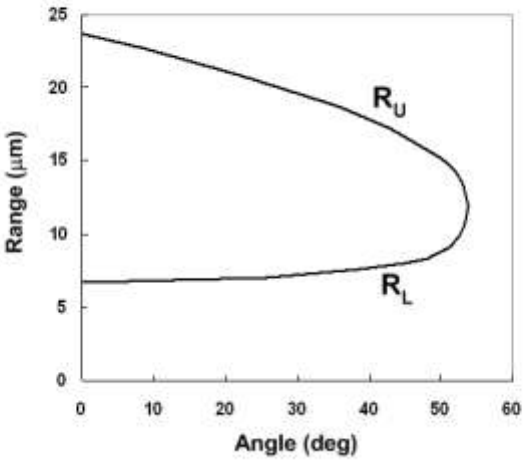

Figure VII. 8. Lower R_L and upper R_U threshold ranges as dependent on the incident angle θ for detector Kodak Pathe LR-115/II. At any θ the detection window is between R_L and R_U.

Response to radon is described in terms of *CF*. According to the above model, the *CF* is given as follows: $CF = CF_1+CF_2+CF_3$, where, for the case of M-absorber:

$$CF_i = \frac{1}{2} K \int_0^{\theta_c} \int_{r_1(\theta)}^{r_2(\theta)} \left(A \exp\left(-\frac{r\cos\theta}{L_D} \right) + B \exp\left(\frac{r\cos\theta}{L_D} \right) \right) \sin\theta\cos\theta d\theta dr = \frac{1}{2} K L_D J_i , \quad \text{(VII.5)}$$

where:

$$J_i = \int_0^{\theta_i} \left(A\left(1 - \exp\left(-\frac{R_i - R_L(\theta)}{L_D}\cos\theta\right)\right) + B\left(\exp\left(\frac{R_i - R_L(\theta)}{L_D}\cos\theta\right) - 1\right)\right)\sin\theta d\theta +$$

$$+ \int_{\theta_i}^{\theta_c} A\left(\exp\left(-\frac{R_i - R_U}{L_D}\cos\theta\right) - \exp\left(-\frac{R_i - R_L}{L_D}\cos\theta\right)\right)\sin\theta d\theta + \qquad \text{.(VII.6)}$$

$$+ \int_{\theta_i}^{\theta_c} B\left(\exp\left(\frac{R_i - R_L}{L_D}\cos\theta\right) - \exp\left(\frac{R_i - R_U}{L_D}\cos\theta\right)\right)\sin\theta d\theta$$

For the case of absorber with homogeneous concentration profile, one obtains:

$$CF_i = \frac{1}{2}K\int_0^{\theta_c}\int_{r_1(\theta)}^{r_2(\theta)} dr \sin\theta\cos\theta d\theta = \frac{1}{2}KH_i = \frac{1}{2}K\int_0^{\theta_c}\left[r_2(\theta) - r_1(\theta)\right]\sin\theta\cos\theta d\theta =$$

$$= \frac{1}{2}K\left\{\int_0^{\theta_i}\left[R_i - R_L(\theta)\right]\sin\theta\cos\theta d\theta + \int_{\theta_i}^{\theta_c}\left[R_U(\theta) - R_L(\theta)\right]\sin\theta\cos\theta d\theta\right\} \qquad \text{. (VII.7)}$$

The equations VII.6 and VII.7 are presented in a general form, suited also for CR-39. To use them for modeling LR-115/II one should substitute θ_i=0. The values of J_i (dimensionless) and H_i (dimension of length) have been numerically calculated. The obtained *CF* is in units of length (e.g. μm if L_D and *H* are expressed in μm). To obtain it in more common units one can use eqn (V.52). Examples of model dependences are illustrated in Fig. VII.9 and Fig. VII.10.

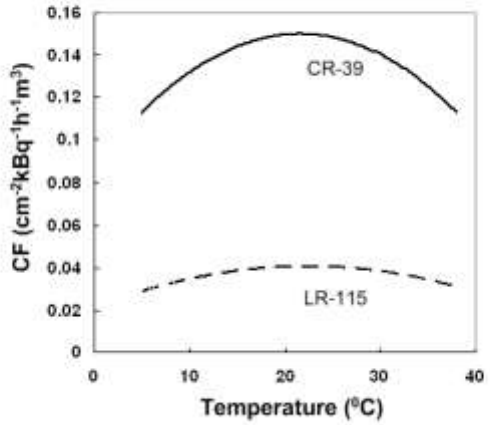

Figure VII.9. Calibration factor for CR-39 and LR-115/II detector with M-absorber of thickness 80 μm at different temperatures.

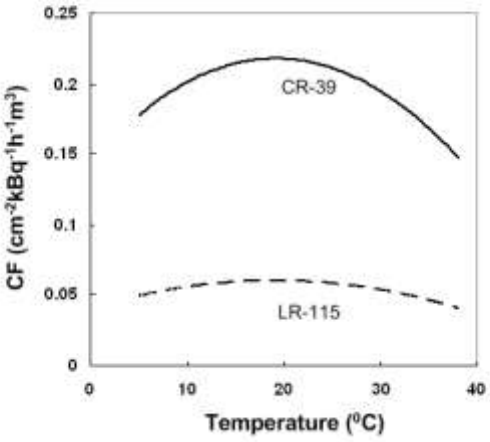

Figure VII.10. Calibration factor for CR-39 and LR-115/II detector with C-absorber of thickness 80 μm (4x20 μm) at different temperatures.

VII.2.2. Experiments with dosemeters with solid absorbers as radiators

To verify the theoretical model dedicated experiments were organized [245]. Two types of polycarbonate material was used: Makrofol DE and Makrofol N. The partition coefficient K for Makrofol DE has been studied in two independent series of experiments [142, 171] which give coherent value of about K = 25 ± 10% at room temperature. For Makrofol N Tommasino et al. [240] reported value of K = 40 ± 5. We have used these as input values in our model calculations. In the conducted experiments detectors with different absorbers were placed in a variety of different packages – film and TLD personal dosemeters, conference badges etc. (Fig. VII.11). In nine of the packages a couple of detectors were arranged – with M-absorber and C-absorber. The absorbers were fixed on Kodak-Pathe LR-115/II detectors as shown in Figs VII.5-6. The designed dosemeters were exposed to known radon activity concentrations using the set-up shown in Fig. VII. 12. The results showed no systematic differences between detectors with identical absorbers placed in different packages (Fig. VII.13). The comparison between theoretical values and experimental results revealed that in all cases the experimental response is about 10% higher than the model estimates. Albeit this difference is within the range of the uncertainties of both experimental and model values, it is systematic, so we cannot exclude a real bias. One possible reason for this can be the difference between the real partition coefficient and the value used in the model. As the present experiments were not conducted under controlled temperature, a difference between the average temperature during exposure and the temperature to which the model value is related can explain this bias.

Figure VII.11. (A) Photo of empty badges and envelopes, used in experiments. (B) Badges and envelopes with radon films inside. In each package a SSNTD with M-absorber and/or C-absorber is placed – in some cases several different absorbers are used.

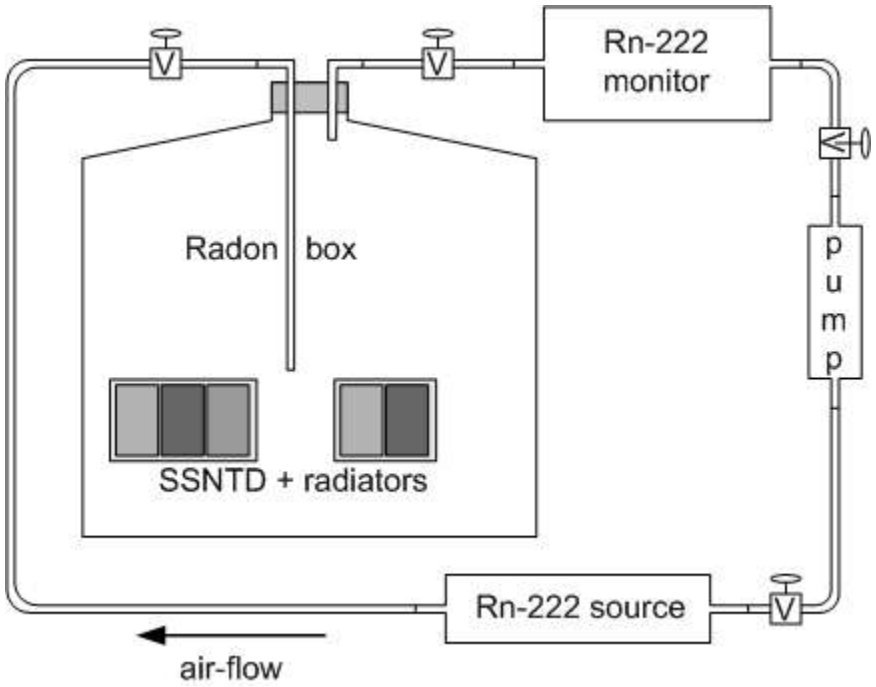

Figure VII.12. A scheme of the experimental set-up used for exposure of the dosemeters. Radon was supplied by a certified emanating radium source. The activity concentration of radon was monitored by an AlphaGuard radon monitor.

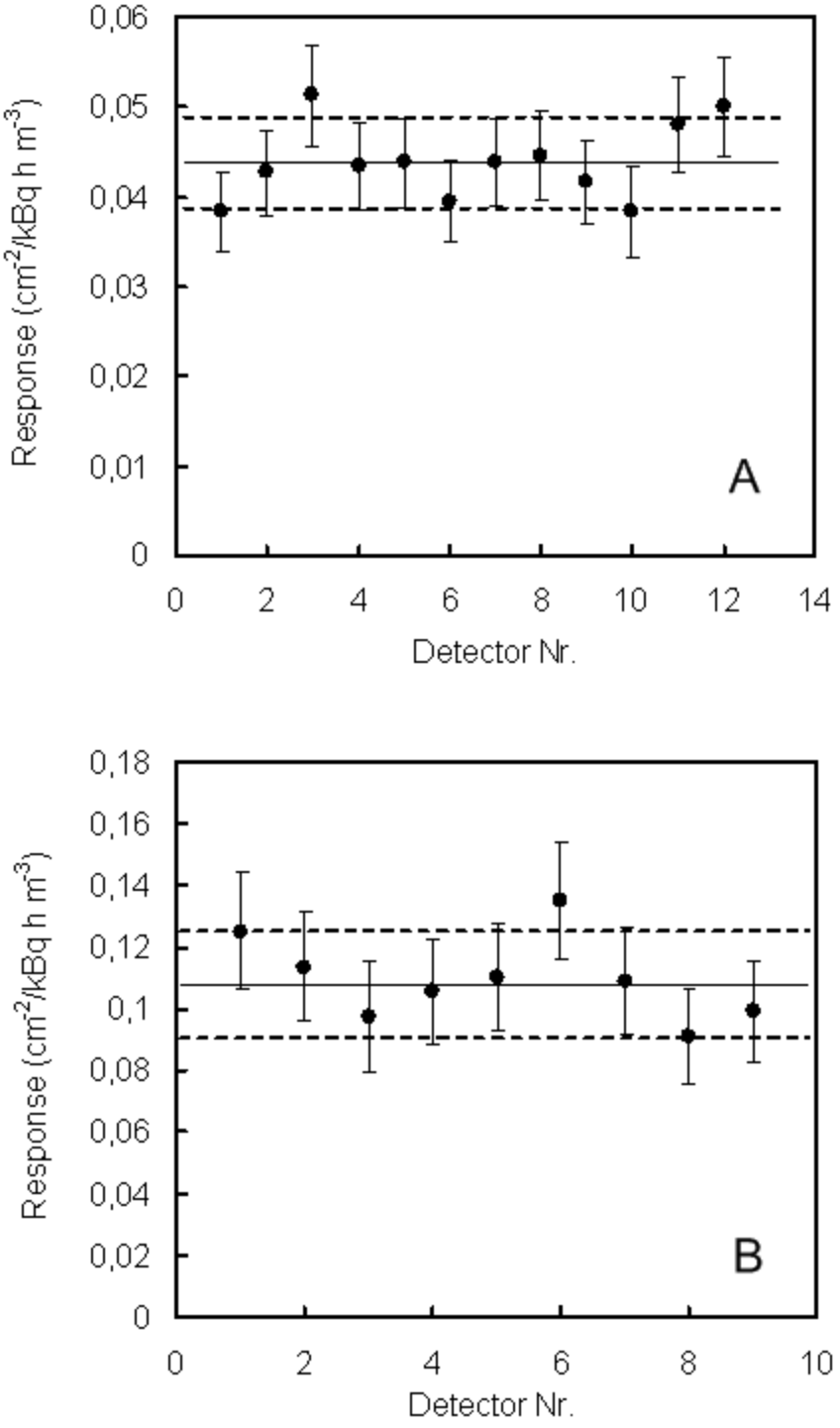

Figure VII.13. Response of detectors with identical absorbers placed in different packages. The lines indicate mean ± 1 SD interval (see [246]). (A) with 250 μm thick M-absorber, (B) with C-absorbers.

VII. 3. Combined Retrospective Measurements of ^{220}Rn and ^{222}Rn

VII.3.1. The concept

In the last years the scientific community became increasingly interested in the thoron (^{220}Rn) problem [191, 247]. The reasons are partly in the non-negligible, in some cases, thoron exposure and partly in the influence of the thoron presence on radon measurements [248]. Analogically to the case of ^{222}Rn, the retrospective dose estimates are representative for the risk related to ^{220}Rn. However, until recently no methods for retrospective ^{220}Rn measurements have been developed. This gap is recognized by the thoron research community and the use of CDs for that purpose was suggested [191].

The task to expand the CD method for retrospective thoron measurements was a challenge. One possibility to do this was proposed by the author in 2011 [249]. The key idea is to study the signal at two depths beneath the surface. The signal in the first (which should be in the interval 64-76 μm) is created by sources, related to ^{220}Rn and to the absorbed ^{222}Rn (R+T signal). The signal in the second depth (that should be >76 μm) is due only to the absorbed ^{222}Rn and its progeny (R-signal). In chapters V and VI the use of this R-signal for measuring ^{222}Rn is described and demonstrated. For the purpose of measuring ^{220}Rn the R-signal is used also to determine and subtract the ^{222}Rn contribution to the R+T signal in the first depth. The remaining "thoron component" (T-signal) is used to measure ^{220}Rn. The sensitivity of this approach is analyzed by theoretical modeling. The results demonstrate promising potential for combined retrospective measurements of thoron and radon.

The irradiation geometry is shown in Figure VII. 14 and the concept of "R" and "T" signal is illustrated in Fig. VII. 15.

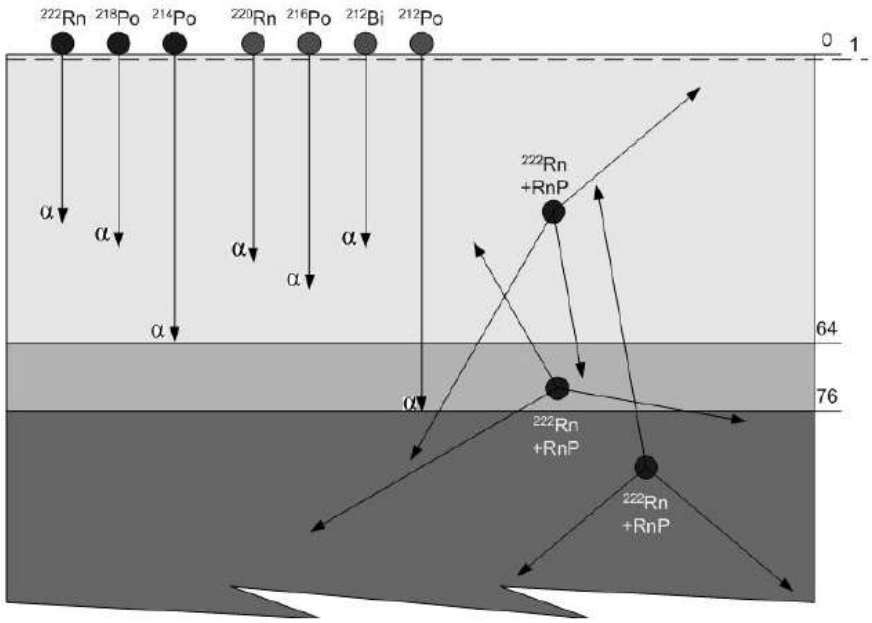

Figure VII.14. Maximum depths at which alpha-tracks could be formed in the disk by the alpha-particles of ^{222}Rn, ^{220}Rn and their decay products present in the air or plated-out on the disk surface. The tracks formed at depths between 64 μm and 76 μm are due only to ^{212P}o (decay product of ^{220}Rn) on the disks surface and to ^{222}Rn absorbed in the disk and its progeny. At depths greater than 76 μm the tracks are formed only by the absorbed ^{222}Rn and its progeny.

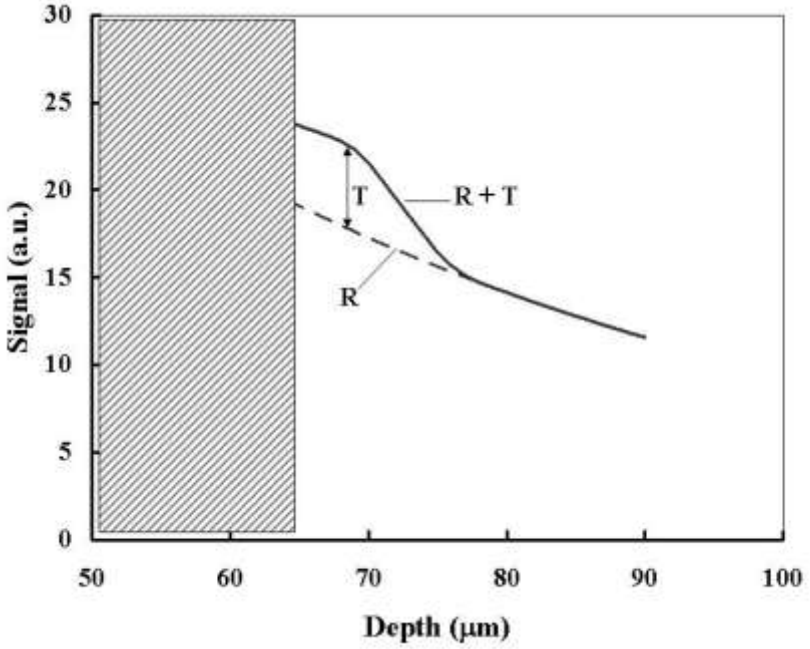

Figure VII. 15. The depth distribution of the signal in a CD. Depths ≤ 64 μm (the marked area) are not used for analysis. The resultant signal at 64-76 μm (R+T) is a sum of two components: R-related to the absorbed ^{222}Rn and T – related to thoron (^{220}Rn). The signal at > 76 μm is related only to the absorbed ^{222}Rn and is used to calculate and subtract the "radon component" from the summary R + T signal at depths 64 – 76 μm, as described in Ref. [249].

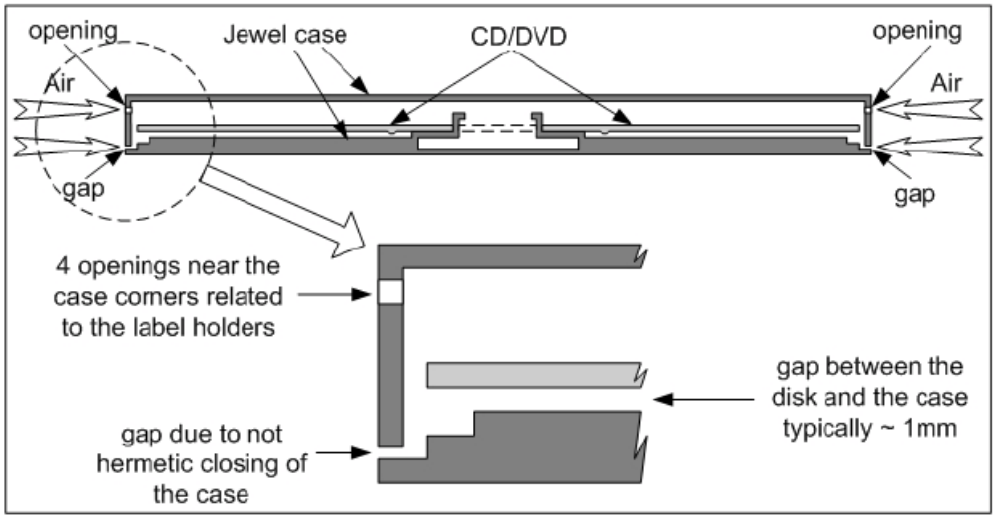

Figure VII.16. Cross-cut of CD/DVD jewel-case. Jewel cases are not hermetic and ^{222}Rn /^{220}Rn can enter inside them. Typically, there is gap of about 1 mm below the CD/DVD. Both radon isotopes present in this gap expose the disk.

VII.3. 2. The model

Almost all the time most of the home CDs/DVDs are stored in their jewel cases. The front side (this is the side of the disk that is hit by the laser beam of the player) looks to the bottom of the jewel case from a small distance (about 1 mm in most cases, considered by the author). The jewel cases are not hermetic and the gases enter and diffuse freely (Fig. VII. 16). Therefore, the air in the internal space of the case contains ^{222}Rn, ^{222}Rn progeny (^{218}Po, ^{214}Pb, ^{214}Bi+^{214}Po), ^{220}Rn, ^{220}Rn progeny (^{216}Po, ^{212}Pb, ^{212}Bi+^{212}Po/^{208}Tl). The sources, related to ^{220}Rn are:

(1) The absorbed ^{220}Rn (and its progeny) in the disk material;

(2) The plate-out of ^{220}Rn progeny on the disk surface and the internal walls of the jewel case;

(3) ^{220}Rn and ^{220}Rn progeny in the internal space air. First, the relative strength of the sources (1), (2) and (3) will be considered.

Source (1): The partition coefficient K of the isotope ^{220}Rn in the polycarbonate material is the same, as that of ^{222}Rn ($K \approx 25$ at room temperature). However, because of the short half-life of ^{220}Rn (55.6 s), the diffusion length ($L_D = (D/\lambda)^{1/2}$, where D is diffusion coefficient of radon in the material: $D = 5.4 \times 10^{-15}$ m^2 s^{-1} at 20^0 C, and λ is the decay constant) of ^{220}Rn is much shorter than that of ^{222}Rn. For instance, the diffusion length of ^{222}Rn in bisphenol-A in the temperature interval 5 – 38^0 C is in the range 42 – 97 μm [139]. In the same temperature interval, the calculated diffusion length of ^{220}Rn is 0.54 – 1.26 μm. Thus, in contrast to ^{222}Rn the absorbed ^{220}Rn and its progeny is concentrated very close to the disk surface. It can be obtained, using the model described in Ref. (171), that the ^{220}Rn absorbed activity per unit disk surface is $A_S^{(abs)} = KC_AL_D$, where C_A is the ambient ^{220}Rn activity concentration. Under radioactive equilibrium each of the surface activities of ^{212}Pb and ^{212}Bi, related to the absorbed ^{220}Rn, is equal to $A_S^{(abs)}$.

Sources (2) and (3): As demonstrated in many studies (e.g. Ref. [250]), there is an extremely high disequilibrium between ^{220}Rn and its progeny in the air. Therefore, the presence of ^{220}Rn decay products, coming from the room air in the interior of the jewel case will be neglected. Only these that originate from ^{220}Rn inside the gap between the disk and the bottom of the jewel case will be considered to contribute to the plate-out of interest. The diffusion coefficient values, reported for the "fresh" radon progeny atoms in air (see e.g. Ref. [69]) are usually in the interval: 0.005 – 0.1 cm^2 s^{-1}. The average time needed for these atoms to diffuse through the distance of 1 mm (the air gap) between the disk front surface and the bottom wall of the jewel case is 0.1 – 2 s. This time is comparable with the half-life of ^{216}Po (0.15 s) and much less than the half-life of ^{212}Pb (10.6 h) or ^{212}Bi (60.5 min). Therefore, one can consider all generated, after ^{220}Rn/^{216}Po decay in the interior, ^{212}Pb and ^{212}Bi atoms to be plate-outed on the internal surfaces and their presence in the air inside (source 3) is fully negligible. Under equilibrium with ^{220}Rn, the plate-out activity of ^{212}Pb or ^{212}Bi on the two surfaces (that of the disk and its projection on the looked by it bottom wall) is equal to that of ^{220}Rn in the interior volume between these two surfaces. Therefore, for the plate-out surface activity $A_S^{(po)}$ of ^{212}Pb or ^{212}Bi, under radioactive equilibrium with ^{220}Rn, one obtains:

$$A_S^{(po)}\, 2S = C_A V = C_A\, S\, h \Rightarrow A_S^{(po)} = C_A h/2, \qquad \text{(VII.8)}$$

where $V=S.h$ is the considered interior volume, S is the area of the disk front surface, as well as the area of its projection on the bottom wall, and h is the air gap width. In the present numerical estimates h = 1 mm is assumed, albeit some variations between different CD/DVD jewel cases are possible. Note that ^{212}Po activity is $\eta\times$(^{212}Bi activity), where η=0.64 is the probability of ^{212}Bi beta decay to ^{212}Po.

The numerical analysis showed that only sources (1) and (2) can contribute (by the alpha particles of ^{212}Po) to the signal at 64-76 μm, while contribution from the source (3) is negligible. Note that with K = 25, L_D = 1.26 μm (1.26×10^{-3} mm) and h = 1 mm one can easily realize that $A_S^{(po)} >> A_S^{(abs)}$. Still, this result was obtained for bisphenol-A based polycarbonates, a material of remarkable high radon absorption ability. The solubility in the plastic material of the jewel case is unknown to the author. The radon absorption in the jewel case material is conditionally neglected in this report, but can be re-considered in the future with more data available.

After consideration of the alpha-particles from the different alpha-emitting isotopes and their ranges in the disk material, together with the energy window for track detection, 3 depth-intervals beneath the disk surface can be distinguished:

- < 64 μm. The origin of the signal in this interval is complicated. Alpha particles from different isotopes can contribute (plate-out from ^{222}Rn and ^{220}Rn progenies, ^{222}Rn and ^{220}Rn in air, absorbed radon etc.). Due to the more complicated analysis needed, the signal in this interval will not be considered in present report;

- 64-76 μm. The tracks ("R+T" tracks) in this interval can be created by 8.78MeV alphas of ^{212}Po (plate-outed and due to the absorbed ^{220}Rn) and by the absorbed in the volume ^{222}Rn and its progeny.

- >76 μm. The "R-tracks" here are created only by the absorbed ^{222}Rn and its progeny.

Using "R" to calculate "T" from "R+T" is not a matter of simple mathematical subtraction, as R-signal is different at different depths. This depth dependence is theoretically modeled in Ref. [171]. The model is based on the volume distribution of the absorbed ^{222}Rn and the response function of electrochemically etched polycarbonate material. This model was applied, using the measured "R-signal" at the second depth to calculate the R-component in the "R+T signal" at the first depth.

VII.3. 3. Efficiency for track production

First, the efficiency for track production (this is the ratio: net track density/number of ^{212}Po decays per unit surface area) at different depths due to the alpha-particles of surface ^{212}Po (8.78 MeV) has been modeled. As the range of 8.78 MeV alpha particles in air (about 8 cm) is much greater than the 1 mm width of the air gap, we will assume that the disk surface is bombarded by alphas of the same energy coming from the plate-out on the two opposite surfaces – those of the disk and the opposite bottom wall. In the depth interval 64-76 μm, the only detectable alpha particles from a surface source are those of ^{212}Po. However, these alphas arrive at any given depth with different energy. Only alphas of energy and incident angle that fall within "energy and angular window" for registration can create etched tracks. Therefore, to model the efficiency for track production, the source geometry was combined with "range-energy" data for alpha-particles in Makrofol and with the response of Makrofol detectors to alpha particles. The model dependence is illustrated in Fig. VII.17. As seen, the efficiency considered has maximum at about 69μm. The next analysis will be done for this depth, considered as optimum. The "R-depth" is taken of 80 μm.

As the emission-rate (per unit surface) of ^{212}Po alpha particles is $\eta\times(2A_S^{(po)} + A_S^{(abs)})$ $= \eta\times(C_A h + C_A K L_D)$, for the net track-density rate related to thoron one obtains:

$$\dot{n} = \varepsilon\eta C_A\left(h + KL_D\right) \qquad \text{(VII.9)}$$

Therefore, for the net track-density:

$$n = \varepsilon\eta I_A\left(h + KL_D\right), \qquad \text{(VII.10)}$$

where n is the net track density (cm^{-2}) $\boldsymbol{\varepsilon}$ (dimensionless) is the efficiency for track production, $I_A = \int_0^{T_{\exp}} C_A dt$ is the time integrated ^{220}Rn activity concentration (e.g. in units kBq h m^{-3}), over exposure time T_{exp}. Respectively, the "thoron calibration factor" (CF_T = T-track density/integrated ^{220}Rn activity concentration) is given by the expression:

$$CF_T = n/I_A = \varepsilon\eta(h+KL_D). \qquad \text{(VII.11)}$$

The numerical value, in conventional units, obtained in the present case (with h = 1 mm) is CF_T = 0.0116 cm^{-2} $kBq^{-1}h^{-1}m^3$.

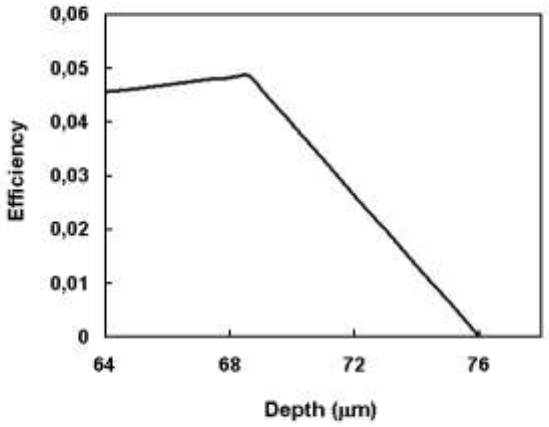

Figure VII.17. Efficiency for track production of ^{212}Po alpha particles (8.78 MeV) from a thin surface at different depths beneath the front surface of CD/DVD.

In real measurements, the experimentally obtained values, after disk etching, will be the net track density at two depths: 69 μm (n_{R+T}) and 80 μm (n_R). Let ρ = (^{222}Rn signal at 69 μm)/(^{222}Rn signal at 80 μm). Numerical values of ρ were calculated using the model of Ref. [171], which describes the depth dependence of the radon signal. The values of ρ within the temperature interval 10^0 – 30^0 C, vary from 1.27 to 1.14. The mean value of ρ = 1.21 was used in present modeling.

Therefore, the "thoron" signal (n_T) at 69 μm is:

$$n_{R+T} - \rho n_R = n_T, \qquad \text{(VII.12)}$$

where n_{R+T} and n_R are the defined above net track densities at 69 μm and 80 μm. Respectively, the integrated thoron concentration is:

$$I_A = n_T/CF_T. \qquad \text{(VII.13)}$$

In the environment the isotopes of radon in air are always present in mixture: ^{222}Rn + ^{220}Rn (^{219}Rn usually negligible). As there is no "pure thoron signal" in any part of the disk volume, the determination of ^{220}Rn is always dependent on the level of ^{222}Rn. The author has modeled n_R, n_{R+T} and n_T for different levels of ^{222}Rn and ^{220}Rn. The modeling was for standard ECE conditions used in previous works with CDs/DVDs. The results indicated that the quantitative measurement of ^{220}Rn in presence of ^{222}Rn is possible in wide range of concentrations that can be met in practice and under various mixtures of ^{222}Rn and ^{220}Rn.

Present evaluations are pilot estimates only. At this first stage the purpose was to study, by modeling, whether home stored CDs/DVDs can be used for retrospective measurements simultaneously of radon and thoron. The answer is yes and the results appear to be feasible. However, the analysis uses several simplifying conditions/assumptions, e.g.:

- The method can be correctly applied only for disks that are exposed to the room air being stored almost all the time in their not hermetic jewel cases;
- The ^{220}Rn concentration in the interior of the jewel case is homogenous and equal to that outside the case. This can be a crude approximation, as the diffusion length of ^{220}Rn in air is relatively short (2.5 - 3 cm) and its concentration can vary over short distances. In addition the place of storage of the disk case can play role, that is hardly to model and should be studied experimentally.
- The interior of the jewel cases, in particular the distance "*h*", can vary between different brands of packed CDs/DVDs. However, this method offers the possibility for individual *a posteriori* calibration. This approach has already been successfully employed for ^{222}Rn measurements by CDs/DVDs. The key concept is part of the analyzed disk to be additionally exposed to controlled concentrations of the measured isotope (^{220}Rn or ^{222}Rn). The increment of the signal in *a posteriori* exposed part over that in the not additionally exposed one is used to determine the individual calibration factor. Still, the technical procedures for such calibration with thoron are to be specified, but the conceptual background remains the same.

Therefore, in practical version of the method an use of an empirical quantity "diffusion resistance" R_D will be necessary ($R_D = CF_{th}/CF_{exp}$). To address these points a dedicated pilot experiments were organized [243].

VII. 3. 4. The Pilot Experiment

In the present experiments the disks were exposed to pure thoron atmosphere, therefore the "R-signal" was actually equal to the background signal. The scheme of the experimental set-up used is shown in Fig. VII. 18. Thoron is supplied by dry old thorium nitrate. The air flushes through the entire loop with flow rate, that is controled by a calibrated rotameter and kept 1 L min^{-1} ± 5%. The reference thoron measurements are made by a calibrated Lucas cell of volume 500 cm^3. At the beginning of a reference measurement the air-flow was stopped and the counter of the

Lucas chamber was switched on simultaneously. During the measurement the decrease of the signal was followed. There are two components in the time dependence of the counting rate (Fig. VII.19). The fast is due to ^{220}Rn + ^{216}Po and decreases with the half-life of ^{220}Rn. The slow component, assumed practically constant for the considered time intervals, is due to the long-lived ^{220}Rn progeny (^{212}Pb, ^{212}Bi + ^{212}Po/^{208}Tl) on the internal cell walls. To estimate these two components two time intervals of the measurement were considered: 0-200 s and 600-800 s. As the fast component effectively fades till the beginning of the second interval, the net-number of counts in the interval 0-200 s corresponding to the fast component was calculated as $n_0=(n_1-n_2)$, where n_1 and n_2 are the counts in the first and the second interval, respectively. The counts n_0 are used as an input value for the calculation of ^{220}Rn activity concetration. This concept for thoron measurement is similar to that used by other authors [252]. Other factors taken into account were Lucas cell calibration data [103] and inflow decay of ^{220}Rn (e.g. [253]). The reference integrated concentration was calculated by multiplying the average ^{220}Rn concentration by the exposure time (with air flow breaks subtracted).

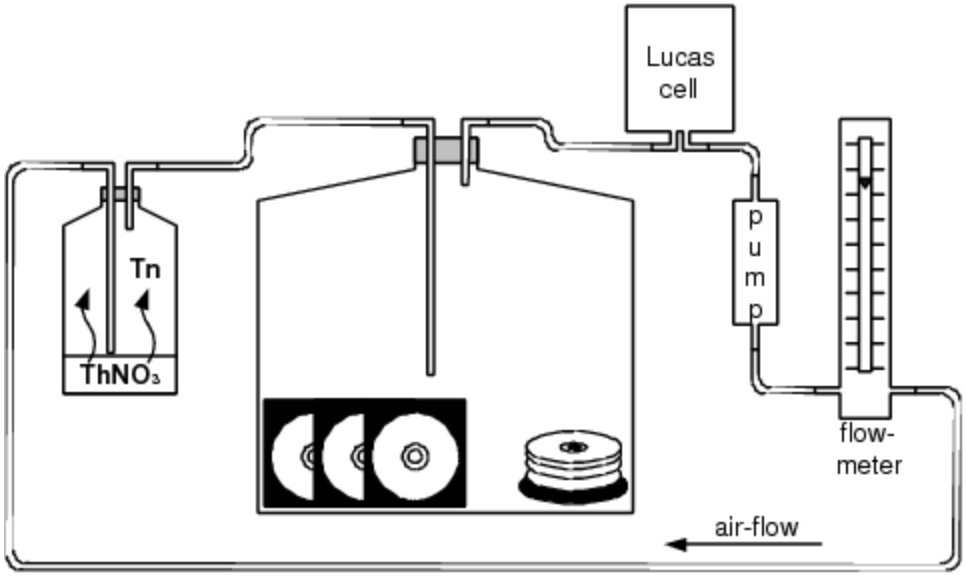

Figure VII.18. Experimental set-up. Continuous air-flow flushes thoron from the source vessel (with old thorium nitrate) to the exposure vessel and Lucas cell.

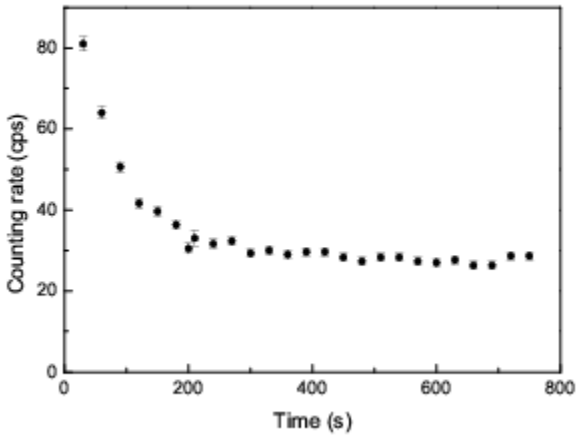

Figure VII.19. Reference thoron measurement. Decay curve (fast + slow component) in the cell after air-flushing is stopped.

In the conducted experiments two exposures of Verbatim DVDs were made. This type of disks were used in previous calibration experiments and they showed sensitivity

Lucas chamber was switched on simultaneously. During the measurement the decrease of the signal was followed. There are two components in the time dependence of the counting rate (Fig. VII.19). The fast is due to ^{220}Rn + ^{216}Po and decreases with the half-life of ^{220}Rn. The slow component, assumed practically constant for the considered time intervals, is due to the long-lived ^{220}Rn progeny (^{212}Pb, ^{212}Bi + ^{212}Po/^{208}Tl) on the internal cell walls. To estimate these two components two time intervals of the measurement were considered: 0-200 s and 600-800 s. As the fast component effectively fades till the beginning of the second interval, the net-number of counts in the interval 0-200 s corresponding to the fast component was calculated as $n_0=(n_1-n_2)$, where n_1 and n_2 are the counts in the first and the second interval, respectively. The counts n_0 are used as an input value for the calculation of ^{220}Rn activity concetration. This concept for thoron measurement is similar to that used by other authors [252]. Other factors taken into account were Lucas cell calibration data [103] and inflow decay of ^{220}Rn (e.g. [253]). The reference integrated concentration was calculated by multiplying the average ^{220}Rn concentration by the exposure time (with air flow breaks subtracted).

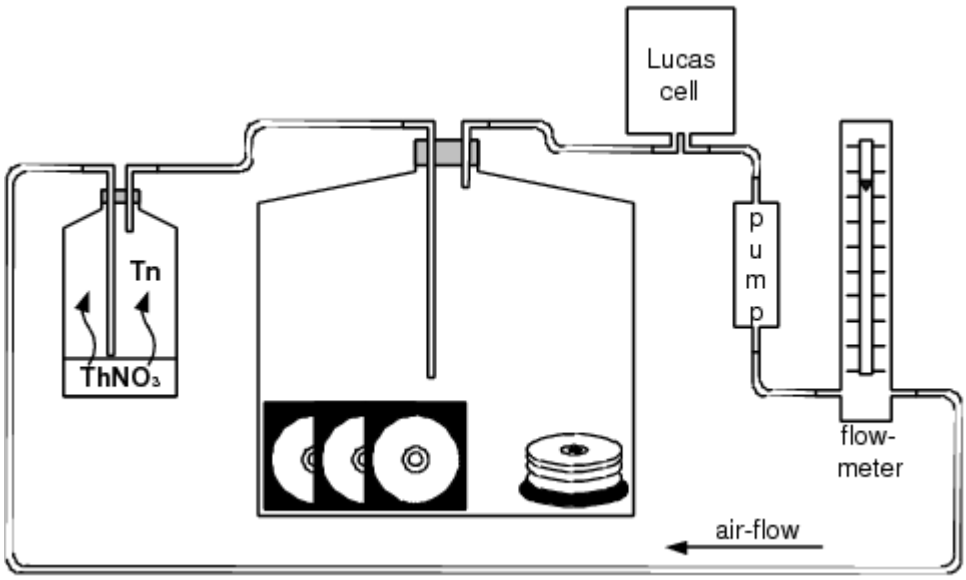

Figure VII.18. Experimental set-up. Continuous air-flow flushes thoron from the source vessel (with old thorium nitrate) to the exposure vessel and Lucas cell.

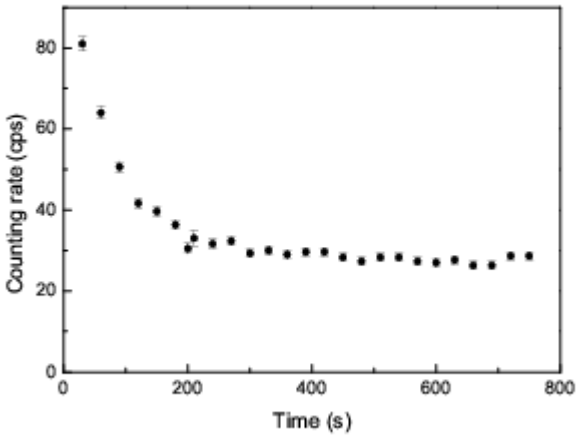

Figure VII.19. Reference thoron measurement. Decay curve (fast + slow component) in the cell after air-flushing is stopped.

In the conducted experiments two exposures of Verbatim DVDs were made. This type of disks were used in previous calibration experiments and they showed sensitivity

to radon close to the average sensitivity of other brands of disks. In the first one DVDs were placed in different jewel cases. This was done at reference integrated ^{220}Rn activity concentration of 34.8 MBq h m^{-3}. The second exposure was of bare disks at reference integrated ^{220}Rn activity concentration of 3.4 MBq h m^{-3}. The combined relative uncertainty in these reference values was about 10%. The combined uncertainties were determined following standard procedures for data processing and propagation of the uncertainties [42, 246]. All presented uncertainties are at the level of one standard deviation uncertainties. The bare disks (second exposure) were either with open front surface or with surface partly shadowed by an external cylindrical object placed close (about 2 cm) to the surface (Fig. VII.20). The shadowed disks were used to see whether external object close to their surface would influence the signal. After exposure the disks were left in thoron-free atmosphere for 3 days before etching, in order to wait for thoron progeny to decay. The removal of the target layers (69 μm and 80 μm) from the surface was by chemical pre-etching (CPE). After that, electrochemical etching (ECE) was applied. The tracks were counted automatically, by a computer scanner and dedicated software [151].

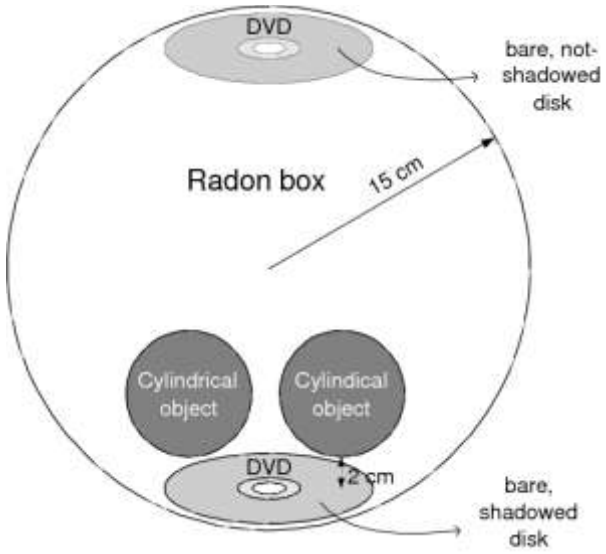

Figure VII. 20. Exposure geometry of bare detectors with open and shadowed disks. The cylindrical objects are ∅75/80 mm metal cans.

The results for the disks exposed in jewel cases are shown in Fig. VII. 21. As seen, there are significant variations between *CF* values for different "detectors". The differences are up to factor of four. We used different jewel cases with different construction and disk's position inside, while all DVDs were from the same brand. Previous experience has shown, that disks of one brand have the same track-etch properties. Therefore, we interpret the differences as due to different "diffusion resistance" of the jewel cases used. The average $\boldsymbol{R_D}$ for disks in different jewel cases was about 14. Without any individual calibration the measurements can be considered more likely semi-quantitative. However, one benefit of the method is the possibility for individual a posteriori calibration, already employed for ^{222}Rn measurements. The concept of this calibration mode is to expose part of the disk to controlled reference ^{222}Rn concentration. As in the case of ^{220}Rn the differences in *CF* are due to differences in the jewel cases' geometries, the a posteriori calibration has to account for that differences. That could be done by exposing a new disk in the particular jewel case. Experiments aiming to study this option are planned for the future. With this procedure more precise quantitative measurements can be targeted.

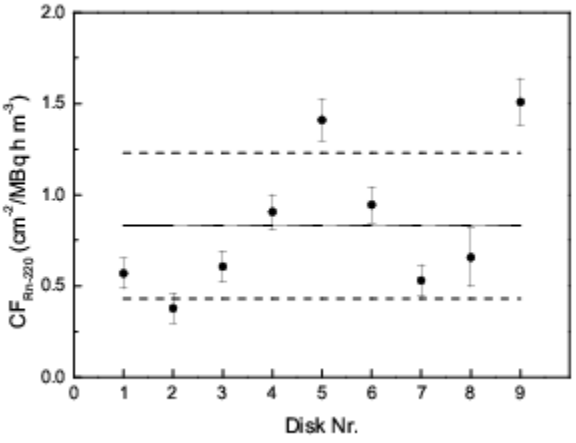

Figure VII. 21. Experimental results for *CF*s of DVDs in different jewel cases. The dashed lines confine the one standard deviation interval around the mean (solid line).

The results from the second exposure experiment are shown in Fig. VII. 22. Clearly, the shadowed disk has twice lower signal than that of the disks with open surface. That demonstrates that the exposure geometry of bare polycarbonate surfaces can hardly be defined precisely. On the other hand the bare disks show much greater CFs than that of disks in cases. This is summarized in Table VII. 2.

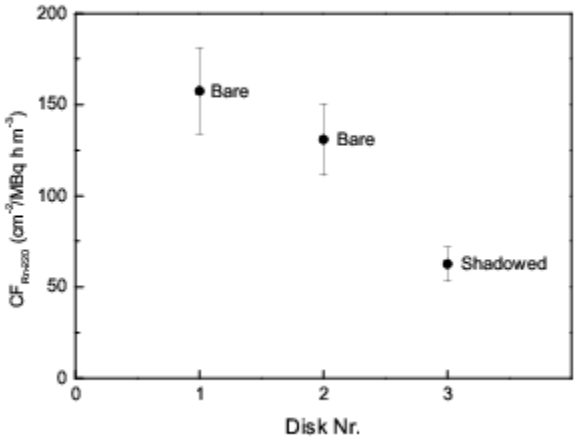

Figure VII. 22. Experimental results for CFs of bare and shadowed DVDs.

The results of the first exposure scenario indicate that the sensitivity is dependent on the specific design of the jewel case in which the disk is stored. The variation among different detectors was up to a factor of four. The CF of bare detectors and the achievable sensitivity are much higher (Table VII. 2). However, for this case an evidence was obtained that the signal depends on presence of nearby external objects that shadow the disk surface. As the deposition of radon/thoron progeny atoms on surfaces is strongly dependent on their geometry, any object placed nearby to the disks surface affects deposition and thus the T-signal, too. Therefore, quantitative measurements by this mode would need further experimental studies and theoretical modeling of thoron progeny deposition. However, it should be mentioned, that the potential for sensitive measurements made by bare CDs/DVDs, and possibly by other open plates of other household objects made of the same polycarbonate material, merit further research in this direction.

Table VII. 2.

Disk exposure	CF (cm^{-2}/MBq h m^{-3})
Bare	144 ± 17
Shadowed	63 ± 8
In jewel case	0.83 ± 0.40

Analysis of disks from real houses for thoron started in 2011, simultaneously with laboratory experiments. In data analysis the average CF for disks in jewel cases (Table VII. 2) was used. Interesting observation was that we found two houses with exceptionally high thoron concentrations in them, while radon concentrations are relatively low (Table VII. 3.). This observation demonstrates the importance of simultaneous retrospective measurements of thoron/radon by CDs/DVDs and the need to facilitate these measurements for practical application. The reason is that many radon measurements are made to identify high radon dwellings that need mitigation. On the other hand, substantial proportion of commercial radon detectors used for that purpose are sensitive to thoron as well [248] and would detect false "high radon concentrations". In such case houses like these detected by us (with high thoron and low radon levels) can be wrongly recommended for mitigation against radon. This would result in wasting significant expenses, as the mitigation systems for radon would have little, if any, effect on thoron. Analysing one CD/DVD can prevent such false alarms, save expenses and draw the attention to the real problem.

Table VII. 3.

House	Radon (Bq m^{-3})	Thoron (Bq m^{-3})
House 1	34 ± 9	830 ± 400
House 2	75 ± 19	3400 ± 1600

Albeit this is a pilot study, it points out a certain potential of the method for practical use. Analysing real disks by the presented methodology, we have observed houses with exceptionally high thoron concentrations, but with normal radon levels. If such houses are studied by commercial radon detectors that are sensitive to thoron (which is typical for many commercial detectors [248]) wrong decision for mitigation can be taken and substantial expenses wasted. At this point, analysing one CD/DVD, even semiquantitatively, can show if thoron is present at such levels that could affect radon detectors and mislead data interpretation and decision process.

VIII. CONCLUSION

In summary the essence of the results presented in this dissertation include:

- Methodological studies of integrated measurements of ^{222}Rn by diffusion chambers with SSNTD and with combined detectors (SSNTD + TLD). The response of Kodak-Pathe LR-115/II detectors and automatization of the track counting are addressed. The calibration and the procedure that ensures traceability to a primary ^{222}Rn standard are described. Special attention was focused on the distribution of ^{222}Rn progeny atoms inside diffusion chambers. Analytical mathematical expressions that describe this distribution are derived.
- A comprehensive mathematical algorithm for grab-sampling methods for measurement of ^{222}Rn progeny and ^{220}Rn progeny is developed. Applications for α-counting methods (both gross counting and spectrometric) are considered, with numerical examples.
- A method for integrated measurements of individual ^{222}Rn progeny (^{218}Po, ^{214}Pb and ^{214}Bi+^{214}Po) and ^{220}Rn progeny (^{212}Pb and ^{212}Bi + ^{212}Po/^{208}Tl) is described. The method employs uniformly rotating filter faced by absorber-covered SSNTDs. The mathematical algorithm for data processing is developed and results from laboratory and field experiments are presented.
- Data for ^{222}Rn progeny exposure of underground miners in major Bulgarian uranium and some metal mines is comprehended. It is used to study the correlation between bronchial pre-neoplastic lesions in miners and their ^{222}Rn progeny exposure.
- Results from radon surveys made in risk areas in Bulgaria are presented. These areas include the village of Eleshnitsa, the town of Rakovski and areas near Sofia affected by the uranium industry.
- A new method for radon measurements is proposed. It employs the high radon absorption ability of bisphenol-A based polycarbonates.

Experimental study of the influence of different factors has been carried out. Theoretical model of the sorption/desorption process and of track detection were developed. Application of the method for measurement of ^{222}Rn in water was proposed and demonstrated.

- On the basis of the polycarbonate method a new method for retrospective ^{222}Rn measurements based on the use of home stored CDs/DVDs was proposed. Procedures for a posteriori calibration and a posteriori temperature correction were proposed and tested. Laboratory studies and measurements in real dwellings were carried-out.
- A method for combined retrospective measurements of ^{220}Rn (thoron) and ^{222}Rn is proposed. It is based on the use of home stored CDs/DVDs and study of the track signal at two specified depths. Theoretical modeling an pilot experiments were carried-out.
- Theoretical and experimental study of radon detectors that employ polycarbonate absorbers/radiators coupled with external SSNTDs is performed. Different designs of radon film dosemeters were tested and results summarized.

REFERENCES

1. World Health Organization. **WHO Handbook on indoor radon: a public health perspective**. Geneva (2009).

2. United Nations Scientific Committee on the Effects of Atomic Radiation. **Sources and Effecrs of Ionizing Radiation.** UNSCEAR 2000 Report to the General Assembly, with Scientific Annexes. UNSCEAR, U.N., N.Y. (2000).

3. Darby S. et al. Residential radon and lung cancer: detailed results of a collaborative analysis of individual data on 7148 subjects with lung cancer and 14208 subjects without lung cancer from 13 epidemiologic studies in Europe. ***Scand. J. Work Environ. Health*** 32, Suppl. 1 (2006) 1-83.

4. Krewski D. et al. Residential radon and risk of lung cancer: a combined analysis of 7 North American case-control studies. ***Epidemiology*** 16 (2005) 137-145.

5. Paracelsus (1567). **Von der Bergsucht und anderen Bergkrankheiten**; s. Schriften aus dem Gesamtgebiet der Gewerbehygiene, Neue Folge, Heft 12. J. Springer, Berlin (1925).

6. Agricola G. (1556) **De Re Metallica**, Libri VI, Basle 1556. English translation by H.C. and L.H. Hoover, Dover Publications, New York (1950).

7. Haerting F. H. and Hesse W. Der Lungenkrebs, die Bergkrankheit in den Schneeberger Gruben. ***V. Gericht. Med. Off. Gesund Wes.*** 30 (1879) 296-309 and 31 (1879) 102-132, 313-337.

8. Schuettman W. Beitrag zur Geschichte der Schneeberger Lungenkrankheit, des Strahlenkrebses der Lunge durch Radon und seine folgerproducte. ***NTM-Schriftenreihe, Gesch. Naturwissenschaf. Tech. Med.*** 25 (1988) 83-96.

9. Ludewig P, Lorenser E. Untersuchungen der Grubenluft in den Schneeberger Gruben auf den Gehalt von Radium-Emanation. ***Z. Phys.*** 22 (1924) 178-185.

10. Pirchan A., Sikl H. Cancer of the lung in the miners of Jachymov (Joachimsthal). ***Am. J. Cancer*** 61 (1932) 681-722.

11. Personal communication from P. D. Evans reported by M. L. Jackson, Thesis. **The biological effects of inhaled radon**. Massachusetts Institute of Technology (1940).

12. Bale W. F. Hazards associated with radon and thoron. Unpublished memorandum to the US-AEC, March 14, 1951, reprinted in ***Health Phys.*** 38 (1980) 1062-1066.

13. Sheets, R. W. Indoor thoron: a review. ***Radioact. & Radiochem***. 4 (1993) 46-58.

14. McLaughlin J. An overview of thoron and its progeny in the indoor environment. ***Radiat. Prot. Dosim.*** 141 (2010) 316-321.

15. Пенчев П. Приносъ къмъ методите за количествено определяне на радия и радиоактивността на някои минерални води в България***. Сп. БАН, Природни науки.*** IX (1914) 1-44.

16. Uzunov I., Dimitrov M., Steinhausler F. Environmental radiation levels and occupational exposure due to uranium mining and milling operations in Bulgaria. ***Radiat. Prot. Dosim.*** 45 (1992) 141-143.

17. United Nations Scientific Committee on the Effects of Atomic Radiation. **Sources, effects and risks of ionizing radiation.** UNSCEAR 1988 Report to the General Assembly, annex A. New York, UN Publications, 1988.

18. United Nations Scientific Committee on the Effects of Atomic Radiation. **Sources, effects and risks of ionizing radiation.** UNSCEAR 1993 Report to the General Assembly, annex A. New York, UN Publications, 1993.

19. ICRP Publication 115. Lung cancer risk from radon and radon progeny and statement on radon. ***Annals of the ICRP*** 40 (2010) 1-64.

20. Young D. A. Etching of radiation damage in lithium fluoride. ***Nature*** 182 (1958) 375-377.

21. Fleischer RL, Price PB and Walker RM. Solid state detectors: Applications to nuclear science and geophysics. ***Ann. Rev. Nucl. Sci.*** 15 (1965) 1-28

22. Bonchev T. et al. A rapid method for investigation of surface alpha-contamination. ***Nucl. Instrum. Meth.*** A 337 (1993) 204-210.

23. Gazibarov V., personal communication (1992).

24. Pressyanov D., Guelev M., Sharkov B. Radon and radon progeny outdoors in a valley with enhanced natural radioactivity. ***Atmos. Environ.*** 29 (1995) 3433-3439.

25. Гинев Г. Дипломна работа, Физически факултет, СУ (1996).

26. Симеонов Г. Дипломна работа, Физически факултет, СУ (1997).

27. Monnin M. Methods of automatic scanning of SSNTDs. ***Nucl. Instrum. Meth.*** 173 (1980) 63-72.

28. Azimi-Garakani D. Intercomparison of automatic fission track counting systems. ***Nucl. Instrum. Meth.*** 225 (1984) 101-103.

29. Popov P. and Pressyanov D. Track density assessment by obstructed total internal reflection of a laser beam. ***Radiat. Meas.*** 27 (1997) 27-30.

30. Harvey J. R. and Weeks A. R. A neutron dosimetry system based on the chemical etch of CR-39. In Fifth Symp. On Neutron Dosimetry, EUR 9762 (1985) 519-529.

31. Harvey J. R. and Weeks A. R. Recent developments in a neutron dosimetry system based on the chemical etch of CR-39. ***Radiat. Prot. Dosim.*** 20 (1987) 89-93.

32. Steele J.D. et al., Development of a reader for track-etch detectors based on a commercially available slide scanner. ***Radiat. Meas.*** 31 (1999) 179-184.

33. Tsankov L., Pressyanov D., Mitev K., Georgiev S., Dimitrova I. Automatic counting of chemically etched tracks by means of computer scanner. ***Radiat. Meas.*** 39 (2005) 557-559.

34. Nikolaev V. A., Ilic R. Etched track radiometers in radon measurements: A review***. Radiat. Meas***. 30 (1999) 1-13.

35. Nikezic D., Yu K.N. Formation and growth of tracks in nuclear track materials. ***Mater. Sci. Eng.*** R 46 (2004) 51-123.

36. Nikezic D., Stevanovic N. Radon progeny behavior in diffusion chamber. ***Nucl. Instr. and Meth.*** B 239 (2005) 399-406.

37. Palacios D., Sajo-Bohus L., Greaves E. D. Radon progeny distributions inside a diffusion chamber and their contributions to track density in SSNT detectors. ***Radiat. Meas.*** 40 (2005) 657-661.

38. Picolo J. L. Absolute measurement of ^{222}Rn activity**.** ***Nucl. Instrum. Meth.*** A 369 (1996) 452-457.

39. Blanchis S. **Realisation d'un logiciel (AngleSol) de calcul d'un angle solide et de son incertitude**. Note technique LPRI-97-019 (1997).

40. Picolo JL, Pressyanov D, Blanchis P, Barbier M, Michielsen N, Grassin D et al. A radon 222 traceability chain from primary standard to field detectors. ***Appl. Radiat. Isot.*** 52 (2000) 427-34.

41. IEC International Standard. **Radiation protection instrumentation-Radon and radon decay product measuring instruments-Part 4: Equipment for the production of reference atmospheres containing radon isotopes and their decay products (STAR)**. IEC 61577-4, edition 1.0 (2009).

42. Taylor B. N., Kuyatt C. E. **Guidelines for evaluating and expressing the uncertainty of NIST measurement results.** Gaithersburg, MD: National Institute of Standards and Technology; NIST Technical Note 1297 (1994).

43. Nikezic D., Baixeras C. Analysis of sensitivity of LR 115 II in cylindrical diffusion chambers for radon concentration determination. ***Nucl. Instrum. Meth.*** A 364 (1995) 531-536.

44. Pressyanov D., Rusinov I., Simeonov G. Radon progeny deposition in track-detection diffusion chambers. ***Nucl. Instrum. Meth.*** A 435 (1999) 509-513.

45. Barillon R. **Contribution a la detection de particules alpha par detecteurs solides de traces nucleaires – application a la mesure du radon.** Ph. D. thesis, Universite de Franche-Comte.

46. Jonsson G. The angular sensitivity of Kodak LR-film to alpha particles. ***Nucl. Instrum. Meth.*** 190 (1981) 407-414.

47. Porstendorfer J. and Mercer T. Influence of electric charge and humifity upon the diffusion coefficient of radon decay products. ***Health Phys.*** 37 (1979) 191-199.

48. Porstendoerfer J., Reineking A. Indoor behaviour and characteristics of radon progeny. ***Radiat. Prot. Dosim.*** 45 (1992) 303-311.

49. Georgiev S., Pressyanov D., Mitev K., Dimitrova I. Calibration of diffusion chambers for measuring ^{222}Rn in air. ***BgNS Trans.*** 12(1) (2008) 3-6.

50. Георгиев С. **Ядренофизични методи за изследване на миграцията на радиоактивни благородни газове.** Дисертация, СУ, Физически ф-т (2012).

51. Tokonami S. Why is ^{220}Rn (thoron) measurement important? ***Radiat. Prot. Dosim.*** 141 (2010) 335-339.

52. Христов Хр. **Математични методи на физиката**. София, Наука и изкуство (1967).

53. Pressyanov D. Radon progeny distribution in cylindrical diffusion chambers. ***Nucl. Instrum. Meth.*** A 596 (2008) 446-450.

54. Mathews J and Walker R.L. **Mathematical Methods of Physics.** W.A. Benjamin Inc., New York, Amsterdam (1964).

55. Abramovitz M., Stegun I. A. (eds.). **Handbook of mathematical functions with formulas, graphs and mathematical tables.** National Bureau of Standards. Applied Mathematics Series, vol. 55 (1964).

56. Busigin A. et al. Nature of unattached RaA (Po-218) particles. ***Health Phys.*** 40 (1981) 333-343.

57. Koo V.S.Y. et al. Experimental study of track density distribution on LR115 detector and deposition fraction of ^{218}Po in diffusion chamber. ***Nucl. Instrum. Meth.*** A 491 (2002) 470-573.

58. Koo V. S. Y. et al. Deposition fractions of ^{218}Po in diffusion chambers. ***Appl. Radiat. Isot.*** 59 (2003) 49-52.

59. Uchrin G. Beta dosimetry, different solutions. ***Radiat. Prot. Dosim.*** 17 (1986) 99-104.

60. Guelev M. et al. A two-element $CaSO_4$:Dy dosemeter for environmental monitoring. ***Radiat. Prot. Dosim.*** 51 (1994) 35-40.

61. Pressyanov D., Guelev M., Klein D., Kritidis P. Measurement of ^{222}Rn in soil gas by combination of thermoluminescent and solid-state nuclear track detectors. ***Environ. Int.*** 22 (1996) S491-S493.

62. Tsivoglou E. C., Ayer H. E., Holaday D. A. Occurrence of nonequilibrium atmospheric mixtures of radon and its daughters. ***Nucleonics*** 11(9) (1953) 40-45.

63. Марков К. П., Рябов Н. В., Стась К. Н. Экспресс-метод оценки радиационной опасности, связанной с наличием в воздухе дочерных продуктов радонал ***Атомная энергия*** 12 (1962) 315-319.

64. Martz D. E. et al. Analysis of atmospheric concentrations of RaA, RaB and RaC by alpha spectroscopy. ***Health Phys.*** 17 (1969) 131-138.

65. Raabe O. G., Wrenn M. E. Analysis of the activity of radon daughter samples by weighted least squares. ***Health Phys.*** 17 (1969) 593-605.

66. Thomas J. W. Measurement of radon daughters in air. ***Health Phys.*** 23 (1972) 783-789.

67. Kritidis P., Uzunov I., Minev L. Precision alpha-counting methods for determination of radon daughters in air. ***Nucl. Instrum. Meth.*** 143 (1977) 299-305.

68. Khan A., Busigin A., Phillips C. R. An optimized scheme for measurement of the concentrations of the decay products of radon and thoron. ***Health Phys.*** 42 (1982) 809-826.

69. Porstendorfer J., Behavior of radon daughter products in indoor air. ***Radiat. Prot. Dosim.*** 7 (1984) 107-113.

70. George A. C., Breslin A. J. The distribution of ambient radon and radon daughters in residential buildings in New Jersey – New York area. IN: Proc. Nat. Radiat. Env. III (1980) 1272-1292.

71. Reineking A., Porstendorfer J. "Unattached" fraction of short-lived Rn decay products in indoor and outdoor environments: an improved single-screen method and results. ***Health Phys.*** 58 (1990) 715-727.

72. Bateman H. Solution of a system of differential equations occurring in the theory of radioactive transformation. ***Proc. Cambridge Philos. Soc.*** 15 (1910) 423-427.

73. Pressyanov D. Short solution of the radioactive decay chain equations. ***Am. J. Phys.*** 70 (2002) 444-445.

74. Pressyanov D. General expressions for determination of ^{222}Rn and ^{220}Rn daughters in air. ***C. R. de l'Acad. Bulg. Des Sciences*** 45(4) (1992) 21-24.

75. Pressyanov D. **Radon and radon progeny: Methodological points and case studies.** Lambert Academic Publishing, Saarbruecken (2012), ISBN: 978-3-8484-8604-5.

76. Skrable K. W. et al. Theoretical response of a ZnS(Ag) scintillation detector to alpha-emitting sources and suggested applications. ***Health Phys.*** 60 (1991) 381-392.

77. Lederer C. M., Shirley V. S. eds. **Table of isotopes**, 7th ed. New York: John Wiley & Sons (1978).

78. Салтыков Л. Д., Шаляев И. Л., Лебедев Ю. А. **Радиационная безопасность при разведке и добыче урановых руд.** Москва, Энергоатомиздат (1984).

79. Наредба за основни норми за радиационна защита (ОНРЗ-2004). Държ. в-к. 73/2004 (в сила до 4.10.2012).

80. Paul A. et al. Measurement of short-lived radon progenies by simultaneous αγ-spectrometry at the German radon reference chamber. ***Nucl. Instrum. Methods*** A 434 (1999) 303-312.

81. Ruzer L. S. Non-emanating samples of the Rn series from ^{226}Ra, ^{228}Th and ^{227}Ac. ***Radiat. Prot. Dosim.*** 46 (1993) 127-128.

82. Pressyanov D., Poffijn A., Meesen G., Van Deynse A., Buysse J. Short-lived alpha sources of energies 6.0 MeV and 7.69 MeV for calibration purposes. ***Radiat. Prot. Dosim.*** 94 (2001) 281-285.

83. Pressyanov D. S, Guelev M. G., Pentchev O. J. **Apparatus for measuring the time-integrated volume specific activities of radon and thoron daughters in the air**. Bulgarian Patent 49984, US Patent 2,225,673 (priority date 4. 01. 1991).

84. Pressyanov D. S., Guelev M. G., Pentchev O. J. Integrated measurements of short-lived ^{222}Rn progeny by rotating filters. ***Health Phys.*** 64: 522-527 (1993).

85. Пресиянов Д. **Кумулативни измервания на дъщерни продукти на ^{222}Rn и на външното бета облъчване от ^{234m}Pa.** Дисертация за научна степен кфн (доктор) (1992).

86. Pressyanov D., Guelev M., Pentchev O., Kritidis P. Statistical precision of integrated measurements of ^{222}Rn and ^{220}Rn decay products in the air by a rotating filter device. ***Environ. Int.*** 22 (1996) S607-S610.

87. Pressyanov D. Integrated measurements of ^{212}Pb and ^{212}Bi in the air by rotating filters. ***Health Phys.*** 68 (1995) 261-265.

88. Pressyanov D. S. Integrated measurements of ^{218}Po, ^{214}Pb and ^{214}Bi+^{214}Po in air under environmental concentrations. ***Nucl. Instrum. Meth.*** A 397 (1997) 448-454.

89. Pressyanov D. S. Integrated measurements of ^{218}Po, ^{214}Pb and ^{214}Bi+^{214}Po in air under environmental concentrations-mathematical supplement. ***Nucl. Instrum. Meth.*** A 397 (1997) 455-457.

90. ICRU. **Stopping powers and ranges for protons and alpha particles**. ICRU Report 49 (1993).

91. Reineking A., Butterweck G., Kesten J., Porstendoerfer J. Thoron gas concentration and aerosol characteristics of thoron decay products. ***Radiat. Prot. Dosim.*** 45 (1992) 353-356.

92. ICRP. Protection against radon-222 at home and at work. ICRP Publication 65, ***Annals of the ICRP***, vol. 23 Nr. 2 (1993).

93. Harley N., Chen J., Chittaporn P., Sorimachi A., Tokonami S. Long term measurements of indoor radon equilibrium factor. ***Health Phys.*** 102 (2012) 459-462.

94. Cote P., Townsend M. G. Mixtures of radon and thoron daughters in underground atmospheres. ***Health Phys.*** 40 (1981) 5-17.

95. Pressyanov D. Study and optimisation of methods for integrated measurements of ^{222}Rn and ^{222}Rn progeny in the human environment. Report of a DWTC 6 months fellowship 1998/99. University of Ghent (1999).

96. Узунов И. Дисертация, СУ, Физически факултет (1972).

97. Uzunov I., Steinhausler F., Pohl E. Carcinogenic risk of exposure to radon daughters associated with radon spas. ***Health Phys.*** 41 (1981) 807-813.

98. ДСО “Редки метали”. Материали на дозиметричната служба (архив).

99. Димитров М., Пресиянов Д.. Вътрешно облъчване от дъщерни продукти на ^{222}Rn на подземните работници от български уранови рудници през1958-1989. ***Докл. БЯД*** 3, 1 (1998) 44-49.

100. Пресиянов Д., Димитров М.. Вътрешно облъчване от дъщерни продукти на ^{222}Rn на подземните работници от Бургаски медни мини през 1962-1999. ***Докл. БЯД*** 3,1 (1998) 39-43.

101. Пресиянов Д. Проблеми при определяне на грешката при измерване на дъщерни продукти на радона. ***Стандартизация, сертификация и метрология*** XLIII(3) (1992) 26-29.

102. Димитров М. Сравнение на методите за измерване на дъщерни продукти на радона и тяхната скрита енергия.. Сб. IV Нац. Конф. Биомед. Физ. Техн. (1984).

103. Критидис П. Дисертация. Физически факултет, СУ (1982).

104. Vapirev E. I. et al. Radioactive sites in Bulgaria contaminated with radium and uranium. Proc. Int. Symp. On Remediation and Restoration of Radioactive-contaminated Sites in Europe, Antwerp, 11-15 Oct. 1993. EC Doc. XI-5027/94 (1994) pp. 929-955.

105. Vapirev E. et al. (1996) Radioactively contaminated sites in Bulgaria. Proc. IAEA first workshop on Environmental restoration for Central and Eastern Europe. IAEA-TECDOC-865, vol. 1, p. 43

106. Michaylov M., Pressyanov D., Kalinov K. Bronchial dysplasia induced by radiation in miners exposed to ^{222}Rn progeny. ***Occup. Env. Med.*** 52 (1995) 82-85.

107. Капитанов Ю. Т., Сердюкова А. С., Коренков А. П. Экспресс-метод для определения концентрации радия-А и отношения концентрации дочерных продуктов радона в воздухе. ***Изв. ВУЗ: Геология и разведка*** 11 (1961) 106-114.

108. ICRP. **Radiation Protection of Miners.** ICRP Publication 47 (1987).

109. Sevc J. et al. Cancer in man after exposure to radon daughters. ***Health Phys.*** 54 (1988) 27-46.

110. E. Radford, K. St. Clair Renard. Lung cancer in Swedish iron miners exposed to low doses of radon daughters. ***New Engl. J. Med.*** 310 (1984) 1485-1494

111. G. Saccomano et al. Development of carcinoma of the lung as reflected in exfoliated cells. ***Cancer*** 33 (1974) 256-270.

112. Saccomano G., Saunders R., Archer V., Auerbach O., Kushner M., Becker P. Cancer of the lung: the cytology of sputum prior to the development of carcinoma. ***Acta Cytol.*** 9 (1965) 413-423.

113. Risse E. K. J., Voijs P.G., Van't Hof M. A. Diagnostic significance of severe dysplasia in sputum cytology. ***Acta Cytol.*** 32 (1988) 629-634;

114. Fulmer C. D. et al. Proposed classification for bronchial epithelial cell abnormalities in the category of dyscariosis. ***Acta Cytol.*** 13 (1969) 459-471.

115. Михайлов М., Дисертация, София, МА (1978).

116. Hosmer D. W., Lemeshow S. **Applied logistic regression.** New York: John Wiley (1989).

117. Димитров М., Тосев И., Пресиянов Д. Оценка на радиоактивното замърсяване на въздуха с радон и дъщерни продукти в някои райони на страната. Сб. XII Кол. "Физиката в опазване на човека и околната среда", с. 135-138 (1990).

118. Sabol J., Weng P. S. **Introduction to radiation protection dosimetry.** World Scientific (1995).

119. Gardner MJ, Altman DG. **Statistics with confidence.** BMJ Publications; 1992.

120. Danon S, Tzvetanski H, Uzunov N. Lung-cancer incidence in the Bulgarian towns in the interval 1971-80. ***Oncologia*** XXII (2) (1985) 69-76 /in Bulgarian/.

121. Pressyanov D, Minev L, Uzunov P, Danon S, Valerianova Z. Excess lung cancer incidence and radon indoors in a Bulgarian town. ***J. Epid. Commun. Health*** 53 (1999) 448.

122. Pressyanov D., Danon S., Valerianova Z. "Radon indoors in a Bulgarian town with increased lung cancer incidence". Proc. Stakeholders' conference on Approaches to the Management of Environmental Radioactivity, Luxembourg, 2-3 Dec. (2002), p. 169.

123. Пресиянов Д., Данон Ш., Валерианова З. Концентрации на ^{222}Rn в жилища в гр. Раковски и потенциалният им принос за повишената заболеваемост от белодробен рак. ***Рентгенология и радиология*** XXXIX (2000) 209-212.

124. Stidley C. A., Samet J. M. A review of ecologic studies of lung cancer and indoor radon. ***Health Phys.*** 65 (1993) 234-251.

125. Ennemoser O. et al. Exposure to unusually high indoor radon levels. The ***Lancet*** 341 (1993) 828-829.

126. Sainz C., Dinu A., Dicu T., Szacsvai K., Cosma C., Quindos L. S. Comparative risk assessment of residential radon exposures in two radon-prone areas, Stei (Romania) and Torrelodones (Spain). ***Sci. Tot. Env.*** 407 (2009) 4452-4460.

127. Lubin JH, Boice JD, Samet JM. Errors in exposure assessment, statistical power and the interpretation of residential radon studies. ***Radiat. Res.*** 1995; 144: 329-41.

128. Pressyanov D. Radon research and practice in Bulgaria – from retrospective measurements to mitigation. ***Nukleonika*** 55 (2010) 477-482.

129. Radon in the human environment in Bulgaria. Final report of research contract Nr. 6139/RB between IAEA and the University of Sofia.

130. Pressyanov D., Mitev K., Georgiev S., Dimitrova I. Radon mapping by retrospective measurements – an approach based on CDs/DVDs. ***J. Env. Radioact.*** 101 (2010) 821-825.

131. Pressyanov D., Mitev K., Dimitrova I., Georgiev S. **Retrospective radon measurements: techniques and perspectives.** Chapter 4 IN**:** ***Handbook on Radon: Properties, Measurements and Health Effects***. Nova Science Publishers, Inc., New York, ISBN: 978-1-62100-369-4 (2012).

132. Пресиянов Д. и съавт. Изследване на радиационния статус на засегнати от уранодобива терени и населени места в Софийското поле. Отчет по Дог. 44-00-37/2003 между НИС-СУ и АЯР, юни 2004.

133. American Association of Radon Scientists and Technologists. **Active soil depressurization radon mitigation standards for low rise residential buildings.** AARST, Fletcher, NC (2006).

134. ASTM. **Standard Practice for Installing Radon Mitigation in Existing Low-Rise Residential Buildings**. ASTM E2121-03, West Conshohocken, PA (2003).

135. Наредба за основните норми за радиационна защита. Държ. в-к бр. 76/5.10.2012 г.

136. Pressyanov D, Van Deynse A, Buysse J, Poffijn A, Meesen G. **Polycarbonates: a new retrospective radon monitor.** Proc. of IRPA Regional

Congress on Radiation Protection in Central Europe, Budapest, 23-27 August 1999: 716-722.

137. Pressyanov D, Buysse J, Poffijn A, Meesen G, Van Deynse A. Polycarbonates: a long-term highly sensitive radon monitor. ***Nucl Instrum Methods*** A 447 (2000) 619-621.

138. Pressyanov D, Buysse J, Van Deynse A, Poffijn A, Meesen G. Indoor radon detected by compact discs. ***Nucl Instrum Methods*** A 457 (2001) 665-666.

139. Pressyanov D, Buysse J, Poffijn A, Meesen G, Van Deynse A. The compact disk as radon detector-a laboratory study of the method. ***Health Phys.*** 84 (2003) 642-651.

140. Pressyanov D, Buysse J, Poffijn A, Van Deynse A, Meesen G. Integrated measurements of ^{222}Rn by absorption in Makrofol. ***Nucl Instrum Methods*** A 516 (2004) 203-208.

141. Pressyanov D. S., Mitev K. K., Stefanov V. H. Measurements of ^{85}Kr and ^{133}Xe by absorption in Makrofol. ***Nucl. Instrum. Methods*** A 527 (2004) 657-659.

142. Pressyanov D., Mitev K., Georgiev S., Dimitrova I. Solubility of krypton, xenon and radon in polycarbonates. Application for measurement of their radioactive isotopes. ***Nucl. Instrum. Methods*** A 629 (2011) 323-328.

143. Durrani S. A., Bull R. K. **Solid State Nuclear Track Detection Principles, Methods and Applications**. Pergamon Press (1987).

144. Möre H. & Hubbard L.M. ^{222}Rn absorption in plastic holders for alpha track detectors: a source of error. ***Radiat. Prot. Dosim***. 74(1997) 85-91.

145. Pressyanov D. The compact disk as a retrospective radon detector – performance of the method. ***Proc. 17th AARST International Radon Symposium***, Jacksonville, Florida, 9-12.09.2007.

146. Pressyanov D., Dimitrova I., Georgiev S., Mitev K. Measurement of ^{222}Rn by absorption in polycarbonates – research and practice. ***Proc. 18th AARST International Radon Symposium***, Las Vegas NV, 14-17 September 2008.

147. Pressyanov D., Dimitrova I., Georgiev S., Hristova E., Mitev K. Measurement of radon-222 in water by absorption in Makrofol. ***Nucl. Instrum. Methods*** A 574 (2007) 202-204.

148. Dimitrova I., Mitev K., Pressyanov D., Georgiev S., Boshkova T. Measurement of ^{222}Rn and ^{226}Ra in water by absorption of radon in polycarbonates and etching alpha-tracks. ***Radiat. Meas.*** 46 (2010) 119-127.

149. Vancraeynest G, Franchoo S, Huyse M, Moons R. Optimisation and modeling of electrochemically etched polycarbonate track detectors. ***Nucl Instrum Methods*** B 129 (1997) 65-72.

150. Vanmarcke H, Janssens A. Study of the properties of electrochemically etched α-tracks in a polycarbonate foil used in a radon diffusion chamber. ***Nucl Tracks*** 12 (1986) 689-692.

151. Mitev K., Madzhunkov Y., Gerganov G., Dimitrova, I. Georgiev S. & Pressyanov D.(2009). Automatic Counting of Electrochemically Etched Tracks in Compact discs. Application to Retrospective Measurements of Rn-222. ***IEEE Trans. Nucl. Sci.***, 57 (2009) 300-308.

152. Turek K, Bednar J, Neznal M. Parallel track-etch detector arrangement for radon measurement in soil. ***Radiat Meas*** 28 (1997) 751-754.

153. Pressyanov D. **Nuclear tracks in polycarbonates with high radon absorption ability: Opportunities for measuring ^{222}Rn.** Chapter 4 IN**:** ***Nuclear Track Detectors: Design, Methods and Applications***. Nova Science Publishers, Inc., New York, ISBN: 978-1-60876-826-4 (2010).

154. Buysse J., personal communications (2002).

155. Kukreja L. M., Chaterjee U. K., Bhawalkar D. D., Bhagwat A. M. & Joshi V. B. Studies on laser cutting of plastic track detector sheets and its effects on track revelation properties. ***Nucl. Tracks*** *9* (1984) 199-208.

156. Lucas H. F. & Woodward D. A. Effect of long decay chains of the counting statistics in the analysis of radium224 and radon222. ***J. Appl. Phys***. 35 (1964) 452-456.

157. Vanmarcke H. (1986). De bijdrage van het woonmilieu tot de blootstelling aan straling afkomstig van nucliden uit de natuurlijke ^{238}U reeks; University Ghent, Dissertation, Department Subatomic and Radiation Physics, (in Dutch).

158. Currie L. A. Limits for qualitative detection and quantitative determination. ***Anal. Chem***. 40 (1968) 586-593.

159. Pressyanov D., Mitev K., Georgiev S. & Dimitrova I. Sorption and desorption of radioactive noble gases in polycarbonates. ***Nucl. Instrum. Methods*** A 598 (2009) 620-627.

160. Тихонов А. Н., Самарский А. А. Уравнения математической физики. Москва, Наука (1977).

161. Dimitrova I., Mitev K., Pressyanov D., Georgiev S. Desorption of 222Rn from polycarbonate samples. ***Trans BgNS*** 12 (2008) 33-37.

162. Пресиянов Д. и колектив. Автоматизирана лабораторна система за прецизни ретроспективни измервания на радон. Договор 08/05 с ФНИ-МОН.

163. Pressyanov D., Georgiev S., Dimitrova I., Mitev K., Boshkova T. Determination of the diffusion coefficient and solubility of radon in plastics. ***Radiat. Prot. Dosim.*** 145 (2011) 123-126.

164. Rovenska K., Jiranek M. 1st international comparison measurement on assessing the diffusion coefficient of radon. ***Radiat. Prot. Dosim.*** 145 (2011) 127-132.

165. Chen, J., Schroth, E., Hnatiuk, S., Frenette, E. and Blain M-F. Radon diffusion coefficients of vapour barrier membranes used in Canadian building construction. ***Radiat. Environ. Biophys.*** 48 (2009)153-158.

166. Fleischer, R. L. Radon in the environment – opportunities and hazards. ***Nucl. Tracks Radiat. Meas.*** 14 (1988) 421-435.

167. Jha, G., Raghavayya, M. and Padmanabhan N. Radon permeability of some membranes. ***Health Phys.*** 42 (1982) 723-725.

168. Hosoda M., Tokonami S., Sorimachi A., Janik M. et al. Experimental system to evaluate the effective diffusion coefficient of radon. ***Rev. Sci. Instrum.*** 80, no. 1: 13501.

169. Durcik M., Havlik F. Experimental study of radon and thoron diffusion through barriers. ***J. Radioanal. Nucl. Chem.*** 209 (1996) 307-313.

170. Rovenska K., Jiranek M. **International intercomparison measurement of the radon diffusion coefficient – challenging results.** IN: Sustainable construction of buildings. Udrzitelna Vystava budov, Prague (2012), pp. 101-106.

171. Pressyanov D. Modeling a ^{222}Rn measurement technique based on absorption in polycarbonates and track-etch counting. ***Health Phys.*** 97 (2009) 604-612.

172. De Vos K. Ontwikkeling van een retro- en prospectieve radondetector gebaseerd op de radonabsorptie in polycarbonaten. Diploma thesis, University of Ghent; 2000 (in Dutch).

173. Turek K. **Study of polymer solid state track detectors for application in neutron detection and dosimetry.** Ph. D. Dissertation, Prague; 1982 (in Czech).

174. Doi M. **Development of the passive radon-thoron discriminative dosimeter for indoor and outdoor surveys.** Dissertation, Nagoya University, Nagoya, Japan (1996).

175. Edling C., Axelson O. Quantitative aspects of radon daughter exposure and lung cancer in underground miners. ***Br. J. Ind. Med.*** 40 (1983) 182-187.

176. Pershagen G. et al. Residential radon exposure and lung cancer in Sweden. ***N. Engl. J. Med.*** 330 (1994) 159-164.

177. Neuberger J. Residential radon exposure and lung cancer: an overview of ongoing studies. ***Health Phys.*** 63 (1992) 503-509.

178. Rericha V., Kulich M., Rericha R., Shore D.L. & Sandler, D.P. Incidence of leukemia, lymphoma, and multiple myeloma in Czech Uranium Miners: a case-control study. ***Environ. Health Perspectives*** 114 (2006) 818-822.

179. Raachou-Nielsen, O., Andersen, C. E., Andersen, H. P., Gravesen, P., Lind, M., Schuz, J. & Ulbake, K. Domestic radon and childhood cancer in Denmark. ***Epidemiol.*** 19 (2008) 536-543.

180. Lubin, J. H. et al. Adjusting lung cancer risks for temporal and spatial variations in radon concentration in dwellings in Gansu Province. ***China Radiat. Res.*** 163 (2005) 571-579.

181. Zhang, Z., Smith, B., Steck, D. J., Guo, Q. & Field, R.W. Variation in yearly residental radon concentrations in the Upper Midwest. ***Health Phys.*** 93 (2007) 288-297.

182. Steck D. Spatial and temporal indoor radon variations. ***Health Phys.*** 62 (1992) 351-355.

183. Steck, D. Annual average indoor radon variations over two decades. ***Health Phys.*** 96 (2009) 37-47.

184. Tomasek L., Darby S.C., Fearn T., Swerdlow A. J., Placek V. & Kunz E. Patterns of Lung Cancer Mortality among Uranium Miners in West Bohemia with Varying Rates of Exposure to Radon and its Progeny. ***Radiat. Res.*** 137 (1994) 251-261.

185. Baverstam, U. & Swedjemark, G-A. Where are the errors when we estimate radon exposure in retrospect? ***Radiat. Prot. Dosimetry*** 36 (1991) 107-112.

186. Lubin, J. H., Boice, Jr. & Samet, J. D. Errors in exposure assessment, statistical power and the interpretation of residental radon studies. ***Radiat. Res.*** 144 (1995) 329-341.

187. Bochicchio, F. Radon epidemiology and nuclear track detectors: Methods, results and perspectives. ***Radiat. Meas.*** 40 (2005) 177-190.

188. Alavanja, M. C., Lubin, J. H., Mahaffey, J. A., Brownson, R. C. Residential radon exposure and risk of lung cancer in Missouri. ***Am. J. Public Health*** 89 (1999) 1042-1048.

189. Mahaffey, J. A., Alvanja, M. C. R., Parkhurst, M. A., Berger, E. & Brownson, R.C. (1999). Estimation of radon exposure history for analysis of a residental epidemiology study. Radiat. Prot. Dosim., 13(5), 571-579.

190. Steck, D. J., Alavanja, M. C. R., Field, R. W., Parkhurst, M. A., Bates, D. J. & Mahaffey, J. A. (2002). 210Po implanted in glass surfaces by long term exposure to indoor radon. Health Phys., 83(2), 261-271.

191. Akiba S., Tokonami S., Bochicchio F., McLaughlin J., Tommasino L. & Harley N. Thoron: its metrology, health effects and implications for radon

epidemiology: a summary of roundtable discussion. Radiat. Prot. Dosim., 141, 477-481.

192. Hahn, O. & Meitner, L. Nachweis der komplexen Natur von Radium C (Proof of the complex nature of radium C). ***Phys. Z.*** 10 (1909) 697-703.

193. Lively, R. S. & Ney, E. P. Surface radioactivity from the deposition of ^{222}Rn daughter products. ***Health Phys.*** 52 (1987) 411-415.

194. Samuelsson, C. Retrospective determination of radon in houses. ***Nature*** 334 (1988) 338-340.

195. Samuelsson, C. Radon retrospective measurements. ***Int. Congr. Ser.*** 1276 (2005) 66-71.

196. Johansson, L., Roos, B. & Samuelsson, C. Alpha-particle spectrometry of large-area samples using an open-flow pulse ionisation chamber. ***Apl. Radiat. Isot.*** 43 (1992) 119-125.

197. Falk, R., Mellander, H., Nyblom L. & Ostergren, I. Retrospective assessment of radon exposure by measurements of ^{210}Po implanted in surfaces using an alpha track detector technique. ***Environ. Int.*** 22 (1996) S857-S861.

198. Samuelsson, C., Falk, R. & Roos, B. Alpha particle emission from reference glass surfaces implanted with ^{210}Po. ***Sci. Total Environ.*** 272 (2001) 175-179.

199. Lively, R. S. & Ney, D. J. Long-term radon concentrations estimated from 210Po embedded in glass. ***Health Phys.*** 64 (1992) 485-490.

200. Roos, B. & Samuelsson, C. Experimental methods of determining the activity depth distribution of implanted ^{210}Pb in glass. ***J. Environ. Radioact.*** 63 (2002) 135-151.

201. Fleischer R. L. et al. Etched tracks and serendipitous dosimetry. ***Radiat. Prot. Dosim.*** 120 (2006) 450-456.

202. Samuelsson, C. Plate-out and implantation of ^{222}Rn decay products in dwellings. ***Environ. Int.*** 22 (1996) S839-S843.

203. Walsh, C. & McLaughlin, J. P. Correlation of ^{210}Po implanted in glass with radon gas exposure: sensitivity analysis of critical parameters. ***Sci. Total Environ.*** 272 (2001) 195-202.

204. Jacobi, W. Activity and potential alpha energy of Rn-222 and Rn-220 daughters in different air atmospheres. ***Health Phys.*** 22 (1972) 441-450.

205. Zhukovsky, M., Onischenko, A. & Bastrikov, V. Radon measurements _ discussion of error estimates for selected methods. ***Appl. Radiat. Isot.*** 68 (2010) 816-820.

206. Schmidt, V. & Hamel, P. Measurements of deposition velocity of radon decay products for examination of the correlation between air activity concentration of radon and the accumulated Po-210 surface activity. ***Sci. Total Environ.*** 272 (2001) 189–194.

207. Steck, D. J. & Field, R. W. The use of track registration detectors to reconstruct contemporary and historical airborne radon ^{222}Rn and radon progeny

concentrations for a Radon-Lung Cancer Epidemiologic Study. ***Radiat. Meas.*** 31 (1999) 401-406.

208. Committee on Health Risks of Exposure to Radon (BEIR VI). National Research Council. Health effects of exposure to radon. National Academy Press,Washington, DC, USA, 1999.

209. Grosche, B., Kreuzer, M., Kreisheimer, M., Schnelzer, M. & Tschense, A. Lung cancer risk among German male uranium miners: a cohort study 1946-1998. ***Br. J. Cancer*** 95 (2006) 1280–1287.

210. McLaughlin, J. P. The application of techniques to assess radon exposure retrospectively. ***Radiat. Prot. Dosim.*** 78 (1998) 1-6.

211. Field, R. W., Steck, D. J., Parkhurst, M. A., Mahaffey, J. A. & Alavanja, M. C. R. Intercomparison of retrospective radon detectors. ***Environ. Health Persp.*** 107 (1999) 905-910.

212. Falk, R, Almren, K. & Ostergren, I. Experience from retrospective radon exposure estimations for individuals in a radon epidemiological study using solid-state nuclear track detectors. ***Sci. Total Environ.*** 272 (2001) 61-66.

213. Birovljev, A., Falk, R., Walsh, C., Bissolo, F., Trotti, F., McLaughlin, J. P., Paridaens, J. & Vanmarcke, H. Retrospective assessment of historic radon concentrations in norwegian dwellings by measuring glass implanted ^{210}Po - an international field intercomparison. ***Sci. Total Environ.*** 272 (2001) 181-188.

214. Bochicchio, F., McLaughlin, J. P. & Walsh, C. Comparison of radon exposure assessment results: ^{210}Po surface activity on glass objects vs. contemporary air radon concentration. ***Radiat. Meas.*** 36 (2003) 211-215.

215. Fitzgerald, B. & Hopke, P. K. A prospective assessment of the ^{210}Po surface collection for estimating ^{222}Rn exposure. ***J. Environ. Radioact.*** 51 (2000) 79-98.

216. Oberstedt, S. Retrospective radon dosimetry. ***Il Nuovo Cimento C*** 304 (1999) 341-344.

217. Oberstedt, S., Vanmarcke, H. Volume traps – a new retrospective radon monitor. ***Health Phys.*** 70 (1996) 222-226.

218. Paridaens, J., Vanmarcke, H., Jacobs, K. & Zunic, Z. Retrospective radon assessment by means of ^{210}Po activity measurements. ***Appl. Radiat. Isot***. 53 (2000) 361-364.

219. Paridaens, J., Vanmarcke, H., Zunic, Z. & McLaughlin, J. P. Field experience with volume traps for assessing retrospective radon exposures. ***Sci. Total Environ.*** 272 (2001) 295-302.

220. Zunic, Z., Yarmoshenko, I.V., Kelleher, K., Paridaens, J., McLaughlin, J. P., Celikovic, I., Ujic, P., Onischenko, A. D., Jovanovic, S., Demajo, A., Birovljev, A. & Bochicchio, F. Comparison of retrospective and contemporary indoor radon measurements in a high- radon area of Serbia. ***Sci. Total Environ.*** 387 (2007) 269-275.

221. Fleischer, R.L. Serendipitous dosimetry - an oppurtunity and an oppurtunity lost. ***Health Phys.*** 52 (1987) 219-221.

222. Hadley, S. A., Meyer, N. R., Fleischer, R. L. & Cavallo, A. Eyeglass lenses for personal radon dosimetry. ***Health Phys.*** 79 (2000) 242-250.

223. Fleischer, R. L., Meyer, N. R.,. Hadley, S. A, MacDonald, J. & Cavallo, A. Personal radon dosimetry from eyeglass lenses. ***Radiat. Prot. Dosim.*** 97 (2001) 251-258.

224. Fleischer R. L. Serendipitous radiation detectors. ***Am. Sci.*** 90 (2002) 324-331.

225. Blanchard R. L., Archer V. E., Saccomano G. Blood and skeletal levels of ^{210}Pb – ^{210}Po as a measure of exposure to inhaled radon daughter products. ***Health Phys.*** 16 (1969) 585-596.

226. Fisher H. L. A model for estimating the imhalation exposure to radon-222 and daughter products from the accumulated lead-210 body burden. ***Health Phys.*** 16 (1969) 597-616.

227. Eisenbud M. et al. In vivo measurement of lead-210 as an indicator of cumulative radon daughter exposure in uranium miners. ***Health Phys.*** 16 (1969) 637-646.

228. Johanston, P. N., Hult, M., Gasparro, J., Martinez-Canet, M-J., Vasselli, R., McKenzie, R. J., Solomon, S.B. & Lambrichts, I. The distribution of ^{210}Po in human bone and its imact on methods for the retrospective estimation of ^{222}Rn exposure from in vivo measurements. ***J. Environ. Radioact.*** 80 (2005) 245-257.

229. McLaughlin, J.P. Aproaches to the assessment of long term exposure to radon and its progeny. ***Sci. Total Environ.*** 272 (2001) 53-60.

230. Pressyanov D., Dimitrova I., Mitev K., Georgiev S. **Retrospective radon measurements: techniques and perspectives.** Chapter 4 IN: ***Handbook on***

Radon: Properties, Measurements and Health Effects. NOVA Science Publishers Inc., New York, ISBN: 978-1-62100-369-4 (2012)101-129.

231. Dimitrova, I., Pressyanov, D., Georgiev, S. & Yankov, P. Logistic of surveys of retrospective radon concentrations by home-stored CDs/DVDs. ***Radiat. Prot. Dosim.*** 145 (2011) 300-304.

232. Димитрова И. **Измерване на ^{222}Rn във въздушна и водна среда чрез абсорбция в поликарбонати.** Дисертация, СУ, Физически факултет (2011).

233. Pressyanov, D., Dimitrova, I., Georgiev, S. & Mitev, K. Radon survey based on home stored CDs/DVDs. *In: Proc. of Third European IRPA Congress*, Helsinki, 14-18 June , 2010.

234. Commission of the European Communities (2001). Commission Recommendation of 20 December 2001 on the protection of the public against exposure to radon in drinking water supplies (notified under document number C (2001) 4580), OJ L 344, 28.12.2001, 85.

235. Trantmannheimer M., Schindermeier K., Hubel K. ***Int. Congr. Ser.*** 1225 (2002) 81.

236. Yurong Y., Ziqiang Z. ***Nucl. Tracks Radiat. Meas.*** 22 (1993) 499.

237. Yasuoka Y. et al. **Anomalous atmospheric radon variation before an earthquake: A case study of the 1995 Kobe earthquake, Japan.** IN: ***Handbook on Radon: Properties, Applications and Health.*** Nova Science Publishers Inc. (2012) pp. 419-433.

238. Salonen L., Hukkanen H. Advantages of low-background liquid scintillation alpha-spectrometry and pulse shape analysis in measuring ^{222}Rn, uranium and 224Ra in groundwater samples. ***J. Radioanal. Nucl. Chem.*** 226 (1997) 67-74.

239. Kitto M. E., Bari A., Haines D. K., Menia T. A., Fielman E. M. **Laboratory intercomparison of radon-in-water standards.** IN: Proc. 2009 Int. AARST Radon Symp., pp. 90-96, St. Luis, MO.

240. Tommasino L., Tommasino M. C., Viola P. Radon-film-badges by solid radiators to complement track detector-based radon monitors. ***Radiat. Meas.*** 44 (2009) 719-723.

241. Tommasino L. Radon film-badges versus existing passive monitors based on track etch detectors. ***Nukleonika*** 55 (2010) 549-553.

242. Tommasino L., Tomasino M. C., Espinosa G. Radon filmbadges based on radon-sorption in solids. A new field for solving long-lasting problems. ***Rev. Mex. De Fisica*** S56 (2010) 1-4.

243. Tommasino L., Tokonami S. Four passive sampling elements (quatrefoil)-II. Film badges for monitoring radon an dits progeny. ***Radiat. Prot. Dosim.*** 145 (2011) 284-287.

244. Pressyanov D. Modeling response of radon track detectors with solid absorbers as radiators. ***Radiat. Meas.*** 46 (2011) 357-361.

245. Brandt S. Data Analysis. **Statistical and Computational Methods for Scientists and Engineers.** Springer, 3rd ed. (1998).

246. Pressyanov D., Georgiev S., Dimitrova I., Mitev K. Experimental study of the response of radon track detectors with solid absorbers as radiators. ***Radiat. Meas.*** (2012), in press.

247. Cheng J., Moir D. The concept of equivalent radon concentration for practical consideration of indoor exposure to thoron. ***Int. J. Environ. Res. Public Health*** 9 (2012) 286-293.

248. Tokonami, S. Why is ^{220}Rn (thoron) measurement important? ***Radiat. Prot. Dosim.*** 141, 335-339 (2010).

249. Pressyanov D. Retrospective measurements of thoron and radon by CDs/DVDs: a model approach. ***Radiat. Prot. Dosim.*** 149 (2012) 464-468.

250. Harley, N., Chittaporn, P., Medora, R. and Merrill, R. Measurement of the indoor and outdoor ^{220}Rn (thoron) equilibrium factor: application to lung dose. Radiat.Prot. Dosim. 141, 357-362 (2010).

251. Pressyanov D., Dimitrova I., Georgiev S., Mitev K. Pilot experiments on retrospective thoron measurements by CDs/DVDs. ***Radiat. Meas.*** (2012), in press.

252. Eappen K., Sapra B., Mayya Y. A novel methodology for online measurement of thoron using Lucas scintillation cell. ***Nucl. Instrum. Meth. Phys. Res.*** A 572 (2007) 922-925.

253. Tang F., Zhuo W., Zhao C., Chen B., Xu Y., He L. A theoretical study on accurate measurement of thoron with airflow-through scintillation cell method. ***Radiat. Prot. Dosim.*** 141 (2010) 448-451.

ANNEX I

GLOSSARY

Some terms might be considered as uncommon. Therefore, we give here their definitions following ICRP Publication 115 [19]:

- **Radon progeny:** ^{218}Po, ^{214}Pb, ^{214}Bi + ^{214}Po; **thoron progeny:** ^{216}Po, ^{212}Pb, ^{212}Bi + ^{212}Po/^{208}Tl.
- **Equilibrium equivalent concentration (EEC):** The activity concentration of radon, in equilibrium with its short-lived progeny that would have the same potential alpha energy concentration as the existing non-equilibrium mixture.
- **Equilibrium factor (F):** The ratio of the equilibrium equivalent concentration to the radon gas activity concentration.
- **Potential alpha energy concentration (PAEC):** The concentration of short-lived radon or thoron progeny in air in terms of the alpha energy released during complete decay to ^{210}Pb for ^{222}Rn progeny or to ^{208}Pb for ^{220}Rn progeny.
- **Working level (WL):** Any combination of the short-lived progeny of ^{222}Rn in one litre of air that will result in the emission of 1.3×10^5 MeV of potential alpha energy. 1 WL = 2.08×10^{-5} J m^{-3}.
- **Working level month (WLM):** The cumulative exposure from breathing an atmosphere at a concentration of 1 WL for a working month of 170 hours.
  1 WLM = 3.54×10^{-3} J h m^{-3}.

ANNEX II

EXAMPLE OF APPLICATION: AN INTEGRATED APPROACH TO THE RADON PROBLEM

Albeit the primary goal in development of the CD/DVD method was for retrospective measurements (needed e. g. for epidemiology) the practical performance of the method suggested, that CDs/DVDs can be used to "pinpoint" radon problem. Our experience indicates, that dwellings with problem (e.g. in which the WHO level of 100 Bq m^{-3} is exceeded) would be detected by any more than one year old disk. In the last years this possibility was used to build an integrated approach to the radon problem.

The common practice to date needs long-term (> 3 months, as recommended by WHO [1], and preferably one year) measurements to be planned and carried-out. The results are usually available months or a year after the detectors are distributed in the studied dwellings. This "too many time" between the decision to test and eventual problem identification affects the stakeholders' attitude and can reduce the concern about the reality of radon hazard and the need of measures to reduce it. However, a step ahead is possible, using CDs/DVDs as available, practically in any dwelling, "radon sensors". This way, one can check almost immediately the radon situation in his house, as the disk processing takes several hours and the results can be available on the same or the next day after the disk is provided. Still, the results are based on long-term integrated measurements as WHO recommends, but concentrations are evaluated "in retrospect".

The concept is to use CDs/DVDs as available serendipitous indoor radon sensors that can be used to pin-point dwellings with problem in short-time after the decision to provide disk for analysis. Any disk purchased more than one year ago is suitable for that purpose. Indeed, as follows from Table V. 2., the minimum detectable ^{222}Rn activity concentration for one year exposure is about 30 Bq m^{-3}. This means that with a disk that is more than one year old there is no danger of omitting buildings with radon levels increased in the range of concern (> 100 Bq m^{-3}, according to the WHO criteria [1]). The probability of "false alarm" is low: The study of the background in 19 different new disks

showed the average value of 6.3 cm^{-2}, with 18 out of 19 disks showing less than 11 cm^{-2} individual track density and only one "outlier" with track density of 49.6 cm^{-2} [232]. If this is considered as representative background distribution between the new disks, there will be no "false alarm" in case of 5 years old disks and only one out of 19 with one year old disks. Such probability for false alarm (about 5% with one year old disks and lower with older disks) is sufficiently low, moreover additional radon measurements can verify the first warning signal.

Consider the basic process: **"detection → diagnostic measurements → mitigation"**. The possibility to detect the problem in short time after decision to provide one or more CDs/DVDs for analysis makes it possible the entire process to be considered as an united whole, with continuous sequence between the individual steps, and which can be controlled and supervised by a single radon expert/team. Somewhat this is an analogy with the process "symptoms → diagnostic → therapy" in medicine that in most cases is supervised by one medical doctor/team, with no significant breaks between the steps. Once the problem is detected and if the stakeholder is concerned, the next step is diagnostic measurements. This step takes normally about one-two weeks. It aims to check once more whether the alarm is real, to analyze radon distribution in the building, to find and explore radon sources and routes of entry.

This approach was used in testing, diagnostic and mitigation of public buildings (kindergartens and schools) in the region of Kremikovtsi. Once ^{222}Rn concentration > 300 Bq m^{-3} was detected comprehensive diagnostic measurements were organized and carried-out when Upon the results, the mitigation plan was prepared and mitigation steps initiated. In diagnostic step the ^{222}Rn measurements were made by calibrated radonometer RAD 7 and that of ^{222}Rn progeny by an aerosol radiometer RV-4. Radon in soil gas measurements were made by diffusion chambers exposed (at 60 cm depth) for few days and radioactivity of soil/building materials was analyzed by gamma spectrometry. A description and methodological details of most of the methods employed in radon diagnostic is given in Chapters II and III. To have an efficient mitigation plan, it is important to study the radon distribution in soil-gas ("the source") and indoors, as in large public buildings the concentrations in different rooms can vary substantially (Fig. AII.1).

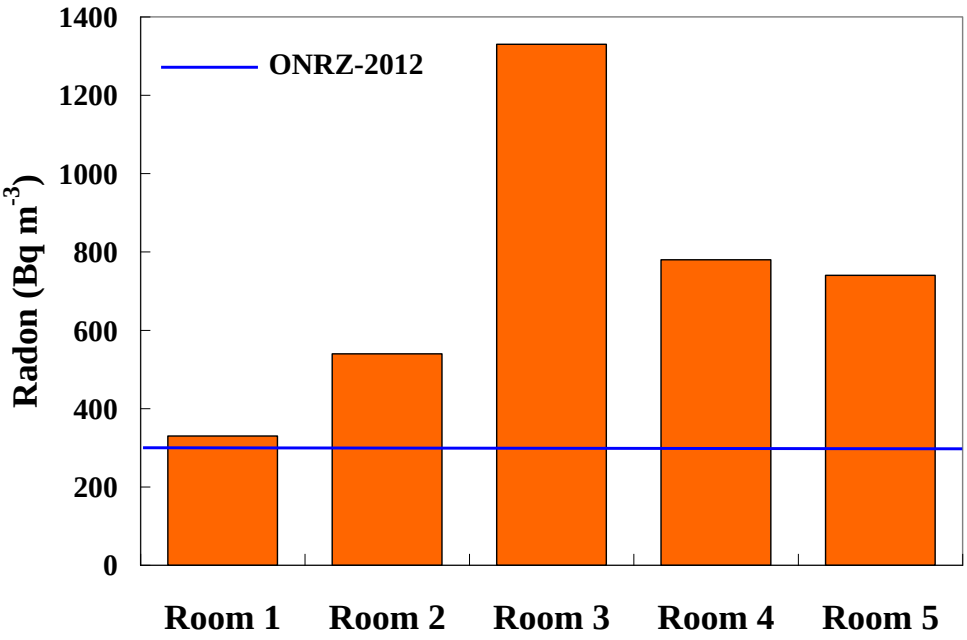

Figure AII.1. Radon distribution in different rooms of one-storey kindergarten.

The third step of the process is mitigation. The choice of mitigation strategy and mitigation plan are much dependent on diagnostic measurements. The mitigation is executed by a company specialized in construction/repair of buildings under the technical supervision of a "radon team/expert" and following available technical standards [133, 134]. Within this integrated approach the interval between the very first indication for the problem to the complete mitigation of the building can be significantly shortened as the stakeholder is not de-motivated by "too many time needed to have some conclusive results". In 2012 in region of Kremikovtsi nine building with elevated radon concentrations were mitigated. The radon problem in some of them was identified by analyzed CDs/DVDs (somewhat curiously, in two of the problem dwellings - one school and one kindergarten the disks were taken from TV-reporters and on 26 January 2012 the national TV (BNT2) arranged "hot reportage" from the author's laboratory to show just obtained results). Later, in April 2012 the Ministry of Health issued official recommendations for reducing radon levels in nine buildings, that were based on independent long term prospective measurements. The author cannot refer to their results as they were neither publicly available nor personally communicated to him. Notably

however, the buildings with problem already identified with our measurements by CDs/DVDs were present in the list. These nine buildings were:

1. Secondary school Nr. 117 (branch Seslavtsi);
2. Kindergarten Nr. 44 (Botunets);
3. Secondary school Nr. 85 (Vrazhdebna);
4. Basic school Nr. 159 (Chelopechene);
5. Kindergarten Nr. 94 (Bouchovo)
6. Kindergarten Nr. 58 (Chelopechene);
7. Kindergarten Nr. 146 (Kremikovtsi);
8. Basic school Nr. 116 (Yana);
9. Kindergarten Nr. 47 (branch Yana).

For all of them the local municipality decided to mitigate against radon (for two of them this was decided even earlier – in March 2012, due to the early warnings for the radon problem). The author provided technical consultancy and supervision for mitigation of all nine buildings. The mitigation works were completed by 15 September 2012 everywhere and the results of mitigation can be seen in Fig. AII.2. Together with other two buildings mitigated in 2007 and 2008, to date the author has supervised mitigation of 11 buildings – one private and 10 public.

A case that illustrates the strength of the integrated approach is taken from our practice in 2012: A disk from the kindergarten Nr. 47 showed ^{222}Rn of about 1100 Bq m^{-3}. Diagnostic measurements confirmed the problem. Under "closed for 24 hours" conditions the measured ^{222}Rn concentrations at the ground floor ranged in different rooms between 1200 and 2200 Bq m^{-3} (average about 1500 Bq m^{-3}). To solve the problem, an active mitigation system with sub-slab depressurization at two points was planned. The position of the aspiration points was chosen taking into account radon distribution indoors and in soil-gas. After the system was started the concentrations dropped everywhere to <100 Bq m^{-3}. The time scale of the entire process was as follows: The CD was analyzed at the end of March 2012, the mitigation works started in the very beginning of April and mitigation was complete in the first week of May 2012. The total

duration of the process was about 6 weeks. With the traditional approach based on prospective integrated measurements only the detection step should need between 3 months and (preferably) one year and the next steps, if any, could be even more delayed. The CD/DVD method allows to develop and put in practice a new integrated approach to the radon problem. Under this approach the entire process "**detection → diagnostic → mitigation**" can be considered as an united whole that can be closely controlled and the risk successfully reduced in sufficiently short time.

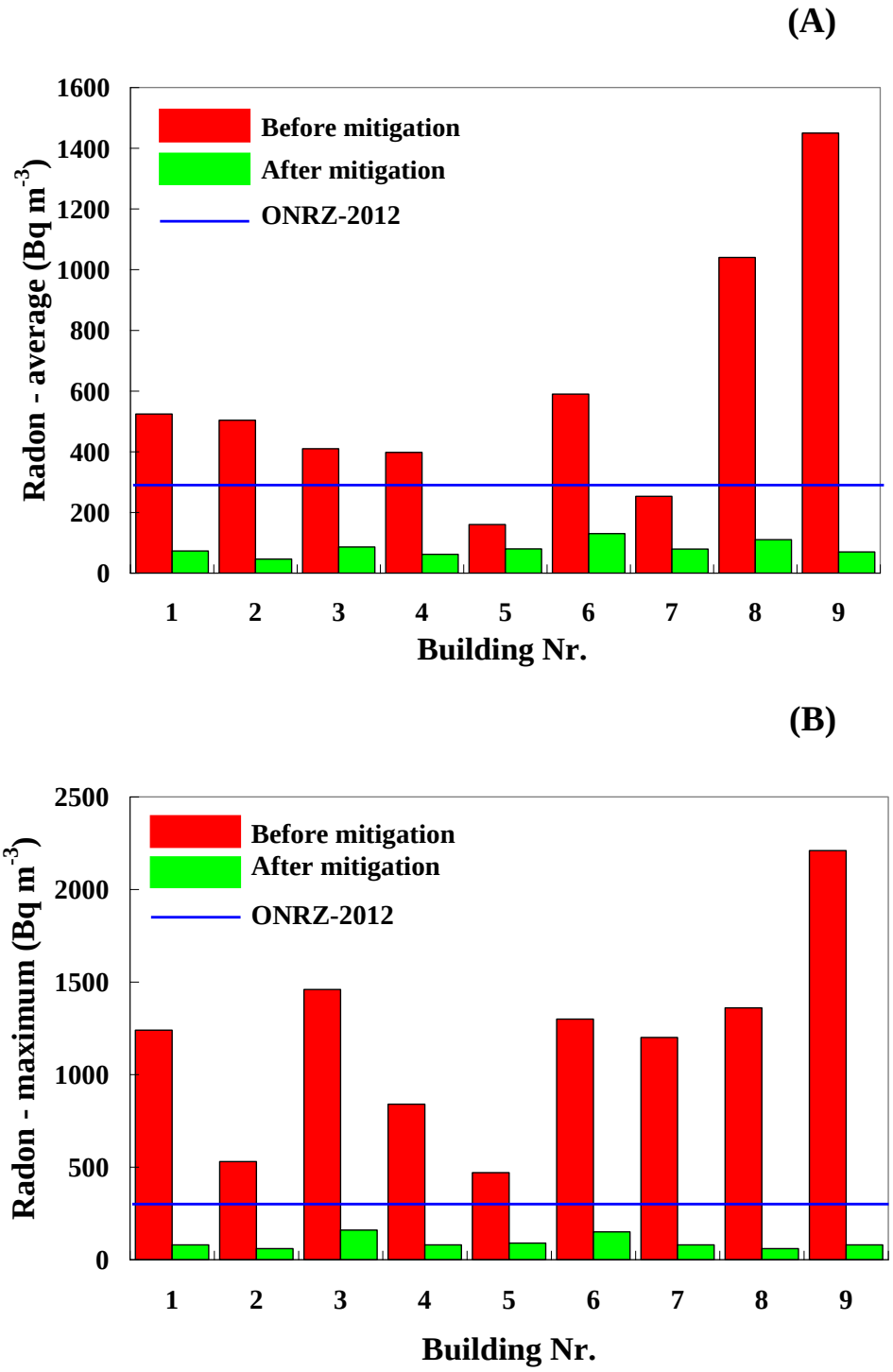

Figure AII.2. Effect of mitigation: (A) average ^{222}Rn concentrations (ground floor); (B) rooms of maximum ^{222}Rn concentrations. The horizontal line represents the current Bulgarian norm for existing buildings [135].